JPRS L/10641

7 July 1982

Translation

PHOSPHATE LASER GLASS

By N. Y. Alekseyev et al.

FBIS FOREIGN BROADCAST INFORMATION SERVICE

FOR OFFICIAL USE ONLY

APPROVED FOR RELEASE: 2007/02/09: CIA-RDP82-00850R000500080015-2

NOTE

JPRS publications contain information primarily from foreign newspapers, periodicals and books, but also from news agency transmissions and broadcasts. Materials from foreign-language sources are translated; those from English-language sources are transcribed or reprinted, with the original phrasing and other characteristics retained.

Headlines, editorial reports, and material enclosed in brackets [] are supplied by JPRS. Processing indicators such as [Text] or [Excerpt] in the first line of each item, or following the last line of a brief, indicate how the original information was processed. Where no processing indicator is given, the information was summarized or extracted.

Unfamiliar names rendered phonetically or transliterated are enclosed in parentheses. Words or names preceded by a question mark and enclosed in parentheses were not clear in the original but have been supplied as appropriate in context. Other unattributed parenthetical notes within the body of an item originate with the source. Times within items are as given by source.

The contents of this publication in no way represent the policies, views or attitudes of the U.S. Government.

APPROVED FOR RELEASE: 2007/02/09: CIA-RDP82-00850R000500080015-2

JPRS L/10641

7 July 1982

PHOSPHATE LASER GLASS

Moscow LAZERNYYE FOSFATNYYE STEKLA in Russia 1980 (signed to press 28 Nov 80) pp 1-352

[Book "Phosphate Laser Glass" by Nikolay Yefimovich Alekseyev, Valentin Pavlovich Gapontsev, Mark Yefremovich Zhabotinskiy, Valeriy Borisovich Kravchenko and Yuriy Petrovich Rudnitskiy, edited by M. Ye. Zhabotinskiy, "Nauka", 2600 copies, 352 pages]

CONTENTS

ANNOTATION

A detailed description is presented of the physical properties of new efficient laser materials--phosphate glass activated by rare earth ions. The possibilities and prospects for their application in various types of lasers are demonstrated.

Information is presented on the structure of phosphate glass, the spectral luminescence, lasing, thermooptical, nonlinear optical characteristics of laser phosphate glass activated by Nd^{3+} ions. The processes of energy transport and quenching of luminescence in phosphate glass, and sensitization of luminescence in glass co-activated by Nd^{3+} and Yb^{3+}, Yb^{3+} and Er^{3+} ions were investigated.

FOREWORD

Phosphate glass, which is now becoming more and more widespread in the basic industrially developed countries, first appeared in the Soviet Union. Phosphate laser glass has especially great significance in creating powerful and superpowerful lasers and lasers that operate in the periodically repeating pulse mode.

At the present time it is possible to talk about the completion of a defined phase of research and development of phosphate laser glass, recognition of its advantages and the beginning of industrial output and application in series laser systems. This determines the urgency of the proposed monograph.

It must be noted that the last exhaustive survey of laser glass was published about 10 years ago and, just as the preceding ones, contained almost no information on phosphate laser glass.

The authors of this book are participants in the development and investigation of many types of phosphate laser glass, including the first, so that a significant part of its content is based on their work, and the book itself does not pretend to encompass the multifaceted problem of laser glass completely.

A discussion is presented of the results of physical and spectral luminescence studies of phosphate laser glass, the study of the processes of excitation of rare earth ions, transmission of excitation and relaxation processes in laser glass. The obtained data indicate both the advantages of phosphate laser glass over other glass and the potential possibilities inherent in these types of glass. Physicochemical and lasing characteristics of this glass is also presented, and phosphate laser glass is compared with silicate laser glass.

The book is designed for physicists interested in studying laser materials and processes occurring in lasers, for technologists involved with improving laser materials and the active elements made from them, and for laser designers in need of specific characteristics of active elements without which it is impossible to design and build lasers.

The book is written in six chapters.

Chapter 1 investigates the requirements on the physical parameters of laser glass arising from the problem of optimizing the characteristics of lasers of various types for various purposes. These parameters include, for example, the spectral luminscence parameters which determine the energy characteristics of lasers, including their efficiency. The corresponding parameters for lasers operating in the free lasing mode differ significantly from those required for the short and supershort pulse modes.

Special attention is given to the parameters determining the applicability of glass in powerful and superpowerful lasers, for which the nonlinear characteristics, optical and thermal stability, and thermooptical distortions become no less important than the efficiency.

Chapter 2 is devoted to the structure of phosphate glass. The structure of phosphate glass differs significantly from the structure of silicate glass, in the final analysis, insuring the advantages of phosphate glass over silicate glass. The physicochemical processes occurring when making phosphate glass determine its structure, having features characteristic of inorganic polymers. This, in turn, determines the nearest vicinity of the ion activators and the structure of subsequent coordination spheres, and at the same time insures exceptionally good spectral luminescence and lasing characteristics of phosphate laser glass and also the possibility of controlling its thermooptical characteristics.

The modern concepts of the mechanisms and laws of occurrence of the processes of nonradiating electron excitation energy transfer in laser glass. An analysis is made of various versions of ion-ion transfer, including the excitation energy migration process and also the processes of multiphonon nonradiating relaxation of the excited states of rare earth ions caused by interaction with the vibrations of admixed hydroxyl groups and structural elements of the glass itself. The discussion is primarily based on original results of the authors, the greater part of which are published for the first time. For exhaustive substantiation of the uniqueness of the properties of phosphate glass, the authors considered it necessary to expand the class of analyzed objects by using other activators and glass-like systems, which lends the obtained results a fundamental nature. The ideas and the results of this chapter played an important role in the development of laser phosphate glass.

Chapter 4 is devoted exclusively to neodymium-doped phosphate laser glass and the possibility of its application in various types of lasers.

The primary content of Chapter 5 is data on the thermooptical properties of phosphate laser glass, the study of which permitted purposeful synthesis of compositions with properties optimized as applied to specific problems. In particular, in this chapter a study is made of the problems arising when making glass for pulsed-periodic lasers and high-energy laser systems. In both cases the advantages of phosphate glass over silicate laser glass are especially clearly manifested.

Chapter 6 analyzes the spectral luminescence and lasing characteristics of erbium-doped phosphate laser glass, and the specific nature of the construction of lasers based on this glass is investigated. Special attention is given to neodymium laser pumped erbium lasers, inasmuch as the combined systems of this type permit the creation of radiation sources in the range of 1.5 microns which are similar with respect to lasing characteristics to neodymium lasers, and in certain respects even superior to them in the short and supershort pulse amplification mode.

The limited size of the book makes it impossible to consider the properties of phosphate laser glass coactivated by neodymium and ytterbium, which is prospective for application in powerful amplifiers. Those who are interested in this subject can refer to the background material [48, 82, 85, 101].

A bibliography containing 545 references was collected up to the end of 1979. It includes the most significant publications, but does not pretend to completeness.

The collective of authors expresses sincere appreciation to all researchers permitting use of figures from their publications. The corresponding footnotes are included in the text or in the captions to the figures.

The authors acknowledge the assistance of coworkers of the IRE [Institute of Radio Engineering and Electronics], and the IONKh [Institute of General and Inorganic Chemistry] of the USSR Academy of Sciences, and the "Rubin" PTO [Production and Technical Association], together with which they studied and made phosphate laser glass. They also acknowledge coworkers of the FIAN [Physics Institute of the USSR Academy of Sciences] and the GOI [State Institute of Optics] imeni S. I. Vavilov for useful discussion.

The materials of this book were distributed among the authors as follows: N. Ye. Alekseyev, §§4.1 to 4.3, 4.8 to 4.10; V. P. Gapontsev, Chapters 3 and 6; M. Ye. Zhabotinskiy, the introduction; V. B. Kravchenko, §§1.4 to 1.6, Chapter 2, §§5.1 and 5.2; Yu. P. Rudnitskiy, §§1.1 to 1.3, §§4.4 to 4.6, 4.7 and 5.3.

M. Ye. Zhabotinskiy

INTRODUCTION

The 20-year mark of the laser age was reached in 1980. Industrial laser production is being engaged in on a large scale and has acquired great significance in the economies of the developed countries. Lasers are widely used in industry, construction, medicine and scientific work. Therefore the literature on lasers initially devoted primarily to investigation of such physical problems as the problems of lasing and amplification, including various operating modes of the laser, such physical characteristics as coherence and fluctuations of laser emission, its divergence and spectral composition, has gradually come to include the analysis of problems arising in the design, development, production and application of lasers.

As is known, the first laser was a ruby laser. It was pumped by a pumping tube. Soon a report came out on the first gas laser using a mixture of helium and neon pumped by electric discharge. Thus, from the very beginning two competing and mutually complementary areas were distinguished--the development of solid-state and gas lasers. Subsequently, semiconductor lasers and liquid lasers using organic (dyes) and inorganic liquids were distinguished as separate areas.

The development of quantum electronics based on studying the physical processes leading to realization of the laser effect had a clearly expressed applied nature. Researchers set the goal of increasing the power of lasers, their efficiencies, assimilation of a broader and broader range of wavelengths, including the possibility of continuous wavelength adjustment, the assimilation of various operating modes from continuous lasing to supershort pulse lasing, and an increase in frequency stability of laser emission, and so on.

This, in turn, stimulated the search for and the investigation of new active media suitable for use in lasers. At the present time hundreds of different gas mixtures are known (including pure gases and metal vapor), which are capable of lasing at different points of the optical band--from the ultraviolet region to submillimeter. A number of crystals, liquids and glass of different composition and an entire series of semiconductor compounds are known, the number of which is growing constantly.

However, the majority of materials for which the laser effect has been studied have not found practical application, for the set of characteristics providing for realization of certain specific goals is encountered relatively rarely.

Thus, the achievement of high pulse energy and maximum high power in the short and supershort pulse mode requires high density of the active particles which is characteristic of solid-state active elements. In spite of persistent research and improvement of the methods of growing artificial single crystals, until recently only two types of active crystals have found application in industrially produced lasers. These are rubies and neodymium-doped yttrium-aluminum garnet. The latter has found especially broad application, for it successfully combines the mechanical and thermooptical properties of yttrium-aluminum garnet with the laser characteristics of the neodymium ions in this crystal. Recently neodymium-doped yttrium aluminate crystals have been added to this list.

Continuous and pulsed-periodic neodymium-doped YAG and yttrium aluminate lasers are being used successfully. They provide an average power on the order of tens and even hundreds of watts, and in unique models, when using special circuits and structures, they provide a power on the order of several kilowatts. However, the cost of large monocrystalline laser elements increases much more rapidly than the obtained power, which is explained by the difficulties of growing large optically homogeneous samples.

Neodymium-doped glass was one of the first materials in which the laser effect was obtained. The superior optical characteristics of the glass, the high technological level of founding and working it, availability and relative cheapness of the raw material insured rapid progress in the creation of laser glass and lasers based on them.

The application of lasers in industrial production processes has required mass output of laser glass, and the problems of laser thermonuclear research have stimulated the manufacture of large active elements with dimensions entirely unattainable by the existing methods of growing crystals.

Thus, glass has become the most important active element for solid-state lasers. For a long time, only silicate glass was used, the manufacturing technology of which was developed to the highest degree in the optical industry. The efforts of physicists and process engineers were aimed at improving the laser characteristics of silicate glass, its physicochemical and optical parameters, such as optical homogeneity, radiation strength (body and surface), and also chemical strength, thermooptical and thermomechanical characteristics, adaptability to manufacture, and so on.

Efforts to create nonsilicate laser glass, for example borate and germanate glass, did not lead to hopeful results.

The presented book has the goal of investigating phosphate laser glass, which has recently become one of the most important materials for making the active elements of solid-state lasers for various purposes.

Phosphate glass was known to specialists as nontechnological, it had a very narrow range of application and was industrially produced in small quantities. For this reason, for a number of years there was no effort made to create phosphate laser glass.

It was only in 1966 that the collective of researchers working at the Institute of Radio Engineering and Electronics of the USSR Academy of Sciences, which included the authors of this book, arrived at the conclusion of the potential advantages of phosphate laser glass if such could be created. The conclusion followed from the results obtained by this collective while studying the luminescence of ions of rare earth elements in polyphosphoric acids and from known concepts regarding the structure of phosphate glass. A collective of coworkers of the Institute of General and Inorganic Chemistry of the USSR Academy of Sciences, among whom V. V. Tsapkin and the late G. V. Ellert played a leading role, became involved in this research.

As a result of purposeful research, a method of synthesizing phosphate laser glass based on alkali and alkali earth element metaphosphates was developed. In the following year neodymium-doped phosphate glass laser elements were made which had satisfactory physicochemical properties and were superior to silicate glass with respect to the primary laser characteristics. Thus, the width of the lasing spectrum of the new glass was 4 angstroms as opposed to 80 to 120 angstroms for silicate glass, and the efficiency was 1.5 to 2 times as high under identical excitation conditions. Soon this glass, under the name of LGS-40, became the first industrial phosphate laser glass. The disadvantage of this glass was relatively low chemical stability.

It must be noted that studies of the possibility of creating phosphate laser glass were performed independently at the same time by Deutschbein and his coworkers in France. They published comprehensive results of spectral luminescence studies of a number of compositions for neodymium-doped phosphate glass, and they reported that lasing had been obtained.

The phosphate laser glass of the IRE Institute of the USSR Academy of Sciences developed jointly with the LZOS and called LGS-40 M, LGS-41 and LGS-42, has improved physicochemical characteristics.

The second generation of phosphate laser glass of the IRE Institute of the USSR Academy of Sciences was intended specially for application in large industrial and research devices in which rigid requirements arise both with respect to thermooptical characteristics of the glass and its efficiency. The athermal characteristics of phosphate laser glass LGS-I were subsequently reproduced also in the corresponding silicate glass.

A number of compositions of neodymium glass developed by the State Institute of Optics imeni S. I. Vavilov and the LZOS and manufactured by industry under the names GLS-21, GLS-22, GLS-23, GLS-24, LGS-55 and LGS-56 must be included in the second generation phosphate laser glass.

The next step in the development of phosphate glass was the creation of "athermal" phosphate glass with reduced temperature dependence of the thermooptical characteristics (type LGS-M), with diminished concentration quenching of luminescence and, correspondingly, with high activator concentration (glass of the LGS-K type developed by the IRE Institute of the USSR Academy of Sciences, lithium neodymium phosphate glass developed by the Physics Institute of the USSR Academy of Sciences). Recently work on highly concentrated glass has been started abroad.

In spite of the progress in improving the characteristics of phosphate laser glass, one area has lagged behind, in which phosphate laser glass cannot compete with yttrium-aluminum garnet. This area involves operation in the rapidly repeated pulse mode. In this mode the thermomechanical characteristics of the material, especially its thermal conductivity and mechanical strength, acquire primary significance. YAG crystals have significant advantages over glass with respect to both of these characteristics.

The known methods of strengthening glass, for example, quenching, have significant disadvantages, among which long buildup to the operating mode and negative effects on the thermooptical characteristics are the most undesirable.

The IRE Institute of the USSR Academy of Sciences developed original methods of strengthening the active elements made of phosphate laser glass. As a result, elements operating at a pulse repetition frequency of 10 hertz develop almost the same average power as YAG active elements of the same dimensions, under identical pumping conditions, but at appreciably less cost and greater availability.

Two more advantages of phosphate laser glass must be noted.

One of these advantages is manifested in large devices designed to obtain high power short and supershort pulses with high emission density. Nonlinear processes leading to the appearance of internal deterioration as a result of self-focusing turn out to be limiting factors in this case. Correspondingly, the limiting energy flux densities in phosphate glass are approximately twice those in silicate glass.

A second advantage is connected with more efficient energy transfer between rare earth ions in phosphate glass compared to silicate glass. The use of this advantage made it possible to develop high quality erbium laser glass sensitized by ytterbium ions. The authors of the monograph obtained lasing in the 1.54 micron range for the first time in this glass in 1969, using free-running neodymium-doped glass lasers as the excitation source. Later, the indicated erbium glass was brought up to industrial standards (type LGS-E), for which, in particular, it was necessary to solve the technologically complicated problem of deep dehydration of it. Systematic studies were also made of the spectral luminescence characteristics of erbium glass and the class of problems connected with optimizing the lasing characteristics of both laser-pumped and tube-pumped erbium lasers. In 1973, one of the authors presented convincing substantiation of the expediency of using erbium re-emitters of neodymium lasers as amplifying stages of powerful laser systems designed for various applications.

Another sensitized phosphate laser glass developed and systematically studied in those years at the IRE Institute of the USSR Academy of Sciences was neodymium (sensitizer) and ytterbium (activator) doped glass which was prospective for use in the terminal stages of power amplifiers for pulses of medium duration, from 10^{-6} to 10^{-4} seconds.

Recently, Soviet industry has developed and is manufacturing a number of types of phosphate laser glass, and active elements for various purposes are being made from it.

The orientation toward silicate glass prevailed for a long time abroad, and there was no serious concern with the development of phosphate glass.

However, in recent years the situation has changed. Industrial phosphate glass was produced in Japan, and later in the United States. This glass is used in large production units and devices for thermonuclear plasma heating in the United States, Japan and France. The developers of laser systems for other applications are also becoming reoriented to phosphate glass.

The possibilities of phosphate laser glass have been far from exhausted. Many laboratories are continuing basic research in order to improve the characteristics of phosphate glass and glass with several glass formers, including phosphorus. A significant increase in the average pulse energy and power of lasers using glass of these types, possibilities of obtaining lasing on new wavelengths, further shortening of the duration of supershort pulses, the application of active fibers, and so on should be expected.

CHAPTER 1. GENERAL REQUIREMENTS ON PHYSICAL PARAMETERS OF LASER GLASS

§1.1. Spectral Luminescence Parameters Determining the Energy Characteristics of Glass

The phenomenon of forced (induced) emission, which forms the basis of the operation of all lasers is observed on interaction of the emission with a set of excited atoms or ions in which the population of one of the excited states with energy E_m is greater than on the lower-lying level with an energy of E_k. The radiation is amplified on frequencies equal to the transition frequencies between the indicated states, as a result of emission of light quanta coherent to the incident radiation by the excited atoms. The probability of forced emission, according to the theory of interaction of radiation with matter is determined by the dipole moment (the oscillator force) of the transition and intensity of radiation. Broadening the energy levels of the atoms as a result of their interaction with the environment decreases the density of states in the given energy range and correspondingly decreases the efficiency of the induced processes. The probability of the forced transition w_{ind} on interaction of an atom with a light beam of intensity $I(\nu)$ is easy to find using the induced emission cross section $\sigma(\nu)$:

$$\underset{(1)}{w_и}(\nu) = \sigma(\nu) I(\nu). \tag{1.1}$$

Key: 1. ind

On interaction with not strictly monochromatic radiation distributed in the frequency range comparable to the width of the spectral transition band $\Delta\nu_{ind}$, the total probability of the induced transition is

$$\underset{(1)}{w_и} = \int\limits_{\Delta\nu_и} \underset{(1)}{w_и}(\nu)\, d\nu = \int\limits_{\Delta\nu_и} \sigma(\nu) I(\nu)\, d\nu. \tag{1.1a}$$

Key: 1. ind

If we consider that at the limits of this band

$$I(\nu) = I = \text{const},$$

then

$$w_и = I \int \sigma(\nu)\, d\nu = I\sigma_0, \tag{1.1b}$$

where σ_0 is the integral radiation cross section.

It is possible to show that on normalization of the function $\Gamma(\nu)$ describing the form of the spectral band, by 1, we obtain

$$\sigma(\nu) = \sigma_0 \Gamma(\nu). \tag{1.1c}$$

In accordance with the theory of interaction of radiation with matter [1], we have

$$w_u \infty |r_{mk}|^2 J, \tag{1.2}$$

where r_{mk} is the dipole moment of the transition, $J=h\nu I$ is the radiation energy flux with frequency $\nu=(E_m-E_k)h^{-1}$.

From expressions (1.1), (1.2), it follows that $\sigma_0 \nu |r_{mk}|^2$, and the induced emission cross section on a frequency corresponding to the maximum luminescence band ν_0 is inversely proportional to the halfwidth $\Delta\nu_0$ of the band, that is,

$$\sigma(\nu_0) \infty \frac{\nu_0}{\Delta\nu_0}. \tag{1.3}$$

Let us consider how the intensity of the light beam with frequency ν_{mk} varies on propagation through a laser active medium. Let the populations of the m-th and k-th levels, that is, the number of particles in the indicated states in 1 cm^3 be N_m and N_k, respectively. The variation of the intensity in the layer of matter dx thick is determined by the difference in probabilities of emission and absorption of photons:

$$dI = (\sigma_{mk}N_m - \sigma_{km}N_k)\, I\, dx = \sigma_{mk}\left(N_m - \frac{g_m}{g_k}N_k\right) I\, dx, \tag{1.4}$$

since $\sigma_{mk} = \frac{g_k}{g_m}\sigma_{km}$; here g_m, g_k are the multiplicities of level degeneration.

In the case of thermodynamic equilibrium $N_m=N_k\exp(-\Delta E/k_BT)$, that is, $N_m<N_k$, and the value of $(g_mN_k-g_kN_m)\sigma_{km}$ defines the absorption coefficient $k(\nu)$.

On integration of equation (1.4), we obtain the well-known Beer-Bouger law:

$$I(x) = I_0 e^{-k(\nu)x},$$

where x is the thickness of the layer of material through which the light has passed. If the difference $g_kN_m-g_mN_k>0$, then an inverse population (inversion) is created in the material, and the radiation is amplified ($dI>0$). The value of

$$(g_kN_m - g_mN_k)\,\sigma_{mk} \tag{1.5}$$

is called the specific gain of the induced emission and is denoted by α_g. In doped crystal or glass lasers, inversion is achieved on excitation of the

activator ions using highly intense light sources, for example, pulsed pumping tubes (ILN), that is, by optical pumping.

The inverse proportion can be created in a set of ions for which the following conditions are met.

The level, the lifetime of which approaches the radiation lifetime, and the quantum luminescence yield is close to one, correspondingly, that is, the interaction of the ion with the surroundings leading to nonradiating loss of excitation is weak, must exist in the energy spectrum of the ions.

Above the indicated level there must be at least one level (better, several levels or a band) on excitation to which the ion quickly relaxes to the indicated lower-lying level. Then this level (band) can be used as the excitation (pumping) channel, and the inverse population can be created on the lower-lying luminescent level called the upper laser level. It is desirable that between the lower laser level on which the ion is incident as a result of induced or spontaneous emission and the basic level an energy gap $\Delta E > k_B T$ exists. Obviously, in this case in order to achieve inversion it is necessary to create a population $\exp\{\Delta E/(k_B T)\}$ times less on the upper laser level than in the case where the lower laser level is the main level.

For realization of induced emission it is also necessary that the absorption from the upper laser level on the lasing frequencies be absent or, in the extreme case, the cross section of this absorption be much less than the cross section of the used induced transition.

Ions, the spectroscopic characteristics of which are determined by their s or p-electron states are unsuitable for obtaining the laser effect. Indeed, the interaction of these ions with a crystal matrix leads to significant broadening of the spectral bands and rapid nonradiating deactivation of the excited states, which creates almost insurmountable difficulties in obtaining sufficient gain for lasers.

Inasmuch as the 4f and 3d-electrons are located in the inner regions of the atoms and interact with the intercrystalline field more weakly than the s or p-electrons [2], the luminescent and spectroscopic characteristics of certain rare earth ions and metal ions of the iron group (primarily neodymium and chromium ions) satisfy the previously enumerated requirements well, and the laser effect was first obtained on them.

Let us present a brief description of the characteristic features of rare earth spectra required for discussion of the interrelation of spectroscopic and laser properties of glass.

As is known, in the spectra of crystals and glass doped with ions of rare earth elements, narrow low-intensity absorption and luminescence bands are observed which correspond to dipole transitions with low oscillator force. These transitions are the result of the effect of intracrystalline fields on the ions, for the transitions between states of identical parity in a free ion according to Laporte's law are forbidden. The standard oscillator force of an optical transition in rare earth ions $f \sim 10^{-6}$ to 10^{-5}, which is approximately 10^3 times less than in the transitions permitted in the dipole approximation.

The interaction of the electron shells of ions with thermal vibrations of the matrix leads to bonding of the spectral lines called uniform, which increases with an increase in temperature. At 300K, its value in the crystals reaches 10 to 30 cm^{-1}.

In glass where the far order is absent, and variations in the structure of coordination spheres nearest to the activator ion are significant, the energy spectrum and permissibility of transitions in the ensemble of activator ions can differ significantly within the limits of the ensemble. The optical spectrum of this ion ensemble is broadened nonuniformly. The magnitude of this broadening in laser glass exceeds the uniform broadening observed at 300K by 2 to 3 times.

The amount of nonuniform broadening can vary noticeably from level to level even within the limits of the same multipleth state, which is connected with some variation in symmetry of the electron states and, correspondingly, interaction with the crystal field.

The existence of electron-phonon interaction also leads to the fact that the transition of excited ions to low-lying levels can take place not only by spontaneous emission of photons, but also in nonradiating fashion, with transfer of the energy to thermal vibrations. The relation between the probabilities of spontaneous emission A and nonradiating transitions w_b defines the quantum yield of the luminescence:

$$q = \frac{A}{A + w_0} = \frac{\tau_л}{\tau_0},$$

where τ_0 is the radiation lifetime of the excited state in glass, and $\tau_л$ is the luminescent lifetime of this excited state.

It must be noted that in cases where the energy gap between the excited and lower-lying electron levels of the activator (ΔE) coincides with the energy of the permitted vibrational transitions in the dielectric matrix, $w_v >> A$ and $q \tilde{} 0$. However, the probability of nonradiating transitions decreases exponentially with an increase in ΔE, and the condition $w_b < A$ is satisfied when the frequency corresponding to the transition between adjacent activator levels falls in the region of transparency of the dielectric. Therefore in crystals and in glass luminescence is observed from levels for which $\Delta E > 5000$ cm^{-1}, and luminescence is induced through levels at a distance of no more than 2000 cm^{-1} from each other and from the metatstable state*;

---

*Here and hereafter the energy is expressed in inverse centimeters. The origin of the unit of inverse centimeter which has become widespread in spectroscopy follows from the expression

$$h\nu = E_2 - E_1,$$

which can be written in the form

$$\frac{1}{\lambda} = \frac{E_2 - E_1}{hc}$$

One electron volt ($1.602 \cdot 10^{-12}$ erg) is equivalent to 8066 cm^{-1}.

The presence in the laser ions of a system of pumping levels and absorption bands corresponding to them offers the possibility of creating a population on the metastable level greater than on the lower-lying level by exciting these ions by intense emission of gas discharge pulse tubes.

The efficiency of optical pumping is determined by the overlap of the emission spectrum of the pulse pumping tubes with the absorption spectrum of the laser ion and also the intensity of the absorption bands and Stokes losses, that is, the fraction of the excitation energy which is transmitted by thermal vibrations during nonradiating relaxation of the ion to the metastable state.

Let us consider the active element (AE) in the form of a flat parallelepiped with dimensions x_0, y_0, z_0. The pumping radiation falls on the AE perpendicular to the faces, that is, parallel to the x-axis.* The power absorbed by an elementary volume ΔV of the active element with the coordinates x, y, z, x+Δx, y+Δy, z+Δz at the time t is

$$\varepsilon_a(x, t) = \int_{\Delta\nu} \varepsilon_0(\nu, t)\,[\exp[-k(\nu, t, x)\,x] + \exp[k(\nu, t, x)\,(x - x_0)]]\,k(\nu, t, x)\,d\nu\,\Delta V, \tag{1.6a}$$

and for the power which is brought to the metastable level and for the Stokes losses we have

$$\varepsilon_m(x, t) = \nu_0 \int_{\Delta\nu} \nu^{-1}\varepsilon_0(\nu, t)\,[\exp[-k(\nu, t, x)\,x] + \exp[k(\nu, t, x)\,(x - x_0)]]\,k(\nu, t, x)\,d\nu\,\Delta V, \tag{1.6b}$$

$$\varepsilon_S = \varepsilon_a - \varepsilon_m. \tag{1.6c}$$

In relations (1.6a) to (1.6c) $\varepsilon_0(\nu, t)$ is the power of the emission incident on a unit of the lateral surface of the element; the value of $\varepsilon_0(\nu, t)$ depends on the quality of the illuminating system and, obviously, cannot exceed the power emitted by a unit surface of the plasma in the pulsed pumping tube; the absorption coefficient $k(\nu, t, x)$ takes into account the decrease in the initial population of the ground state N_0 on transition of part of the ions N_1

*The calculations performed on a computer for a flat AE made of neodymium glass excited by a system of pumping tubes located along the large faces of the AE parallel to the y-axis with a plane mirror behind them, gave results close to (1.6a). The peculiarities of the pumping of a cylindrical AE in an elliptic and other types of illuminators were investigated in [3, 4].

to the excited states; the factors exp[-k(ν, t, x)x] and exp[k(ν, t, x)(x-x_0)] describe the attenuation of the light flux on its propagation in an active element. Integration is carried out in the frequency range bounded by the emission frequency of the laser ν_0 and the frequency of the edge of the fundamental band in the absorption spectrum of the dielectric matrix ν_ϕ.

Since the noted population is created only on the metastable level, on the transition frequencies to this level the absorption coefficient is

$$k_m(\nu, t, x) = k_m(\nu)\left(1 - \frac{2N_m(t, x)}{N_0}\right), \tag{1.7a}$$

and for the remaining frequencies

$$k_i(\nu, t, x) = k_i(\nu)\left(1 - \frac{N_m(t, x)}{N_0}\right); \tag{1.7b}$$

here $k_i=\sigma(\nu)_i N_0$ in the absence of degeneration of the levels.

Here the population of the metastable level $N_m(t, x)$ is defined by the system of equations

$$\frac{dN_m(t, x)}{dt} = (h\nu_0)^{-1} e_m(t, x) - N_m(t, x)\frac{1}{\tau_л}, \tag{1.8a}$$

$$N_0(t, x) + N_m(t, x) = N_0. \tag{1.8b}$$

In lasers using Nd^{3+} ions $N_m(t, x) \ll N_0(t, x) \approx N_0$, and therefore the solution of equation (1.8a) has the form

$$N_m(t, x) = (h\nu_0)^{-1} \exp\left(\frac{t}{\tau_л}\right) \int_0^t e_m(t, x) \exp\left(-\frac{t}{\tau_л}\right) dt. \tag{1.9}$$

The efficiency of using pumping can be characterized by the expression

$$F = \frac{\int_V e_a(x, y, z, t)\, dV}{S \int_{\Delta\nu} e_0(\nu, t)\, d\nu}; \tag{1.10}$$

integration is carried out with respect to the entire body of the AE, S is the surface area of the AE illuminated by the ILN.

As calculations and direct measurements performed for AE made of neodymium glass indicate [3-5], the value of F can reach approximately 50% of the energy emitted by the ILN. In a real illumination system $F \sim \varepsilon_a$ increases as $(\mathcal{N}_0 L)^{1/2}$ (L is the transverse dimension of the AE) where $(\mathcal{N}_0 L) < 10^{21}$ см$^{-2}$ (Figure 1.1). The relation between the Stokes losses and energy fed to the metastable level of Nd^{3+} is 0.7:1 for brightness temperature of the ILN of about 8000K.

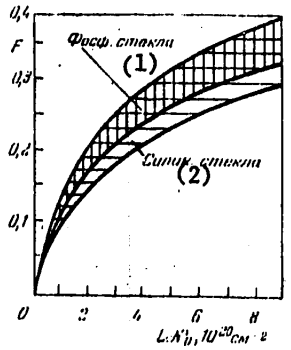

Figure 1.1. Fraction of the radiation energy absorbed by the glass as a function of the product of the Nd^{3+} ion concentration times the thickness of the flat AE.
The radiation source was xenon discharge with current density of 1 kiloamp/cm^2.

Key:
1. Phosphate glass
2. Silicate glass

The fraction of the energy absorbed by the Er^{3+} for laser concentrations $N_{Er} \approx 5 \cdot 10^{19}$ $см^{-3}$ or Yb^{3+} for $N_{Yb} \approx 2 \cdot 10^{20}$ $см^{-3}$, does not exceed 10% of the energy emitted by the ILN. Therefore sensitization of their luminescence, for example, by Nd^{3+} greatly improves the use of the pumping and correspondingly improves the energy parameters of Yb^{3+} or Yb^{3+} and Er^{3+} lasers.

The following condition must be satisfied for lasing: amplification of the emission in the active material must compensate for losses in the laser system. This condition is realized when the inverse population on the metastable level is equal to

$$N_{\underset{(1)}{\text{пор}}} = \frac{\Pi\,[см^{-1}]}{\sigma(\nu)\,[см^2]}, \qquad (1.11)$$

Key: 1. threshold

where Π is the losses in the laser system reduced to a unit length of the inverse medium, including absorption in the AE, the losses on the mirrors and to diffraction. If the lower laser level is the main level (a three-level induced emission system), it is necessary to create a population equal to

$$N_m = \frac{1}{2} N_0 + N_{\underset{(1)}{\text{пор}}}$$

on the upper laser level. If an energy gap ΔE_l exists between the lower laser level and the main level, condition (1.11) is satisfied for

$$N_m = N_0 \exp\left\{-\frac{\Delta E_l}{k_B T}\right\} + N_{\underset{(1)}{\text{пор}}}.$$

Key: 1. threshold

When $\Delta E_\ell >> k_B T$ and $N_m \sim N_{threshold}$, the four-level induced emission system is realized. Here the characteristic setup time for the thermal equilibrium between the main and lower laser level τ_ℓ defines the minimum laser pulse duration, the generation of which occurs by the four-level system. During induced emission or amplification of the pulses with duration $t_{pulse} \sim \tau_\ell$ on the lower laser level, an additional nonequilibrium population is created, which decreases the inversion, and in these cases degeneration of the four-level amplification system to a three-level system is indicated. When $t_{pulse} << \tau_\ell$, the laser pulse can "discharge" only a defined fraction of the population of the metastable level, that is, the maximum energy lost to induced emission decreases noticeably.

For exact consideration of the degeneration effects, in addition to the value of τ_ℓ, it is also necessary to know the structure of the lower laser level. Since thermal equilibrium between the Stark components of the multipleth level is established much faster than between the different states, an additional population created by induced transitions in one component or a group of components of the lower laser level, is redistributed according to Boltzmann's law between all the Stark components of this laser level, and the negative influence of degeneration decreases.

The induced emission cross section of the laser transition for an ensemble of activator ions with uniform broadening is defined by the formula

$$\sigma(\nu) = \sigma_0 \gamma(\nu),$$

where $\gamma(\nu)$ is a function describing the form of the line (gaussian or Lorentian), σ_0 is the integral emission cross section which is related to the probability of spontaneous emission A as follows:

$$\sigma_0 = \frac{Ac^2}{8\pi\nu^2} \frac{g_2}{g_1}. \qquad (1.12a)$$

Here g_1 and g_2 are the multiplicities of degeneration of the levels.

In the case of a nonuniformly broadened spectrum $\sigma(\nu)$ is equal to the integral of cross sections of induced emission of all particles on a frequency ν:

$$\sigma(\nu) = \int_{\Delta\nu}\int_{0}^{\infty} \rho(A, \nu')\, \sigma_0(A)\, \gamma(\nu, \nu')\, d\nu' dA, \qquad (1.12b)$$

where $\rho(A, \nu')$ is the fraction of the particles for which the probability of spontaneous emission is equal to A, and the maximum of the uniform line is located on a frequency of ν'; $\sigma_0(A)\gamma(\nu, \nu')$ is the emission cross section of these particles on the frequency ν.

Let us express the lasing threshold and energy efficiency of the laser in terms of the spectral luminescence parameters of the glass. Let us consider a four-level induced emission system and a square pumping pulse for which $\varepsilon 0(\nu, t) = \varepsilon_0(\nu)$ for $0 < t \leq t_{pumping}$, and for simplicity we shall consider that it is possible to neglect the variation of the pumping intensity with respect to the AE cross section.

From expressions (1.9) to (1.12) it follows that

$$\Pi = \int N_m(A, \nu', t)\,\sigma_0(A)\,\gamma(\nu, \nu')\,d\nu'dA = \\ = \frac{1}{h\nu_0}\varepsilon_m \int \rho(A, \nu')\,\sigma_0(A)\,A^{-1}q\left(1-\exp\left(-\frac{At_{\text{пор}}}{q}\right)\right)\times \\ \times\gamma(\nu, \nu')\,d\nu'dA, \tag{1.13}$$

where $(h\nu_0)^{-1}\varepsilon_m$ is the total number of particles excited by pumping per cm^3 of AE per unit time, q is the quantum yield of the luminescence which is assumed to be identical for the entire ensemble of excited particles.

The pumping energy for which the lasing threshold is reached is

$$\mathscr{W}_{\substack{\text{пор}\\(1)}} = (F\xi)^{-1}\varepsilon_m t_{\substack{\text{пор}\\(1)}} V, \tag{1.14}$$

Key: 1. threshold

where $\xi \equiv \varepsilon_s/\varepsilon_m$ is the relative magnitude of the Stokes losses averaged with respect to the activator absorption spectrum, V is the volume of the AE, $t_{\text{threshold}}$ is the time the lasing threshold is reached (as a rule, $t_{\text{threshold}} \ll \tau_l$). Using expression (1.13), we obtain

$$\mathscr{W}_{\substack{\text{пор}\\(1)}} = \frac{h\nu_0 (F\xi)^{-1}\Pi V}{\int\limits_{\Delta\nu}\int\limits_{0}^{\infty}\rho(A, \nu')\,\sigma_0(A)\,\gamma(\nu, \nu')\,dAd\nu'}. \tag{1.14a}$$

Key: 1. threshold

It is possible to express the integral in the denominator in terms of the experimentally defined luminescence parameters of the glass: the quantum yield of the luminescence q, characteristic attenuation time of the luminescence $\tau_l(t_{\text{threshold}})$ excited by a light pulse of duration $t_{\text{threshold}}$, and $\Gamma(\nu_0)$ is the amplitude of the function normalized by one describing the shape of the luminescence band on a frequency of ν_0:

$$\int\limits_{\Delta\nu}\int\limits_{0}^{\infty}\rho(A, \nu')\,\sigma_0(A)\,\gamma(\nu, \nu')\,d\nu'dA = \frac{c^2\Gamma(\nu_0)\,q}{8\pi\tau_{\substack{n\\(1)}}(t_{\text{пор}})}. \tag{1.14b}$$

Key: 1. threshold

In a laser the lasing frequency ν_0 usually coincides with the frequency of the maximum luminescence band, and in this case

$$\mathscr{W}_{\substack{\text{пор}\\(1)}} \approx \text{const}\,\frac{\Delta\nu_0\tau^n(t_{\text{пор}})}{qF\xi}. \tag{1.15a}$$

Key: 1. threshold

In the case of steady-state pumping the pumping power for which lasing occurs is

$$\underset{(1)}{\varepsilon_{пор}} = h\nu (F\xi)^{-1} \underset{(1)}{N_{пор}} \tau_л^{-1} V \infty \text{ const} \frac{\Delta\nu_0}{F\xi q}. \tag{1.15b}$$

Key: 1. threshold

The intensity of the induced emission I passing through a unit surface of the working cross section of the active element S_0 under steady-state lasing conditions is related to the pumping emission power absorbed by the AE as follows:

$$h\nu_0 I S_0 = F\xi \varepsilon_0 \left(1 - \frac{\underset{(1)}{\varepsilon_{пор}}}{\varepsilon_0}\right) \frac{w_и}{w_и + w_л}, \tag{1.16a}$$
$$\underset{(2)}{}$$

Key: 1. threshold; 2. ind

where $w_{ind} = \tilde{k}\sigma I$ is the probability of induced emission; $\tilde{k}$ is a coefficient indicating how many times the photon field inside the resonator is larger than outside it; $w_л = 1/\tau_л$ is the probability of luminescent processes.

Using formulas (1.11) and (1.15b) and integrating with respect to time, we obtain the expression for the radiation energy of a laser:

$$\underset{(1)}{\mathscr{W}'_и} = F\xi \underset{(3)}{\mathscr{W}_п} \left[1 - \frac{\underset{(2)}{\mathscr{W}'_{пор}}}{\underset{(3)}{\mathscr{W}'_п}} (1 + (\tilde{k}\Pi l)^{-1})\right]; \tag{1.16b}$$

Key: 1. ind; 2. threshold; 3. pumping

for glass lasers the value of $\tilde{k}\Pi л$ is approximately equal to one, л is the active element length. Here the energy expenditures on maintaining the threshold population and on the luminescence processes which naturally are not curtailed during lasing are proportional to the value of

$$\underset{(1)}{\varepsilon_{пор}} (1 + (\tilde{k}\Pi l)^{-1}) \infty \text{ const} \frac{2\Delta\nu_0}{F\xi q}, \tag{1.16c}$$

Key: 1. threshold

the efficiency of the laser

$$= \frac{\mathscr{W}_и}{\mathscr{W}_п} = \underset{(1)}{F\xi} \left[1 - \frac{\underset{(2)}{\mathscr{W}_{пор}}}{\mathscr{W}_и} (1 + (k\Pi l)^{-1})\right]; \tag{1.16d}$$

Key: 1. ind; 2. threshold

for $\mathscr{W}_{ind} >> \mathscr{W}_{threshold}$, the efficiency $\simeq F\xi$. During pumping by the emission of xenon ILN with discharge current density on the order of 1 kiloamp/cm^2, the value of $F\xi$ for phosphate glass $\lesssim$12% of $\mathscr{W}_{pumping}$. As we shall see, the lasing threshold and efficiency of the laser depend to a significant degree on the spectral luminescence parameters of the glass: the intensity of the absorption bands and their overlap with the pumping emission spectrum, the luminescence quantum yield, the magnitude of nonuniform broadening of the luminescence band and also the magnitude of the Stark splitting of the upper and lower laser levels.

The width of the induced emission spectrum, as numerous experimental and theoretical papers [6, 7] have demonstrated, is determined by the ratio of the uniform and nonuniform broadening, the shape of the luminescence band, and, in cases where the probability of the excitation transfer processes between the active ions is comparable to the probability of induced emission, by the energy migration rate. For illustration let us compare some of the spectroscopic parameters of neodymium-doped borate, silicate, phosphate and germanate glass, using the data presented in [47].

The quantum yield for silicate, germanate and phosphate glass with a neodymium ion concentration of $2 \cdot 10^{-20}$ cm^{-3} is 0.5 to 0.8, and for borate glass the quantum yield is no more than 0.1 to 0.2. The fraction of the pumping energy absorbed by the AE from the phosphate glass is 20 to 50% more than for the majority of silicate glasses. The laser silicate glass ED-2 which absorbs pumping radiation just as well as phosphate based glass constitutes an exception. With respect to magnitude of overlap of the absorption spectra of the Nd^{3+} ions with the ILN spectrum, the germanate and borate glasses, in our opinion, are similar to silicate glass. In phosphate glass the minimum width of the laser transition luminescence band is observed equal to 150 to 220 cm^{-1}; in other types of glass, this value is 1.5 to 2 times higher.

It must be noted that fluophosphate glass has spectroscopic characteristics similar to phosphate glass. This is investigated in more detail in §1.6.

A comparison of the spectroscopic parameters of neodymium-doped glass of various types permits a unique conclusion to be drawn--phosphate glass has optimal spectral luminescence parameters for laser application: namely, quite intense bands in the absorption spectrum larger than in other types of glass, induced emission cross sections, minimum width of the luminescence band of the transition $^4F_{3/2} \rightarrow {}^4I_{11/2}$, the quantum yield of luminescence in them is 0.7 to 0.8. Phosphate glass coactivated by Yb^{3+} and Er^{3+} or Nd^{3+} and Yb^{3+} ions also has good properties.

§1.2. Nonlinearity of the Index of Refraction of Glass

As is known, the relation between the index of refraction of a transparent dielectric and its microparameters is defined by the Lorenz-Lorentz formula

$$(n^2 - 1)(n^2 + 2)^{-1} = \frac{4\pi}{3} \mathcal{A} \rho M^{-1} \alpha, \tag{1.17}$$

where A is Avogadro's number, M is the molar mass, ρ is the density, α is the polarizability of molecules which on optical frequencies is basically caused by polarization of the electron shells of the ions.

Under the effect of intense light fields (energy flux density $>10^6$ watts/cm^2), the electrostriction compression of the material and increase in polarizability lead to an increase in n by an amount proportional to the square of the intensity amplitude of the light field:

$$n = n_0 + n_2 |\mathcal{E}|^2. \tag{1.18}$$

The term which is linear with respect to E in isotropic glass, just as in centrosymmetric crystals, is equal to zero.

The coefficient of nonlinearity of the index of refraction n_2 is a characteristic of the material, and for glass it has values of $(3 \text{ to } 0.5)\cdot 10^{-13}$ cm^2/volt^2.

As the calculations show [8, 9], with a light pulse duration less than 10^{-9} second, the primary contribution to n_2 (up to 80%) is made by the electron polarizability caused by light induced dipole moments (these dipole moments determine the intensity of the Raman scattering lines in the material). The characteristic time for establishment of equilibrium between the nonlinear electron polarizability and electromagnetic field is on the order of 10^{-16} sec. Other nonlinear mechanisms include the following: the electrostriction mechanism and also orientation (Kerr) and nuclear polarizabilities--have characteristic setup times on the order of 10^{-12} sec, and their joint contribution does not exceed 20% of the observed values of n_2 of glass.

The nonlinearity of the index of refraction leads to the fact that on propagation of a laser beam with gaussian or any other convex intensity distribution with respect to the beam cross section in the glass, a positive nonlinear lens is "induced." Its focal length is determined by the magnitude of n_2 and the power of the radiation; if the focusing effect of the nonlinear lens exceeds the divergence of the light beam, self-focusing of it is observed. The power for which the nonlinear lens compensates the divergence of the emission is called the critical or threshold power of self-focusing. For radiation powers significantly exceeding the critical power, small scale distortions develop in the laser beam which not only have a negative effect on the quality of the wave front, but with sufficient length of path of the light in the glass, lead to breakdown of the beam into individual filaments with very high power density and optical breakdown of the glass. The self-focusing theory and experiment performed to study it are investigated in considerable detail in the survey books [10, 11]. We shall only consider the basic laws here.

If a quasicylindrical light beam with cross section diameter D and light field intensity E is propagated in a nonlinear optical medium, then the index of refraction of the medium inside the beam will be $n = n_0 + n_2\mathscr{E}^2$, where n_0 is the index of refraction of the medium outside the beam. Here, the rays incident on the surface from the inside, bounding the beam, make the transition from a medium which is optically more dense to a medium optically less dense, and with sufficiently large angles of incidence undergo total internal reflection. The critical angle of incidence for which the reflected ray is propagated parallel to the interface is defined by Snell's law $n \sin\phi_{cr}=n_0\sin(\pi/2)$. Since the angle of divergence of the beam θ is related to the angle of incidence ϕ by the expression $\phi=\pi/2-\theta$, then

$$\underset{(1)}{\theta_{пр}} = \arccos\left(\frac{n_0}{n_0+n_2\mathscr{E}^2}\right) \approx \left(\frac{2n_2\mathscr{E}^2}{n_0}\right)^{1/2}. \qquad (1.19)$$

Key: 1. cr

A light beam with divergence $\theta>\theta_{cr}$ will remain diverging; for $\theta<\theta_{cr}$ it will be focused. For diffraction divergence $\theta_d=1.22\ \lambda/D$ the critical intensity of the light field E_{cr} and the critical power of the beam ε_{cr} for which $\theta_{cr}=\theta_d$ are defined by the expressions

$$\frac{\theta_{\text{д}}^2}{2}=\frac{n_2\mathscr{E}_{\text{кр}}^2}{n_0}=\frac{\gamma J_{\text{кр}}}{n_0},\quad J_{\text{кр}}=\frac{(1{,}22\lambda)^2 n_0}{2D^2\gamma}, \tag{1.20}$$

$$\varepsilon_{\text{кр}}=\frac{\pi D^2}{4}J_{\text{кр}}=\frac{(1{,}22\lambda)^2\pi n_0}{8\gamma}, \tag{1.20a}$$

(1)

Key: 1. cr

where [12] $\gamma=n_2[\text{cm}^2/\text{volt}^2]4\pi\cdot10^7/n_0c$, J s the energy flux density (in units of watts/cm^2).

Obviously, in the case of a wave with divergence $\theta=M\theta_d$, the radiation power must be M^2 times greater than ε_{cr} in order to obtain self-focusing.

The distance at which the light flux with plane phase front is self-focused, being propagated in a nonlinear medium, is equal to

$$R_{\underset{(1)}{\text{нл}}}=\frac{D}{2}\sqrt{\frac{n_0}{2n_2\mathscr{E}^2}}=\frac{D^2}{4}\sqrt{\frac{\pi n_0}{2J\gamma}}. \tag{1.21}$$

Key: 1. nonlinear

For divergence of the emission θ and power in the beam exceeding the self-focusing threshold, the light beam is focused at a distance R_{sf}:

$$\frac{1}{R_{\underset{(1)}{\text{сф}}}}=\frac{1}{R_{\underset{(2)}{\text{нл}}}}-\frac{1}{R_0},\text{where}\ R_0=\frac{D}{2\theta}. \tag{1.21a}$$

Key: 1. sf; 2. nonlinear

Using Snell's law, in the limiting case it is easy to show that for gaussian distribution in the beam

$$J(r)=J_{\max}\exp\left\{-\frac{2r^2}{D^2_{\underset{(1)}{\text{эфф}}}}\right\}, \tag{1.22}$$

$$R_{\underset{(2)}{\text{нл}}}=\frac{D_{\underset{(1)}{\text{эфф}}}}{2}\sqrt{\frac{n_0}{\gamma J_{\max}}}. \tag{1.22a}$$

Key: 1. eff; 2. nonlinear

where D_{eff} is the effective beam diameter, J_{max} is the maximum flux density in the beam. In laser beams of high (supercritical) power $R_{sf}\sim R_{nonlinear}$.

Applying the above-presented formulas, it is necessary to consider that they are valid only for nonlinear media in which amplification or attenuation of

the emission does not occur. In the presence of absorption k the minimum power for which self-focusing is still possible is determined from the equation $R_{nonlinear}=k^{-1}$. The physical meaning of this equation is obvious: the nonlinear effects become insignificant at distances exceeding the length of free path of the photon in the medium. In an active medium with specific gain α_g the self-focusing develops faster than in a nonamplifying medium. If the condition $R_{nonlinear}\alpha_g>>1$ is satisfied, then $R_{sf}=\ell n(R_{nonlinear}\alpha_g)/\alpha_g$.

It must be noted that for an emission power much higher than critical, instabilities develop in the light beam which, with sufficient length of the nonlinear medium, lead to breakdown of the beam into a number of individual small-scale beams and, consequently, significantly distort the wave front of the emission. The instability of the laser beam increases significantly when small-scale distortions occur in the distribution of the emission intensity. These distortions are the result of interference of the main high-power laser beam with low intensity emission propagated at small angles ϕ to the basic. The variations in the intensity lead to spatial modulation of the index of refraction of the medium, which, in turn, increases the fraction of the energy in the scattered emission and induced optical inhomogeneity. In reference [13] it is demonstrated that the distortions in the intensity distribution with transverse dimension $a\sim\lambda/(\phi n)$ increase at a distance L, as $\exp\{\kappa L(\gamma\bar{J}-\kappa^2/4\tilde{k}^2)^{-1/2}\}$, where $\kappa=2\pi/a$ and $\tilde{k}=2\pi n/\lambda$, $\bar{J}$ is the average value of the radiation flux density in a laser beam.

The distortions with characteristic dimension determined by the equality $\kappa^2_{max}=2\tilde{k}^2\gamma\bar{J}$ are the most unstable. Their amplitude J_{max} increases as

$$J_{\max}(L)=J_{\max}(0)\exp\left\{\tilde{k}\gamma\int_0^L\bar{J}(l)\,dl\right\},$$

and the self-focusing length is

$$R_{c\phi(1)}^{max}=\frac{n_0}{\gamma\bar{J}}\frac{2}{\tilde{k}}. \tag{1.23}$$

Key: 1. sf

In reference [14] a study is made of the development of small-scale distortions in the laser beam propagated in an amplifying nonlinear medium. Here it was considered that $\bar{J}(L)=\bar{J}_0\exp(\sigma N_{ind}L)$.

According to the calculations using the above-presented formulas for a medium having gain G>6.5, the inhomogeneities (distortions) with $\kappa_{max}=0.8\tilde{k}\sqrt{\gamma\bar{J}_{inp}G/n_0}$ are most unstable, the magnitude of which increases by the law

$$J_{\max}(L)=J_{\max}(0)\exp\left\{0{,}725\tilde{k}\frac{\gamma\bar{J}_{\text{вх}(1)}G}{n_0}(\sigma N_{\text{и}})^{-1}\right\}, \tag{1.24}$$

Key: 1. inp

where $\bar{J}_{inp}$ is the average energy flux density of laser emission at the input of the amplifying medium, (σN_{ind}) is the specific gain of the medium.

Consequently, for fixed emission power at the exit of the laser system, the buildup increment of the instabilities is inversely proportional to the specific gain of the inverse medium, and the energy flux density which can be obtained at the output of the laser system for given distortions of the wave front is proportional to the square of the specific gain. With a gain $G<6.5$, as the gain increases, the value of $\varkappa_{max}$ varies from $\tilde{k}\sqrt{2\gamma\bar{J}_{inp}G/n_0}$ to $0.8\tilde{k}\sqrt{\gamma\bar{J}_{inp}G/n_0}$ [14]. Let us again note that the above-presented formulas are valid under the condition $\int J_\varkappa d\varkappa/J_0 \ll 1$, where $\int J_\varkappa d\varkappa$ is the total energy flux density of the emission responsible for small-scale self-focusing. For $\int J_\varkappa d\varkappa/J_0 \sim 1$ the self-focusing theory is significantly complicated and becomes less obvious than the linear theory of development of small-scale instabilities.

Let us present the characteristic self-focusing parameters calculated for phosphate glass of the LGS-M type: $n_2 \approx 1.0\cdot10^{-13}$ cm^2/volt^2, $\gamma=2.76\cdot10^{-16}$ cm^2/watt, the critical power in the beam is $2.5\cdot10^7$ watts. In glass with absorption coefficient $k=10^{-3}$ cm^{-1}, self-focusing of a laser beam 2 cm in diameter is observed with the flux density greater than $5\cdot10^9$ watts/cm^2. In the same glass small-scale focusing begins to develop at $\bar{J}>2\cdot10^8$ watts/cm^2. With a density $\bar{J}\approx3\cdot10^9$ watts/cm^2, the radiation components with a divergence of $1.5\cdot10^{-3}$ rad are the most amplifying. They cause transverse modulation in the intensity distribution of the laser beam with a wavelength of 0.7 mm. The gain of the distortions is $6\cdot10^{-2}$ cm^{-1}, and the self-focusing length is about 50 cm. If a flux density of $\sim3\cdot10^9$ watts/cm^2 is obtained at the output of an amplifier about 50 cm long with G-7.5, then self-focusing does not develop, and 5 times less energy goes into the small-scale distortions than in the nonamplifying glass.

According to the data presented in [12, 14], it is possible to neglect the influence of self-focusing (small and large-scale) if the condition

$$\frac{2\pi n}{\lambda}\gamma\int_0^L \bar{J}(l)\,dl < 3, \tag{1.25}$$

is satisfied, where $\bar{J}(\ell)$ is the average flux density (watts/cm^2) in the cross section lagging a distance ℓ behind the input cross section of the nonlinear medium (glass), L is the total length of the nonlinear medium. The physical meaning of this condition is clear: as a result of nonlinearity of the index of refraction, the emission phase advance must not exceed $\lambda/2$, and the variation of the divergence angle must be less than the diffraction angle.

The value of n_2 for glass was determined by the interference method with a laser pulse duration on the order of 10^{-10} second. The increase in the index of refraction in the investigated glass with an increase in emission intensity leads to shift of the interference bands proportional to n_2.

In performing these measurements, it is important to insure space and time coincidence of the integrating beams on the recording instrument and also sufficient time resolution when recording the interferograms [15, 16].

Table 1.1

Types of glass	n_D	ν_D	n_2, 10^{-13} cm^2/volt^2	
			experiment	calculation
Silicate				
LGS-247-2(GLS-7)	1.5494	52	1.5±0.2	1.70
GLS-1	1.534	58	1.41±0.14	1.40
ED-2	1.567	54	1.52±0.3	1.70
Phosphate				
GLS-22	1.595	57	-	1.70
LGS-I	1.580	65	1.2±0.2	1.35
LGS-M	1.532	66	1.0±0.15	1.15
KGSS-1161	1.530	64	-	1.18
GH-6	1.532	66	1.01±0.1	1.15
EV-2	1.512	68	0.95	1.05
Fluophosphate				
LGS-F	1.490	82	-	0.70

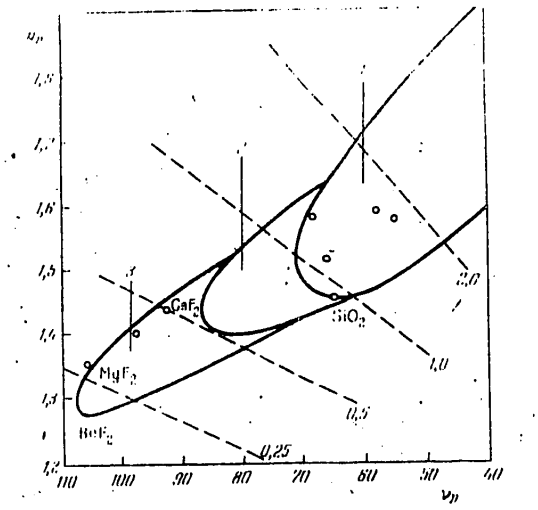

Figure 1.2. n_2 as a function of n_D and ν_D for silicate and phosphate glass (1), fluosilicate and fluophosphate glass (2) and fluoberyllate glass (3). The numbers on the dotted curves indicate values of n_2 in units of 10^{-13} cm^2/volt^2.

The value of n_2 can also be calculated, defining the focal length of the nonlinear lens[2] created on propagation of the light beam with known power and gaussian distribution of the intensity [17].

Using the Lorenz-Lorentz formula, the authors of reference [18] derived a formula in which n_2 is expressed in terms of the optical constants of glass n_D and the Abbe number (or dispersion coefficient) $\nu_D=(n_D-1)/(n_F-n_C)$ (n_D, n_F, n_C are the indexes of refraction of glass on wavelengths of 587.6, 486.1 and 656.3 nm, respectively) as follows:

$$n_2 = \frac{68\,(n_D-1)\,(n_D^2+2)^2}{\nu_D\left\{1{,}517+\left[(n_D^2+2)\,(n_D+1)\,\nu_D\right]\frac{1}{6n_D}\right\}^{1/2}}\,10^{-13}\ \text{cm}^2/\text{volt} \qquad (1.26)$$

The values of n_2 calculated by this formula agree well with the experimentally measured values[2] (with an error to 10 to 15%), including when $n_2<2.5\cdot10^{-13}$ cm^2/volt^2. For materials with $n_2>2.5\cdot10^{-13}$ cm^2/volt^2, the calculated values are systematically less than the experimental values.

The values of n_2 measured experimentally and calculated by formula (1.26) are presented in Table 1.1 for Soviet and foreign laser glass.

The dotted lines in Figure 1.2 show the possible values of n_2 for different glass [14-17]. The index of refraction n_D and dispersion coefficient ν_D are plotted on the coordinate axes. In phosphate glass the values of n_2 are much less than in silicate glass. Fluophosphate and fluoberyllate glass has minimum values. However, these types of glass are inferior to phosphate glass with respect to technological characteristics and magnitudes of the cross sections of the induced emission of the Nd^{3+} ion.

§1.3. Resistance of Glass to Laser Emission

The first papers in which breakdown of transparent dielectrics by laser emission was noted were published in 1964 to 1965. Since that time basic research has been done both with respect to the physical principles of optical breakdown and the methods of increasing the resistance of dielectrics (including glass) to laser emission; the results of this research are generalized in the surveys [19-21].

The problems of optical breakdown in materials used in optics are the subject of conferences held annually by the National Bureau of Standards of the United States beginning in 1969 [22].

It must be noted that the physical picture of optical breakdown in laser glass does not differ from that observed in other types of glass. On the surface of the glass the damage appears at lower energy and flux densities than in the body of the glass. In the case of damage to glass and light breakdown, the threshold power on the entrance surface of the sample is always lower than on the exit surface, which is explained by the difference in electric field intensities of the emission at the entrance and exit of the dielectric.

Deterioration of the exit surface begins with the formation of small spallations, which, as the radiation intensity grows, increase in size, forming a network of transverse cracks. The deterioration of the entrance surface occurs in the majority of cases for flux densities of $J>>J_p$ where J_p is the

energy flux density for which sparks begin to be observed. The damage is manifested in the form of individual burns which with high radiation intensity form continuous ring projections, and on exceeding (3-5) Jp, traces of continuous fusion and chips occur in the glass.

In references [23, 24] it was demonstrated for the first time that a reduction in optical surface density of a dielectric by comparison with the body density is caused by the presence of absorbing admixtures. Such admixtures include the remains of abrasives, hydration of salt entering into the composition of the glass by atmospheric moisture, and so on. The concentration of the absorbing admixtures in the surface layer up to $2 \cdot 10^{-4}$ cm thick is estimated at 10^8 cm^{-3}, and the absorption cross section is 10^{-9} to 10^{-11} cm^2. Absorbing the radiation energy, the admixtures are heated to high temperatures, and the adjacent volume of the glass is heated as a result of thermal conductivity.

With high radiation intensity, part of the material evaporates, and further heating of it to the state of a low temperature plasma and the formation of holes on the surface of the glass take place. On cooling of the heated region, stresses and cracks appear in the glass.

It must be noted that multiple reflections in the crack layer of the glass increasing the local intensity of the emission also lead to significant lowering of the breakdown threshold.

It is obvious that the admixtures and defects in the glass surface have distribution with respect to size and absorbing capacity. Therefore the threshold of optical breakdown which depends on the parameters of the irradiated admixture also has high dispersion. With an increase in the transverse cross section of the laser beam incident on the surface of the glass, the probability that an admixture capable of initiating optical breakdown for given flux density will be irradiated increases, and the glass breakdown threshold is lowered. On variation of the laser beam cross section from 3 to 130 mm^2, a monotonic decrease (up to tenfold) in the radiation flux causing damage to the surface of the glass K-8 from the first shot with a probability of about 50% was observed. It is also obvious that the body of the glass adjacent to the admixture and heated as a result of thermal conductivity, increases with an increase in pulse duration t_{pulse} even in the case where the thermal conductivity of the glass and the absorbing capacity of the admixture do not change on heating. The radiation energy causing damage to the glass must increase as the square root of the pulse duration.

The values of the flux density for which damage to the surface of the K-8 glass and GLS-1 laser glass begins for different laser pulse durations t_{pulse} are presented in Table 1.2 [26]. The experimental results presented in it were obtained for light beam cross sections of about 1 cm^2. The relation between J_p and t_{pulse} is described quite well by the expression

$$J_p(t_1)/J_p(t_2) = (t_2/t_1)^{1/2}.$$

According to the data presented in [21, 22], the failure threshold also decreases monotonically with an increase in the pulse duration, but it does not always follow such a simple function.

Numerous experiments indicate that the application of any of the methods of obtaining a surface of increased purity leads to an increase in the optical breakdown threshold [21, 22]. The application of pickling of the glass surface during the polishing process is especially efficient. The failure threshold rises with the process of machining the surface by more than an order--to 300-350 joules/cm^2 for $t_{pulse} \sim 50 \cdot 10^{-9}$ second. Unfortunately, the pickling effect turns out to be unstable. With time the light strength of the surface spontaneously drops to the usual values. The reason for this probably is looseness of the surface during hydration and contamination by the dust particles in the air.

Table 1.2

$t_и$, с (1)	Разрушающая плотность потока, Вт/см^2 (2)	
	стекло К-8 (3)	стекло ГЛС-1 (4)
$9 \cdot 10^{-11}$	—	$(1-2) \cdot 10^{10}$
$4 \cdot 10^{-9}$	$1,1 \cdot 10^9$	$0,8 \cdot 10^9$
$4 \cdot 10^{-8}$	$\sim 10^7$	—
$1 \cdot 10^{-7}$	$\sim 10^6$	$4,8 \cdot 10^6$
$1 \cdot 10^{-3}$	$2,5 \cdot 10^6$	$1,5 \cdot 10^6$

Key:
1. t_{pulse}, second
2. Failure flux density, watts/cm^2
3. Glass K-8
4. Glass GLS-1

The body failure of the glass can be broken down into two types: the different types of internal chipping (cracks) and long hairline damage. The chipping, as a rule, is obtained in glass during lasing and amplification of the laser pulses with high energy density (10 joules/cm^2 and higher), which is usually achieved with a pulse duration of 10^{-2} to 10^{-8} second. The hairline damage 1 to 5 microns in diameter and 10 cm long (and more) appears in the glass under the effect of light pulses with energy flux densities exceeding 10^8 watts/cm^2. The radiation energy density can be low (0.1 joule/cm^2).

The thresholds of the hairline damage practically coincide with the thresholds of small-scale self-focusing which sharply increases the local intensity of radiation. Quite simple data about this type of damage is presented in [21, 22].

The cause of the low threshold of body breakdown of glass is the presence in the body of the glass of large (10^{-3} to 10^{-2} cm) defects of process origin. Their concentration is less than 10 defects per liter of glass. The process causes of the formation of these inclusions in laser glass is rupture of the founding vessel (including platinum) by the glass melt, contamination of the initial glass charge with admixtures, microcrystallization and microliquation processes. The rupture thresholds of glass on metal platinum inclusions under the effect of a quasicontinuous pulse of duration on the order of 10^{-3} sec vary from 100 to 500 joules/cm^2 depending on the type of glass. The chips on the ceramic inclusions appear at somewhat higher densities (200 to 800 joules/cm^2). The nodal stria cause rupture of the glass for energy densities exceeding 10^3 joules/cm^2.

In the case of the above-enumerated defects, the failure thresholds with laser pulse duration of 10^{-7} to 10^{-8} sec are an order lower than indicated.

Heating by laser emission of the inclusions of smaller dimensions (0.1 to 1 micron) leads to the appearance of stresses in the adjacent microvolumes of glass and quite strong scattering of light. On repeated irradiation, the regions scattering the light spread, the magnitude of the thermoelastic stresses in them reaches the ultimate strength of the glass, and cracks appear. The failure threshold for $t_{pulse} \sim 10^{-3}$ sec in this case is greater than 10^3 joules/cm^2. In defect-free regions of glass, the flux density threshold leading to rupture coincides with the threshold for the case of development of an electron avalanche and is about $6 \cdot 10^{10}$ watts/cm^2 for $t_{pulse} \simeq 5 \cdot 10^{-8}$ sec.

The theory of thermal failure of glass for the case where the parameters of the medium and the absorption coefficient of the inclusions do not depend on the temperature, developed in [24], agrees well with the experiment for sizes of the inclusions of 0.1 micron or more. The nonlinear theory of thermal failure, considering the dependence of the absorption and thermal conductivity coefficients on temperature and considering failure as thermal explosion of the inclusions, predicted a decrease in the "dangerous" size of the inclusions by almost an order, and it also explained the threshold nature of the light breakdown of glass and the existence of threshold glow [27].

Unfortunately, the literature has no data on the thresholds of optical breakdown of phosphate laser glass. However, the operating experience of AE made from phosphate glass in lasers for various purposes indicates that with respect to radiation resistance, they do not differ from silicate glass.

§1.4. Thermooptical Distortions in Active Laser Elements

During lasing, the laser active element (AE) heats up. The primary causes of heating are absorption of the pumping emission by the glass matrix (fundamental and admixture), Stokes losses on transition from high excited levels to the metastable level of the activator, nonradiating losses as a result of difference in quantum yield of the luminescence from the metastable level from one, nonradiating transitions from the lower operating levels (for the four-level lasing system) to the main level of the activator. Usually during operation of the laser, efforts are made to achieve uniform absorption of the ILN emission in the body of the AE; here the heat release with respect to the volume will also be uniform. However, the temperature with respect to cross section of the AE varies as a result of finite (and very small) thermal conductivity of glass and differences in the cooling conditions between the edges and the center of the AE. Other possible causes of temperature variation are inhomogeneities of the emission of the pumping tubes and absorption of the emission with respect to the body of the AE (deviation from uniformity of pumping), thermal heating of the surface of the element from the pumping tube, and so on. These causes are related to peculiarities in the structural design of the illuminator and can be eliminated on improvement of it; therefore we shall not consider them here.

The optical properties of the active element during heating vary, but the front of the lightwave passing through it, as a rule, is distorted. These distortions are called thermooptical. For laser elements this effect was noted for the first time obviously in reference [28]. In this item we shall present general formulas which describe the thermooptical distortions, brief information about the thermooptical characteristics of phosphate and (for comparison) silicate laser glass, and we shall demonstrate the influence of the thermooptical distortions on the energy and divergence of the glass laser emission. The dependence of the variation of the thermooptical properties of phosphate glass and its composition will be investigated in more detail in §5.1 and then in §§5.2 and 5.3 the general arguments of the given section will be more specifically defined for two important cases of practical application of phosphate glass, in pulse periodic lasers and powerful laser systems.

Thermooptical distortions are related to two basic causes. First, the index of refraction of the glass n varies with temperature and, consequently, the length of the optical path in the element varies. This case is realized in a uniformly heated AE in the form of a rectangular plate with unattached ends. In the presence of a temperature gradient with respect to cross section of the active element, the length of the optical path at different points of the cross section is different. A platy AE with linear temperature gradient along one of the coordinate directions of the cross section is an example. In both of the indicated cases, mechanical stresses do not arise in the active element. The optical properties of such elements are investigated in [29-32], and they are characterized by the thermooptical constant $\tilde{W}=dn/dT+\alpha_T(n-1)$, where α_T is the coefficient of linear thermal expansion, T is the temperature. For an element of length L, the difference of the optical paths Δp for points of the cross section in which the temperatures differ by ΔT, is defined by the simple relation [29-33]

$$\Delta p = L\tilde{W}\Delta T. \tag{1.27}$$

This formula serves for determination of the value of $\tilde{W}$ either with uniform heating of the optical element and simultaneous recording of the variation of Δp [34] or with creation in the platy AE of a linear temperature gradient along one coordinate and comparison of the optical paths for beams traveling through the sections of the cross section with different temperature [32].

The second cause of thermooptical distortions is the photoelastic effect. We shall consider two types of the most widespread AE here--the above-mentioned rectangular plate L in length and 2h thick, and a cylinder of radius R and length L (here two versions are possible--a long cylinder with $L\gg R$ which we shall consider in the greatest detail, and a disc with $R\geq L$. On heating, mechanical stresses arise in the cylindrical AE and in the plate AE with fastened ends or nonlinear temperature distribution with respect to cross section. The orientation of the two principal axes η_1 and η_2 of the stress tensor in the cross section of the cylinder and the plate is illustrated in Figure 1.3 [35]. The stress with respect to the third axis $\eta_3=\eta_{zz}$ is directed along the elongation L of the plate or the cylinder (perpendicular to the plane of the drawing). For a cylindrical AE, the two main components

of the stress tensor in the circular cross section are directed along the radius of the AE ($\eta_1=\eta_{rr}$) and perpendicular to the radius ($\eta_2=\eta_{\phi\phi}$). For the plate AE the stresses $\eta_1=\eta_{xx}$ and $\eta_2=\eta_{yy}$ in the cross section perpendicular to the elongation, are parallel to the faces of the plate except the regions near the boundaries of the AE noted in Figure 1.3 by the crosshatched area where the boundary effects are felt (just as on the fastened ends of the long plates; see, for example [35, 36]). These regions are not considered further.

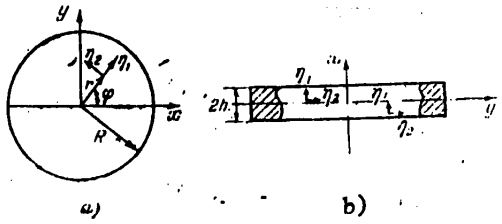

Figure 1.3. Orientation of the principal axes η_1 and η_2 of the stess tensor in the cross section of a cylindrical (a) and plate (b) AE [35]. The areas in which boundary effects are observed are crosshatched.

Let us first analyze the thermooptical distortions in a cylindrical AE. Usually it is assumed that the temperature distribution in such an element is radially symmetric and does not vary with respect to length of the AE. The directions of the principal axes of the stress tensor in such a case corresponds to Figure 1.3, and the components of the stress tensor reduced to the principal axes are [31, 37, 38]:

$$\begin{aligned}\eta_{rr} &= \frac{\alpha_T E}{1-\mu}\left(\frac{\overline{T}_R}{2}-\frac{\overline{T}_r}{2}\right),\\ \eta_{\varphi\varphi} &= \frac{\alpha_T E}{1-\mu}\left(\frac{\overline{T}_R}{2}+\frac{\overline{T}_r}{2}-T(r)\right),\\ \eta_{zz} &= \eta_{rr}+\eta_{\varphi\varphi}.\end{aligned} \tag{1.28}$$

Here α_T is the coefficient of thermal expansion (KTR), E is the modulus of elasticity, μ is the Poisson coefficient, $\overline{T}_R$ and $\overline{T}_r$ are the average temperature with respect to the entire cross section of the AE and with respect to the cross section of radius r, respectively:

$$\overline{T}_R = \frac{2}{R^2}\int_0^R T(r)\,r\,dr,$$

$$\overline{T}_r = \frac{2}{r^2}\int_0^r T(r)\,r\,dr.$$

In the presence of stresses, the indexes of refraction for beams with linear polarization in the direction of the radius of the element and perpendicular to it will differ as a result of the photoelastic effect, which for a body

isotropic in the free state is characterized by the photoelastic constants C_1 and C_2 describing the variation of the index of refractions of light with oscillations parallel and perpendicular to the direction of the stresses [37, 39]. (In some experiments the values of $B_{\parallel}$ and $B_{\perp}$ having signs opposite to the signs of C_1 and C_2 are used instead of the values of C_1 and C_2.)

Knowing the magnitudes of the stresses in the AE, it is possible to calculate the variations in length of the optical path. The calculation for the steady-state case--lasing in the continuous mode or in the steady-state mode with periodic pulse repetition with off-duty factor exceeding the thermal relaxation time in the AE--is the simplest. If the directions of the principal axes of the stress tensor r and ϕ (the radial and tangential polarization) lie in the polarization plane of the light wave, the variation in length of the optical path Δp at a distance r from the axis of the cylindrical AE is given by the following expressions [31, 37, 38]:

$$\Delta p_r(r) = L\left\{\left[\frac{dn}{dT} - \frac{2\alpha_T E}{1-\mu}C_2\right]T(r) - \right.$$
$$- \frac{\alpha_T E}{2(1-\mu)}(C_1 - C_2)\,\overline{T}_r + \left[\alpha_T(n-1) + \right.$$
$$\left. \left. + \frac{\alpha_T E}{2(1-\mu)}(C_1 + 3C_2)\right]\overline{T}_R\right\}, \quad (1.29)$$
$$\Delta p_\varphi(r) = L\left\{\left[\frac{dn}{dT} - \frac{\alpha_T E}{1-\mu}(C_1 + C_2)\right]T(r) + \right.$$
$$+ \frac{\alpha_T E}{2(1-\mu)}(C_1 - C_2)\,\overline{T}_r + \left[\alpha_T(n-1) + \right.$$
$$\left. \left. + \frac{\alpha_T E}{2(1-\mu)}(C_1 + 3C_2)\right]\overline{T}_R\right\}. \quad (1.29)$$

Here the notation is analogous to that used previously. In these formulas the temperature dependence of the physical characteristics of the glass (except n) is not considered, and dn/dT is assumed constant. This is admissible only for small average pumping powers per unit volume of AE and for lightly varying operating temperature of the laser. Below, we shall demonstrate how important it is in a number of cases to consider the temperature variations of the properties of the glass. The above-presented formulas pertain to the steady-state case. In the single and rare pulse mode, the temperature of the AE depends on the time. This case and also the operating mode of the laser transitional to steady-state are discussed in detail in a number of papers [31, 38, 40-43].

For plate AE usually the case most frequently realized in laser systems is considered where the temperature varies only along the thickness of the plate (the coordinate x in Figure 1.3, b). Then under the assumption that surface forces are absent, the regime of the two-dimensional stressed state is realized for the AE with the following values of the principal components of the stress tensor [29, 31]:

$$\eta_{zz} = \eta_{yy} = \frac{\alpha_T E}{1-\mu}\left[\frac{1}{2h}\int_{-h}^{h} T(x)\,dx - T(x)\right], \quad (1.30)$$
$$\eta_{xx} = 0.$$

The corresponding expressions for the differences in optical paths in the plate AE have the form [29, 31]

$$\Delta p_x(x) = L\left[\frac{dn}{dT} - \frac{\alpha_T E}{1-\mu} 2C_2\right] T(x),$$
$$\Delta p_y(x) = L\left[\frac{dn}{dT} - \frac{\alpha_T E}{1-\mu}(C_1 + C_2)\right] T(x). \tag{1.31}$$

In [38, 42] it was demonstrated that when determining the absolute magnitude of the variation of the index of refraction of glass it is necessary also to consider the contribution from the excited activator ions which will be considered below. However, in the majority of cases the radial dependence of n for small temperature gradients in the cylindrical AE is described well by the formulas analogous to (1.29).

These formulas are simplified significantly if we use the so-called thermooptical characteristics P, W and Q which are combinations of other physicochemical parameters of the glass and, what is very significant, can be determined independently [33, 44, 45]:

$$\widetilde{W} = \frac{dn}{dT} + \alpha_T (n-1),$$
$$P = \frac{dn}{dT} - \frac{\alpha_T E}{2(1-\mu)}(C_1 + 3C_2), \tag{1.32}$$
$$Q = \frac{\alpha_T E}{2(1-\mu)}(C_1 - C_2).$$

The value of $\widetilde{W}$ already mentioned earlier characterizes the variation of the optical path in the AE free of stresses, P characterizes the magnitude of the optical inhomogeneity averaged for two polarizations in the AE with mechanical stresses, Q characterizes the magnitude of the optical anisotropy induced by the stresses (birefringence). Now expressions (1.29), (1.31) can be rewritten in the form [31]

$$\Delta p_{r,\varphi}(r) = L[(P \pm Q) T(r) \mp Q\bar{T}_r + (\widetilde{W} - P) T_n]. \tag{1.33}$$

Here the top signs pertain to the radial stress (r-polarization), and the lower signs, to the tangential stress (ϕ-polarization. For plate AE [31], we have

$$\Delta p_{x,y}(x) = L\left[(\widetilde{W} - P + Q)\frac{1}{2h}\int_{-h}^{h} T(x)\,dx + (P \pm Q) T(x)\right]. \tag{1.34}$$

The upper sign here pertains to light polarized along the x-axis, and the lower sign, along the y-axis. Values of $\widetilde{W}$, P and Q and their temperature derivatives for a number of silicate and phosphate laser glasses are presented in Table 1.3. More detailed data can be found in [47, 48]. The thermooptical characteristics vary linearly with the temperature in the first approximation [34, 48, 49]. $\widetilde{W}$ and P increase with an increase in temperature, their temperature coefficients are similar, and for laser glass they amount to $(0.09 \text{ to } 0.25)\cdot 10^{-7}$ K^{-2} [34, 49]. The value of dQ/dT is appreciably smaller: $(-0.01 \text{ to } 0.03)\cdot 10^{-7}$ K^{-2}, and the temperature variation of Q can be neglected. In formulas for thermooptical distortions it is necessary to use values of P and $\widetilde{W}$ corresponding to the temperature of the medium surrounding the laser AE.

Table 1.3

Types of glass	$\tilde{W}$, 10^{-7} K^{-1}	P, 10^{-7} K^{-1}	Q, 10^{-7} K^{-1}	$\frac{d\tilde{W}}{dT}$, 10^{-7} K^{-2}	$\frac{dP}{dT}$, 10^{-7} K^{-2}	$\frac{dQ}{dT}$, 10^{-7} K^{-2}
Silicate						
GLS-1	38	32	6	0,16	0,23	—0,01
GLS-2	27	22	8	0,14	0,21	0,01
LGS-247-2	10,5	5	4,5	—	0,17	0,03
KGSS-1080	—	5	7	—	0,18	0,01
Phosphate						
GLS-2	0	—2	4	0,13	0,14	0,01
LGS-55	—2,5	—	10	—	—	—
LGS-56	9,5	—	11,5	—	—	—
LGS-1-2**	6	—4	4,7	0,14	—	—
LGS-M**	4	—6	5,8	0,09	—	—
KGSS-V-16*	9	—3	1,5	—	—	—
KGSS-V9199*	17,5	3	1	—	—	—
KGSS-V133*	14,5	1	1	—	—	—
KGSS-V133*	10	—1	1,5	—	—	—

*Lead phosphate glass with small values of Q [49]; the characteristic $\tilde{W}$ for this type of glass is measured for 70°C at λ =0.644 micron. For the majority of other types of glass the characteristics are presented for 0°C and λ=1.06 microns.
**λ=0.63 micron.

For practice, it is not the absolute value of the difference in optical paths for a defined cross section of AE that is important, but the variation of Δp with respect to cross section, which depends on the form of the AE and the temperature distribution. The case of heat release which is uniform with respect to volume and constant in time is considered most frequently. Under these steady-state conditions the temperature distributions in the AE are parabolic [31, 35, 50] and for cylindrical and plate AE they have the form

$$T(r) = T_0 + \Delta T_{\text{ц}}^{(1)}\left(1 - \frac{r^2}{R^2}\right), \tag{1.35}$$

Key: 1. cyl

$$T(x) = T_0 + \Delta T_{\text{п}}^{(1)}\left(1 - \frac{x^2}{h^2}\right). \tag{1.36}$$

Key: 1. rect

Here r and x are current coordinates for the cylindrical and rectangular plate AE, respectively, ΔT_{cyl} and ΔT_{rect} are the temperature gradients between the center and the surface (having a temperature T_0) of the cylindrical and rectangular AE. For small ΔT, where it is possible to neglect the temperature dependence of the thermooptical characteristics, the differences in the optical paths between the center of the AE and some point of the cross section for the cylindrical and rectangular AE are equal to the following, respectively [31, 35, 50]:

$$\Delta p_{r,\varphi}(0) - \Delta p_{r,\varphi}(r) = \underset{(1)}{L\left(P \pm \frac{Q}{2}\right)\Delta T_{\text{ц}}\frac{r^2}{R^2}}, \tag{1.37}$$

Key: 1. cyl

$$\Delta p_{x,y}(0) - \Delta p_{x,y}(x) = \underset{(1)}{L(P \pm Q)\Delta T_{\text{п}}\frac{x^2}{h^2}}. \tag{1.38}$$

Key: 1. rect

Here let us determine the differences of the optical paths for beams with orthogonal polarizations coinciding with respect to directions with the principal axes of the stress tensor in the transverse cross section of the AE:

$$\Delta p_r(r) - \Delta p_\varphi(r) = \underset{(1)}{L\Delta T_{\text{ц}}Q\frac{r^2}{R^2}}, \tag{1.39}$$

Key: 1. cyl

$$\Delta p_x(x) - \Delta p_y(x) = \underset{(1)}{2L\Delta T_{\text{п}}Q\frac{x^2}{h^2}}. \tag{1.40}$$

Key: 1. rect

The phase shift between these beams can be obtained by multiplying the right-hand sides of the last two formulas by $2\pi/\lambda$, where λ is the wavelength of the light. The quadratic dependence of the phase shift on the coordinate indicates that the cylindrical AE is equivalent to a spherical lens, and the plate AE is equivalent to a cylindrical lens. Here, for the plate AE the light linearly polarized with respect to x or y axis retains linear polarization on passage through the AE.

The energy characteristics and divergence of the laser emission depend on the thermooptical distortions. In a resonator with flat mirrors and AE, with respect to the cross section of which the difference of the optical path changes, the angular divergence θ is proportional to the square root of the difference of the optical paths in the AE [51, 52]. This difference is considered equal to the sum of the moduli of the maximum and minimum (having ordinarily another sign and the maximum) distortions of the light wave front passing through the AE. We shall discuss this problem in more detail in §5.2 devoted to pulse-periodic lasers. In accordance with the formulas (1.37) and (1.38) for difference of the optical paths, the divergence increases with an increase in the average pumping power determining the temperature gradient in the AE and with an increase in the values of (P±Q/2) or (P±Q). The closer to zero these values, the smaller the divergence and for the same lasing energy, the higher the radiation brightness. In Figure 1.4 the angular divergence is presented for the emission of a periodic laser with cylindrical cooled AE 7 mm in diameter and 120 mm long as a function of the temperature gradient in the AE. The values of P and Q for the majority of these types of glass are presented in Table 1.3.

For small pumping powers where the temperature gradients and the thermooptical distortions are small, the lasing energy increases with an increase in the pumping power (Figure 1.5). Then as the optical strength of the thermal lens increases, the lasing energy begins to decrease. For GLS-1 glass, the focal length of the induced positive lens decreases with an increase in pumping power (Figure 1.6). Figure 1.7 shows the variation in lasing energy in each pulse with an increase in pumping power for glass with different values of (P±Q/2). Here the lasing energy drop takes place faster the larger the dispersing effect of the thermal lens, that is, the smaller the value of (P-Q/2) in the negative region. Since the thermooptical characteristics vary with temperature, in reference [42] the concept of the optimal temperature T_0 was introduced, for which the values of (P-Q) or (P-Q/2) are equal to zero for rectangular and cylindrical AE, respectively, for neodymium containing glass on a wavelength of 1.06 microns. From Figure 1.7, where the data are presented for room temperature, it is obvious that for (P-Q/2)=0 the energy parameters of the laser are the best.

The measurement of the values of P and Q entering into the formulas (1.37), (1.38) is quite labor intensive, and therefore in a number of papers efforts are made to relate the values of the focal lengths of the thermal lenses and the generating characteristics of the lasers to the more easily measured value of W. Thus, in [57] it was found that the focal length of the thermal lens in the AE increases with a decrease in absolute magnitude of W. Values of W, the angles of divergence θ in the single pulse mode and in the periodic mode and the relative efficiency of the laser (with respect to the efficiency of GLS-1 glass) are presented in Table 1.4 for a number of types of laser glass [54]. In the periodic mode the measurements were taken on cylindrical AE 20 mm in diameter and 260 mm long which together with the IFP-5000 tube were placed in a block of LK-318 glass silvered on the outside. The cooling of the rod and the tube was realized by running water. The pulse frequency was equal to 0.1 hertz, the average pumping power was 400 watts. In the single pulse mode the pumping was carried out in an illuminator with four tubes IFP-5000, the pumping energy was 18 kilojoules, the pulse duration was 1 millisecond. As we shall see, in order to increase the radiation brightness as a result of decreasing divergence while retaining the efficiency, the value of $|\tilde{W}|$ must not exceed $10 \cdot 10^{-7}$ K^{-1} [54]. The correlation of the values of $\tilde{W}$ and the thermooptical distortions characterized by (P±Q/2) (see (1.37)), is related to the linear relation between $\tilde{W}$ and P for a series of glass types found in reference [55] when investigating a large number of types of glass of different composition. The situation changes for the "athermal" glasses with small values of P [48]. As an example, in Figure 1.8 the variation of the focal power of the thermal lens in cylindrical AE 7 mm in diameter by 130 mm with an increase in temperature gradient is illustrated for two types of glass [56]. For large values of the thermooptical characteristics W and P, when the contribution of the value of Q is small (the values of Q for the majority of ordinary types of laser glass do not exceed $1 \cdot 10^{-6}$ K^{-1}), W can be used with admissible error for estimating the magnitude of the thermooptical distortions. For "athermal" types of glass with P≈Q, use of $\tilde{W}$ in place of P and Q can lead to improper conclusions regarding the magnitude and nature of variation of the induced optical inhomogeneity (the glass GLS-22, previously KGSS-1621). However, even in this case by the value of $\tilde{W}$ it is

possible to judge that the given glass must belong to the class of "athermal" glass. The value of $\tilde{W}$ depends on the dispersion of the index of refraction

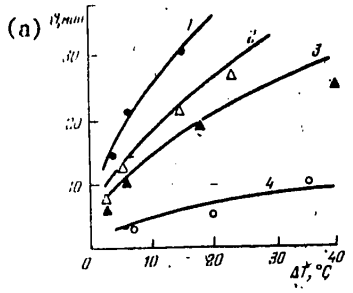

Figure 1.4. Angular divergence of the emission of a periodic laser with cylindrical AE made of GLS-1 glass (1), GLS-2 glass (2), KGSS-3 glass (3) and GLS-22 glass (4) [52].
The dots are the experimental data, and the curves are the calculated data.
Key:
a. θ, minutes

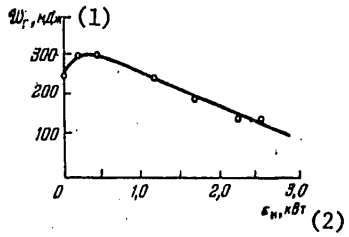

Figure 1.5. Lasing power per pulse W_g as a function of pumping power ε_{pump} for a cylindrical active element 6 mm in diameter by 130 mm made of GLS-1 glass (50]
Key:
1. W_g, millijoules
2. ε_{pump}, kilowatts

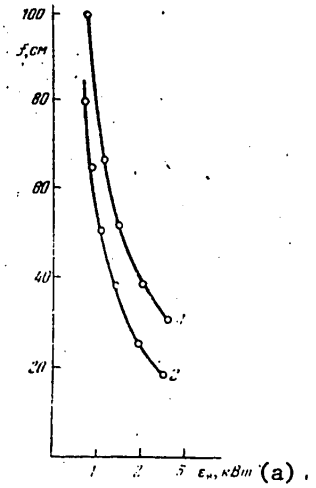

Figure 1.6. Focal length f of the induced positive lens as a function of pumping power for a cylindrical AE 6 mm in diameter by 130 mm made of GLS -1 glass [50].
1 -- ϕ-polarization, 2 -- r-polarization
Key: a. ε_{pump}, kilowatts

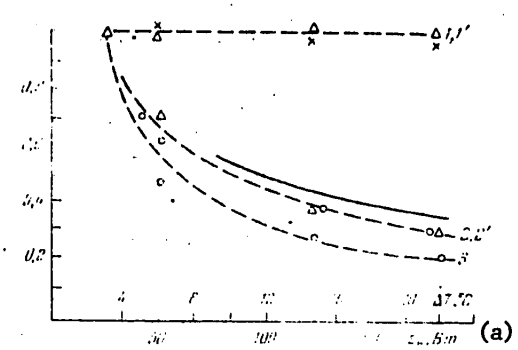

Figure 1.7. Variation of the lasing power with an increase in average pumping power [56].
Glass KGSS-1621 (1), KGSS-9199 (1'), KGSS-V-16 (2), KGSS-91 (2') and KGSS-V-70 (3). $(P-Q/2)=0$ (1), $0.5\cdot10^{-7}$ (1'), $-4\cdot10^{-7}$ (2), $-5\cdot10^{-7}$ (2') and $-12\cdot10^{-7}$ K^{-1} (3); $(P+Q/2)=4\cdot10^{-7}$ (1), $1.5\cdot10^{-7}$ (1'), -2.5×10^{-7} (2), $-3\cdot10^{-7}$ (2'), and $-10\cdot10^{-7}$ K^{-1} (3).
The solid line is the calculated values for $(P+Q/2)=-4\cdot10^{-7}$ K^{-1}.
The ratios of W_g for the investigated pumping powers to W_g in the single pulse mode are plotted on the y-axis.

Key:
a. ε_{pump}, watts

Table 1.4

Types of glass	Nd^{3+} concentration, % by weight	$\tilde{W}$, 10^{-7} K^{-1}, λ=1.06 microns	θ in the periodic mode, minutes	Relative efficiency	θ in the single pulse mode, minutes
LGS-36-2	2	55	18	1.1	5.6
GLS-1	2	38	16	1.0	5.2
KGSS-3	2	17	9	0.8	3.7
Silicate	3	11	10	1.0	3.1
Silicate	3	8	8	0.9	2.8
Silicate	2	6	6	0.8	2.0
Borophosphate LGS-41	3.5	4	8	1.2	-
Silicate	2	2.5	7	-	-
Silicate LGS-44	2	-1	7.5	0.7	1.5
Phosphate LGS-40	3.5	-16	15.5	1.1	5.6

[39, 49]. Table 1.5 shows the most probable values of $\tilde{W}$ on wavelengths of 644 and 508 nm for silicate and phosphate glass corresponding to the zero values of the thermooptical characteristics of P for a wavelength of 1.06 microns at a temperature of 30°C, depending on the differences in the indexes of refraction for two spectral lines of hydrogen λ_F and λ_C (wavelengths of

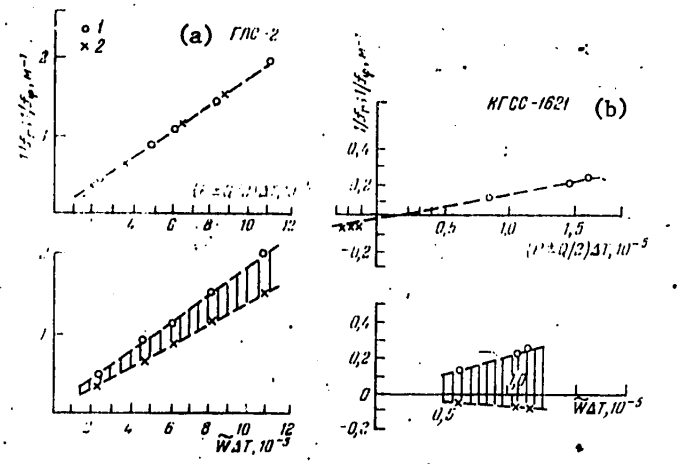

Figure 1.8. Relation of the focal power of a thermal lens to the glass parameter [56].
The experimental values of the focal power of the thermal lens corresponding to radial $1/f_r$ (1) and tangential $1/f_\phi$ (2) polarization power respectively

Key:
a. GLS-2
b. KGSS-1621

Table 1.5

$(n_F - n_C)\cdot 10^5$	$\tilde{W}$, 10^{-7} K^{-1} for 70°C	
	λ=644 nm	λ=508 nm
1000	13,5	19
1500	15	23
1900	17	30

Table 1.6

Type of glass	Cylindrical AE		Plate AE	
	T_{or}, °C	$T_{o\phi}$, °C	T_{ox}, °C	T_{oy}, °C
GLS-1	—152	—125	—165	—113
GLS-2	—113	—78	—130	—61
LGS-247-2	—42	—16	—56	—3
KGSS-1080	—47	—8	—67	11
GLS-22	0	29	—14	43

486.1 and 656.3 nm) [46]. The values of $\tilde{W}$ in Table 1.5 are somewhat higher than those found in [54] when looking for laser glass insuring high radiation brightness. Measuring $\tilde{W}$, it is thus possible to select the compositions of the "athermal" glasses with small P and then more precisely determine the thermooptical characteristics for compositions close to optimal.

For large average pumping power the temperature gradient in the AE can reach 100K or more [57, 59]. In this case it is necessary to consider the temperature dependence of the thermooptical characteristics, primarily P, for $dQ/dT \simeq 0$ [49]. Then the expression for the difference of the optical paths between the center of the AE and the points with the coordinates ξ equal to r/R or x/h, respectively, for a cylinder and a plate, acquires the following form [52]:

$$\Delta\bar{p}_{r,\varphi;x,y}(\xi) = L\Delta T\,[n_{2(r,\varphi;x,y)}(T, \Delta T)\,\xi^2 + n_4(\Delta T)\,\xi^4], \tag{1.41}$$

where $n_4 = -\theta\,\Delta T$, $\theta = \frac{dP}{dT} \approx \frac{d\tilde{W}}{dT}$,

$$n_{2(r,\varphi)}(T, \Delta T_{\text{п}}) = P_0 \pm Q_0/2 + \theta\,(T + 2\Delta T_{\text{п}}), \tag{1.42}$$

$$n_{2(x,y)}(T, \Delta T_{\text{п}}) = P_0 \pm Q_0 + \theta\,(T + 2\Delta T_{\text{п}}). \tag{1.43}$$

Here T is the temperature of the lateral surface of the AE reckoned from the standard for which the values of P_0 and Q_0 are introduced (for example, 0°C). Thus, in order to decrease the thermooptical distortions, glass is needed with small values not only of P_0 and Q_0, but also θ. Considering formulas (1.42), (1.43), the values of the "optimal" temperature minimizing the values of $n_{2(r,\phi;\ x,y)}$, in accordance with [44] are defined by the following expressions for cylindrical and plate AE:

$$T_{\text{or},\varphi} = -(P_0 \pm Q_0/2)/\theta, \tag{1.44}$$

$$T_{\text{ox},y} = -(P_0 \pm Q)/\theta. \tag{1.45}$$

The optimal operating temperatures of lasers with cylindrical and plate AE calculated by these formulas are presented in Table 1.6 [52]. GLS-22 is phosphate glass, and the remainder of the glass is silicate glass. Figure 1.9 shows the temperature dependence of the angular divergence and lasing energy of the periodic laser with cooled cylindrical AE 10 mm in diameter by 120 mm made of GLS-2 and GLS-22 glasss with a temperature gradient ΔT between the axis and the surface equal to 20°C. As we shall see, the minimum divergence of the emission is reached in the temperature range between the values of T_{or} and $T_{o\phi}$ (for rectangular AE, between T_{ox} and T_{oy}, respectively). The optimal temperature previously determined in reference [49] for lasers with small temperature gradient usually decreases in this interval, but the values of T_o considering the temperature dependence of the thermooptical properties are physically more substantiated. For $T<T_{or}$ the radiation pulse energy (Figure 1.9, b) decreases, which can be explained [52] by an increase in losses in the resonator as a result of deflections of the beams by the peripheral zones of the AE permits access and exit of them from the resonator.

The formulas (1.44) and (1.45) are inexact, for they consider vanishing only of the value of $n_{2(r,\phi;\ x,y)}$ (see (1.42), (1.43)). Here additional distortions determined by n_4 and depending on the coordinates, θ and ΔT are retained. In §5.2 when analyzing the thermooptical distortions in the AE of pulse-periodic lasers, it will be demonstrated that with an increase in n_4 at least for one polarization the thermal lens in the AE with the temperature gradient can be completely eliminated only for glass with $\theta=0$. In real optical glass, however, $\theta \geq 0.04 \cdot 10^{-7}$ K^{-2}, and for ordinary laser glass $\theta \geq 0.14 \cdot 10^{-7}$ K^{-2} (Table 1.3). In [58-60] it was demonstrated that during operation of the laser in a wide temperature range the angular divergence and the emission energy vary sharply as a function of the temperature behavior of W and P, and this dependence turns out to be the weakest for phosphate glass type LGS-M with $\theta \approx 0.09 \cdot 10^{-7}$ K^{-2} [59, 60].

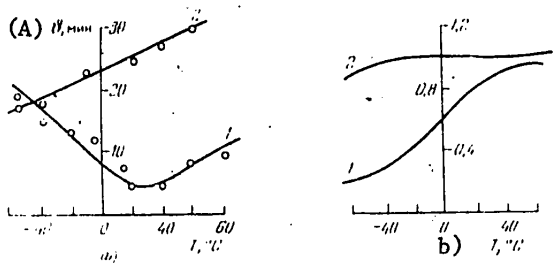

Figure 1.9. Temperature dependence of angular divergence θ (a) and lasing energy W_g (b) for GLS-22 glass (1) and GLS-2 glass (2) [52].
The ratios of the values of W_g are plotted on the y-axis in Figure 1.9, b for the investigated temperatures and at room temperature.

Key:
A. θ, minutes

On introduction of polarizing elements into the laser cavity, the birefringence effects in the AE become significant. They can have a sharp negative influence on the output characteristics of such lasers [61, 62]. Only one characteristic --the value of Q--enters into the expressions (1.39), (1.40) for the difference in optical paths of the beams of mutually orthogonal polarizations. One of the possible methods of improving the characteristics of lasers with polarizing elements is creation of glass with very small values of Q. The requirement of thermooptical distortions must be satisfied also in this case, and, consequently, the glass must simultaneously have small values P. Such glass can be created only on a phosphate base [46] (Table 1.3). The variation of Q for phosphate glass will be considered in detail in §5.1.

Up to now we have talked about long active elements in the shape of a cylinder or rectangular plate. In the case of discs, the thermooptical distortions are characterized not by the previously indicated values of P and Q, but by the parameters $\tilde{W}$, R and Q_1 [63], where

$$\mathcal{R} = \alpha_T (n-1)\mu - \alpha_T E \frac{C_1 + C_2}{2}, \quad Q_1 = \alpha_T E \frac{C_1 - C_2}{2}.$$

The variation in length of optical path of two polarizations of light is

$$\Delta p_{r,\varphi}(r) = L[(\tilde{W} + \mathcal{R} \pm Q_1) T(r) - \mathcal{R} T_{\text{ср}} \mp Q \bar{T}_r], \quad (1)$$

Key: 1. ave

where T_{ave} is the average temperature of the entire disc, $\bar{T}_r$ is the average temperature of the section of the disc with the radius r. The variation of the thermooptical parameters with temperature is not considered here, although in disc lasers operating in the periodic pulse mode, the temperature gradient between the center and the edge of the disc can reach 60°C [64]. It is possible that the absence of considering the temperature dependence of $\tilde{W}$, R and Q_1 led in reference [63] to significant divergence of the experimental and calculated values of the sums of $\tilde{W}+R$. For the glass investigated in [63], R is a positive value. and therefore in order to obtain the minimum thermooptical distortions, when the sum $\tilde{W}+R$ must be close to zero, the value of $\tilde{W}$ must be negative. Actually, the minimum distortions are observed in discs made of glass with negative values of $\tilde{W}$ [63, 65]. The glass based on phosphate can have $\tilde{W}$ to $-60 \cdot 10^{-7}$ K^{-1} [34]; therefore these types of glass are well suited to use for disc lasers. However, thermooptical distortions in the disc active elements and the laws of variation of the values of R and Q_1 with the composition of the glass have now been investigated insufficiently well.

The thermal lens determined by variations of the index of refraction which are caused by the temperature gradients in the AE was discussed above. The variation of this thermal lens in time is determined by thermophysical and geometric parameters of the active element; the time constant of the thermal lens for the single pulse mode is seconds and more. The other cause of variation of the index of refraction in glass is variation of the polarizability of the activator ions for transition of them to the excited state which takes place with time constant corresponding to the lifetime of the activator luminescence and the component part Nd^{3+} 0.1 to 1 millisecond. The different variation rate of the index of refraction offers the possibility of separating these two effects in the AE [66]. The measurements performed in [66] indicate that for Nd^{3+} ions in the glass, the variation of the polarizability $\Delta\alpha_{1.06}$ on the lasing wavelength for different glass is on the average $(0.8 \pm 0.1) \cdot 10^{-25}$ cm^3. The corresponding variation of the index of refraction with respect to cross section of the AE for neodymium-doped glass is

$$\underset{(1)}{\Delta n_{\text{п}}} = 2\pi \Delta\alpha_{1,06} \Delta N_{\text{инв}}, \quad (2)$$

Key: 1. refr; 2. inv

where ΔN_{inv} is the variation of the inverse population with respect to cross section of the AE. Its value is not measured directly. If we assume [66] that it is about 25% of the threshold inverse population $(1.5 \text{ to } 2) \cdot 10^{18}$ cm^{-3}, the value of ΔN_{refr} will be about $(2 \text{ to } 3) \cdot 10^{-7}$. For glass with $(P \pm Q) >> 0$, this additional variation of n almost has no influence on the focal power of the total induced optical lens, for the temperature gradient arising in the AE as a result of one pumping pulse is approximately (0.5 to 20) K [31, 42],

and Δn is $(20 \text{ to } 100)\cdot 10^{-7}$ or more, respectively. For $(P \pm Q) \neq 0$, the value of Δn_{refr} for one of the polarizations will become comparable to the variation of n as a result of thermal effects during the operation of the laser in the single pulse mode (small ΔT), and it will be negligibly small by comparison with the therml variation of n when operating in the periodic mode (large ΔT).

§1.5. Thermophysical Properties and Thermal Strength of Laser Glass

In this section we shall consider the thermal mode of the AE, the thermal strength of the AE and methods of increasing it and also certain methods of decreasing the temperature gradients in the AE during operation of the laser. As a result of poor thermal conductivity of glass, the temperature gradients in the AE made of glass are appreciably greater than in crystals. For description of the thermal conditions of the AE it is sufficient to consider the case of uniform heat release with respect to volume in the approximation of a continuously operating internal heat source. This approximation is the most justifiable for the steady-state with continuous operation of the laser or with pulse periodic mode with pumping pulse repetition period appreciably less than the thermal relaxation time of the AE (for example, the repetition frequency is much greater than 0.1 hertz for a cylindrical AE made of glass with radius of 0.4 cm [31]). In this approximation the temperature field T(r, t) for the cylindrical AE with radius R at a distance r from the AE axis at the time t is defined as follows [31, 57]:

$$T(r,t) - T_0 = \frac{qR^2}{4\lambda_h}\left[1 + \frac{2}{\mathrm{Bi}} - \frac{r^2}{R^2} - \sum_{n=1}^{\infty} \frac{4}{\mu_n^2} A_n I_0\left(\frac{\mu_n r}{R}\right) \exp\left(-\mu_n^2 \frac{at}{R^2}\right)\right]. \quad (1.46)$$

Here T_0 is the surface temperature, q is the power of the heat release per unit volume, λ_h is the coefficient of thermal conductivity, a is the temperature of thermal diffusivity, A_n and μ_n are the coefficients which depend on the Biot number $Bi=\tilde{\alpha}R/\lambda_h$ ($\tilde{\alpha}$ is the heat exchange coefficient) characterizing the heat exchange conditions, I_0 is the Bessel function. The temperature gradient between the center and the edge of the AE is relatively small for the single pulse mode, it increases in the periodic mode with an increase in the pulse repetition frequency and it reaches a maximum value of ΔT_{st} in the steady-state mode [31]; it is

$$\Delta T_{\underset{(1)}{\text{ст}}} = T(0,t) - T(R,t) = \frac{qR^2}{4\lambda_h}. \quad (1.47)$$

Key: 1. st

In other words, ΔT depends on the radius of the AE and on the thermal conductivity of the material. The transient heating processes were investigated in a number of papers, for example [38, 40-42, 67, 68]. In these cases the temperature gradient is less than ΔT_{st}, and therefore in order to discover the limiting possibilities of the AE made of glass, it is sufficient to consider only the steady-state mode. For plate AE the temperature gradient

between the center and the side surface in the direction of the x-axis (Figure 1.3, b) is determined analogously:

$$\Delta T_{\underset{(1)}{\text{ст}}} = \frac{qh^3}{2\lambda_h}.$$

Key: 1. st

Then we shall consider only the cylindrical AE. For the calculations it is convenient to characterize the heating state of the AE by the relative temperature Θ [31] defined as

$$\Theta = \frac{T_\infty - T_0}{\Delta T_{\underset{(1)}{\text{имп}}}},$$

Key: 1. pulse

where T_∞ is the temperature at the given point of the cross section under steady-state conditions, T_0 is the surface temperature, ΔT_{pulse} is the increase in the temperature of the AE in one pumping pulse, $\Delta T_{pulse} = \tilde{Q}/c\rho$, where $\tilde{Q}$ is the energy absorbed by a unit volume of the AE in one pumping pulse, c and ρ are the specific heat capacity of the glass and its density, respectively. The results of calculating the relative temperature on the axis of the AE made of silicate glass under steady-state conditions as a function of the pulse repetition frequency and radius of the cylindrical AE are presented in Table 1.7. The Biot numbers correspond to liquid cooling of the AE. As follows from the table, the heating is approximately proportional to the pumping pulse repetition frequency.

The magnitude of the relative temperature Θ under steady-state conditions for a ruby rod with R=0.2 cm for Bi=10 is 1.1 for 5 hertz and 9.4 for 100 hertz, that is, as a result of high thermal conductivity the ruby element is heated 10 to 20 times less than the glass element (for the same value of ΔT_{pulse}). Since the temperature gradient in the cylindrical rod increases proportionately to the square of the radius, for glass lasers with high average lasing power it is expedient to select thin active elements of long length (or in the case of discs, large cross sectional area). An important characteristic is the thermal conductivity of the glass which must be selected as large as possible. The value of λ_h for glass is usually 0.6 to 1.4 watts/(m·K) (0.0014-0.0032 cal/(cm-sec-K) [31, 47, 48]). The variation of the values of λ_h for phosphate glass of different composition will be analyzed in §5.2.

The temperature gradients lead to the occurrence in the AE of mechanical stresses. The corresponding expressions are presented in §1.4 (formulas (1.28)). For a limiting value of the temperature gradient, the stresses exceed the strength of the glass, which usually is 3 to 10 kg/mm^2 [31, 39, 69], and then failure of the AE takes place. For cylindrical AE 10 mm in diameter and 130 mm long made of silicate glass with the upper defective layer removed by pickling, the maximum temperature gradient is 70 to 90 K [47, 69]; for phosphate glass 25 to 40 K [47, 69, 70] (for more detail see §5.2).

Table 1.7

f, hertz	Values of Θ for R=0,1 см		R=0,2 см		R=0,4 см	
	Bi=60	Bi=100	Bi=60	Bi=100	Bi=60	Bi=100
5	3,6	3,6	13,3	13,1	52,1	51,4
10	6,9	6,8	26,2	25,9	104	102
20	13,3	13,1	52,1	51,4	207	204
50	32,7	32,3	130	128	517	510
100	65,0	64,1	259	255	1034	1020

As is obvious from Table 1.7 and expressions (1.46), (1.47), the temperature gradient in the AE increases with an increase in the pumping pulse energy and repetition frequency. The limiting frequency for cylindrical AE (above which failure of it occurs) under steady-state conditions is determined from the expression [31]

$$\tilde{f} < \eta_{\text{пред}} \frac{1-\mu}{\alpha_T E} \frac{8a}{\Delta T_{\text{имп}} R^2}, \qquad (1.48)$$

(1) (2)

Key: 1. pre; 2. pulse

where η_{pre} is the stress leading to failure of the material, a is the coefficient of thermal diffusivity ($a=\lambda_h/c\rho$). For $\Delta T_{pulse}=1$ K and standard values of the parameters for silicate glass $\eta_{pre}=400$ kg/cm^2, $\alpha_T=100\cdot10^{-7}$ K^{-1}, $E=6.5\cdot10^5$ kg/cm^2, $\mu=0.24$, $a=4\cdot10^{-3}$ cm^2/sec and R=0.2 cm, we have $\tilde{f}<37$ hertz. Using elements made of silicate laser glass with small transverse cross section, it is possible to obtain a pulse repetition frequency of 100 or more hertz [71, 72] and also lasing in the continuous mode [72, 73]. However, as a result of large temperature gradients and the thermal lens effect, such lasers have poor energy characteristics and their efficiency is 0.02 to 0.1%.

The thermal strength of phosphate glass is usually 2 to 3 times lower than silicate glass [47, 69, 70]. In [73], a study was made of the limiting resistance to pumping power of AE 2.5 mm in diameter made of phosphate, fluoberyllate and silicate glass. The lasing threshold in a single pulse for rods made of phosphate, fluoberyllate and silicate glass was 1.5, 2.6 and 4 joules respectively. The pumping power for which failure of the AE occurred was 650, 800-1000 and 3000 watts. Phosphate glass turned out to be insufficiently strong, and lasing in the continuous mode could be realized only on silicate glass. In the quasicontinuous mode on phosphate glass with the composition $ZnLi_4(PO_3)_6$, lasing was obtained on pumping by the emission of a xenon tube operating on alternating current with a frequency of 50 hertz [74] (Chapter 4).

It is known that the mechanical and thermal strength of glass can be increased by special treatment [39, 75]. In order to harden silicate laser glass, special mechanical treatment of the surface of the AE with selection of the optimal height of the unevennesses on the surface [76], fire polishing [76], pickling of the defective surface layer [47, 69, 77], ion exchange [71, 79],

and quenching [70, 80] were used. The last three methods are especially effective. Thus, the ion exchange method increases the strength of the silicate laser glass ED-2 by five times [78, 79], the quenching method increases the maximum temperature gradient which the AE withstands without failure by more than threefold [70]. The process of strengthening phosphate glass has been studied appreciably less, and only in the most recent years has it been possible significantly to increase the thermal resistance of AE made of phosphate glass [58, 59, 70, 81]. This is very important, for it permits efficient use of "athermal" phosphate glass with small magnitudes of the thermooptical characteristics P and Q in order to increase the average lasing power of lasers with small angle of divergence of the emission (§5.2)

As is obvious from the preceding discussion, decreasing the radius of a cylindrical AE or the plate thickness leads to a decrease in temperature gradient in the AE. Therefore it is possible to use fibers of films made of glass where cooling can be made most effective, and the temperature gradient, small. However, decreasing the transverse dimensions of the AE unavoidably leads to an increase in the radiation divergence. A survey of earlier papers with respect to glass fiber can be found in [82-85]. In recent years, in addition to the study of the lasing and amplification effects in fibers made of ordinary glass (see, for example [86, 87]), a study was also made of fibers made of especially pure quartz with Nd_2O_3 [88, 89], on which it was possible to realize lasing during pumping using a semiconductor injection laser [90]. Lasing and amplification of light were also obtained in films made of silicate glass using the diffusion light guides created in the silicate glass [91-93]. Efforts to make phosphate glass films with the composition NdP_5O_{14} [94] by radio frequency spraying of the crystals of the same composition with decreased concentration quenching of luminescence of the Nd^{3+} ions did not give good results: the lifetime of the Nd^{3+} luminescence in the films was approximately 8 microseconds, which is appreciably less than in the initial crystals (55 to 120 microseconds). The laser effect on films made of phosphate glass has still not been obtained.

Let us consider another factor, which determines the temperature conditions of the AE--the power of the heat release q. This heat release power is connected with the absorption of pumping light in the AE and with nonradiating losses enumerated in §1.4. The pumping light is absorbed by the glass matrix as a result of the presence of inactive admixtures; there is also natural absorption in the short wave, as a rule, ultraviolet part of the spectrum and absorption by the activator ions. The absorption by the matrix takes place only on heating the AE, and it is desirable to reduce it to a minimum by using pure reagents and filtering the shortest wave part of the pumping tube emission. However, with such filtration part of the useful absorption is also lost simultaneously (in the activator absorption bands). Let us consider this briefly in the example of glass doped with Nd^{3+} ions (the spectroscopic properties of Nd^{3+} are discussed in more detail in Chapter 4). The absorption spectrum of Nd^{3+} consists of narrow bands which can be broken down into three groups in the range of 350 to 530, 580 and 680 to 880 nm [5]. Figure 1.10 shows the absorption spectra for GLS-4 silicate glass and LGS-40 phosphate glass together with the transmission curves of filters made of three types of glass--K-208, OS-12, KS-14 [5]. In contrast to phosphate

glass, silicate glass usually does not have absorption bands at 350 nm, and therefore a filter made of K-208 glass has no influence on the activator absorption or the lasing characteristics of the glass. The use of the other two filters significantly decreases the lasing energy, especially for phosphate glass (Figure 1.11). Efforts were made to decrease the reduction in lasing efficiency during filtration, for example, by the application of luminescing liquid filters, the material of which absorbs the shortwave emission and emits the longer wave emission (see, for example [96]); however, such filters have ordinarily low light strength.

The role of Stokes losses in the heating of the AE for individual groups of absorption bands of Nd^{3+} is illustrated in Figure 1.12, b [5]. It varies with variation of the absorptivity of the neodymium glass, which for cylindrical AE depends on its diameter d and on the activator concentration N_{Nd} (as the square root of the product of these values). The energy absorbed in the 680 to 880 nm bands makes 20% contribution to the heat release and about 40% contribution to the maximum admissible lasing power (Figure 1.12, a); the latter was calculated in [5] by the total tube pumping energy absorbed by the activator, under the assumption that the quantum yield of the luminescence of the Nd^{3+} is equal to one, and the energy losses to heat are connected only with the Stokes shift between the given excitation band and the Nd^{3+} lasing band by 1.06 microns. The total pumping energy absorption for the cylindrical AE 10 mm in diameter by 130 mm is 6 to 12% of the electric pumping power [47, 5, 97, 98]; approximately half of the absorbed energy can be converted to lasing power with these dimensions of the AE [5]. The actually attainable efficiency of the glass lasers with small AE usually is less inasmuch as the lasing power decreases not only as a result of Stokes losses. Figure 1.12 shows that on variation of the absorptivity of the AE, the contribution of the blue green and yellow absorption bands to the lasing power and heat varies sharply. For $N_{Nd}d=1$ to 45% the maximum admissible lasing power is given by the yellow band and only about 20% by the blue green bands; for $N_{Nd}d=15$, the role is reversed. Here the contribution of the short wave bands to the heat release for large values of $N_{Nd}d$ reaches 65%. The thermal conditions of the AE vary correspondingly for identical filtration conditions. In spite of improvement of the thermal conditions of the AE on filtration of the short wave part of the pumping emission, in this case, the decrease in lasing efficiency that occurs makes consideration of the thermophysical and strength characteristics of the glass permitting a decrease in the requirements on the pumping filters highly significant.

The use of narrow-band pumping sources of the type of semiconductor light diodes and heterolasers, dye lasers, Raman lasers, and so on operating in the range of 500 to 900 nm and matched with the absorption bands of the activator is a radical method of decreasing the heat release as a result of Stokes losses and absorption of the energy by the glass matrix. With these pumping sources, in particular, continuous lasing was obtained on the AE made of neodymium-doped phosphate glass [99]. However, the power and efficiency of the existing narrow-band pumping sources still are insufficient, and they are used predominantly in experimental devices. For powerful systems, "double" conversion of the energy, for example, tube pumping of the Nd^{3+} lasers and

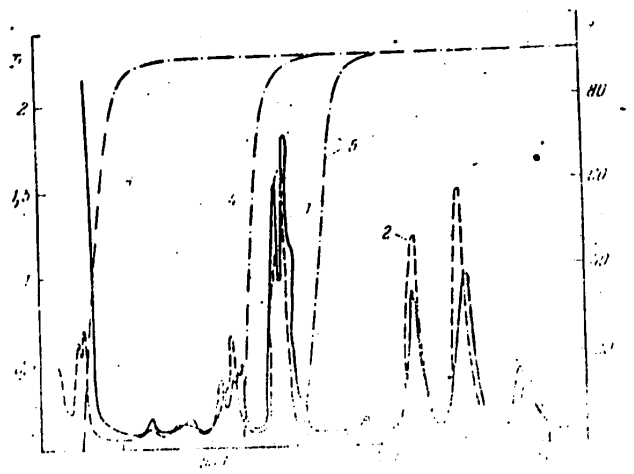

Figure 1.10. Curves for the optical density D of GLS-4 glass (1) and LGS-40 glass (2) 5 mm thick and the transmission curves t of filters made of K-208 glass (3) 3 mm thick, OS-12 glass (4) and KS-14 glass (5) 1 mm thick [95]

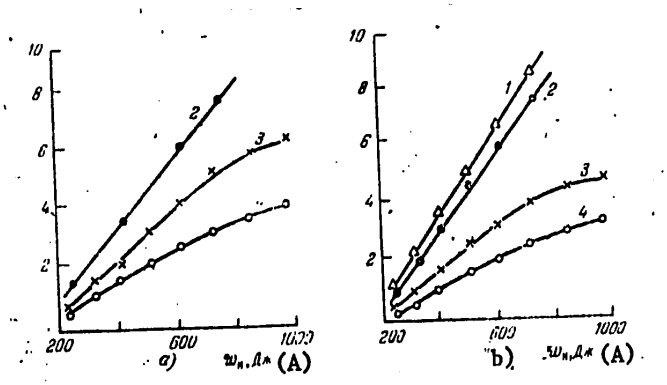

Figure 1.11. Lasing power as a function of the pumping power for GLS-4 glass (a) and LGS-40 glass (b) without filtration (1) and using filters made of K-208 glass (2), OS-12 glass (3) and KS-14 glass (4) [95]. The ratios of the lasing power for the investigated energy to the lasing power near the threshold are plotted on the y-axis.

Key:

A. joules

subsequent use of these lasers to pump the AE made of Yb^{3+} and Er^{3+} doped glass can turn out to be effective. This significantly improves the thermal conditions of the output stage of the laser system. Such a converter is described in Chapter 6.

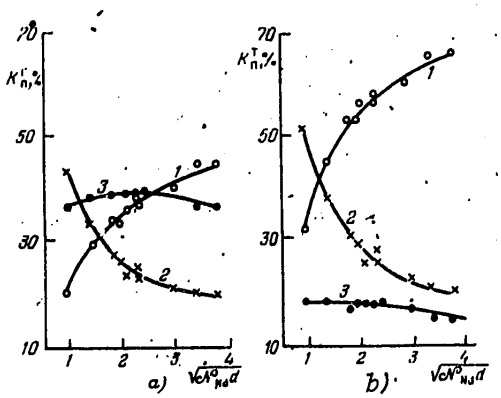

Figure 1.12. Variation of the contribution K_{π} of the energy in the 0.43 to 0.53 band (1), 0.58 band (2), 0.68-0.88 micron band (3) to the maximum lasing power (a) and heat (b) as a function of the activator concentration and diameter d of the active element [95]. $N_{Nd}=10^{20}$ cm^{-3}, the diameter d in cm.

§1.6. General Description of Laser Glass

Now, after discussing the information about the most significant characteristics of laser glass, we can compare glass-like laser materials with other types of materials for lasers. The laser effect is now obtained in solid, liquid and gaseous media. The materials of solid-state lasers are divided into two basic types--semiconductor crystals and films and materials with predominantly ion structure containing rare earth elements or certain 3d-ions (Cr, Co, Ni) or having color centers as the activators. Each type of laser has its own area of application. Materials with ion structure can be crystalline (including in the form of thin monocrystalline films or fibers) and vitreous. Laser crystals are investigated in the monograph [100]. Three crystal materials basically now have practical significance: ruby $Al_2O_3:Cr^{3+}$, yttrium aluminum garnet (YAG) $Y_3Al_5O_{12}:Nd^{3+}$ and yttrium aluminate $YAlO_3:Nd^{3+}$.

The vitreous laser materials primarily belong to the classes of inorganic oxides or fluorides of glass. Glass as a laser material has a number of advantages by comparison with crystals [48, 83, 84]: namely,

1) The possibility of obtaining it in large volumes with comparatively low cost.

2) Simplicity of manufacturing products of almost any shape and size.

3) High optical homogeneity and small losses (~0.001 cm^{-1}) to inactive absorption on the lasing wavelength.

4) The possibility of variation of the physicochemical, spectral luminescence and lasing characteristics within significant limits for glass technology and for the development design of lasers and selection of the optimal combination of these characteristics.

5) The possibility of selecting thermooptical parameters which insure minimum distortion of the light wave front (§1.4) and selection of nonlinear optical properties insuring that maximum lasing power will be obtained for short duration pulses (§1.2).

6) Broader absorption bands of the activators, improving the matching with the pumping sources; the possibility of eliminating polarization effects (variation of the optical transparency of the active medium under prolonged exposure to pumping light) as a result of the corresponding additives.

The deficiencies of glass by comparison with crystals reduce to the following.

1) Worse thermal conductivity (by more than an order less than in crystals):

2) Worse mechanical properties--less hardness, lower modulus of elasticity and strength. This is illustrated by the data in Figure 1.8, in which some physical properties of ruby, YAG and glass are compared [31, 84].

3) Greater luminescence band width, smaller induced radiation cross section of rare earth activators; consequently, smaller gains and higher lasing thresholds. For Nd^{3+} ion and YAG, the maximum cross section of the induced emission for the main laser transition is $8 \cdot 10^{-19}$ cm^2 [100], in glass $(1\text{-}4.7) \cdot 10^{-20}$ cm^2 [47, 48, 101-104]. However, this factor turns out to be useful during the operation of active elements in the amplification and Q-switching modes, especially in powerful systems, for it offers the possibility of obtaining high radiation energy from one element.

Table 1.8

Properties	Ruby	YAG	Glass
Thermal conductivity, watts/(m-K)	23	14	0.3-1.3
Microhardness, kg/mm^2	2100-2400	1320-1380	300-600
Modulus of elasticity, 10^7 kg/cm^2	4.25-4.6	0.294	0.05-0.09
Bending strength, 10^3 kg/cm^2	3-6	1.75-2.1	0.3-0.8
dn/dT, 10^{-6} K^{-1}	1.0-1.4 (for n_0)	9.86	-10-(+10)

Lasing is obtained in glass for an entire series of rare earth ions. In Table 1.9 some of the laser parameters of glass with different activators are presented. The studies were performed in different laser systems and on elements differing with respect to size, optical quality, inactive absorption and other parameters, and therefore the results can be compared only with great caution. The use of sensitizers permits significant improvement of the characteristics of the glass with certain activators, for example, with Er, Tm, Ho. However, on the whole, the lasing thresholds for glass doped with Yb^{3+}, Ho^{3+}, Gd^{3+}, Tb^{3+}, Tm^{3+} ions, are very high, and the lasing efficiency is low. Therefore only Nd^{3+} doped glass and, to a lesser degree, Yb^{3+} and Er^{3+} doped glass have acquired practical significance at the present time.

Table 1.9

Типы стекла (1)	Ион-активатор (2)	Рабочая температура, К (3)	Переход (4)	Длина волны генерации, нм (5)	Размер цилиндрического элемента, мм (6)		Порог генерации, Дж (9)	Источник данных (10)
					диаметр (7)	длина (8)		
Силикатное (11)	Nd^{3+}	300	$^4F_{3/2}\rightarrow{}^4I_{11/2}$	1,06	0,1	(волокно в оболочке) (12)	0,9	[83]
»	»	»	»	»	2,5	55	4	[73]
Фторбериллатное (13)	»	»	»	1,05	»	»	2,6	[73]
Фосфатное (14)	»	»	»	1,06	»	»	1,5	[73]
Боратное (15)	Tb^{3+}	»	$^5D_4\rightarrow{}^7I_5$	0,542	6,5	70	1200	[83]
Силикатное (16)	Ho^{3+}	77	$^5I_7\rightarrow{}^5I_8$	2,046			3600	[83]
»	Er^{3+}	»	$^4I_{13/2}\rightarrow{}^4I_{15/2}$	1,55	4	24	1100	[83]
»	Yb^{3+}	»	$^2F_{5/2}\rightarrow{}^2F_{7/2}$	1,015	4	24	1300	[83]
»	Pr^{3+}	»	$^1G_4\rightarrow{}^3H_4$	1,047	6,7	53	150	[83]
»	Gd^{3+}	78	$^6P_{7/2}\rightarrow{}^8S_{7/2}$	0,3125	4	24	4300	[83]
»	Tm^{3+}	77	$^3H_4\rightarrow{}^3H_6$	1,85	4	27	55	[105]

Key:

1. Types of glass
2. Activator ion
3. Operating temperature, K
4. Transition
5. Lasing wavelength, nm
6. Size of cylindrical element, mm
7. Diameter
8. Length
9. Lasing threshold, joules
10. Data source
11. Silicate
12. (fiber in sheathing)
13. Fluoberyllate
14. Phosphate
15. Borate
16. Silicate

Let us consider the basic groups of Nd^{3+}-doped laser glass in somewhat more detail. Ordinary inorganic glass includes compounds of modifier elements (oxides and halides of the majority of metals) and glass forming elements (SiO_2, B_2O_3, P_2O_5, GeO_2, BeF_2, TeO_2, in some cases Al_2O_3, and so on). The spectroscopic and lasing studies were performed for silicate, phosphate, borate, germanate, fluophosphate and fluoberyllate glass. The spectroscopic properties of Nd^{3+} have also been studied for tellurite, sulfate, chloride, fluozirconate, nitrate and acetate glass. The lasing data for such glass are almost unavailable, and we shall not consider these systems in more detail. Let us only indicate the possibility of obtaining quite high induced radiation cross sections σ for Nd^{3+} in tellurite glass--approximately $9\cdot10^{-20}$ cm^2 for the transition $^4F_{3/2}\rightarrow{}^4I_{11/2}$, by the spectroscopic estimates made in [106]. At the same time, other authors give significantly smaller values of σ: $4.7\cdot10^{-20}$ cm^2 in [107], where continuous lasing is obtained

on tellurite glass with Nd^{3+} for longitudinal pumping by an argon laser, and $2.3 \cdot 10^{-20}$ cm^2 in [102]. Recently synthesized glass based on sulfides and oxysulfides of rare earth elements and gallium can turn out to be highly prospective [108, 109]. In these types of glass, the intensity of the absorption and luminescence bands of Nd^{3+} is appreciably higher than in an ordinary oxide or fluorine containing glass as a result of an increase in the degree of covalence of the bond between the activator and the atoms surrounding it. The studies of such glass are only beginning.

Laser glass is characterized by several tens of parameters describing the physicochemical, thermooptical, spectroluminescent and lasing properties. Comparing laser glass with respect to all parameters is a problem which goes far beyond the framework of the given paper. We shall try to give an analysis in general form of some of the most significant properties for use in laser systems for the most important groups of laser glass. Basically the characteristics already investigated in §§1.1 to 1.5 and also the mechanical and chemical strengths, the adaptability for manufacture and cost of production of the glass will be compared. Then, in Chapters 3 to 6, when analyzing the individual properties of phosphate glass, a more detailed comparison of it will be made with other classes of laser glass, and the advantages of phosphate glass for use in different laser systems will be demonstrated.

The summary picture of the properties of various classes of laser glass with Nd^{3+} ions is presented in Table 1.10. The ranges of variation of the physicochemical properties are presented approximately with the use of references [47, 48, 101, 103, 110-116], spectroluminescent and lasing properties, using the results of [47, 48, 73, 101-103, 112-118]. The omissions in the table indicate the absence of systematic studies.

The most widespread now are silicate laser glasses [47, 48, 119]. About 40 types of silicate laser glass have been developed in the USSR and abroad. They are the cheapest and are the most adaptable for manufacture, they have good mechanical and chemical strength, they offer the possibility of obtaining large castings of high optical quality. The magnitude of the cross section of the induced emission of Nd^{3+} ions does not exceed approximately $3 \cdot 10^{-20}$ cm^2; the coefficient of nonlinearity of the index of refraction n_2 is comparatively large (more than $1.4 \cdot 10^{-13}$ $cm^2/volt^2$), which limits the possibility of using the glass in powerful systems with small pulse durations (fractions of a nanosecond). Detailed information about the properties of industrial silicate laser glass are presented in [47]. A deficiency of silicate glass is the relatively high values of the thermooptical characteristics $\tilde{W}$ and P ($\tilde{W} \geq 10 \cdot 10^{-7}$ K^{-1}, $P \gtrsim 5 \cdot 10^{-7}$ K^{-1} for a wavelength of 1.06 microns, §1.4), which does not permit selection of the compositions combining good thermooptical and lasing properties.

Germanate glass almost has no advantages over silicate glass, but it is significantly more expensive, which makes industrial use of it inexpedient.

Borate glass has comparatively large induced emission cross sections of Nd^{3+} (to $3.8 \cdot 10^{-20}$ cm^2) and satisfactory thermooptical characteristics, but low

Table 1.10

Properties	Type of glass					
	Silicate	Phosphate	Borate	Germanate	Fluo-phosphate	Fluo-beryllate
Index of refraction n_D	1.48-1.8	1.48-1.8	1.47-2.2	1.6-2.0	1.46-1.6	1.28-1.4
Coefficient of nonlinearity of the index of refraction n_2, 10^{-13} $cm^2/volt^2$	1.40-2.0	0.90-1.3	-	-	0.55-1.1	0.23-0.4
Coefficient of thermal expansion α_T, 10^{-7} K^{-1}	20.0-150	50-250	50-160	60-150	100-170	70-200
Thermal conductivity λ_h, 10^{-3} watts/(cm-K)	5-15	2-13	-			
Microhardness, kg/mm^2	300-800	150-600	200-60 0	350-600	300-550	180-315
Young's modulus E, 10^{10} Pa	5-80	3-7	2-9	4-7	-	3.6-5.0
Maximum of the Nd^{3+} luminescence band ($^4F_{3/2} \rightarrow {}^4I_{11/2}$), nm	1060	1049-1055	-	1060	-	1046-1050
Halfwidth of the luminescence band of Nd^{3+} ($^4F_{3/2} \rightarrow {}^4I_{11/2}$, nm	26-36	15-23	28-30	35	18-30	15-24
Luminescence lifetime, microseconds	300-1000	300-600	50-150	-	300-500	530-1000
Induced emission cross section σ, 10^{-20} cm^2	0.9-3.0	1.8-4.7	2.8-3.8	2	2.1-4.3	1.2-4.0
Thermooptical characteristics:						
$\tilde{W}$, 10^{-7} K^{-1}	10-200	-100-120	-10-100	-	-	-
P, 10^{-7} K^{-1}	5-150	-100-100	-	-	-	-
Q, 10^{-7} K^{-1}	0-12	0-12	0-12	-	-	-

quantum yield and short luminescence lifetime of Nd^{3+} (no more than 150 microseconds) complicate its use for the existing pumping systems.

Phosphate glass is now the second most important group of laser glasses, and in recent years it is finding broader and broader application in lasers of various types [47, 48, 52, 58, 59, 81, 121, 122]. The advantages of phosphate glass [47, 48, 52, 59, 120-123] are higher cross sections of induced emission of Nd^{3+} (to $4.7 \cdot 10^{-20}$ cm^2), high gain, narrow lasing spectrum and high efficiency. The thermooptical characteristics of phosphate glass vary within broad limits, which offers the possibility of selecting compositions with optimal lasing and thermooptical properties. The smaller coefficient of nonlinearity of the index of refraction, higher induced emission cross section and good thermooptical properties are the advantages of phosphate glass by comparison with silicate glass when it is used in powerful systems for amplifying supershort pulses [14, 120-122]. Phosphate glass is sufficiently adaptable for manufacture, and it can be obtained in large volumes with high optical quality. The deficiencies include increased cost by comparison with silicate glass, lower mechanical and chemical strength than for silicate glass. The latter deficiency pertains especially to the first phosphate laser glass assimilated in the USSR about 10 years ago, types LGS-40 and LGS-41 [47] and some of the modern foreign types of glass, for example, EV-2 and Q-88 [122]. Elements made of glass of the last two types begin to break down after a few days on contact with water [122]. The phosphate glass presently produced in the USSR has good chemical stability [47]. The mechanical, and especially the thermal strength of phosphate glass can be raised by using special methods of treatment [58, 59, 70, 81].

The phosphate base permits significant replacement of P_2O_5 by oxides and fluorides of other elements playing the role of glass formers and permitting improvement of certain physicochemical characteristics of the glass, a decrease in the crystallization capacity, variation of the interaction between activators, and so on. Such glass nevertheless retains the most important advantages of purely phosphate glass related to its spectral luminescence, thermooptical and lasing properties. Silicophosphate, borophosphate, germanium phosphate, niobium phosphate, aluminum phosphate glass are known. The spectral luminescence properties are known for many of these types of glass, and the lasing properties are known for some. Thus, the term "phosphate glass" can actually refer to a very broad class of compositions in which the role of the basic glass forming component is played by phosphorus pentoxide.

In essence, the same class includes fluophosphate glass containing significant amounts of metal fluorides. This glass is similar to phosphate glass with respect to physicochemical properties [113-115], it has somewhat smaller cross section of induced emission Nd^{3+}, but even smaller coefficient of nonlinearity of index of refraction n_2, which makes it prospective for use in powerful laser systems with heated plasma [14, 113]. Increased aggressiveness and volatility of fluorine-containing melts complicate obtaining large optically homogeneous billets and require additional development of the process of founding such glass.

The study of fluoberyllate glass was started comparatively recently [115, 124, 125]. As was discovered recently, BeF_2 and fluoberyllate glass have the least coefficients of nonlinearity of the index of refraction n_2 for inorganic materials [112]. In fluoberyllate glass the symmetry of the surroundings of the activator is the highest, and in such glass the ionicity of the bond between the activator and the ligands is the highest [125]; the luminescence band width of Nd^{3+} and the magnitude of the induced emission cross sections of neodymium for fluoberyllate glass are close to these characteristics for phosphate glass [73, 112, 115]. Fluoberyllate glass has lower mechanical and chemical stability than phosphate glass. It is very difficult to obtain optically homogeneous castings from fluoberyllate glass. The thermooptical properties of fluophosphate and fluoberyllate glass have still been studied insufficiently.

The complex of physical properties required for laser glass depends on the specific purpose and required parameters of the laser system. Thus, the requirements imposed on the thermooptical characteristics of glass are different when using active elements in the form of cylinders, discs or plates (§1.4), the requirements on the active elements of lasers operating in the single pulse mode and in the periodic frequency mode are different, and so on. It is necessary to select the glass for powerful systems where the expenditures on materials are large, especially carefully. An example of such a choice of glass used in systems for studies of laser thermonuclear fusion is presented in reference [126], where the expenditures on creating the active elements from glass are compared with systems with high power or high lasing energy. Here phosphate glass can turn out to be a highly prospective material (§5.3). The requirements on glass for systems of another important type--pulse periodic lasers--are analyzed in §5.2.

CHAPTER 2. STRUCTURE OF PHOSPHATE GLASS

Phosphate glass, just as the majority of other types of inorganic glass [110, 127-129] contains two types of coordination groupings of atoms--compact polyhedra of glass former ions (in the given case, PO_4^{3-} tetrahedra) with powerful covalent bonds between the anions and the central ion and larger polyhedra of modifier ions, where the bonds have a more ionic nature. The properties of glass are determined to a significant degree by the structure of the anion motif, the method of combining the polyhedra of the glass former (isolated groups of polyhedra, rings, chains, strips, layers, frames) and the type of modifier ion. In ordinary silicate glass the SiO_4^{4-} tetrahedra, joined by the apexes through bridge (that is, bound to two glass former ions) oxygen atoms, form a comparatively strong three-dimensional silicate frame, in the cavities of which the modifiers are located [110]. This frame can be characterized by the degree of binding m determined by the average number of bridge oxygen atoms per ion of glass former. The degree of binding is equal to 4 in pure SiO_2, and it decreases as the molar concentration of the modifier increases, to 0 for transition to "inverted" glass, in which the molar content of the modifier is higher than in SiO_2 [130]. Another useful characteristic of the anion motif (especially for phosphates) is the density of the transverse bonds [131, 132], which is defined as (m-2). In essence, it is equal to the average number of additional bonds per glass former ion by comparison with the number of bonds in an infinite polymer chain of polyhedra of glass formers joined by the apexes, in which there are two bridge oxygen atoms for every glass former ion.

The same situation exists with the binding of the anion motif in crystals. Phosphates containing more than 50 mole % metal oxide are constructed from island (isolated) phosphate groups and polyhedra of the cations connecting these groups located between them. With a univalent and bivalent metal oxide content of 50 mole %, that is, in "metaphosphates" with the formula $MePO_3$ or $Me(PO_3)_2$, every tetrahedron of PO_4^{3-} is connected to two other tetrahedra through common (bridge) oxygen atoms; here rings or infinite chains of tetrahedra are formed. The density of the transverse bonds is equal to 0, that is, they are absent. In the region of crystals with predominance of P_2O_5, "ultraphosphates" appear, where part of the PO_4^{3-} tetrahedra ("ultra-tetrahedra") are already connected to three other tetrahedra, the binding of the anion motif increases. In one of the versions of P_2O_5 (O-form), every tetrahedron is bound to three others, forming a frame [133, 134],

and this means that the binding of the phosphate motif is correspondingly equal to three, and the density of the transverse bonds is equal to one. Thus, phosphates and phosphate glass have less binding of the anion motif than silicate glass. Usually the higher the binding of the anion motif, the higher the mechanical properties of the glass (with identical modifier cation). Correspondingly, phosphate glass has lower microhardness, lower modulus of elasticity, higher coefficient of thermal expansion and lower softening points than silicate glass with the same cation.

In order more clearly to represent the basic types of phosphate groupings which can exist in phosphate glass, let us briefly consider the structure of phosphate crystals in the example of th Me_2^+O-$Me^{2+}O$-P_2O_5 system, the diagram of which is shown schematically in Figure 2.1 [135]. Here Me^+ and Me^{2+} are univalent and bivalent metal, respectively. With an increase in the P_2O_5 content in crystal phosphates, the anion groupings are complicated in the following sequency: orthophosphates with isolated tetrahedra PO_4^{3-}→ pyrophosphates with double tetrahedra $[P_2O_7]^{4-}$→short chain polyphosphates with the formula of the anion motif $[P_nO_{3n+1}]^{(n+2)-}$→ the ring phosphates with the formula of the anion $[PO_3]_n^{n-}$ + metaphosphates with infinite chains of $[PO_3]_\infty^-$→ strip and layered ultraphosphates with the anions $[P_4O_{11}]^{2-}$, $[P_6O_{17}]^{2-}$, $[P_5O_{14}]^{3-}$ [135-142]→frame P_2O_5 (O-form).

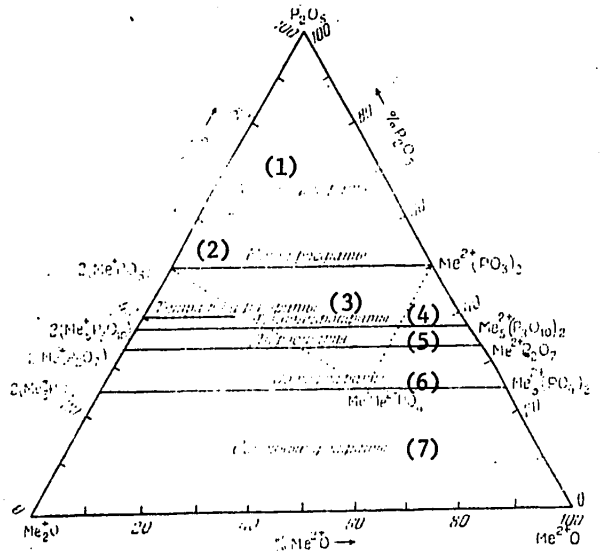

Figure 2.1. Ternary diagram of the system Me_2^+O-$Me^{2+}O$-P_2O_5 [135]. The basic types of compounds are indicated.

Key:

1--ultraphosphates; 2—metaphosphates; 3--tetrapolyphosphates; 4--tripolyphosphates;5--diphosphates; 6--orthophosphates; 7--basic phosphates

Certain types of phosphate groupings are depicted in Figures 2.2 to 2.5. It must be noted that for each type of phosphate grouping, several versions of the mutual spatial orientation of the tetrahedra PO_4^{3-} can exist; various methods of combining the tetrahedra are also possible [133, 134, 142, 143].

As an example, Figure 2.3 shows several different types of infinite phosphate chains with the general formula $[PO_3]^-_\infty$; Figure 2.4 shows two types of ultraphosphate strips with a general formula $[P_5O_{14}]^{3-}$ encountered in ultraphosphates of the type of MeP_5O_{14}, where Me is a rare earth element or Bi; Figure 2.5 shows layers of eight member and 14 member rings constructed from metatetrahedra PO_4^{3-} connected with two other tetrahedra and ultratetrahedra connected with three tetrahedra.

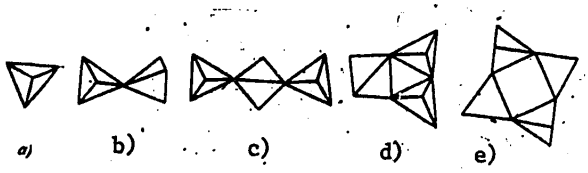

Figure 2.2. Some island phosphate groupings. a) Tetrahedron PO_4^{3-}; b) pyrophosphate ion $P_2O_7^{4-}$; c) tripolyphosphate ion $P_3O_{10}^{5-}$; d) cyclic triphosphate ion $P_3O_9^{3-}$; e) cyclic tetraphosphate ion $P_4O_{12}^{4-}$

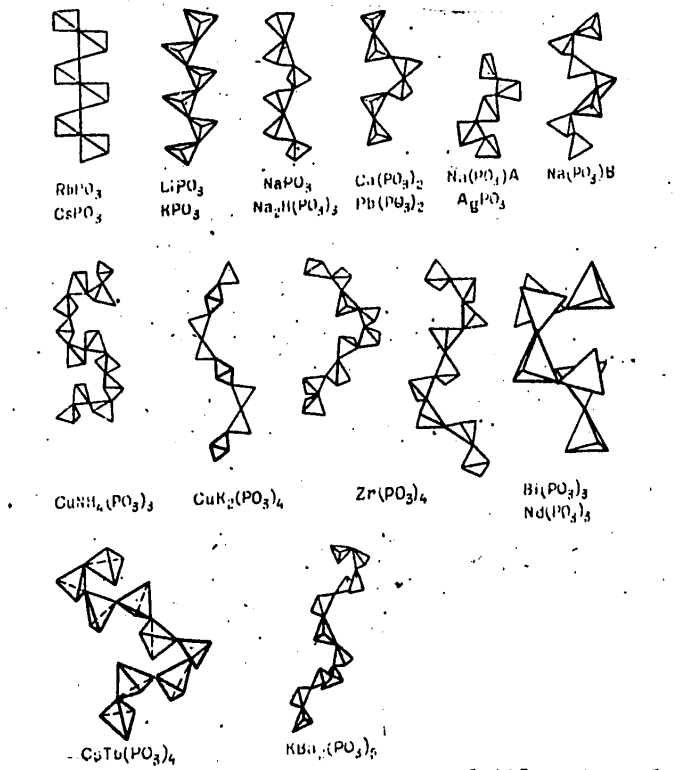

Figure 2.3. Various polyphosphate chains [142]. The relative orientation of the tetrahedra PO_4^{3-} along the axes of the chains is demonstrated.

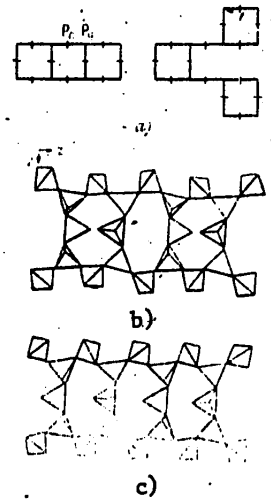

Figure 2.4. Phosphate motifs in certain strip ultraphosphates.
a) Possible methods of joining 8 member rings of PO_4^{3-} tetrahedra in ultraphosphates (P_c--middle PO_4^{3-} group connected to two others, P_y--ultraphosphate group PO_4^{3-} connected to three others); b) ultraphosphate strips of 8 member rings in NdP_5O_{14} lattices and c) rhombic version of HoP_5O_{14} [139].

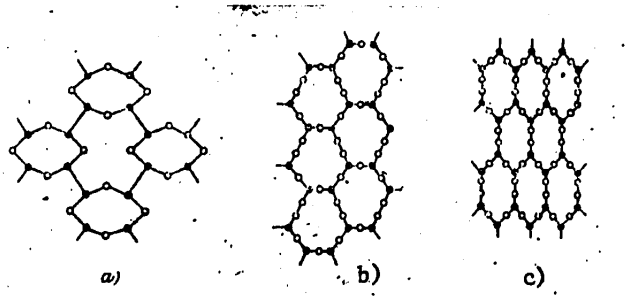

Figure 2.5. Phosphate grids in lattices of certain ultraphosphates [143].
a) MnP_4O_{11}; b) $Sr_2P_2O_{17}$; c) $Cd_2P_6O_{17}$. The black circles are ultraphosphate tetrahedra, the white circles are the middle (meta) phosphate tetrahedra. Only the P atoms are indicated, the oxygen atoms are omitted.

In the isolated PO_4^{3-} tetrahedra, all four P-O bonds are approximately equivalent and usually are 0.154±0.001 mm long [133, 134, 152]. The multiplicity of the P-O bond is greater than one. There are no final data on the electron structure of a phosphate tetrahedron [142], although it is assumed that in addition to the ordinary σ-bonds of P-O, a π-bond is formed in the tetrahedron as a result of overlap of the d-orbitals of phosphorus and the p-orbitals of oxygen [133, 134, 142]. In the phosphates containing motifs from bound tetrahedra, the P-O bonds become nonequivalent. The spacings of the P-O (-P) with bridge atoms O (2 oxygen atoms in the meta and three in the ultratetrahedron) are 0.154 to 0.167 nm for different polyphosphates and ultraphosphates and usually are greater than the P-O spacing (the terminal oxygen) in the same tetrahedra (0.144 to 0. 152 nm) [133, 134, 142, 143]. Consequently, the proportion of the π-bond is higher for the phosphorus bond with the terminal O-atoms entering into the coordination sphere of the modifier cation.

As we have seen (Figure 2.1), in anhydrous systems, as the P_2O_5 concentration increases, the process of joining, polycondensation, of the tetrahedra PO_4^{3-} takes place with the formation first of island and then chain, strip and layered phosphate motifs. The cation polyhedra bind the phosphate groups, forming characteristic structures--usually frames, layers or chains--in the crystals with high metal oxide content, predominantly isolated groups or simply isolated polyhedra in the ultraphosphates. The analogous picture of complication of the phosphate motifs also occurs in the melts of polyphosphoric acids containing water: with an increase in temperature, the phosphates crystallize successively with all the more complex phosphate radicals [144]. The process of polycondensation of the phosphate tetrahedra takes place with an increase in binding of the anion motif (just as for certain other groups of oxygen compounds, for example, borates [145]), under the effect of several factors--variation of the concentration of the metal oxide in the system, the temperature, acidity of the medium, pressure and so on.

The type of phosphate groupings formed depends on the metal cation. For example, anion groups are distinguished for ultraphosphates of bivalent and trivalent metals [138, 140, 142, 143]. In the H_2O-P_2O_5 system at 170°C, the main part of the P atoms is in the form of the pyrophosphate ion $P_2O_7^{4-}$, and on addition of the trivalent metal oxide to the solid phase, bismuth orthophosphate $BiPO_4$, ytterbium polyphosphate $YbHP_2O_7$, gallium tripolyphosphate $GaH_2P_3O_{10}$ and the metaphosphate of lanthanum $La(PO_3)_3$ are isolated [144]. This can be explained from the point of view of the theory of random arrangement of phosphate melts proposed by Van Vezer [146] in which dynamic equilibrium exists between the free PO_4^{3-} groups and the groups bound to 1, 2 and 3 other tetrahedra. Introduction of the metal oxide leads to a shift of the equilibrium in the direction of formation of the most soluble compound. The metal cations, in accordance with the views of Belov [147, 148], can play the role of a matrix or a nucleating center, around which the formation of the most energetically advantageous anion structure takes place.

As is obvious, phosphate glass is obtained by cooling melts; therefore an entire set of phosphate groupings with predominance of any defined form must exist in them. The structure of phosphate glass, as is shown in a number of

experiments by the methods of x-ray diffraction, spectroscopy and chromatography [129-155] is theoretically analogous to the structure of crystalline phosphates, and it is distinguished by a lower degree of ordering. In alkali glass with high metal oxide concentration, linear polyphosphate groups predominate. The average number $\bar{n}$ of PO_4^{3-} tetrahedra in such groups depends on the ratio R of the mole fractions of the metal oxide and P_2O_5: $\bar{n}=2/(R-1)$. Then the number of groupings per 100 atoms of phosphorus $T=100/\bar{n}$. With a ratio of $Me_2O:P_2O_5=1$, we have $n=\infty$, which corresponds to 100% content of infinite monophosphate chains. In reality, along with the linear phosphate groupings, there is always some number of cyclic groupings in the glass. Figure 2.6 shows the variation in content of various anion groupings in alkaline glass with variation of the molar concentration of the alkali oxide [153]. With an increase in the P_2O_5 content, the proportion of more condensed groups increases, and anion groupings appear in the ultraphosphate region, in which part of the PO_4^{3-} tetrahedra are bound to three other tetrahedra (branch points), and not to two, as in the alkali groupings. Correspondingly, the binding of the anion motif increases, the vitrification point and Young's modulus increase for the glass [131, 132].

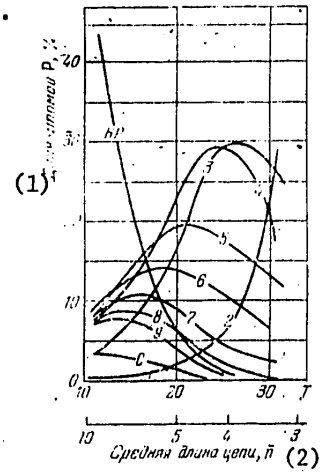

Figure 2.6. Proportion of phosphorus atoms (in %) entering into the composition of various phosphate polyions in alkali potassium phosphate glass as a function of the average length $\bar{n}$ of the phosphate chains [153].
The numbers on the curves are the number of phosphorus atoms n in the linear polyion with the composition $P_nO_{3n+1}^{(n+2)-}$;
C is the proportion of phosphorus atoms entering into the cyclic phosphate groupings; HP is the proportion of P atoms in linear phosphates with n>9.

Key:
1. Proportion of P atoms, %
2. Average chain length, $\bar{n}$

Glass with island anion groupings is easily crystallized. In phosphate systems stable glass is formed in the metaphosphate and ultraphosphate regions, where the binding of the anion motif is high. The bond strength between the phosphate groupings depends on the type of modifier cation. Cations with

high field strength, that is, with large charge and small anion radius (Mg^{2+}, Al^{3+}, Nb^{5+}, and so on) form strong bonds with oxygen, the strength of which differs little from the P-O bond strength. The introduction of these cations into the glass decreases the coefficient of thermal expansion, increases the thermal stability and chemical stability of the glass, its microhardness, and the temperature of the beginning of deformation. It is provisionally possible to consider that such cations together with the polyhedra of the glass former form a "mixed motif," which was investigated, for example, for titanium-containing and zirconium-containing silicate glass [156, 157]. The conditionality consists in selecting the boundary between the extreme cases: the structural motif formed only by polyhedra of the glass former (SiO_2, GeO_2, B_2O_3, P_2O_5, and so on) and the "standard glass" containing an anion motif (with powerful cation-oxygen bonds) and large low-charge ions (for example, alkali metals), having weak binding to oxygen. Even the transition from single-charge cations to larger bivalent Ba^{2+} causes a sharp change in properties of the metaphosphates, for example, a significant decrease in the electrical conductivity of the melts [158]. The difference between strengthening of the phosphate motif itself as a result of increasing its binding and strengthening of the mixed phosphate cation motif on introduction of "strong" cation modifiers decreases with an increase in field strength of the cation. Therefore, for example, it is possible to talk about alkali niobium phosphate glass [159, 160], considering that the bond strength of Me^{+}-O is much less than the P-O bond strength or the Nb-O bond strength, which means P and Nb can play an analogous role structurally.

Of course, the most similar in this respect are the P atoms and the glass former ions which can under defined conditions form mixed tetrahedral motifs with the phosphate tetrahedra, for example, Si^{4+}, B^{3+}, As^{5+}, sometimes Al^{3+} [161-178]. For laser phosphate glass, B^{3+} is especially important, for it is demonstrated that the introduction of BPO_4 into phosphate glass significantly improves its mechanical and chemical stability [166, 167]. Boron orthophosphate has a frame structure with alternation of tetrahedra BO_4^{5-} and PO_4^{3-}. The addition of BPO_4 to metaphosphate glass leads to the appearance of additional bonds between the polyphosphate chains, an increase in binding of the anion motif and, consequently, to an increase in its overall strength for the same cation modifiers. In order to keep the interaction of the activator with the glass matrix small (see Chapter 3) it is essential that up to a defined B_2O_3 concentration in the glass with BPO_4 additive, the boron atoms in the phosphate glass have predominantly tetrahedral coordination. However, at the present time there are no exact data on the relation between the boron atoms in the tetrahedral coordination and in the other possible, trigonal coordination. As an example, let us present data on the fraction of the boron atoms n_4 in tetrahedral coordination determined recently for several glass compositions in the K_2O-B_2O_3-P_2O_5 system by two independent methods--by the Raman scattering spectra of glass [168] and by the nuclear magnetic resonance spectra of B^{11} [170] (Table 2.1). As we shall see, the results do not agree. Comparison of the available data from infrared spectroscopy, electron microscopy, nuclear magnetic resonance spectroscopy, the results of studying the electron paramagnetic resonance of boron phosphate glass with admixtures of paramagnetic ions and irradiated glass, the

studies of the processes of extinguishing luminescence of RZI* which depend on the frequencies of the highest-energy oscillations of the matrix and, consequently, on the coordination of the boron atoms (see Chapter 3), provides a basis for considering that high values of n_4 obtained by the method of nuclear magnetic resonance are more reasonable. In the region with large B_2O_3 content with respect to the P_2O_5 content obviously the trigonal coordination of the boron atoms predominates; usually in boron phosphate glass of this type, liquation is observed [164, 165, 173, 176]. In such glass, the interaction of the rare earth activators is intensified both between each other--as a result of liquation and an increase in the local activator concentration--and with the glass matrix as a result of high energy of the vibrations of the B-O bond for boron atoms in trigonal coordination.

Table 2.1.

Glass composition, molecular %			n_4 [170]	n_4 [168]
K_2O	B_2O_3	P_2O_5		
25	50	25	0,64	0
30	40	30	0,75	0,08
40	20	40	0,70	0,26
23	54	23	0,56	0,03
•16,7	66,7	16,7	0,43	0,52

The addition of small amounts of SiO_2 to phosphate glass usually leads to cross linking of the phosphate groupings, an increase in the binding of the anion frame, a decrease in the crystallization capacity of the glass [171, 172, 177]. Large amounts of SiO_2, on the other hand, have a depolymerizing effect on the phosphate grouping, in a number of cases having a negative effect on the chemical strength of the glass and increasing its inclination to crystallization [174, 175]. Sometimes the negative influence of large amounts of SiO_2 on the chemical stability of the glass can be compensated by the addition of Al_2O_3, which obviously leads to the formation of stable $AlPO_7$ groups with aluminum atoms in tetrahedral coordination in the glass [174].

In the properties of laser glass, variations not only in the cation, but also in the anion composition of the glass are felt strongly. The most important is replacement of the oxygen ions by OH-groups and halide ions, primarily fluorine. If we do not take special measures with respect to careful dehydration of phosphate glass, it will always contain a significant amount of residual water (fractions of a percentage by weight and even percentages [179], which corresponds to several mole percentages [179-184]). This has a strong influence both on the optical transparency of the glass in the regions corresponding to the absorption frequencies of the OH-groups and the luminescence properties of rare earth activators [181-183, 185] (Chapter 3). In phosphate groupings the OH-groups are terminal, and increasing their concentration decreases the degree of binding of the phosphate motif [131]. On the contrary, the process of removal of the water leads to combination of the phosphate groupings, an increase in the average degree of polymerization and the degree of binding of the phosphate motif [131, 180]. Of course, the degree of polymerization (that is, the number of PO_4^{3-} tetrahedra in the phosphate grouping) with identical initial composition of the

* RZI = rare earth ions

glass, in addition to the water content, can also be influenced by other factors: the possibility of volatilization of part of the P_2O_5, variation in the ratio between the ring and the chain groupings, and so on [186]. The dehydration is felt most strongly in the properties of ultraphosphate glass, where it causes an increase in the transformation temperature and Young's modulus of the glass [131, 132].

Inasmuch as the presence of OH-groups has a significant negative effect on the luminescence, and in certain cases, the lasing characteristics of the glass with rare earth activators, various methods are used for dehydration of laser glass [117, 181-183, 185, 187]: bubbling of the glass melt with dry gas, founding in a protective atmosphere, deuteration of the melt, evacuation, the addition of halides. In particular, the addition of fluorides, leading to replacement of the terminal OH-groups by F ions essentially having no influence on the luminescence properties of the activator, permits us to obtain almost anhydrous glass [183]. The amount of fluorides which can be introduced into the phosphate glass is very high: phosphate glass can consist of about 80 percent fluorides [114, 188, 189]. Up to defined concentrations of fluorides in the fluophosphate glass, polymer phosphate groupings are retained [114, 190], then the pyrophosphate and ring phosphate groups begin to increase. The PO_3F anion intermediate between the purely fluoride and purely phosphate components of the structure plays an important role in phosphate glass [114]. The presence in the coordination sphere of an activator of fluorine and oxygen atoms causes multitype nature of the centers distinguished with respect to resolution of the transitions, luminescence lifetimes, and so on. With respect to width of the luminescence bands and cross sections of the induced emission of the activators, the fluophosphate glass is similar to phosphate glass [115, 191, 192], but the processes of excitation energy transport in it differs significantly [193] (Chapter 3), which is connected to a significant degree to variation in the glass structure.

The activator ions in the phosphate glass are located in the vicinity of the oxygen ions. Rare earth ions with completed 4f-shell are distinguished with respect to coordination capacity in oxygen compounds both from large cations with small field strength, high degree of ionicity of the bond and coordination numbers and cation-oxygen distances varying within significant limits, and from 3d-ions with powerful covalent bonds and comparatively rigid coordination polyhedra. Ions of this type, for example, Cu^{2+}, V^{4+}, form a characteristic environment in the glass which is different for different glass formers, but depends comparatively little on the type of cation modifier (if it does not cause changes in the structure of the glass). [194]. The complex forming capacity of rare earth ions (RZI) in compounds with oxygen is less than for 3d-ions, and the set of coordination polyhedra and the interval of variation of the interatomic spacings and valence angles in them is correspondingly larger [195-200]. There is also a difference in the coordination properties of different RZI [197-200] and variation in the surroundings of the activator as a result of loss of order in the glass. For glass usually a study is made of the average statistical shape of the nearest coordination in the vicinity of the activator which can be found with a defined degree of reliability either by comparing the luminescence and absorption spectra of the activator

in the glass and in the crystal with known coordination of the activator or by comparing the spectra calculated by the methods of crystal field theory with the experimental data. Several such studies are known for phosphate glass.

In [201], on the basis of a comparison of the calculated and experimentally obtained absorption and luminescence spectra of Yb^{3+}, the conclusion is drawn that in the investigated phosphate, silicate and germanate glass, this ion is in six coordination with the D_3 symmetry. In [202] it was demonstrated that the structure of the Nd^{3+} terms in alkaline niobium phosphate glass is close to the structure of the Nd^{3+} terms in $LaPO_4$ [203], where the La ions have nine nearest O atoms and surroundings with C_1 symmetry, and the proposition is stated that in glass Nd^{3+} ions have analogous surroundings. In references [204] and [205], on the basis of analysis of the splitting of the energy levels of the Tm^{3+}, Er^{3+} and Nd^{3+} ions, the conclusion is drawn that the surroundings of these ions in phosphate glass have symmetry no higher than C_2. In reference [204] the proposition is stated that in oxide glass rare earth ions are surrounded by eight nonbridge oxygen ions from the anion groups. For Nd^{3+}, this is confirmed by compiling the values of Stark splittings of the levels and resolution of the transitions for crystal phosphates of the type $Me^{+}NdP_4O_{12}$ (Me^{+}=Li^{+}, Na^{+}, K^{+}), $Nd_xMe_{1-x}P_5O_{14}$ (Me=La, Gd, Y, Yb) and for phosphate glass of analogous composition [206, 207]. It is known that in the majority of the indicated crystals the coordination number of the RZI is equal to 8, rarely 7 or 6 [115-137, 143], the nearest surroundings of the Nd^{3+} ions have C_1, C_2 or C_s symmetry. It is therefore possible to consider that the coordination number of the RZI varies in phosphate glass from 6 to 9, and the nearest surroundings have quite low symmetry. Of course, as a result of disorder of the glass structure, a set of coordination polyhedra is realized in it for the activator, which, along with the absence of far order, leads to broadening of the luminescence and absorption bands of the RZI [83].

The oxygen atoms entering into the first coordination sphere of the activator are usually related also to the glass former atoms (phosphorus in purely phosphate glass) and the cation modifiers. In phosphate glass with anion motif, predominantly from the chains of PO_4^{3-} tetrahedera, there are no significant steric obstacles to the formation of the nearest vicinity of the activator ions located between the chains, in contrast to the silicate glass with rigid silicate frame. In such a case the fluctuations of the local electric fields acting on the RZI depend primarily on the field strength of the cation modifiers located in the second coordination sphere of the activator, increasing with an increase in charge and a decrease in the radius of the modifier. Here usually the width of the absorption and luminescence bands of the activator also increases.

With variation of the anion motif, for example, on introduction of B_2O_3, BPO_4, Nb_2O_5, Al_2O_3, on making the transition to ultraphosphate glass with a higher degree of binding of the anion motif, first of all steric obstacles to free formation of the surroundings of the activator can arise as a result of an increase in rigidity of the anion motif and, secondly, the number of possible combinations of atoms in the second coordination sphere of the activator increases. The oxygen ions of the first coordination sphere of the

activator can now be bound not only to the phosphorus and modifier atoms, but also to other atoms forming the anion motif--B, Nb, Al. Therefore introduction of the additives B_2O_3, BPO_4, Nb_2O_5, Al_2O_3 to phosphate glass leads to an increase in variations of the surroundings of the rare earth ions and to broadening of the energy spectra of these surroundings [83, 117, 159, 162, 167, 208].

The interaction of the activators in the glass depends on the spacing between the active ions. With usual laser concentration of Nd^{3+} ions on the order of $2 \cdot 10^{20}$ cm^{-3} the average distance between the activator ions is about 2.1 mm. However, the actual spaces can differ sharply from the average. As a result of the processes of chemical differentiation, the glass is inhomogeneous, there are two types of regions in it--polar (ionogenic) regions enriched with modifiers and covalently bound regions containing predominantly glass former polyhedra [83, 110, 209]. The size of the region depends on the glass composition and the conditions of its heat treatment, and it increases in the liquefying glass. The activator, which usually plays the role of a modifier, has a tendency to accumulate in the ionogenic regions where its local concentration can greatly exceed the average and where segregation of the activator takes place [210]. This leads to the formation of pairs of groups of close RZI analogous to the clusters of paramagnetic ions (see, for example, [211-214]). Increasing the local activator concentration can be connected with microstratification of the glass [215]. However, this obviously is not mandatory [209, 216, 217]. Such processes are most strongly expressed in quartz glass [211, 218], in silicate glass inclined toward liquation with relatively low modifier content and in glass with two or more glass former ions (boron silicate, boron phosphate, and so on) with defined concentration ratios of such ions (see, for example, the survey [209]). As a result, intensification of the interaction of the active ions takes place-- quenching of the luminescence of part of the activator ions forming associates [117, 209], variation of the energy transfer efficiency between the activators [209, 216, 217, 219-221] (Chapter 3).

The processes of segregation of phosphate glass depend on the composition and structure of the glass, and for ordinary activator concentrations $(2\text{-}6) \cdot 10^{20}$ cm^{-3} for Nd^{3+} dions, they can be expressed either very weakly (which, according to [222], occurs for GLS-22 glass) or, on the contrary, strongly (as for alkaline boron phosphate glass [117]). In purely phosphate glass, the average distance between the Nd^{3+} ions for which the luminescence lifetime in the 1.06 micron region becomes half that in glass with low Nd^{3+} concentration, is less than for other types of glass--silicate, germanate, borate [223]. This can also indicate comparatively uniform distribution of the activator in such glass.

The segregation effects apparently are manifested most weakly in phosphate glass with predominantly trivalent cation modifiers with high P_2O_5 concentration (more than 60 mole %), in which the concentration quenching of the luminescence of the activator is most sharply expressed [206, 207, 224-229]. The study of such glass began after detection of intense Nd^{3+} luminescence in a series of neodymium-containing crystals with Nd^{3+} concentration of $(3 \text{ to } 4) \cdot 10^{21}$ cm^{-3}, exceeding by more than 20 times the Nd^{3+} concentration

in ordinary YAG crystals $Y_3Al_5O_{12}:Nd^{3+}$. Here we are talking about phosphate crystals NdP_5O_{14} [206, 230, 231], $Me^+Nd(PO_3)_4$ [230, 232] (where $Me^+=Li^+$, Na^+, K^+, Rb^+), $NdAl_3(BO_3)_4$ and certain other materials [230, 232, 233].

The most significant structural peculiarity of such crystals obviously is the location of the active ions in the common cation motif. The form of the aluminum grouping in this case can be different. For example, the concentration quenching of the Nd^{3+} luminescence is low in $RbNd(P_4O_{12})$ crystals with ring tetraphosphate ion $[P_4O_{12}]^{4-}$ [234], in $MeNd(PO_3)_4$ (Me=Li, Na, K) with infinite metaphosphate chains $(PO_3)^-_\infty$ and in the ultraphosphate NdP_5O_{14} with $P_5O_{14}^{3-}$ strips [230, 232]. In all these structures with different anion motifs, the activator polyhedra are isolated, that is, there are no Nd-O-Nd bonds in the structure, and the Nd-Nd spacing exceeds 0.5 nm. Even a small (to 0.481 nm) decrease in the shortest Nd-Nd distance leads to $K_3Nd(PO_4)_2$ [235], where the Nd^{3+} polyhedra also have no common peaks, to an increase in the concentration quenching of Nd^{3+} luminescence, although not to such a degree as in phosphate crystals, in which two neodymium atoms are bound directly through a common oxygen (for example, in (La, Nd)PO_4) [203]. These crystal chemical characteristics are insufficient for the decreased concentration quenching of Nd^{3+} luminescence; the structure of the energy levels of the neodymium ion, the phonon spectrum of the matrix, and so on are also significant [231, 236]. However, for oxygen compounds this obviously is necessary. Such conditions can be satisfied in two cases: either in the cation motif of the lattice the activator ions and other cations alternate in ordered fashion or in the compound containing only the activator as a cation, the anion motif creates steric obstacles for direct cation-cation contacts. The first case is realized in the phosphates $Me^+Nd(PO_3)_4$, in $YAl_3(BO_3)_4$, in $Na_5Nd(WO_4)_3$, $K_5Nd(MoO_4)_3$ [237], and so on. In known structures of this type the activator cations make up no more than half of the total number of cations. The anion groupings can be discrete, just as in $RbNd[P_4O_{12}]$ (rings of 4 tetrahedra) or chain, as in $Me^+Nd(PO3)4$ ($Me^+=Li^+$, Na^+, K^+). The representatives of structures of the second type are ultraphosphates of rare earth ions of the MeP_5O_{14} type, ultraphosphates MeP_4O_{11} (Me=Mn, Ca). Analysis of the spatial relations of the cation polyhedra and anion motif in these structures led to [136-138, 142, 143]. It is interesting that the ultraphosphate motif does not necessarily insure absence of contacts of the cation polyhedra: in the ultraphosphate $Cd_2P_6O_{17}$, the Cd cations are arranged in pairs [143]; in the $Sr_2P_6O_{17}$, the Sr polyhedra are bound into infinite chains [140, 143].

Thus, two groups of phosphates are now known in which the polyhedra of the rare earth cations are arranged in isolated fashion, and the spacings between the cations are quite large: these are compounds of alkali and rare earth cations and ultraphosphates of rare earth ions. The similarity of the energy structures of the levels and lifetimes of luminescence in both types of dehydrated crystalline and vitreous phosphates with high Nd^{3+} concentration indicates closeness of their structure. Concentration quenching of the luminescence in such glass is rather weakly expressed Let us note that the conclusion of reference [204] that glass belonging to the ultraphosphate region of compositions has anomalously weak concentration quenching of the Nd^{3+} luminescence independently of the chemical composition of the modifying oxides, appears to be inaccurate. First, as follows from the above-presented

investigation of crystal phosphates of RZI, the anomalously weak quenching of the luminescence must not be a property of ultraphosphate compounds alone. This is confirmed completely by the studies of the luminescence of a number of metaphosphate glasses of the type $Me^{+}Nd(PO_3)_4$ and $Me^{2+}Nd(PO_3)_5$ containing Nd^{3+} ions and ions of alkali and alkali earth metals [224, 229]. Secondly, the cation motif of crystalline ultraphosphates can be constructed differently, as has already been noted above, and, consequently, the structure and properties of the different ultraphosphate glasses can differ. The structural investigations of the ultraphosphates were started only recently and demonstrated large crystal chemical uniqueness of these compounds [143]. The spectral luminescence properties of glass have now been studied only for the simplest ultraphosphate systems with close structural characteristics, and further work is needed in this area.

As has already been pointed out above, the Nd-Nd spacing, which exceeds about 0.5 nm, is one of the necessary conditions of low concentration quenching of the Nd^{3+} luminescence, which is connected with strong dependence of the interaction of the active ions on the distances between them (Chapter 3). The total probability of the loss of excitation of the activator characterizing the degree of extinguishing of its luminescence ΣW_{DA} is proportional to $\Sigma(1/R^6)$, where the interacting activator ions located at a distance $\leqslant R$ are considered together [231]. Let us consider how this lattice sum varies for different distribution of the distances between the active ions for Nd^{3+} concentration of $2.7 \cdot 10^{21}$ cm^{-3} used in references [225-228, 238]. The average volume calculated for the Nd^{3+} ion is $370 \cdot 10^{-3}$ nm^3. For the most tightly packed arrangement of the spheres, they take up 74.05% of the total volume [148]; consequently, if we consider such packing, then the volume of the sphere corresponding to one Nd^{3+} ion is $275 \cdot 10^{-3}$ nm^3, and its radius is about 0.4 nm. The spacing between the centers of the spheres 0.8 nm is the average distance between the Nd^{3+} ions. For the tightest packing of the spheres, each sphere is surrounded by 12 adjacent ones, the lattice sum with respect to which is 46 nm^{-6}. Now let the spacings differ from the average and let two activator ions approach the central ion to 0.4 nm each, which corresponds approximately to the Nd-Nd in the chain of polyhedra connected along the edges. Then the lattice sum increases to 530 nm^{-6}, that is, by more than tenfold by comparison with the ordered distribution. If the two closest ions are removed by a distance of not 0.4, but 0.5 nm, then the lattice sum decreases to 170 nm^{-6}, that is, by 3 times. Thus, it is not the average distances, but the nearest activator-activator distances that are significant.

The study of the concentration quenching of Nd^{3+} luminescence in phosphate glass indicates [206, 229, 232, 233, 238], that its probability is only insignificantly--by 1.5 to 2 times--greater in glass than in crystals of analogous composition with low concentration quenching of the Nd^{3+} luminescence for concentrations to $(3.6 \text{ to } 4) \cdot 10^{21}$ cm^{-3}. This pertains both to ultraphosphate glass of the type $(NdLa)P_5O_{14}$, Li-Nd-FS, and so on, and to metaphosphate glass type $MeNd(PO_3)_4$ (Me=Li, Na, K, Rb). Hence, two important conclusions about the structure of the glass follow. First, the Nd^{3+} ions are comparatively uniformly (just as in crystals of this type) distributed with respect to the body of the glass, not forming associates with small Nd-Nd distances (less than about 0.5 nm). Secondly, the ordered alternation of the alkali cations and Nd^{3+} ions characteristic of crystals of double metaphosphates $MeNd(PO_3)_4$ is also retained in glass, preventing

the formation of Nd^{3+} polyhedra bound along the edges or at the apexes. The last conclusion indicates the active role of the cations in the construction of the phosphate glass structure as was noted above also for crystals.

The crystal chemical investigation of the structure of the glass and the structure of the active centers permits explanation of the laws of variation of the spectral luminescence and physicochemical properties of glass and provides a basis for structurally substantiated selection of the compositions of phosphate glass with the most expedient combination of properties for the specific applications.

CHAPTER 3. NONRADIATING ELECTRON EXCITATION ENERGY TRANSFER IN LASER GLASS

§3.1. Classification of Nonradiating Transfer Processes

In the physics of laser glass, just as other types of luminophors, an exceptional role is played by nonradiating electron excitation energy transfer (BPV), which can be defined as the physical process in which primarily the excited particle--the energy donor D*--as a result of weak interaction with another particle--the energy acceptor A--makes the transition to the electron or electron vibrational state with lower energy, with simultaneous transition of the particle A to the state with higher energy. Photon emission does not occur in this case, that is, the process is nonradiating. For significant concentrations of rare earth ions (RZI) it is necessary also to consider the possibility of the appearance of radiating transfer caused by reabsorption by the acceptor of the emission energy of the excited donor. However, the influence of this factor on the spectral luminescence and lasing characteristics of the glass is limited.

In glass which is prospective as an active medium for lasers, as a rule, the energy donors are trivalent RZI excited to one of the high electron states. Sometimes a study is also made of BPV from certain transition metal ions, for example, Cr^{3+}, Mn^{2+}, Mo^{3+}, or molecular groups, for example, UO_2^{2+} excited to the metastable electron vibrational state. The circle of energy acceptors is much wider. For any donor the acceptors can be any impurity ions or ions belonging to the glass lattice capable of absorbing transitions, isoenergetic or resonance, with the investigated radiating transition D*. As an example, let us indicate the ions Sm^{3+}, Dy^{3+}, Pr^{3+}, Yb^{3+}, Cu^{2+}, V^{4+}, Fe^{2+}, and so on for D*-ions Nd^{3+} or the ions Nd^{3+}, Sm^{3+}, Pr^{3+}, and so on for the D*-ions Er^{3+}. The requirement of isoenergetic nature is not strict. Cases are known where BPV takes place quite effectively with an energy difference in the radiating and absorbing transitions to 4000 cm^{-1} (the pairs Tb^{3+}-Yb^{3+}, Eu^{3+}-Yb^{3+}, and so on [209]). The energy acceptors must also include molecular groups, overtones of high frequency vibrations which sometimes are manifested in the infrared absorption spectra with sufficient intensity for effective BPV to energies of 5000 to 10000 cm^{-1}. As examples we have the hydroxyl groups OH^- or glass-forming anions $(SiO_4)^{4-}$, $(PO_4)^{3-}$, and so on.

Thus, beginning with the nature of the transitions participating in the BPV act, it is possible to talk about two types of BPV with participation of RZI, namely, the ion-ion (1) and ion-vibrational (2). Each of these types has, in turn, several variations.

Let us enumerate the variations of the ion-ion BVP:

1a) BPV with complete excitation energy degradation in A to thermal lattice vibrations as a result of nonradiating relaxation of the excitation between the levels to the ground state (Figure 3.1, a) (examples: $Nd^{3+}(^4F_{3/2}\rightarrow{}^4I_{9/2}$; $^4I_{11/2})$-Fe^{2+}; $Er^{3+}(^4I_{13/2}\rightarrow{}^4I_{15/2})$-$Nd^{3+}(^4I_{9/2}\rightarrow{}^4I_{15/2})$, and so on (see Figure 3.3 below).

1b) BPV with nonradiating relaxation in A to the metastable state with subsequent emission of a quantum of energy $h\omega_A<h\omega_D$ (Figure 3.1, b) (examples: $Nd^{3+}(^4F_{3/2}\rightarrow{}^4I_{9/2})$-$Yb^{3+}(^2F_{7/2}\rightarrow{}^2F_{5/2})$; $Yb^{3+}(^2F_{5/2}\rightarrow{}^2F_{7/2})$-$Er^{3+}(^4I_{15/2}\rightarrow{}^4I_{11/2})$, and so on).

1c) Cross relaxation of the excitation energy through one or two intermediate levels in the D*-A pair from the identified particles (Figure 3.1, c) (classical example: $Nd^{3+}(^4F_{3/2}\rightarrow{}^4I_{15/2}$; $^4I_{13/2})$-$Nd^{3+}(^4I_{9/2}\rightarrow{}^4I_{13/2}$; $^4I_{15/2})$).

1d) Multiple BPV with respect to like particles without significant nonradiating relaxation of the excitation energy for a unit act of BPV usually called the process of excitation energy migration with respect to the donor subsystem (Figure 3.1, d) (examples: $Nd^{3+}(^4F_{3/2}\rightarrow{}^4I_{9/2})$-$Nd^{3+}$ $(^4I_{9/2}\rightarrow{}^4F_{3/2})$-...-$Nd^{3+}$ and so on).

1e) BPV to the acceptor which is in the excited state (A*) (Figure 3.1, e) (examples: $Nd^{3+}(^4F_{3/2}\rightarrow{}^4I_{9/2})$-$Nd^{3+}(^4F_{3/2}\rightarrow{}^2P_{3/2})$; $Nd^{3+}(^4F_{3/2}$-$^4I_{9/2})$- -$UO_2^{2+}(^3\Pi_{ou}\rightarrow{}^1\Sigma_{oul})$ [246] and so on).

1f) Cooperative BPV or simultaneous excitation energy transfer from two or more donors to one unexcited acceptor with summation of the energy quanta [216, 245] (Figure 3.1, f) (example: $Yb^{3+}(^2F_{5/2}\rightarrow{}^2F_{7/2})$+$Yb^{3+}(^2F_{5/2}\rightarrow{}^2F_{7/2})$- -$Tb^{3+}(^7F_6\rightarrow{}^5D_4)$).

The versions of ion vibrational BPV (Figure 3.2) are as follows:

2a) BPV to overtones of the vibrations of the impurity molecular groups.

For oxide glass acceptors of this type can be oxyhydryl groupings $(O_nH_m)^-$ dissolved in the majority of them, of which the hydroxyl groups $(OH)^-$ have the greatest significance. In the general case, the $(OD)^-$, CH, and other groups can be analogous quenchers.

2b) Intracenter BPV to vibrations of glass forming molecular groups enter into the first coordination sphere of the D*.

These groups include the anions $(SiO_4)^{4-}$, $(PO_4)^{3-}$, $(BO_3)^{3-}$, $(GeO_4)^{4-}$, and so on.

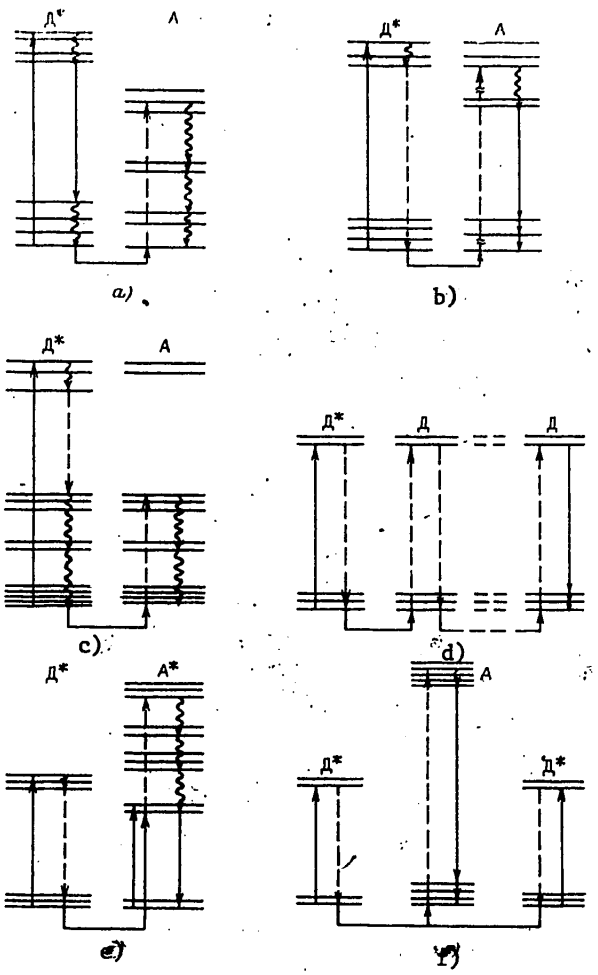

Figure 3.1. Versions of ion-ion nonradiating electron excitation energy transfer. Solid lines--radiating transitions; dotted lines--BPV D*-A; wavy lines--nonradiating transitions.

Type 2b is the most specific variation of the BPV phenomenon, for, in contrast to the others, it is present in all types of glass for any activator concentrations. All other versions of BPV are of an intercenter nature, and they can theoretically be eliminated by decreasing the acceptor concentration.

Let us also emphasize that all versions of ion-ion BPV are at least three-particle processes (D*-A-lattice phonon), inasmuch as they are continuously related to the ion-phonon interactions: direct (single phonon), multiphonon, Orbach [242, 243], and so on. These interactions permit dispersion of the excess energy during the BPV act or, vice versa, they cover the energy shortage in the case of antiStokes BPV ($h\omega_D < h\omega_A$). The ion-vibrational BPV can also be two-particle (D*+molecular group).

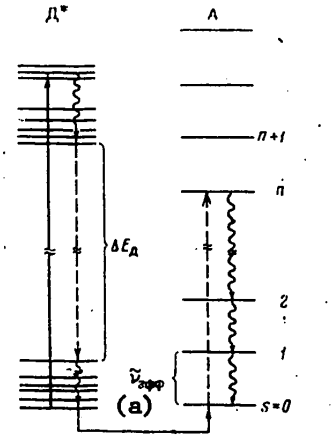

Figure 3.2. Diagram of the ion-vibrational nonradiating electron excitation energy transfer; s-- number of the vibrational mode

Key:

a. $\tilde{\nu}_{eff}$

The influence of BPV on the spectral luminescence and lasing characteristics of laser glass is dual. On the one hand, the BPV, primarily versions 1a, 1b, 1c, 2a, 2b, has negative influence on these characteristics, for it leads to nonradiating energy degradation of the metastable states of the donors and, therefore, to a reduction in quantum yield q, average duration of the luminescence τ_ℓ, a reduction in lasing efficiency and an increase in the lasing thresholds. Here BPV type 1c can be the cause of concentration quenching of the D* luminescence even in the absence of foreign quenching admixtures. The excitation migration process with respect to the D* ions does not directly cause quenching of their luminescence, but promotes it indirectly, leading to spatial convergence of excited donors with the quenching centers.

The BPV type 2b serves as a cause of negligibly small quantum yield of luminescence of the RZI from the majority of upper excited states, which sharply limits the number of potentially possible laser transitions. As for BPV type 1e and 1f, they have a nonlinear nature, that is, they depend on the excitation level. At high excitation levels characteristic of laser operating modes, their contribution to the quenching of luminscence of the metastable states of the activators in some dases also must be considered.

On the other hand, BPV is very useful, for example, when it is accompanied by the effects of sensitizing the luminescence of RZI not having natural intense absorption bands (BPV type 1b), and therefore it permits expansion of a number of ions prospective for the creation of lasing media. Thus, obtaining effective lasing on Er^{3+} and Yb^{3+} ions turned out to be possible in practice only as a result of sensitizing their luminescence by Yb^{3+} and Nd^{3+} ions respectively. The process of migration of the excitation under the conditions of strong nonuniform broadening characteristic of luminescence

and absorption bands of RZI in glass insures effective energy exchange between the activators, restoring their equilibrium distribution disturbed during the lasing process, and thus it has a positive influence on the efficiency, lasing spectrum and other characteristics of the laser. The process of nonradiating deactivation of high excited states as a result of BPV type 2b turns out to be useful if we consider the efficiency of the accumulation of excitation energy absorbed in various activator bands in the metastable state. In some cases, for example, for a laser-pumped erbium laser (Chapter 6), the energy relaxation rate between the excited states can have decisive influence on the operating efficiency of the laser. The processes type 1e and 1f are used for visual display of the infrared radiation [245].

Thus, the manifestations of BPV in laser glass are extraordinarily varied both with respect to nature and with respect to effect on the spectral luminescence and lasing characteristics of the glass. Selecting the glass composition and concentration of the activators and sensitizers, carefully purifying it of harmful admixtures and introducing useful ones, it is possible to suppress or amplify the efficiency of certain versions of the BPV and as a result, significantly to improve the lasing characteristics of the glass or create new types of glass lasers. Examples of the progress made in this approach are erbium lasers with laser pumping [101, 247], minilasers and microlasers based on concentrated neodymium glass [207, 225, 228, 229] and ytterbium lasers. However, for this purpose it is necessary carefully to study both the general laws and mechanisms of various versions of BPV and the dependence of their efficiency on the structure and composition of the glass and also the specific nature and quantitative characteristics of BPV in various pairs especially important for applications. The indicated problem was stated in general form at the dawn of the "laser age," at the beginning of the 1960's. A number of experimental and theoretical studies have been performed in the past, but we are still a long way from a really complete solution of it. The primary cause of this situation is complexity of the objects of investigation: as a rule, in real systems, several versions of BPV appear in parallel, frequently competing with each other. In addition, in the framework of each of them usually several pairs of resonance and nonresonance transitions compete with the participation of various Stark components of the initial and final state of D and A.

Let us demonstrate this in the relatively simple example of neodymium-doped glass. The luminescence from the intermediate excited states of the ions Nd^{3+}, $^4I_{11/2}$, $^4I_{13/2}$, $^4I_{15/2}$ (Figure 3.3), just as from the high excited states, is fully quenched as a result of type 2b BPV. Luminescence from the metastable state $^4F_{3/2}$ is quenched by uncontrolled admixtures from the series Fe^{2+}, Cu^{2+}, V^{4+}, Dy^{3+}, Pr^{3+}, Sm^{3+}, Er^{3+}, Tm^{3+}, Yb^{3+}, Ni, Co and so on [248] (the transitions in the Nd^{3+} ion to the $^4I_{9/2}$ and $^4I_{11/2}$ levels compete) and also on vibrations of the OH -groups (transitions to the $^4I_{13/2}$ and $^4I_{15/2}$ levels compete), and in some cases on the matrix vibrations. In addition, already for moderate concentrations of Nd^{3+} ions, approximately 1 to 2 % by weight, the cross relaxation process begins to be manifested (type 1c), where transitions compete with the participation of the $^4I_{13/2}$ and $^4I_{15/2}$ levels. The process of excitation energy migration with respect to the system of Nd^{3+} ions deepens the effect of all of the impurity quenchers. Finally, with high populations of the state $^4F_{3/2}$ (greater than 10^{19} cm^{-3}), nonlinear quenching as a result of BPV type 1e is also possible

[249]. The picture of the microscopic effects connected with BPV is still more complicated by the irregularity of the distribution of the donors and acceptors in the glass.

The noted factors complicate interpretation of the experimental data in the case of single center crystals. In glass, new complications are added to them:

1) Powerful nonuniform broadening of the spectral bands (NUP) of D* and A which lowers the probability of exact resonance of the transitions even for like interactions of the centers; in addition, spectral dependence of the probabilities of the radiating transitions [250] and, as recently demonstrated, the force of ion-phonon interaction arise [251].

2) In glass matrices consisting of like structural elements, the vibrational spectrum is richer, including, in particular, the shorter wave modes, than in the majority of ion crystals, which promotes increased probability of nonradiating transitions, and as will be demonstrated below, greater effectiveness of the nonresonating BPV.

3) A tendency toward segregation or selective entry of the activator causing its nonuniform distribution, which is observed in a number of types of multicomponent technical glass (Chapter 2).

New highly informative experimental methods have appeared only recently which permit quantitative study of various versions of BPV in glass on the level of the elementary act of interaction. These methods are primarily related to the development of procedures and equipment for selective laser excitation [252, 253] and highly sensitive systems for counting phonons with high time resolution [254].

In this chapter, on the basis of the latest experimental data an effort is made to discuss modern concepts of mechanisms and basic laws of the BPV processes in laser glass from united points of view, especially affecting the location and specific nature of phosphate systems in the general series.

§3.2. Ion-Ion Excitation Transfer--Theoretical Concepts

The modern state of the art with respect to theoretical concepts of BPV in condensed media has been discussed in the monographs [239, 240], surveys [243, 244] and other works. During this analysis it is necessary clearly to delimit the theory of the elementary BPV acts and the theory of the interrelation of the latter to the macrocharacteristics of transfer in the set of excited and unexcited donors and acceptors. The former is devoted to analysis of the mechanisms of elementary acts considering the effect on them of the solvent matrix. The latter presupposes various relations relating the macroscopic characteristics of the BPV (the kinetics of the luminescence of the donors and acceptors, the quantum yield of the donor luminescence, the effective relations of the luminescence, and so on) to the parameters of the elementary acts as a function of the nature and dynamics of the mutual arrangement of the particles D* and A and the distribution of the transition energies.

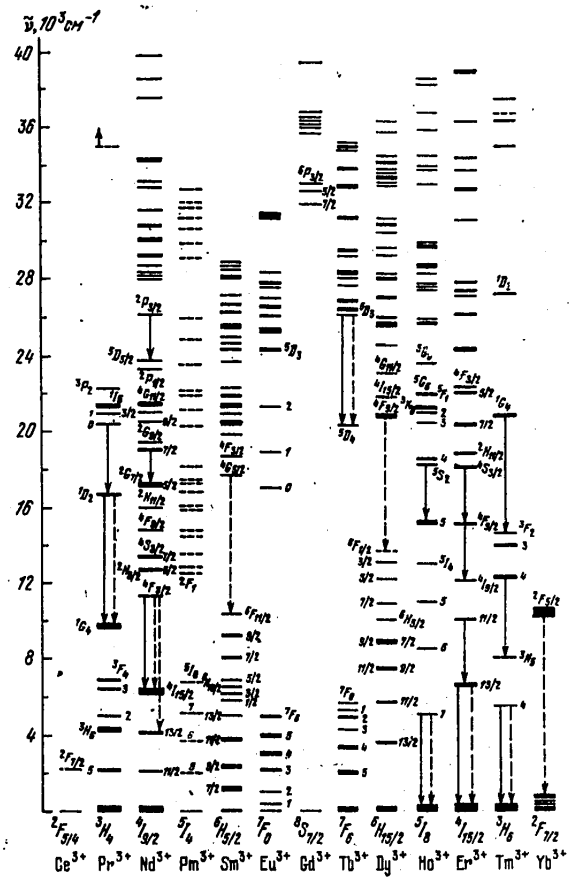

Figure 3.3. Diagram of the energy states of rare earth ions in glass [95]. Vertical solid lines--transitions investigated by the authors in the case of quenching on matrix vibrations; dotted lines--on OH-group vibrations

BPV Elementary Act. As is known, the ^{4}f-electrons of rare earth ions are shielded to the maximum and are localized by comparison with the optical electrons of all other known luminescent ions. As a result, overlap of their wave functions with the wave functions of even the nearest neighbors is very small, and the rare earth ions are weakly bound through the crystal field of the ligands to the surroundings; in other words, both for interion and for ion oscillatory interactions with the participation of rare earth ions, the case of very weak bonding is realized. The spectroscopic attributes of the weak ion-ion bond are absence of any significant (by comparison with

$\Delta\tilde{\nu}_{single}$) splitting of the spectral lines with an increase in the RZI concentration, and the ion-phonon, low intensity (especially in glass) of the electron-vibrational satellites of the electron transitions. For example, for Nd^{3+} ions in glass, they are almost undetectable, and for Yb^{3+} ions, they are observed in the absorption and luminescence spectra with an intensity, approximately 100 times less than the intensity of the phononless lines. What has been stated above must be constantly taken into account when analyzing the applicability of the general principles of the theory of the elementary act of BPV to the case of RZI in glass. At the limit of weak bonding, the probability of this act in the D*-A pair usually is recorded within the framework of the nonsteady theory of perturbations in the form [239]

$$W_{DA} = \frac{2\pi}{\hbar} |\langle H_{DA} \rangle|^2 \rho(E), \tag{3.1}$$

where $\langle H_{DA} \rangle$ is the matrix element of the Hamiltonian of interaction causing nonradiating transition, and $\rho(E)$ is the density of the finial states of the D* + A + lattice system. The form of $\langle H_{DA} \rangle$ depends on the mechanism of electron interaction in the D*-A pair and also on the propositions with respect to the nature of the ion-phonon interactions active in the BPV act. The electron interaction in the general case can be caused by electrical multipolar, magnetic dipole or exchange interactions. However, for RZI in dielectric matrices, the contribution of the magnetic dipole transitions to the optical BPV is negligibly small [242, 244], even when the electric dipole transitions are forbidden by the rules of symmetry. Strong localization of 4-f-electrons and significant minimal distances in the D-A[1] pair by comparison with the dimensions of the interacting oscillators prevent effective manifestation of the exchange interactions, inasmuch as for the latter the value of $|\langle H_{DA} \rangle|^2$ decreases with distance exponentially with the index of the order of the dimensions of the electron shells D and A. In any case, in spite of the many efforts up to the present time convincing experimental proof of noticeable contribution of the exchange interactions to the BPV between the RZI was not obtained. Thus, preference should be given to the electrostatic coulomb multipolar interaction of quantum oscillators corresponding to the interacting transitions. This type of interaction in the adiabatic approximation is characterized by the inverse exponential dependence of the square of the matrix element on the distance R_{DA} between D and A [257]:

$$|\langle H_{DA} \rangle|^2 = R_{DA}^{-m}, \tag{3.2}$$

where m is the multipole parameter equal respectively to 6, 8, 10 for the dipole-dipole, dipole-quadrupole and quadrupole-quadrupole transitions.

---

[1]The dimensions of the RZI-oscillators are less than the dimensions of the ions and the dimension of the 4-f-shell of the ion, where the transition is realized, that is, less than 0.5 to 0.6 angstroms. At the same time, the least distance from these ions to the nearest coordinating atoms of the matrix is more than 2 angstroms and, consequently, more than 3.5 angstroms to the adjacent RZI-center.

Proper consideration of the nature of the ion-phonon interactions presents a more difficult problem. The first quantitative theory of the elementary act of BPV was the theory of resonance Foerster transfer [256] later generalized by Dexter [257]. In this theory the participation of the matrix is considered phenomenologically through the overlap integral of the radiation spectrum D* and the absorption spectrum A. Here adiabatic approximation and the proposition of independence of the vibrational wave functions of D* and A are used. The theoretical result is presented below in experimentally measured values for dipole-dipole BPV:

$$W_{ДА} = \frac{9\chi^2}{128\pi^5 N_A n^4 \tau_{0Д} R_{ДА}^6} \int g_Д(\tilde{\nu})\, k_A(\tilde{\nu})\, \tilde{\nu}^{-4} d\tilde{\nu}, \qquad (3.3)$$

where $g_D(\tilde{\nu})$ is the form factor of the luminescence band or the quantum spectrum of the emission D* normalized with respect to area; $k_A(\tilde{\nu})$ is the linear absorption coefficient of the acceptor on the scale of wave numbers (cm^{-1}); τ_{0D} is the radiation lifetime of the excited state D* (sec); N_A is the concentration A (cm^{-3}); n is the index of refraction of the matrix; $\chi 2$ is the "orientation" factor taking into account the averaging of $\langle H_{DA} \rangle$ with respect to orientations of the dipole moment.

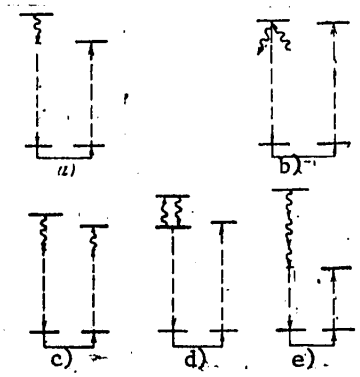

Figure 3.4. Possible diagrams of the resonance and nonresonance processes of ion-ion BPV.
a) single-phonon nonresonance; b) Raman resonance; c) two-phonon nonresonance; d) Orbach resonance; e) multiphonon nonresonance.

The simplicity of practical determination of the values entering into (3.3) and good agreement in a number of cases with the experiment gave rise to wide popularity of the Foerster theory. It was subjected several times to theoretcial checking in order more precisely to define the limits of applicability (see [239, 240]). In this respect, another phenomenological approach turned out to be fruitful--the method of the density matrix which, in particular, permits more precise determination of the weak bond condition [240]. Further progress is connected with the development of the quantum microscopic theory, in which ion-ion interaction in different approximations is considered directly. Figure 3.4 shows the basic diagrams of the ion-ion BPV

(two-level approximation) with the participation of different ion-phonon interactions.[1] Table 3.1 gives a brief summary of the results obtained in the framework of microtheory. For the two-phonon processes of type b and d its conclusions coincide with accuracy to the correction factor with the results of the phenomenological approach. This is not unexpected inasmuch as the indicated processes, as is known from [240], determine the mechanisms of uniform broadening of the spectral bands. With respect to all data, they make a decisive contribution to the total efficiency of the BPV in the resonance region $\tilde{\varepsilon}<\Delta\tilde{\nu}_{single}$ where $\tilde{\varepsilon}=|E_D-E_A|$. The single-phonon process

Table 3.1

(1) №№ по рис. 3.4	(2) Зависимость $W_{ДА}(\tilde{\varepsilon})$	(3) Зависимость $W_{ДА}(T)$: $T\ll\theta_D$	(3) $T>\theta_D$	(4) Источник данных
a	$W_{ДА}\propto\tilde{\varepsilon}^s$ $s=1-3$	$\propto\left[\exp\frac{\tilde{\varepsilon}}{k_Б T}-1\right]^{-1}$	$\propto T$	[240, 242, 243, 261—266, 269—271]
b	$W_{ДА}\propto\tilde{\varepsilon}^{-3}$	$\propto T^7$	$\propto T^2$	[265]
c	$W_{ДА}=\text{const}$	$\propto T^3$	$\propto T^2$	[265]
d	$W_{ДА}\propto\tilde{\varepsilon}^{-3}$	$\propto\Pi_i\exp\left(-\frac{\Delta E_i}{k_Б T}\right)$	$\propto T^2$	[265]
e	$W_{ДА}\propto\exp(-\alpha\tilde{\varepsilon})$	$\propto\left[\exp\frac{\tilde{\varepsilon}}{k_Б T}-1\right]\left[-k_Б\theta_D/\tilde{\varepsilon}\right]$	$\propto T^{k_Б\theta_D/\tilde{\varepsilon}}$	[258]

θ_D is the Debye temperature of the given matrix; ΔE_i is the energy difference between the operand and the metastable states; α is a parameter.

Key:
1. Numbers according to Figure 3.4
2. Function $W_{DA}(\tilde{\varepsilon})$
3. Function $W_{DA}(T)$
4. Data source

type a is ineffective here on the basis of low density of the phonon states of the matrix which for $\tilde{\varepsilon}<<\tilde{\nu}_D$, where $\tilde{\nu}_D$ is the Debye frequency (on the scale of the wave numbers); is usually proportional to $\tilde{\varepsilon}^2$ [242]. The above-mentioned correction factor depends on R_{DA} and can be appreciably less than one for small R_{DA} on the order of several lattice constants [273, 274]. Inasmuch as for an effective interaction radius of the RZI R_0 determined from the condition $W_{DA}=(\bar{\tau}_{\ell D})^{-1}$, where $\bar{\tau}_{\ell D}$ is the average duration of D* luminescence in the absence of A, these parameters are characteristic,

[1] The BPV diagrams with the participation of virtual phonons [240, 260, 259] and excitons [240] of the matrix have still not been taken into account, for it is assumed that the investigated transitions are located far from the fundamental bands in the infrared and ultraviolet absorption spectra of the glass.

this factor must be considered. However, its numerical estimates for RZI in glass are unknown. When analyzing the resonance BPV it is also necessary to consider the type b process, the probability of which does not have a simple relation to the band widths.

The single-phonon BPV process becomes weighty in the region $\Delta\tilde{\nu}_{single}<\tilde{\varepsilon}\lesssim\tilde{\nu}_D$. Depending on the propositions regarding the mechanism of ion-phonon interaction by the magnitude of the parameter $q_\nu=2\pi c\tilde{\nu}R_{DA}/v_{sound}$ (v_{sound} is the speed of sound in the medium) characterizing the relation between R_{DA} and the wavelength of the active phonon in the BPV act, various relations $W_{DA}(\tilde{\varepsilon})$ are obtained for it. However, it must be emphasized that in all cases they turn out to be increasing, having an exponential form with the exponent s=1-3. In references [271, 272], in the expression for W_{DA} for $q_\nu>>1$, an additional dependence on R appears in the form of the factor proportional to R_{DA}^{-2}. Let us also note that one of the investigated mechanisms of single phonon nonresonance BPV corresponds in Foerster theory to overlap of the phononless bands and single-phonon wings in the D* and A spectra. However, in [240, 266, 271] it is demonstrated that this concept is valid only in the region $q_\nu>>1$, that is, for $\tilde{\varepsilon}>100$ cm^{-1}, if R_{DA}=10 angstroms, $v_{sound}\sim 5\cdot 10^5$ cm·sec^{-1}. Nevertheless, for RZI in glass, the region $\tilde{\varepsilon}\lesssim 100$ cm^{-1} is of greatest interest, inasmuch as the values of $\Delta\tilde{\nu}_H$=5-100 cm^{-1} and $\Delta\tilde{\nu}_{single}$ from 10^{-4}-10^{-3} cm^{-1} at low temperatures to 5-20 cm^{-1} at 300 K are characteristic for them.

In the multiphonon region $\tilde{\varepsilon}>\tilde{\nu}_{max}\gtrsim\tilde{\nu}_D$, where $\tilde{\nu}_{max}$ is the boundary frequency of the spectrum of basic vibrations of the matrix, the function $W_{DA}(\tilde{\varepsilon})$ again becomes decreasing close to the exponential curve. Thus, the microtheory of BPV has made it possible more precisely to define the limits of applicability of the Foerster theory and has proposed several mechanisms, for the phenomenological approach obviously not considered. Unfortunately, on the basis of indeterminacy of the approximations made in different models and also as a result of the presence of parameters not subject to direct experimental determination, the microtheory of BPV does not permit calculation of absolute and relative efficiencies of the interactions caused by these mechanisms, which complicates the selection between the transfer models in specific experimental situations. Nevertheless, the conclusions of the theory of the nature of the functional dependencies $W_{DA}(\tilde{\varepsilon})$, $W_{DA}(R_{DA})$ and $W_{DA}(T)$ put the "keys" in the hands of the experimenter for checking its principles and discovering the predominating mechanisms of the ion-ion transfer between RZI.

Interrelation of the Macrocharacteristics of BPV with the Parameters of the Elementary Acts. With respect to nature of occurrence of the energy transfer processes in the D*+A system, usually two situations are distinguished: static and dynamic. The sign of the static nature of the BPV is absence of spatial wandering of the excitation with respect to the donor subsystem, which is typical of small donor concentrations. The procedure of averaging the probabilities of elementary acts with respect to configurations of the set of statistically uniformly distributed particles of the donor with respect to the acceptor was first proposed by Foerster [256]. Later, it was developed

in references [274-279] and a number of other studies. In the case of multiple approximation of the donor-acceptor interaction the luminescence damping kinetics D* are described by the expression

$$N_{Д}(t) = Y(t)\exp\left\{-\frac{4\pi}{3}\mathcal{N}_{A}\Gamma\left(1-\frac{3}{m}\right)C_{ДA}^{3/m}t^{3/m}\right\} \qquad (3.4)$$

and, in particular, for dipole-dipole interaction by the relation

$$N_{Д}(t) = Y(t)\exp\left[-\gamma\sqrt{t}\right], \qquad (3.4a)$$

where $N_D(t)$ is the population of the radiating state D*; the function $Y(t)$ expresses the luminescence damping law D* in the absence of A (in the general case, nonexponential); $\Gamma(x)$ is the gamma function; C_{DA} is the microparameter of the interaction D*-A related to W_{DA} by the expression $W_{DA}(R)=C_{DA}R_{DA}^{-m}$; γ is the parameter determined from the expression

$$\gamma = \frac{4\pi^{3/2}}{3}C_{ДA}^{1/2}\mathcal{N}_{A}. \qquad (3.5)$$

The formulas (3.4), (3.4a) are valid for the following restrictions: 1) the inverse transfer A*→D is absent; 2) $\mathcal{N}_{D^*} \ll \mathcal{N}_{D}$; 3) $\mathcal{N}_{A}/\mathcal{N}_{max} \ll 1$, where $\mathcal{N}_{max}$ is the total number of places which could be occupied by acceptors per unit volume. The last restriction provides that the averaging be carried out within the limits of the statistically uniform distribution of D* with respect to A without considering a finite number of places which can be occupied by the acceptors in the nearest coordination spheres near D*; this is admissible only for small A concentrations. The case $N_A/N_{max}\to 1$ was investigated in [274, 279]. It was demonstrated that here the luminescence decay kinetics approach exponential with characteristic time determined by the total sum of the probabilities of the interaction with respect to all nodes of the acceptor sublattice. The exponential kinetics are manifested first of all in the initial phase of the process of luminescence decay. In [280], consideration is given to the influence of the minimum distance of approach of the donor and the acceptor R_{min}. It is demonstrated that in the initial stage of decay (for $t \ll R_{min}^6/C_{DA}$) there is a relatively short exponential section which can be noted for $N_A \to N_{max}$ or for very small interactions, that is, for $C_{DA}\tau_D \to R_{min}^6$.

The formulas (3.4), (3.4a) are derived for the case of excitation by a δ-pulse. The damping law for any other type of excitation can be written in the form of a convolution in time:

$$N'_{Д}(t) = \int_0^t N_{Д}(\tau)\lambda(t-\tau)\,d\tau, \qquad (3.6)$$

where $\lambda(t)$ is the shape of the optical excitation pulse. For example, after switching off the steady-state excitation, the luminescence damping kinetics are significantly closer to exponential than (3.4) [275]. The decay law with an exchange nature of the interactions in the pairs D*-A also differs sharply from that described by formula (3.4) [278]. Nevertheless, in spite of the indicated restrictions, the law (3.4) is quite universal and applicable

according to [286], also to the media with nonuniform broadening if instead of W_{DA} we use the probability $\overline{W}_{DA}$ averaged with respect to the transition energies.

With increased concentrations of D, the process of quenching by the acceptor is stimulated by migration of the excitations with respect to the donor subsystem and when finding the function $N_D(t)$ it is necessary to consider the dynamics of the spatial distribution of D* with respect to A. This situation is more complicated for interpretation and it is described within the framework of various models of quenching [274, 278-288]. Qualitatively, the energy migration with respect to D leads in all models to an increase in the rate of the luminescence decay process and its exponentialization in the final phase. The parameter of the exponential curve $\overline{W}$ defining the rate of migrations controlled quenching of luminescence of D* depends not only on N_A and C_{DA}, but also on the concentration of the donors N_A and probability of the elementary act of donor-donor interactions $W_{DD}=C_{DD}R_{DD}^{-m}$. However, the form of this function is essentially different in different theoretical models. Analysis of the conditions of applicability of one model or another, their approximations and limitations can be found in references [281, 284]. The results of such an analysis reduce to the following.

First, it is necessary to distinguish the migration controlled phase of quenching from the kinetics phase.[1] The condition of realizing migration controlled quenching has the form $W_{DA}<<\xi$, where $\xi=W_{DA}^{min}(\tau_A)^{-1}/(W_{DA}^{min}+(\tau_A)^{-1})$ defines the rate of irreversible energy runoff to the acceptor subsystem; W_{DA}^{min} is the probability of the elementary act of BPV at a minimum distance R_{min}; $(\tau_A)^{-1}$ is the average energy relaxation rate in the acceptors. Thus, the bottleneck in the given case is the migration rates of the energy with respect to the donor subsystem. In the kinetic stage of quenching ($W_{DD}>>\xi$) the limiting factor is the excitation energy discharged through the acceptors. Here the luminescence quenching rate can be limited by the transport D*-A ($W_{DA}^{min}<<(\tau_A)^{-1}$) or the excitation relaxation in the acceptors $W_{DA}^{min}>>(\tau_A)^{-1}$).

Secondly, in the migration controlled phase the quenching kinetics are described within the framework of the diffusion or jump limits. The former is applicable for a ratio of $C_{DA}>>C_{DD}$. The solution of the diffusion equations is found in different approximations in references [274, 279, 280, 283, 284, 287-289, 291, 292]. The asymptotics obtained by different authors do not agree with each other. For resonance dipole-dipole interactions in the pairs D*-D and D*-A for uniformly broadened transition bands, the process can be approximated by the following analytical function [281, 293]:

$$N_D(t) = \exp\left(-\frac{t}{\tau_{0D}} - \gamma\sqrt{t} - \overline{W}t\right), \qquad (3.7)$$

[1] The latter is sometimes called "supermigration" [281].

where

$$\overline{W} = A\mathcal{N}_{\text{А}}\mathcal{N}_{\text{Д}}(C_{\text{ДА}})^{(1-x)}(C_{\text{ДД}})^{x}, \tag{3.8}$$

different authors use different values of the coefficient A, and the value of x varies from 5/6 to 3/4.

For $C_{DD}>C_{DA}$ the application of a jump limit is more substantiated. In this case the results of references [273, 274, 279, 282-286, 289, 291, 292] are much closer to each other:

$$\overline{W} = B\mathcal{N}_{\text{А}}\mathcal{N}_{\text{Д}}C_{\text{ДА}}^{0,5}C_{\text{ДД}}^{0,5}. \tag{3.9}$$

However, the values of the coefficient B do not coincide here, varying as a function of the simplifying assumptions made within the limits of 16 to 27. Uniformity of expressions (3.8) to (3.9) was also confirmed by numerical simulation [287], but here the coefficient B turned out to be smaller: B was equal to approximately 14 for ordered arrangement of D and 3.5 for random arrangement. Finally, the calculations performed in [289] demonstrated that the function (3.9) is maintained with an error to 10% in the region $C_{DD}\geq 0.5C_{DA}$.

Thirdly, the kinetic stage of quenching is realized in a broad range of concentrations $N_D>N_D^{cr}$, where $N_D^{cr}=\left(\frac{2\pi}{3}\right)^{-1,5}\left(\frac{C_{\text{ДА}}}{C_{\text{ДД}}}\right)^{0,5}(R_{\min})^{-3}$, except in the jump model.

Here

$$\overline{W} = \frac{2}{3}\pi^2\mathcal{N}_{\text{А}}C_{\text{ДА}}(R_{\min})^{-3} \tag{3.10}$$

and does not depend on N_D and C_{DD} [284, 285]. At the diffusion limit the kinetic phase is attainable only in the region $N_D/N_{max}\to 1$.

The above discussed results are obtained under the assumption of resonance dipole-dipole nature of the interaction of the donors with uniformly broadened bands. The equation for $N_D(t)$ considering nonuniform broadening was obtained at the jump limit in reference [290]. Its approximate solution when replacing real probability distribution of the elementary acts of energy migration in the donor subsystem by δ-distribution with some average probability $\overline{W}_{\text{ДД}}=\frac{8\pi^3}{27}\overline{C}_{\text{ДД}}\mathcal{N}_{\text{Д}}^2$ has the form [516]

$$\overline{W} = \int_0^\infty \frac{\overline{W}_{\text{ДА}}(R)\,g'(R)\,dR}{1+\overline{W}_{\text{ДА}}(R)/\overline{W}_{\text{ДД}}}, \tag{3.11}$$

where g'(R) is the distribution density of the acceptor around D*. Formula (3.11) is quite common, for it is valid both in the case of multipole and for exchange nature of D-D and D-A interactions, and it describes the migration controlled and kinetic stages of luminescence quenching. In the limiting cases $\overline{W}_{DD}\ll\xi$ and $\overline{W}_{DD}\gg\xi$ with dipole-dipole nature of the interactions its asymptotics coincide with (3.9) and (3.10), respectively.

Thus, at the present time theory presupposes quite simple relations between the relation of the integral kinetics of luminescence decay D* and the micro-parameters of the elementary act of D-D and D-A-interactions, and certain stipulations used also in the case of activated glass. They provide the basis for the method of precision investigation of the integral kinetics of luminescence or the method of microparameters most comprehensively developed in [281, 283, 293]. This method permits certain definition of the micro-parameters averaged with respect to energies of the D-A interactions $\overline{C}_{DA}$ and m and in the case of realization of the kinetic phase of quenching, estimation of the distance R_{min}. At the same time, the estimates of the parameter $\overline{C}_{DD}$ are less exact and possible only in the presence of preliminary information about the multipole nature of the interactions D-D. In real experimental situations, the choice between models of migration controlled quenching of luminescence is also complicated.

More complete information about the microparameters and mechanisms of donor-donor interactions is permitted to be obtained by the methods of investigating spectral migration in the donor subsystem. This migration is specifically characteristic of media with NUP, and it is manifested for the corresponding setup of the experiment, for example, for low temperatures or selected excitation, in the time evolution of the spectral composition of luminescence. Efforts at theoretical description of the spectral migration were undertaken in references [252, 266, 290, 294-301]. The most successful of them obviously is reference [290], in which it was possible to obtain, in particular, relations generalizing formula (3.4) to the case of the luminescence quenching law of spectrally isolated centers in various sections of the resonance NUP curve:

$$N_{Д}(E, t) = g(E)\, Y(E, t) \exp\left[-\frac{4\pi}{3}\Gamma\left(1-\frac{3}{m}\right) N_{Д} t^{3/m} F(E)\right], \qquad (3.12a)$$

where

$$F(E) = \int_0^E [C_{ДД}(\tilde{\varepsilon})]^{3/m}\, g(E-\tilde{\varepsilon})\, d\tilde{\varepsilon}. \qquad (3.12b)$$

For known $N_D(E, t)$ and $Y(E, t)$ expressions (3.12) permit determination of the parameter m and the functional dependence $C_{DD}(\tilde{\varepsilon})$ which sheds light on the mechanism of the interactions D-D, which was used as the basis for the method of selective observation of the kinetics of the quenching of luminescence on the shortwave branches of the resonance lines (SNKL) [254]. Additional information about the mechanisms of interactions and relative contribution of transitions between different Stark components can be given by the temperature functions $\overline{C}_{DA}(T)$ and $\overline{W}(T)$ [290].

Thus, the results of investigating the integral and selective kinetics of the damping of the D* luminescence carry sufficient information to determine the microparameters and mechanisms of donor-donor and donor-acceptor interactions and their interrelation to the structure of laser glass. Let us emphasize that the study of the concentration and temperature dependence of other characteristics of BPV, for example, the quantum yield q or the average

duration of the luminescence $\bar{\tau}_{\ell D}$ does not have analogous informativeness, and it is necessary to take a critical position with respect to the conclusions drawn on the basis of it regarding the mechanisms of pair interactions.

§3.3. Ion-Ion Transfer--Experimental Results

Analysis of the Published Data. At the present time a number of experimental papers have been concluded, in which certain characteristics of the BPV processes are presented for different pairs of rare earth ions in glass. The known reviews of these papers became obsolete long ago [82-85, 302]. An effort is made below to classify the published data and to some degree analyze their quality and reliability.

The greater part of the experimental papers are devoted to studies of such macroscopic characteristics of the BPV as dependence of the density of luminescence, quantum yield and some "effective duration of luminescence" of the donors on the concentration of the acceptors and in a number of cases on the composition of the glass and temperature. The data presented in Table 3.2, not pretending to completeness, permit an idea to be formed of the volume and the accents in the performed research. As we shall see, primary attention is given to silicate systems and then phosphate systems, and among the investigated pairs, the pairs important for laser applications Nd^{3+}-Nd^{3+}, Nd^{3+}-Yb^{3+}, Yb^{3+}-Er^{3+} and certain others predominate. The series of indicated papers is characterized by an arbitrary choice of compositions of glass, imperfection of procedures and experimental equipment and absence of clarity in defining the concept of "effective luminescence duration." In many cases when analyzing the quenching processes, consideration is not given to possible competition on the part of the accompanying impurities which are not taken into account, for example, the OH-groups. The conclusions of these papers regarding the mechanisms of pair interactions, as has already been noted above, must be approached with caution. Nevertheless, the research has made it possible to obtain primary information about the efficiency and specific nature of the BPV processes in one pair or another, and it has created defined prerequisites for deeper research.

In another group of papers laser methods of studying transport processes are developed. This group must include the cycles of works in which investigations are made of the dynamics of the reproduction of the equilibrium curve of the luminescence band of rare earth ions after clearing of the latter by passage of a single band laser pulse through the sample [346, 348, 380-382], the dynamics of development of the generation spectra [202, 384], lasing kinetics [202, 335, 353] and other processes. The limited nature of the laser methods consists in the fact that for implementation of them it is necessary to have a powerful pulse source of coherent radiation with lasing frequency coinciding with the frequency of the luminescence band of the investigated transition of the rare earth ions; in some cases the lasing mode must be implemented in the investigated sample itself. Therefore at the present time the circle of BPV processes investigated by such methods is limited to migration of the excitation energy with respect to the Nd^{3+} ions in silicate and phosphate glass. In addition, the obtained results reduce only to estimating the phenomenological characteristics of energy migration defined in one way or another, the unique relation of which to the parameters of the elementary acts cannot be traced.

In recent years various versions of the chronospectroscopic or spectroscopic method with time selection for investigation of resonance luminescence of rare earth ions in glass combined with the methods of selective excitation of individual types of luminescing centers have developed quickly [389, 394]. Selective excitation of rare earth ions in glass was used for the first time in reference [415] to investigate Eu^{3+} ions, and the presence of spectral migration was discovered, which insures establishment of equilibrium in the set of luminescence centers. The method of selective excitation supplemented by the chronospectroscopic method of recording was later used many times to study the parameters of the spectral and spatial migration of energy with respect to the ions Nd^{3+} [370, 379, 383, 387, 388], Yb^{3+} [301, 351, 377], Eu^{3+} [251-253, 349, 371, 375, 377, 379, 389, 390] in phosphate, silicate, borosilicate, fluoberyllate and germanate glass. In the majority of indicated papers, only qualitative estimates were obtained for the phenomenological migration parameters. In some cases conclusions were drawn regarding the mechanism of elementary acts of the interactions. However, the procedures for processing the results of such studies have still been insufficiently developed, and they do not permit reliable identification of the mechanism of interaction or the obtaining of quantitative data on the microparameters of migration. In this sense, the situation with investigation of migration in Eu^{3+}-doped glass is characteristic. In reference [252], the mechanism of the elementary act is defined as dipole-dipole nonresonance single-phonon, in [253], as quadrupolar-quadrupolar resonance, in [375], as dipole-dipole two-phonon nonresonance, and, finally, in [390], as dipole-dipole resonance.

More reliable and complete results can be obtained on combination of the chronospectroscopic method of recording, selective excitation and low temperatures ($k_BT<<\Delta\tilde{\nu}_H$) where the processes of phonon absorption are "frozen" and BPV within the limits of the NUP curve proceeds only in the direction of lower energies. Obviously, this fact was first indicated in [372], where for 4.2 K in silicate glass, a long wave shift of the luminescence band of the Yb^{3+} ions is noted (the transition $^2F_{5/2}(1)\rightarrow{}^2F_{7/2}(1)$) on excitation of them by quasimonochromatic emission with frequency $\tilde{\nu}_H=10330$ cm^{-1} to the short wave edge of the resonance absorption band, and a valid interpretation of it is given qualitatively. Later, long wave concentration shift of the luminescence band of Yb^{3+} ions, and then Nd^{3+} was investigated in detail during wide-band excitation in silicate, phosphate and fluophosphate glass in the cycle of papers [294, 356, 357, 369, 373, 384, 392]. The authors of these papers, confirming the conclusion of [372] regarding the single phonon nonresonance mechanism of BPV between the Yb^{3+} ions in glass of $k_BT<<\Delta\tilde{\nu}_H$, tried many times to calculate the relation from the experimental data for the phenomenological value introduced in a defined way which characterizes the effective spectral migration rate of the excitation as a function of the difference in energies of the interacting transition ε. However, such efforts do not give any unique result. Only recently when using selective excitation of Yb^{3+} ions, were qualitatively valid data obtained [301]. In Figure 3.5, for phosphate glass with $N_{Yb}=7\cdot10^{20}$ cm^{-3}, the form of the resonance luminescence band of Yb^{3+} ions is presented for narrow band excitation by krypton tube emission with $\tilde{\nu}_B=10254$ cm^{-1} (1) and absorption (2) corresponding to the transition

Table 3.2

D*	Переход (1)	A	(1) Переход	Тип БПВ (2)	Источник данных (3)
Nd^{3+}	$^4F_{3/2} \rightarrow {}^4I_{13/2;15/2}$	Nd^{3+}	$^4I_{9/2} \rightarrow {}^4I_{13/2;\ 15/2}$	1в	[74(ф), 83(с, ф), 84(ф), 85(с), 209(с, б/с), 223 (с, ф), 225 (ф), 226 (ф), 229 (ф), 236 (с, ф), 303 (с, б), 304 (с, ф), 305 (с), 306 (с, ф, б, г, б/с), 307 (к), 308 (с), 309 (ф), 310 (с, г), 311 (с), 368 (с), 470 (с)]
	$^4F_{3/2} \rightarrow {}^4I_{15/2}$	Nd^{3+}	$^4F_{3/2} \rightarrow {}^2G_{7/2}$	1д	[249 (с)]
	$^4F_{3/2} \rightarrow {}^4I_{9/2}$	Yb^{3+}	$^2F_{7/2} \rightarrow {}^2F_{5/2}$	1б	[82 (с), 101 (ф), 304 (с), 315 (с), 318 (б), 320 (б), 331 (с), 339 (с), 336 (ф/б), 347 (ф, с), 358 (б/с), 360 (б), 369 (ф), 385 (с)]
		UO_2^{2+}	$^3\Pi_{0u} \rightarrow {}^1\Sigma^-_{0u}$	1д	[246 (с, ф, б/ф), 359 (с, ф, б/ф)]
		Er^{3+}	$^4I_{15/2} \rightarrow {}^4I_{11/2}$	1б	[248 (с, ф), 338 (ф, ф/ф), 361 (ф, с)]
	$^4F_{3/2} \rightarrow {}^4I_{11/2}$	Pr^{3+}	$^3H_4 \rightarrow {}^1G_4$	1б	[248 (с, ф)]
		Sm^{3+}	$^6H_{5/2} \rightarrow {}^6F_{9/2}$	1а	Тот же (4)
	$^4F_{3/2} \rightarrow {}^4I_{11/2;9/2}$	Dy^{3+}	$^6H_{15/2} \rightarrow {}^6F_{5/2};\ {}^6H_{5/2}$	1а	Тот же
	$^4F_{3/2} \rightarrow {}^4I_{13/2}$	Tm^{3+}	$^3H_6 \rightarrow {}^3H_5$	1б	Тот же
	$^4F_{3/2} \rightarrow {}^4I_{11/2}$	Ho^{3+}	$^5I_8 \rightarrow {}^5I_5$	1б	Тот же
	$^4F_{3/2} \rightarrow {}^4I_{15/2}$	Tb^{3+}	$^7F_6 \rightarrow {}^7F_{0;\ 1}$	1а	Тот же
		Eu^{3+}	$^7F_0 \rightarrow {}^7F_6$	1а	Тот же
	$^4F_{3/2} \rightarrow {}^4I_{9/2;11/2}$	Cu^{2+}		1а	Тот же
		V^{4+}		1а	Тот же
		Ni^{2+}		1а	Тот же
		Fe^{2+}		1а	Тот же
Yb^{3+}	$^2F_{5/2} \rightarrow {}^2F_{7/2}$	Er^{3+}	$^4I_{15/2} \rightarrow {}^4I_{11/2}$	1б	[48 (ф, с), 85 (с, ф), 101 (ф), 312 (с), 326 (с), 332 (с), 338 (ф/ф, г), 339 (с), 360 (б), 361 (с, ф/ф, ф), 386 (с)]
		Er^{3+}	$^4I_{13/2} \rightarrow {}^4F_{9/2}$	1д	[343 (г)]
		Ho^{3+}	$^5I_8 \rightarrow {}^5I_6$	1б	[317 (с), 332 (с), 366 (с, ф)]
		Tm^{3+}	$^3H_6 \rightarrow {}^3H_5$	1б	[317 (а/с)]
		Tm^{3+}	$^3H_4 \rightarrow {}^3F_3;\ {}^3F_4 \rightarrow {}^1G_4$	1д	[343(г)]
		Nd^{3+}	$^4I_{9/2} \rightarrow {}^4I_{15/2}$	1а	[374 (б)]
		UO_2^{2+}	$^3\Pi_{0u} \rightarrow {}^1\Sigma^-_{0u}$	1д	[359 (с, ф)]
$Yb^{3+}+Yb^{3+}$	$^2F_{5/2} \rightarrow {}^2F_{7/2}$	Tb^{3+}	$^7F_6 \rightarrow {}^5D_4$	1е	[362 (ф, г)]
Er^{3+}	$^4I_{13/2} \rightarrow {}^4I_{15/2}$	Tm^{3+}	$^3H_6 \rightarrow {}^3I_4$	1б	[317 (а/с), 344 (ф, б)]
		Ho^{3+}	$^5I_8 \rightarrow {}^5I_7$	1б	[332 (с), 345 (ф/ф), 366 (с, ф)]
		Nd^{3+}	$^4I_{9/2} \rightarrow {}^4I_{15/2}$	1а	[339 (с), 361 (с, ф)]
		Er^{3+}	$^4I_{13/2} \rightarrow {}^4I_{9/2}$	1д	[338 (ф, фт, ф/ф, г)]
Eu^{3+}	$^5D_0 \rightarrow {}^7F_{0;\ 1}$	Yb^{3+}	$^2F_{7/2} \rightarrow {}^2F_{5/2}$	1б	[241 (с, ф, г, б/с)]
	$^5D_0 \rightarrow {}^7F_{0;\ 1;\ 2;\ 3}$	UO_2^{2+}	$^3\Pi_{0u} \rightarrow {}^1\Sigma^-_{0u}$	1д	[246 (ф, с), 359 (ф, с)]

Key: 1--Transition; 2--Type of BPV; 3--Data source; 4--the same

[Table 3.2, continued]

D*	Переход (1)	A	Переход (1)	Тип БПВ (2)	(3) Источник данных
Tb^{3+}	$^5D_4 \rightarrow {}^7F_0$	Yb^{3+}	$^2F_{7/2} \rightarrow {}^2F_{5/2}$	1б	[241 (с, ф, г, б/с)]
		Nd^{3+}	$^4I_{9/2} \rightarrow {}^2G_{9/2}$	1б	[363 (ф)]
	$^5D_3 \rightarrow {}^5D_4$	Pr^{3+}	$^3H_4 \rightarrow {}^3F_2$; 3	1а	[352 (ф)]
		Tb^{3+}	$^7F_6 \rightarrow {}^7F_0$; 1; 2	1е	Тот же (4)
		Tm^{3+}	$^3H_6 \rightarrow {}^3H_4$	1б	Тот же
		Dy^{3+}	$^6H_{15/2} \rightarrow {}^6H_{11/2}$	1а	Тот же
		Nd^{3+}	$^4I_{9/2} \rightarrow {}^4I_{15/2}$	1а	Тот же
		Sm^{3+}	$^6H_{5/2} \rightarrow {}^6F_{1/2}$; 3/2	1а	Тот же
Sm^{3+}	$^4G_{5/2} \rightarrow {}^6H_{5/2}$; 7/2	Eu^{3+}	$^7F_0$; $_1 \rightarrow {}^5D_0$	1б	[313 (ф), 314 (ф, б)]
Tm^{3+}	$^1D_2 \rightarrow {}^3H_6$	Er^{3+}	$^4I_{15/2} \rightarrow {}^2G_{7/2}$; 9/2	1б	[313 (ф, б), 364 (ф, б)]
Gd^{3+}	$^6P_{7/2} \rightarrow {}^8S_{7/2}$	Tb^{3+}	$^7F_6 \rightarrow$	1б	[313 (ф, б), 321 (с)]
Cu^+	—	Tb^{3+}	—	1б	[328 (с)]
Ce^{3+}	—	Nd^{3+}	—	1б	[315 (а/с), 316 (а/с), 319 (с), 327 (с)]
	—	Yb^{3+}	—	1б	[316 (а/с)]
	—	Tb^{3+}	—	1б	[328 (с)]
	—	Tm^{3+}	—	1б	[367 (б)]
Cr^{3+}	—	Nd^{3+}	$^4I_{9/2} \rightarrow {}^4F_{3/2}$; 5/2; 7/2	1б	[327 (с), 329 (с)]
	—	Yb^{3+}	$^2F_{7/2} \rightarrow {}^2F_{5/2}$	1б	[330 (с), 333 (с), 361 (с, ф)]
Mn^{2+}	—	Nd^{3+}	—	1б	[295 (с), 325 (с), 327 (с), 337 (ф)]
	—	Er^{3+}	—	1б	[337 (с)]
	—	Ho^{3+}	—	1б	[337 (с)]
Mo^{2+}		Er^{3+}	—	1б	[330 (с)]
UO_2^{2+}	$^3\Pi_{0u} \rightarrow {}^1\Sigma_g^+$	Nd^{3+}	$^4I_{9/2} \rightarrow {}^2G_{9/2}$; 7/2; $^4S_{5/2}$	1б	[246 (ф, б/ф, с), 315 (с), 324 (с), 325 (с), 354 (с), 359 (ф, с, б/ф), 365 (с)]
	—	Eu^{3+}	$^7F_0$; $_1 \rightarrow {}^5D_0$	1б	[246 (ф, с, б/ф), 322 (б/с), 354 (ф), 359 (ф, с, б/ф)]
	—	Er^{3+}	$^4I_{15/2} \rightarrow {}^4S_{3/2}$; $^2H_{11/2}$	1б	[323 (с)]

The letter in parentheses indicates which glass is investigated in the given paper: с--silicate, ф--phosphate, б--borate, б/с--boroscilicate, б/ф--borophosphate, г--germanate, ф/ф--fluophosphate, ф/б--fluoberyllate, ФТ--fluoride, а/с--alumosilicate, к--quartz.

Key: 1--Transition; 2--Type of BPV; 3--Data source; 4--the same

$^2F_{5/2}(1) \rightleftarrows {}^2F_{7/2}(1)$, and in Figure 3.6, the spectral dependence of the macroscopic characteristic of the energy migration process w_ϕ using the expression $w_\phi(\tilde{\varepsilon} = \tilde{\nu}_в - \tilde{\nu}) \sim I_л(\tilde{\nu})/g(\tilde{\nu})$. This relation confirms on the phenomenological

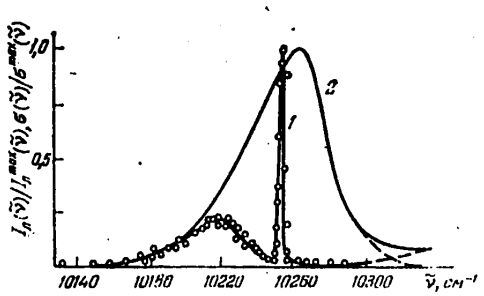

Figure 3.5. Form of the resonance band corresponding to the transition $^2F_{5/2}(1) \rightleftarrows {}^2F_{7/2}(1)$ of Yb^{3+} ions in phosphate glass [301].
1--luminescence with selective excitation, 2--absorption.
$N_{Yb} = 7 \cdot 10^{20}$ см$^{-3}$.

level the theoretically important results previously established [254] using the SNKL method: a sharp increase in probability of the elementary BPV act within the limits of the NUP with an increase in $\tilde{\varepsilon}$ which is valid at least for $K_BT \lesssim \Delta\tilde{\nu}_H$ and refutes the widespread opposite opinion based on preference given to the resonance mechanisms of BPV.[1] Let us note that the function $w_\phi(\tilde{\varepsilon})$ does not have a simple relation to the probability of the elementary act so that it is at least difficult to use it to determine the microparameters of the D-D interaction and the functional form of the relation $C_{DD}(\tilde{\varepsilon})$.

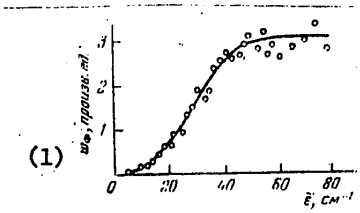

Figure 3.6. Spectral dependence of the probability of transmission $w_\phi(\tilde{\varepsilon})$ for phosphate glass with $N_{Yb}=7 \cdot 10^{20}$ cm^{-3} [301]

Key:
1. w_ϕ, arbitrary units

[1]The results obtained using the SNKL method are discussed in more detail on pp 103-105.

In Table 3.3 data are presented from experiments in which the method of investigating the integral kinetics of luminescence was used successively. There are very few of these papers, and in the majority they are devoted to determining the microparameters of BPV in neodymium-doped glass. Their authors unanimously come to the conclusion of dipole-dipole nature of the interactions in the investigated papers, but for the interactions D-D, this conclusion is not confirmed by convincing experimental proofs. The conclusion that the migration quenching of luminescence in neodymium-doped glass must be considered within the framework of the jump model appears to be reliable. Quantitative estimates are made of the microparameters C_{DD} and C_{DA} for a number of pairs. However, in some cases they are questionable (see the remarks to Table 3.3) and for 4.2 K for C_{DD} using formula (3.9), they are in general not incorrect. The temperature dependence of C_{DA} and C_{DD}, in particular, the relations obtained for the pair Eu^{3+}-Cr^{3+} in [350] giving information about the BPV mechanisms, are of interest. In [205] an effort was made to trace the dependence of the parameters C_{DD} and C_{DA} for Nd^{3+} ions on the type of glass former, but it was not possible to obtain complete, sufficiently reliable data. In [238] an effort was made to explain the reduced concentration quenching in Li-La-Nd-phosphate glass: namely, the combination of a small value of the parameter C_{DA} characterizing the process of cross relaxation of the ions Nd^{3+} (about $3 \cdot 10^{-41}$ cm^6-sec^{-1}), and the relatively large value of R_{min} (about 4.7 angstroms). However, the causes of significant developments in the degree of concentration quenching in the series of phosphate systems, in our opinion, remain still unclear and require additional study.

In the papers mentioned in Table 3.3, it was proposed in accordance with the theoretical concepts discussed in §3.2, that the functions $\overline{W}=f(N_D)$ and $\overline{W}=f(N_A)$ in the migration controlled phase of quenching are linear. Experimental testing of this proposition (with the exception of the case of concentration quenching in neodymium glass which is complicated for interpretation [238]) was not carried out. Moreover, in references [340, 341, 395], in which the BPV was investigated in 12 pairs of rare earth ions (Nd^{3+}-Yb^{3+}, Yb^{3+}-Er^{3+}, Nd^{3+}-Sm^{3+}, Dy^{3+}-Dy^{3+}, Dy^{3+}-Eu^{3+}, Sm^{3+}-Eu^{3+}, and so on) in phosphate glass it is pointed out that in the latter, in contrast to the silicate glass, the functions $\overline{W}=f(N_D)$ are nonlinear, and $\overline{W}$ increases appreciably faster than the concentration N_D. It is demonstrated there that the experimental values of the excitation energy diffusion coefficients with respect to the investigated donors in phosphate glass exceed by an order or more the ones calculated for dipole-dipole interactions using the overlap integrals of the spectra with respect to the formula (3.3), at the same time as the indicated values are close in silicate and germanate glass.

On the basis of these results, the conclusion is drawn of exchange nature at least the donor-donor interaction phosphate glass. However, the set of results obtained recently on a large number of objects using the precision methods of investigating BPV, in particular, the SNKL method, does not confirm this conclusion (see below). In addition, it is necessary to recognize the use of the diffusion model for description of the migration controlled stage of quenching in the majority of investigated pairs as unconvincing, inasmuch as the efficiency of the D-D interactions, as was indicated in these papers, exceeds the efficiency of the D-A interactions (see § 3.2). At the same time, the indications of nonlinearity of the concentration functions $\overline{W} - f(N_D)$ require fixed attention.

Table 3.3

B*	Transition	A	Transition	BPV type
1	2	3	4	5
Nd^{3+}	$^4F_{3/2}\rightarrow{}^4I_{9/2}$	Nd^{3+}	$^4I_{9/2}\rightarrow{}^4F_{3/2}$	1г
	$^4F_{3/2}\rightarrow{}^4I_{13/2;\ 15/2}$		$^4I_{9/2}\rightarrow{}^4I_{13/2;\ 15/2}$	1в
Nd^{3+}	$^4F_{3/2}\rightarrow{}^4I_{13/2};\ {}^4I_{15/2}$	Nd^{3+}	$^4I_{9/2}\rightarrow{}^4I_{13/2;\ 15/2}$	1в
	$^4F_{3/2}\rightarrow{}^4I_{9/2}$		$^4I_{9/2}\rightarrow{}^4F_{3/2}$	1г
Yb^{3+}	$^2F_{5/2}\rightarrow{}^2F_{7/2}$	Er^{3+}	$^4I_{15/2}\rightarrow{}^4I_{11/2}$	1б
Yb^{3+}	$^2F_{5/2}\rightarrow{}^2F_{7/2}$	Yb^{3+}	$^2F_{7/2}\rightarrow{}^2F_{5/2}$	1г
Nd^{3+}	$^4F_{3/2}\rightarrow{}^4I_{9/2};\ {}^4I_{11/2}$	Sm^{3+}	$^6H_{5/2}\rightarrow{}^6F_{11/2;\ 9/2}$	1а
		Nd^{3+}	$^4I_{9/2}\rightarrow{}^4F_{3/2}$	1г
		Ho^{3+}	$^5I_8\rightarrow{}^5I_5$	1б
Nd^{3+}	$^4F_{3/2}\rightarrow{}^4I_{13/2;\ 15/2}$	Nd^{3+}	$^4I_{9/2}\rightarrow{}^4I_{13/2;\ 15/2}$	1в
	$^4F_{3/2}\rightarrow{}^4I_{9/2}$		$^4I_{9/2}\rightarrow{}^4F_{3/2}$	1г
Eu^{3+}	$^5D_0\rightarrow{}^7F_{0;\ 1;\ 2}$	Cr^{3+}	$^4A_2\rightarrow{}^4T_2$	1б
		Eu^{3+}	$^7F_{0;\ 1}\rightarrow{}^5D_0$	1г

[Table 3.3, continued]

Matrix	T, K	$\bar{c}_{ДА}$, 10^{-40} см^6 сек$^{-1}$	m	Other results	Data source	Remarks
6	7	8	9	10	11	12
Ba—K—SiO_2	300 500	7,8	6	СМ; $\gamma(T)$, $\bar{F}$	[283]	(1)
	700 900	0,25—0,9	6			(1)
Na—SiO_2	4,2 300 450 600	0,13 0,3 0,4 0,6	6		[205]	(1)
Na—GeO_2	300	1,6	6			(1)
Na—B_2O_3	300	11	6			(4)
Na—P_2O_5	4,2 300	0,5 5—7	6	$\bar{F}$ ~ (2—3) $\times 10^5$ см$^{-1}$		(2)
Na—SiO_2	4,2 300 450 600	3,9 4,0 4,4 4,4	6	СМ; $\bar{F}$		(1, 5) (1) (1) (1)
Na—GeO_2	300	17	6	СМ		(1)
Na—P_2O_5	4,2	2,2	6	СМ; $\bar{F}$		(2, 5)
K—Ba—Sb—SiO_2	300 500 700	184	6		[355]	(1)
K—Ba—Sb—SiO_2	300	24	6	ДМ; $\bar{F}$	[355]	(1, 3)
	300	95	6			(1)
	300	8,5	6	ДМ; $\bar{F}$		(1, 3)
	300	20	6	ДМ		(1, 3)
Li—La—P_2O_5	4,2 300	0,3 0,3	6	R_{min}=4,7 Å	[238]	
	4,2 300	2,0 100	6	СМ		(5)
$La(PO_3)_3$	77— — 700	[illegible]	6	$\nu_Д(T)$; $\bar{F}(T)$ R_0=22 Å	[350]	
		2,8(300 K)	6	ДМ		

[Table 3.3]. Notes. (1) The dispersion τ_{OD} with respect to the NUP curve is not taken into account; (2) the competition on the part of quenching on the OH-groups is not considered; (3) the use of the diffusion model is questionable; (4) the quenching on the matrix vibrations is not considered; (5) the use of formula (3.9) to determine $\overline{C}_{DD}$ at 4.2K is invalid.

The following abbreviations are used: CM--jump model of migration quenching; DM--diffusion model; $\overline{F}$--effective macroscopic energy migration rate with respect to donors; $\gamma(T)$--dependence of the macroparameter of BPV γ (3.5) on temperature; $\overline{D}(T)$--diffusion coefficient as a function of temperature.

On the whole it can be stated that there are insufficient data presented in the above investigated papers to put together a clear representation of the mechanisms and relations of the BPV process parameters in glass or their dependence on the type of glass former, modifier or glass structure.

The original experimental data are presented below (the greater part of them are published for the first time[1]) fill the indicated gaps to some degree. The described results are obtained by analyzing the luminescence decay kinetics, including with spectral selection with respect to the excitation channel and with respect to the recording channel, in a wide temperature range on a large number of samples with specially selected relations of the activator concentrations. Here use was made of the precision experimental setup (Figure 3.7) providing for recording the luminescence decay kinetics in the multichannel photon counting mode in the dynamic range to 80 decibels with sensitivity to 10 photons per excitation pulse, spectral resolution to 0.5 angstrom and time resolution to 10 microseconds, with automated processing of the experimental results. The recording of the luminescence decay kinetics in the infrared range was insured in an analogous mode in the 45 decibel range using the cooled germanium photoresistance, signal from which after preamplification was normalized with respect to intensity and averaged in the two-channel gate integrator with time resolution to 100 nanoseconds, and then input through a matching device to the minicomputer memory. The latter was used to approximate the curves obtained by calculation with output of the results on the display screen for visual comparison.

Donor-Acceptor Interaction of Rare Earth Ions. Measurements of the D-A interaction parameters were performed on samples with very small donor concentration (on the order of $1 \cdot 10^{19}$ cm^{-3}) which excluded migration of excitation energy with respect to them. The acceptor concentration varied within broad limits, from $1 \cdot 10^{20}$ to $2 \cdot 10^{21}$ cm^{-3}. The program for processing the experimental results on a computer considered the presence of dispersion of the radiative probability with respect to the set of donor centers manifested in the nonexponential nature of the curves for the radiation luminescence decay [250]. In Figure 3.8a, in the example of the Yb^{3+}-Er^{3+} pairs in phosphate

[1] Some studies were performed jointly with Yu. Ye. Sverchkov and S. M. Matytsin on samples fixed by A. A. Izyneyev, A. K. Gromov, V. B. Kravchenko, V. M. Kozyukov, and U. Ya. Sedmalis.

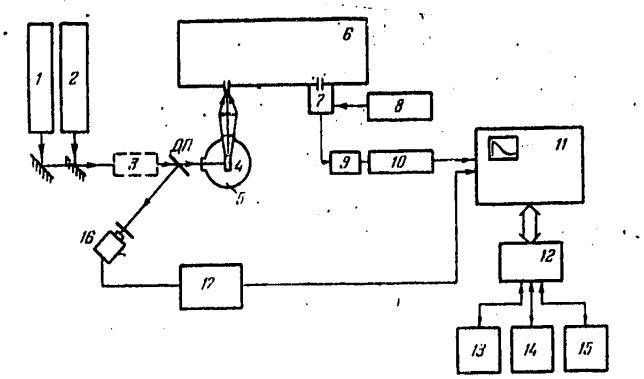

Figure 3.7. Functional diagram of a modern experimental setup for kinetic studies of BPV processes.
1--nitrogen laser (λ=0.337 micron, τ_{pulse}=10 nanoseconds, F_{repeat}=0 to 500 hertz); 2--YAG laser: Nd^{3+} (λ=1.064, 0.532, 0.355 micron; τ_{pulse}=15 nanoseconds; F_{repeat}=0-100 hertz); 3--the tunable dye laser (λ=0.4 to 0.75 micron) or LiF crystal laser: F_2^+ (0.85 to 1.1 microns); 4--sample; 5--helium cryostat (2-300 K); 6--double monochromator (dispersion 5 angstroms/mm); 7--cooled photomultiplier; 8--photomultiplier cooling system; 9--preamplifier; 10--module for sampling single photon events; 11--multichannel statistical pulse analyzer (1024 memory channels; scanning rate with respect to channels 10 microseconds/channel); 12--minicomputer; 13--storage element based on flexible magnetic discs; 14--terminal; 15--digital plotter; 16--avalanche photodiode; 17--delayed pulse generator in the synchronization channel

glass with the composition $Ba_3AlLa(PO_3)_{12}$, into which the activators were introduced by replacement of La, standard experimental luminescence decay curves of D* are presented which were measured with high precision in the dynamic range of intensities occupying more than three orders. On approximation of these curves by the expression (3.4) with variation of the introduced values of the parameters m and C_{DA} the best matching in the entire investigated time interval was achieved for m=6±0.1, that is, the process of static quenching was described well within the framework of the concept of the dipole-dipole interaction. An increase in concentration of A was not accompanied by significant changes in the nature of the functional dependence $N_D(t)$ or the value of the parameter C_{DA}, but in the initial section ($t\to 0$) a trend was traced to an exponentialization of the decay. In glass with high A concentration (to 2.10^{21} cm^{-3}), this trend was expressed quite clearly, indicating upper bounding of the luminescence quenching rate as a result of minimum distance between rare earth ions R_{min} (see §3.2) and, on the other hand, absence of a noticeable contribution of other, shorter acting types of interactions even in the closest pairs.

The pair Yb^{3+}-Er^{3+} is characterized by almost complete overlap of the luminescence spectrum of D* and absorption spectrum of A (Figure 3.9a). Analogous studies of samples with different acceptor concentration were performed for standard nonresonance pairs Yb^{3+}-Tm^{3+} and Yb^{3+}-Ho^{3+} and also for the pair of ions Nd^{3+}-Yb^{3+}, the spectra of which partially overlap in their wings (Figure 3.9b). For example, in Figure 3.8b, the experimental curve is shown for the luminescence decay of Yb^{3+} in glass with high Ho^{3+} ion concentration (about $2.1 \cdot 10^{21}$ cm^{-3}). A calculated relation is presented there which was obtained using formula (3.4) for $\overline{C}_{DA}=1.3 \cdot 10^{-40}$ cm^6-sec^{-1} measured on samples with low Ho^{3+} concentration. As is obvious, the experimental curve differs from the calculated curve by the initial, more gently sloping and exponential section in the dynamic range of intensities of more than one order. Using the relation of [238]

$$R_{\min} = \left(\frac{12}{\sqrt{2}} \frac{\overline{C}_{DA} N_A}{\overline{W}_e} \right)^{1/s}, \qquad (3.13)$$

it is possible to estimate $R_{min} \approx 5.0$ angstroms by the luminescence decay rate in this section $\overline{W}_e$. This value is close to the known data for crystal phosphates, for example, NdP_5P_{14} ($R_{min}=5.19$ angstroms) or $LiNdP_4O_{12}$ ($R_{min}=5.64$ angstroms) [238], and it indicates the isolated location of the RZI (rare earth ions] in phosphate glass.

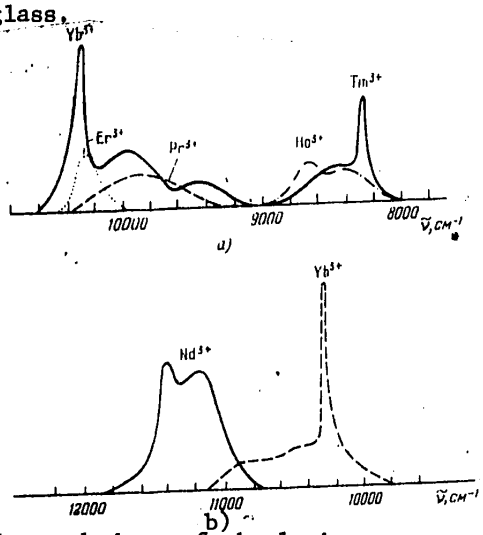

Figure 3.9. Position and shape of the luminescence and absorption bands of rare earth ions connected with excitation energy transfer in the pairs Yb^{3+}-Er^{3+}, Yb^{3+}-Pr^{3+}, Yb^{3+}-Ho^{3+}, Yb^{3+}-Tm^{3+} (a) and Nd^{3+}-Yb^{3+} (b); T=300 K.
For Er^{3+} and Ho^{3+}, the scale on the y-axis has been doubled, and for Pr^{3+}, it has been multiplied by five.

For the Nd^{3+}-Yb^{3+} pair studies were also made of the laws of burning of luminescence of the acceptor, and their correspondence on the whole to the nature of the damping curves was discovered.

Thus, the obtained results indicate that the Foerster theory is applicable for measuring the averaged parameters of the elementary acts of donor-acceptor interactions of m and $\bar{C}_{DA}$ in glass in a wide range of acceptor concentrations. The measurements for high A concentrations permit additional estimation of R_{min}.

Experimental values are presented in Table 3.4 for the parameters of the pair interactions m, $\bar{C}^{e}_{DA}$ and R_0, where $R_0=(\bar{C}^{e}_{DA}\cdot\tau_{\ell D})^{1/6}$ is the critical Foerster radius for a large number of pairs of rare earth ions in phosphate glass with the composition $Ba_3AlLa(PO_3)_{12}$. The calculated values of the parameter $\bar{C}^{calc}_{DA}$ obtained from the integrals of overlap of the spectra under the assumption of dipole-dipole resonance nature of the BPV using (3.3) are given for a number of pairs in the same table.[1] For nonresonance pairs the upper bounds of $\bar{C}^{calc}$ are presented considering the resonance overlap of the electron spectra or D* and A with the electron vibrational satellites of the partners, the intensities of which could not always be determined because of their smallness. As was obvious from Table 3.4, in all cases, dipole-dipole interactions (m=6) predominate, and, therefore, the conclusions of the authors of certain papers regarding effective manifestation in the BPV between the rare earth ions in glass of other types of interactions--dipole-quadrupole [352, 363], exchange [340], and so on--are not confirmed. For resonance pairs (Yb^{3+}-Er^{3+}, Yb^{3+}-Pr^{3+}, and so on), quite good correspondence of the values of $\bar{C}^{e}_{DA}$ and $\bar{C}^{calc}_{DA}$ is observed, and for nonresonance pairs, the experimental values are systematically an order (or more) larger than the calculated values. The divergences increase sharply with an increase in energy deficit during the transfer act $\tilde{\varepsilon}_{min}$, where $\tilde{\varepsilon}_{min}$ is the minimum energy difference of the transitions between the Stark components of the interacting multipleths D* and A. It is remarkable that the experimental values of $\bar{C}^{e}_{DA}$ and, the more so, R_0 for variation of $\tilde{\varepsilon}_{min}$ in broad limits (sometimes to 1000 cm^{-1}) differ relatively little for transitions with close integral cross sections. This is easily traced in the example of quenching of the luminescence by Yb^{3+} ions from the series Er^{3+}, Pr^{3+}, Ho^{3+}, Tm^{3+} (see Figure 3.9 and Table 3.4). The differences in values of $\bar{C}^{e}_{DA}$ for these pairs do not exceed one order, and the values of R_0 differ by one and a half times and correlate with the differences in the transverse cross sections of the absorption bands of the acceptors. Only for $\tilde{\varepsilon}_{min}$>1000 to 1200 cm^{-1} ($\tilde{\varepsilon}_{max}$>2000 cm^{-1}, where $\tilde{\varepsilon}_{max}$ is the energy mismatch between the most intense components of the transitions D* and A) a sharp decrease in the value of $\bar{C}_{DA}$ is observed of which it is easy to be convinced in the example of the pairs Eu^{3+}-Yb^{3+} ($\tilde{\varepsilon}_{min}\sim$1300 cm^{-1}), Yb^{3+}-Eu^{3+} ($\tilde{\varepsilon}_{min}\sim$3000 cm^{-1}), Yb^{3+}-Tb^{3+} ($\tilde{\varepsilon}_{min}\sim$3500 cm^{-1}), and so on. Attention is attracted by the fact that the admissible ineteraction energy deficit corresponds to the maximum frequencies of the vibrational spectrum of phosphate glass ($\tilde{\nu}_{max}\sim$1200 cm^{-1}). Thus, the

[1] The values of $\bar{C}^{calc}_{DA}$ obtained in this way are somewhat high, for the corrections for NUP are not taken into account.

Table 3.4

D*	Transition	A	Transition	Type of BPV	$\tilde{\nu}_{min}$, $см^{-1}$	$\tilde{\nu}_{max}$, $см^{-1}$	m	$\tau_{лД}$, 10^{-3} с	$\overline{C}^{э}_{ДА}$, 10^{-40} $см^6 \cdot с^{-1}$	$\overline{C}^{ср}_{ДА}$, 10^{-40} $см^6 \cdot с^{-1}$	R_0, Å
Nd^{3+}	$^4F_{3/2} \rightarrow {}^4I_{9/2}$	Yb^{3+}	$^2F_{7/2} \rightarrow {}^2F_{5/2}$	1б	0	1200	6	0,37	16	6,5	9,2
		Ho^{3+}	$^5I_8 \rightarrow {}^5I_5$	1б	250	800	6	0,37	7	<0,1	8,0
	$^4F_{3/2} \rightarrow {}^4I_{11/2;9/2}$	Sm^{3+}	$^6H_{5/2} \rightarrow {}^6F_{5/2;7/2;9/2;11/2}$	1а	0	250	6	0,37	90	16	12,2
	$^4F_{3/2} \rightarrow {}^4I_{13/2}$	Nd^{3+}	$^4I_{19/2} \rightarrow {}^4I_{15/2}$	1в	800	1400	6	0,37	0,45	0,06	5,1
	$^4F_{3/2} \rightarrow {}^4I_{15/2}$	Eu^{3+}	$^7F_0 \rightarrow {}^7F_6$	1а	0	800	6	0,37	4	1,2	7,3
		Tm^{3+}	$^3H_6 \rightarrow {}^3H_4$	1б	350	1200	6	0,37	12	<1	8,7
Yb^{3+}	$^2F_{5/2} \rightarrow {}^2F_{7/2}$	Er^{3+}	$^4I_{15/2} \rightarrow {}^4I_{11/2}$	1б	0	0	6	1,15	22	12	12,0
		Tm^{3+}	$^3H_6 \rightarrow {}^3H_5$	1б	700	2000	6	1,15	3,8	<0,5	8,7
		Ho^{3+}	$^5I_8 \rightarrow {}^5I_6$	1б	650	1600	6	1,15	1,4	<0,1	7,5
		Pr^{3+}	$^3H_4 \rightarrow {}^1G_4$	1а	0	450	6	1,15	10	5	10,2
		Sm^{3+}	$^6H_{5/2} \rightarrow {}^6F_{9/2;\ 11/2}$	1а	—	—	6	1,15	12	4	10,6
		Tb^{3+}	$^7F_6 \rightarrow {}^7F_0$	1а	3500	—	6	1,15	<0,01	<0,001	<3,2
		Eu^{3+}	$^7F_0 \rightarrow {}^7F_6$	1а	3500	—	6	1,15	<0,01	<0,001	<3,2
	$^2F_{5/2}(3) \rightarrow {}^2F_{7/2}(1)$	Nd^{3+}	$^4I_{9/2} \rightarrow {}^4I_{15/2}$	1б	~600	—	6	1,15	0,008	0	3,2
Er^{3+}	$^4I_{13/2} \rightarrow {}^4I_{15/2}$	Nd^{3+}	$^4I_{9/2} \rightarrow {}^4I_{15/2}$	1а	0	300	6	8,2	1	1,3	9,7
		Ho^{3+}	$^5I_8 \rightarrow {}^5I_7$	1б	750	1400	6	8,2	1,5	<0,1	10,4
		Tm^{3+}	$^3H_6 \rightarrow {}^3H_4$	1б	0	650	6	8,2	3,0	2	11,6
		Eu^{3+}	$^7F_0 \rightarrow {}^7F_6$	1а	850	1900	6	8,2	1	<0,01	9,5
		Pr^{3+}	$^3H_4 \rightarrow {}^3F_3$	1а	0	60	6	8,2	60	70	19,1
		Sm^{3+}	$^6H_{5/2} \rightarrow {}^6F_{3/2}$	1а	0	0	6	8,2	50	43	18,0
Eu^{3+}	$^5D_0 \rightarrow {}^7F_{6;\ 5}$	Dy^{3+}	$^6H_{15/2} \rightarrow {}^6F_{3/2;\ 5/2}$	1а	0	300	6	2,3	0,1	—	5,3
	$^5D_0 \rightarrow {}^7F_{0;\ 1;\ 2}$	Pr^{3+}	$^3H_4 \rightarrow {}^1D_2$	1б	0	100	6	2,3	0,4	—	6,7
		Cr^{3+}	$^4A_2 \rightarrow {}^4T_2$	1б	0	0	6	2,3	650	530	23
Sm^{3+}	$^4G_{5/2} \rightarrow {}^6H_{5/2;\ 7/2}$	Eu^{3+}	$^7F_{0;\ 1} \rightarrow {}^5D_0$	1б	0	0	6	3,1	0,1	—	5,6
	$^4G_{5/2} \rightarrow$ $\rightarrow {}^6F_{3/2;5/2;7/2;9/2}$	Dy^{3+}	$^6H_{15/2} \rightarrow$ $\rightarrow {}^6F_{3/2;5/2;7/2;9/2}$	1а	0	0	6	3,1	3	—	9,9
Pr^{3+}	$^1D_2 \rightarrow {}^3H_4$	Eu^{3+}	$^7F_0 \rightarrow {}^5D_0$	1а	~130	~130	6	0,25	5,5		7,2
UO_2^{2+}	$^3\Pi_{0u} \rightarrow {}^1\Sigma_g^+$	Eu^{3+}	$^7F_{0;\ 1} \rightarrow {}^5D_{0;\ 1}$	1б	0	0	6	0,45	2,7	—	7
		Nd^{3+}	$^4I_{9/2} \rightarrow ?$	1б	0	0	6	0,45	16	—	9,5

presented results indicate the significant contribution of the single phonon nonresonance mechanism to the total efficiency of the donor-acceptor transfer. Consequently, the degree of overlap of the emission spectra D and absorption spectra A or their resonance is not a decisive factor determining the efficiency of the BPV process. The requirement that the difference in energies of interacting transmissions not exceed the value of $\tilde{\nu}_{max}$ for the given matrix is much more important.

Table 3.5.

Matrix	$\overline{C}^e_{Nd-Yb}$	$\overline{C}^a_{Yb-Er}$	$\overline{C}^a_{Yb-Ho}$	$\overline{C}^e_{Yb-Tm}$
	10^{-40} см^6 сек$^{-1}$			
Ba—Al—La—metaphosphate	16	22	1,3	3,9
Na—Mg—metaphosphate	14	20	1,3	3,8
K—La—metaphosphate	18	23	—	3,9
Pb—La—ultraphosphate	24	40	1,35	4,0
Li—Na—K—Ba—silicate	6,5	8,1	1,0	2,9
Li—Ca—Al—silicate	12	21	—	—
Ba—La—borate	15	24	2,3	5,0
Na—Mg—borophosphate	13	16	1,2	3,6
Na—Mg—Ba—Ca—Al—fluophosphate	15	22	—	—
Pb—La—germanium phosphate	13	16	1,2	3,6
Na—K—Ba—germanate	12	18	—	—

The drawn conclusion is confirmed also by the results of studying the dependence of the values of C_{DA} on the type of glass former. In Table 3.5 the parameters of the elementary acts of the interactions are presented for two pairs of interest for laser applications: Nd^{3+}-Yb^{3+} and Yb^{3+}-Er^{3+} and standard nonresonance pairs Yb^{3+}-Tm^{3+}, Yb^{3+}-Ho^{3+} in glass of different composition. It turns out that the value of C_{DA} for the pair Yb^{3+}-Er^{3+} depends weakly on the type of glass former. Only the following types of glass are distinguished with respect to BPV efficiency: lead phosphate glass with an excess of phosphorus (in the direction of higher efficiency) and alkaline silicate glass (in the direction of lower efficiency). Replacement of phosphorus oxides by other glass formers (GeO_2 or SiO_2) leads to some decrease in the values of C_{DA} (Figure 3.10). However, the noted differences are small. The dependence of C_{DA} on the type of modifier is still less significant (Figure 3.11). The influence of the matrix on the transfer in the Nd^{3+}-Yb^{3+} pair and especially the Yb^{3+}-Tm^{3+} pair turns out to be more significant. In the latter case borate glass is distinguished, for which the value of $\overline{C}^e_{Yb-Tm}$ is higher. As is known [412], for borate glass the greatest extent of the spectrum of basic matrix vibrations is characteristic ($\tilde{\nu}_{max} \approx 1450$ cm^{-1}), which promotes involvement of a greater number of transitions between components of the multipleths $^2F_{5/2}$ and $^2F_{7/2}$ of the donors (Yb^{3+}) and $^3H_6$, $^3H_5$ of the acceptors (Tm^{3+}), including the most

intense, in the BPV process. In other glass, the latter do not participate in the transfer, for $\tilde{\varepsilon} > \nu_{max}$ for them. Obviously this explains the higher efficiency of transfer in the borate matrix in the pair Yb^{3+}-Tm^{3+}. The analogous situation is realized also in the case of the pair Yb^{3+}-Ho^{3+}. On the contrary, for the BPV between the ions Nd^{3+} and Yb^{3+}, for which $\tilde{\varepsilon}_{max} \sim 900$ cm^{-1}, and the edges of the spectra even overlap (Figure 3.9b), the dependence of $\bar{C}^{e}_{DA}$ on the type of glass former is significaltly weaker, and borate glass is not distinguished.

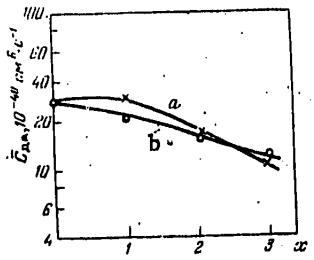

Figure 3.10. Variation of the probability of the elementary act of BPV in the pair Yb^{3+}-Er^{3+} for molar replacement of P_2O_5 by the oxides SiO_2 (a) and GeO_2 (b) in the systems

$$R_2O_3 \cdot PbO \cdot (8-x) \times P_2O_5 \cdot x \begin{matrix} SiO_2 \\ GeO_2 \end{matrix},$$

where R is rare earth elements.

It is remarkable that even with almost complete overlap of the spectra, in spite of the closeness of the values of $\bar{C}^{e}_{DA}$ and $\bar{C}^{calc}_{DA}$ entering into the error, the contribution of the nonresonance transfer channel turned out to be highly significant. This is indicated both by the fact that the experimentally measured values exceed the calculated values (in spite of the high estimation of the latter) and the complex nature of the temperature functions $\bar{C}^{e}_{DA}(T)$ for resonance pairs illustrated in the example of BPV between Yb^{3+} and Er^{3+} (Figure 3.12). The observed temperature growth by more than tenfold in the range of 4.2 to 300 K with two sharp inflections at 12 and 80 K is difficult to explain within the framework of resonance BPV. Indeed, for the first time, the values of $\bar{C}^{calc}_{DA}$ for 4.2 and 300 K differ by no more than 1.5 times. The emission spectrum of Yb^{3+} is overlapped with the components of the absorption spectrum Er^{3+} uniformly broadened as a result of the relaxation processes even for 4.2 K; thus, the calculated value of $\bar{C}^{calc}_{DA}$ (4.2 K) cannot greatly exceed the true value. Secondly, the influence of the temperature broadening of the lines must be manifested in the region of high temperatues, when the values of $\Delta\tilde{\nu}_{single}$ and $\Delta\tilde{\nu}_{H}$ approach, and, consequently, it cannot be accompanied by sharp breaks in the functions $\bar{C}^{e}_{DA}(T)$ at low temperatures. Nevertheless, the nonresonance processes of BPV with phonon absorption possible in the given pair can have energies of activation corresponding to low temperatures. In particular, the break at 80 K can be fully explained by thermal activation of the nonresonance transfer with absorption of a phonon with an energy of about 50 cm^{-1} required for compensation of the energy deficit between the most intense transitions corresponding to the luminescence band peaks of the Yb^{3+} ions (about 10265 cm^{-1}) and the absorption band of the Er^{3+} ions (about 10315 cm^{-1}).

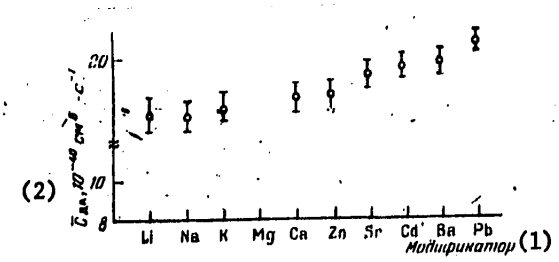

Figure 3.11. Magnitude of the microparameter of the donor-acceptor interaction for the pair Yb^{3+}-Er^{3+} as a function of the type of modified (Me^{+} or Me^{2+}) in the phosphate systems $Me^{+}PO_3$ with $R(PO_3)_3$ and $Me^{2+}(PO_3)_2$ with $R(PO_3)_3$, where R are rare earth elements.

Key:
1. Modifier
2. $\bar{C}_{DA}$, 10^{-40} cm^6-sec^{-1}

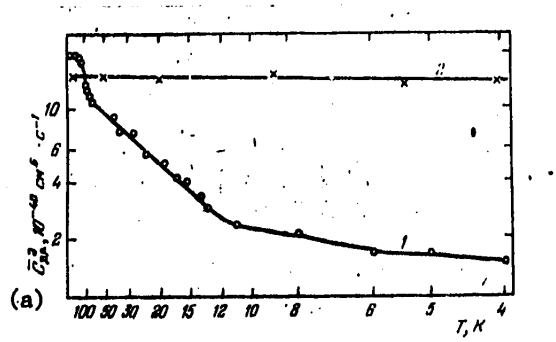

Figure 3.12. Temperature dependence of the microparameters of donor-acceptor interactions $\bar{C}^{e}_{DA}$ in the pair Yb^{3+}-Er^{3+} (1) and Nd^{3+}-Yb^{3+} (2) in glass with the composition $Ba_3AlLa(PO_3)_{12}$

Key:
a. $\bar{C}^{e}_{DA}$, 10^{-40} cm^6-sec^{-1}

For the other pair, Nd^{3+}-Yb^{3+}, the temperature dependence of $\bar{C}^{e}_{DA}$ (T) is almost absent (Figure 3.12), inasmuch as in the given case the transfer process is accompanied by generation of phonons, and it does not require thermal activation. An analogous picture was observed when investigating such relations for the pairs Yb^{3+}-Tm^{3+} and Yb^{3+}-Ho^{3+}.

Now let us consider the process of cross relaxation of the electron excitation energy of the Nd^{3+} ions from the applied point of view (BPV type 1c, Figure 3.1) responsible for concentration quenching of the luminescence of neodymium-doped glass. This process is difficult to subject to interpretation,

inasmuch as it is caused by competition of three relaxation channels: 1) quasiresonance caused by weak overlap of the luminescence and absorption bands corresponding to the transitions $^4F_{3/2}\rightarrow{}^4I_{15/2}$ ($\tau_0^{-1}\approx 15$ sec^{-1}, where τ_0 is the radiating lifetime) and $^4I_{9/2}\rightarrow{}^4I_{15/2}$ ($\sigma\approx 5\cdot 10^{-22}$ cm^2) 2) nonresonance connected with the transitions $^4F_{3/2}\rightarrow{}^4I_{13/2}$ ($\tau_0^{-1}\approx 280$ sec^{-1}) and $^4I_{9/2}\rightarrow{}^4I_{15/2}$ ($\tilde{\varepsilon}_{min}\approx 700$ to 800 cm^{-1}, $\tilde{\varepsilon}_{max}\approx 1400$ cm^{-1}); 3) nonresonance connected with the transitions $^4F_{3/2}\rightarrow{}^4I_{15/2}$ and $^4I_{9/2}\rightarrow{}^4I_{13/2}$ ($\sigma\approx 2\cdot 10^{-21}$ cm^2, $\tilde{\varepsilon}_{min}\approx 750$ cm^{-1}, $\tilde{\varepsilon}_{max}\approx 1200$ cm^{-1}). For channel 1 estimation of $\overline{C}_{DA}^{calc}$ in phosphate glass with the composition $Ba_3AlLa(PO_3)_{12}$ gives $(5\text{-}6)\cdot 10^{-42}$ cm^6-sec^{-1}, which is almost an order less than the experimental value of $\overline{C}_{DA}^{e}=5\cdot 10^{-42}$ cm^6-sec^{-1} (see Table 3.4). In addition, this process presupposes a sharp decrease in C_D^{calc} for low temperatures on the basis of disappearance of the overlap of the spectra and satisfaction of the condition $E_D<E_A$, and the experiment demonstrated that $\overline{C}_{DA}^{e}$ depends little on the temperature (see also [238]). On the other hand, the values of $\tilde{\varepsilon}_{min}$ for nonresonance channels 2 and 3 do not exceed $\tilde{\nu}_{max}$ and, consequently, their efficiency must be quite high, but the temperature dependence is insignificant. Preference must be given to channel 2, for it is connected with more intense transition in the donor. Actually, the calculated values of C_{DA} for channel 2 give a value of about $5\cdot 10^{-42}$ cm^6-sec^{-1}, and for channel 3, about $1\cdot 10^{-41}$ cm^6-sec^{-1}. The closeness of the value of $\tilde{\varepsilon}_{max}$ to the high-frequency boundary of the phonon spectrum of the matrices forces expectation of significant dependence of $\overline{C}_{DA}^{e}$ for channel 2 on the type of glass former. The study of the processes of concentration quenching of luminescence of Nd^{3+} in borate glass confirmed this proposition, demonstrating that $\overline{C}_{DA}^{e}\approx(1.3\pm 0.4)\cdot 10^{-40}$ cm^6-sec^{-1}. The lower accuracy of the measurements is connected with strong competition on the part of the quenching process on the matrix vibrations (see below).

Donor-Donor Interactions of Rare Earth Ions. The first problem in stating the experimental studies of donor-donor interactions was checking the applicability of the basic principles of the theory of integral kinetics of luminescence decay of a set of impurity centers in the migration-controlled and kinetic phases of quenching to actual vitreous systems. Therefore for a number of pairs of rare-earth ions in different matrices, a careful study was made of the concentration functions $\overline{W}=f(N_A)$ and $\overline{W}=f(N_D)$. Figure 3.13 shows a typical function $\overline{W}=f(N_A)$ in the example of the pair Yb^{3+}-Er^{3+} in phosphate glass with the composition $Ba_3AlLa(PO_3)_{12}$. It is linear in a wide range of Er^{3+} concentrations (in the selected coordinate grid this corresponds to 45-degree slope of the experimental curve). The relations of this type had analogous form in all of the investigated cases, for example, for the pairs Yb^{3+}-Tm^{3+}, Nd^{3+}-Yb^{3+}, and so on. Another picture was found for the dependence of $\overline{W}$ on the donor concentration. In Figure 3.14 curves 1-4 correspond to the laws in the pair Yb^{3+}-Er^{3+} in phosphate, borate, silicate and fluophosphate glass. The first two of them are explicitly nonlinear. For example, in phosphate glass at low concentrations of Yb^{3+} $(3\text{-}12)\cdot 10^{20}$ cm^{-3}), the curve is closer to quadratic, and for high ($N_D>1.3\cdot 10^{21}$ cm^{-3}) the growth of $\overline{W}$ is slowed sharply, which obviously is connected with the transition

to the kinetic phase of quenching. For silicate and fluophosphate glass the measured relations turned out to be close to linear within the limits of accuracy of the experiment.

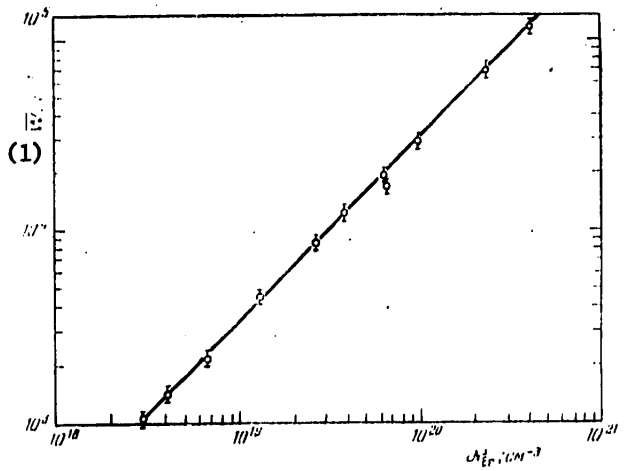

Figure 3.13. Probability of migration-controlled quenching of $\overline{W}$ as a function of the acceptor concentration for the pair Yb^{3+}-Er^{3+} in glass with the composition $Ba_3AlLa(PO_3)_{12}$; $N_{Yb}=1.3\cdot10^{21}$ cm^{-3}

Key:
1. $\overline{W}$, sec^{-1}

In order to establish the generality of the observed laws in phosphate glass, a study was also made of the pairs Yb^{3+}-Tm^{3+} and Nd^{3+}-Yb^{3+}. In the first case (Figure 3.14, curve 5) the concentration growth of $\overline{W}$ also turned out to be nonmonotonic. The transition to the kinetic stage was observed even for $N_D\sim6\cdot10^{20}$ cm^{-3}; in the second case (Figure 3.14, curve 6), the function $\overline{W}(N_D)$ within the limits of accuracy of the experiment (low as a result of competition on the part of the cross relaxation process in the subsystem of Nd^{3+} ions) can be considered linear.

Thus, the conclusion of references [340, 341, 395] regarding deviations from linearity in the concentration functions $\overline{W}(N_D)$ in phosphate glass was confirmed. The analogous effect was detected for borate systems. It was demonstrated that the nature of the functions $\overline{W}(N_D)$ is different in the given matrix for different pairs of rare earth ions, which obviously is connected with differences in the ratios of the parameters C_{DD} and C_{DA}. The causes of the observed effect are still unclear and do not find explanation within the framework of the above-discussed theoretical concepts of the kinetics of migration-controlled quenching. Therefore the use of the method of integral kinetics of luminescence for estimating the values of the parameters of C_{DD} at least in phosphate and borate glass is questionable and in practice is

possible only for pairs for which the linearity of the functions $\overline{W}(N_D)$ has been established in a defined concentration range of D. Here all of the above stipulations remain valid.

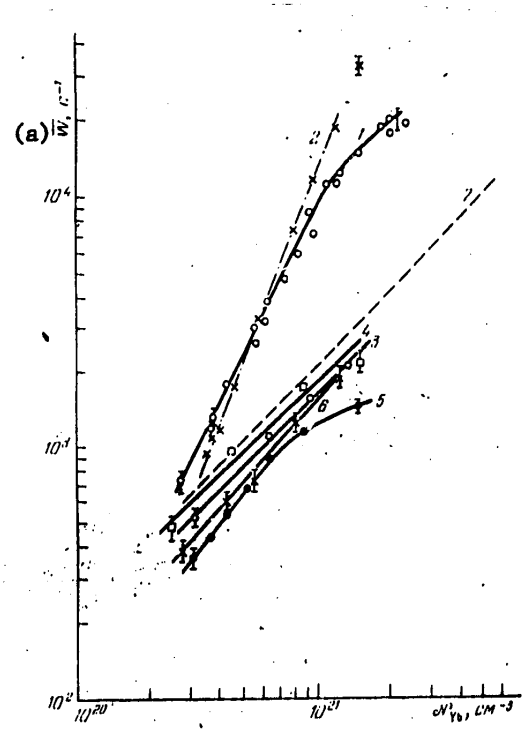

Figure 3.14. Probability of migration-controlled quenching $\overline{W}$ as a function of the donor concentration for the pair Yb^{3+}-Er^{3+} in phosphate (1), borate (2), fluophosphate (3), silicate (4) glass, for the pairs Yb^{3+}-Tm^{3+} (5) and Nd^{3+}-Yb^{3+} (6) in phosphate glass (N_A=3.5·10^{19} cm^{-3}) and also the calculated linear function (7)

Key:
a. $\overline{W}$, sec^{-1}

The experimental results discussed hereafter were obtained using the new method of investigating donor-donor interactions of rare earth ions already mentioned above in random media, and the method of selective observation of luminescence kinetics in the short-wave wings of the resonance lines at low temperatures [254]. The essence of this method consists in the following. At low temperatures ($k_BT<<\Delta\nu_H$), the donor centers in the media with NUP, as a result of freezing of the transitions from the upper Stark components of the metastable state to the sharp decrease in uniform broadening of the resonance components ($\Delta\nu_{single}<<\Delta\nu_H$) and a decrease in the efficiency of the BPV with phonon absorption are becoming spectrally nonequivalent. As a result, the possibility appears for direct experimental observations of

the effect of BPV from centers with greater energy resonance transition to centers with smaller energy by investigating the kinetics of the decay of spectrally isolated luminescence centers after photoexcitation by a δ-pulse. Actually, the experiments for 4.2 K demonstrated that for donor centers on the short-wave edge of the resonance lines, concentration-dependent decrease in duration and variation of the luminescence decay kinetics from almost exponential at small N_D to sharply exponential close to Foerster for high N_D, is observed. The effect increased sharply on shift of the spectral slot to the edge of the resonance NUP (Figure 3.15). On the contrary, on wavelengths close to maximum NUP and also increased temperatures it is almost absent. The nature of the dependence of the luminescence decay kinetics of the observation wavelength indicates growth of the probability of BPV with an increase in the energy deficit $\tilde{\varepsilon}$ between the transitions in the interacting centers, and it permits the conclusion to be drawn that the transfer mechanism is a single-phonon, nonresonance process, and the process of spectral migration is nonstationary, bounded by one or several jumps to the centers with maximum transition energies at which excitation is localized. Careful studies of the kinetics of luminescence decay curves as a function of λ permit us to obtain detailed quantitative information about the parameters of the elementary acts of D-D interactions and their dependence on the energy shortage in the interaction $\tilde{\varepsilon}$. The experimental procedure is discussed in detail in [254]. Measurements performed for a large number of types of glass based on phosphate, borate and silicate doped by Yb^{3+}, Nd^{3+} and Eu^{3+} ions in different concentrations demonstrated reliably that the donor-donor interactions are of a dipole-dipole nature ($m=6\pm0.1$), and the functional dependence $C_{DD}(\tilde{\varepsilon})$ in the energy range of $\tilde{\varepsilon}\lesssim100$ to 150 cm^{-1} is approximated well by the exponential curve (Figure 3.16). The latter result was unexpected, and, in our opinion, does not find acceptable explanation within the framework of the known theories of the elementary act of single-phonon, nonresonance BPV (see above). Let us also note that for different RZI in one matrix, the functional form of the functions $C_{DD}(\tilde{\varepsilon})$ it is almost identical, whereas on replacement of the matrix, the exponent of the same activator changes significantly. This result indicates that the form of the curves $C_{DD}(\tilde{\varepsilon})$ is determined by the peculiarities of the spectral distribution of the density of the phonon states in different matrices and depends weakly on the specifics of the electron transitions.

Another experimental result consists in the fact that the absolute value of C_{DD} for any value of $\tilde{\varepsilon}$ almost does not depend on the activator concentration for variation of the latter within very broad limits, for example, for the ions Nd^{3+} from $3\cdot10^{20}$ to $4\cdot10^{21}$ cm^{-3}. This fact indirectly confirms the correctness of the drawn conclusions regarding the dipole-dipole nature of the donor-donor interactions.

With an increase in temperature of the sample, the nonresonance BPV with respect to the NUP curve becomes two way, and the process of spatial migration is activated, acquiring a quasistationary nature for $k_BT>\Delta\tilde{\nu}_H$. It is obvious that the greatest contribution is made to it by the excitation jumps connected with phonons with an energy on the order of the halfwidth of the NUP. Consequently, the value of $C_{DD}(\Delta\tilde{\nu}_H)$ can serve as a characteristic of the efficiency of the process of nonresonance spatial migration of

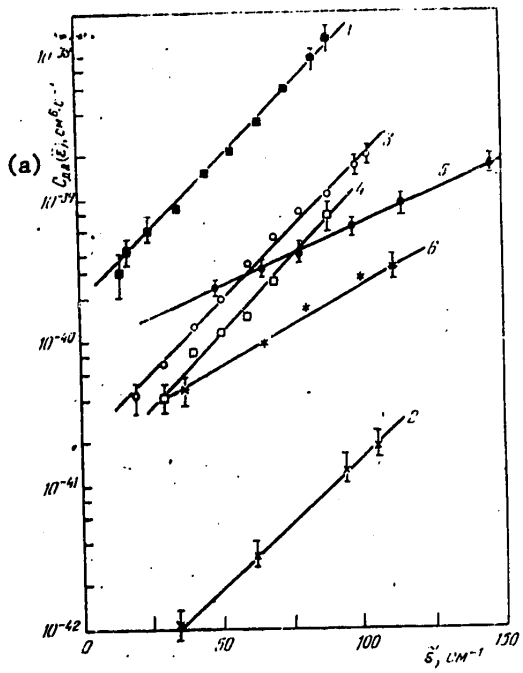

Figure 3.16. Microparameter of the elementary act of D-D interaction $C_{DD}(\tilde{\varepsilon})$ as a function of the energy of the emitted phonon $\tilde{\varepsilon}$.
1--Nd^{3+} in glass with the composition $Ba_3AlLa(PO_3)_{12}$, 2--Eu^{3+} in the same glass, 3--Yb^{3+} in the same glass, 4--Yb^{3+} in Na-Mg-phosphate glass, 5--Yb^{3+} in borate glass, 6--Yb^{3+} in alkali silicate glass. The values of C_{DD} for the Eu^{3+} ions are multiplied by 10.

Key:
a. $C_{DD}(\tilde{\varepsilon})$, cm^6-sec^{-1}

excitations at high temperatures. According to [290], for $k_BT>>\Delta\tilde{\nu}_H$ it is related to $\overline{C}_{DD}$ by the expression

$$\overline{C}^{\tau}_{\text{дд}} \approx C_{\text{дд}}(\Delta\tilde{\nu}_{\text{я}})\cdot k_{\text{в}}T/\Delta\tilde{\nu}_{\text{н}}. \qquad (3.14)$$

In Table 3.6 comparative data are presented with respect to the efficiency of nonresonance migration of excitation with respect to Yb^{3+} ions in different matrices. As we shall see, phosphate glass has increased efficiency compared to other systems. It is also of interest to compare the values of $\overline{C}^{T}_{DD}$ with the estimated values of $\overline{C}^{e}_{DD}$ obtained using the formula (3.9) from an analysis of the integral luminescence decay kinetics of the rare earth ions in the presence of an acceptor in the linear region of the concentration functions $\overline{W}(N_D)$ and also with the calculated values of $\overline{C}^{calc}_{DA}$ formed from the overlap integrals of the absorption and luminescence spectra of the rare earth ions. In Table 3.7 data are also presented for the ions Nd^{3+}

(quencher Yb^{3+}), Yb^{3+} (OH-groups), Er^{3+} (Nd^{3+}) in phosphate glass with the composition $Ba_3AlLa(PO_3)_{12}$. When estimating $\overline{C}_{DD}$ B≈20 according to [284] was

Table 3.6

Composition \ Parameter	$\widetilde{\Delta\nu}_H(1=e)$, $см^{-1}$	N_{Yb}, 10^{21} $см^{-3}$	$C_{ДД}(\widetilde{\Delta\nu}_H)$, 10^{-40} $см^6 \cdot с^{-1}$
$BaLa_{(1-x)}Yb_x(PO_3)_5$	63	0,64	3,5
		1	3,5
		1,75	3,5
		3,5	3,5
KGSS-46 (silicate)	45	1	0,55
ED-2 (silicate)	48	1	0,7
Ba—La—B_2O_3-glass	80	1	4,0
LGS-K (phosphate)	55	1	2,7
Composition \ Parameter	$\overline{C}^T_{ДД}$(300 K), 10^{-40} $см^6 \cdot с^{-1}$	$\overline{\tau}_л$(4.2 K), 10^{-6} с	$C_{ДД}$(60$см^{-1}$), 10^{-40} $см^6 \cdot с^{-1}$
$BaLa_{(1-x)}Yb_x(PO_3)_5$	13	1150	3,3
	13	1150	3,3
	13	1150	3,3
	13	1100	3,3
KGSS-46 (silicate)	2,5	1900	0,7
ED-2 (silicate)	3,0	1400	0,9
Ba—La—B_2O_3-glass	10	850	3,0
LGS-K (phosphate)	10	1250	2,9

$\overline{C}^T_{DD}$ (300 K) is the calculated value of the integral parameter of donor-donor interactions at 300 K using expression (3.14); $\overline{\tau}_л$ (4.2 K) is the effective luminescence time of the ion Yb^{3+} for low concentrations and a temperature of 4.2 K; C_{DD} (60 cm^{-1}) is the value of the spectral parameter of the donor-donor interactions for $\tilde{\varepsilon}$=60 cm^{-1}.

used. A comparison of the presented data indicates that the value of $\overline{C}^T_{DD}$ is comparable or even exceeds the value of $\overline{C}^{calc}_{DD} \approx \overline{C}^{e}_{DD}$. This fact permits the conclusion to be drawn of significant contribution of nonresonance single-phonon processes to the total efficiency of excitation energy migration at room temperatures. The studies of the temperature functions $\overline{W}(T)$ confirmed

this conclusion. For example, in Figure 3.17, the relation was presented for phosphate glass coactivated by the ions Yb^{3+} ($1.3 \cdot 10^{21}$ cm^{-3}) and Tm^{3+} ($1.3 \cdot 10^{20}$ cm^{-3}). For this pair, as was demonstrated above, weak temperature dependence of the parameter C_{DA} is demonstrated, which permits the observed temperature behavior to be completely attributed to the process of activation of spatial migration of excitations with respect to the Yb^{3+} ions. Here the energy of activation (~60 cm^{-1}) turns out to be the corresponding value of $\Delta\tilde{\nu}_H$ for the Yb^{3+} ions in the given matrix.

Table 3.7

Activator	$\overline{C}^{T}_{дд}$	$\overline{C}^{e}_{дд}$	$\overline{C}^{p}_{дд}$
	10^{-40} см^6 · sec^{-1}		
Yb^{3+}	.13	46	52
Nd^{3+}	130	30	35
Er^{3+}	—	55	48

Conclusions. The above discussed experimental data permit the following conclusions to be drawn.

1. The dipole-dipole interactions of rare earth ions are responsible for the BPV between rare earth ions in vitreous matrices and, as a rule, there is no necessity for calling on interactions of other types for interpretation of the experimental results.

2. The nonresonance single-phonon processes of transport make a highly significant contribution to the total efficiency of the BPV, and both in the case of D-D and in the case of D-A interactions with respect to efficiency they turn out to be close to quasiresonance.

3. The mechanisms of single-phonon nonresonance processes of the BPV remain unexplained. In particular, the experimental data require careful theoretical analysis with respect to the exponential nature of the functional relations $C_{DD}(\tilde{\varepsilon})$ in the range of phonon energies of $\tilde{\varepsilon}<\tilde{\nu}_D$ and also deviations from linearity in the concentration functions $\overline{W}(N_D)$ in a number of types of glass.

4. The type of matrix which includes RZI has significant influence on the transfer efficiency, primarily as a result of differences in intensity, extent and structure of the spectrum of the vibrational mode in the vicinity of the interacting rare earth centers.

5. Phosphate glass differs from other vitreous systems by increased BPV efficiency between the RZI, which makes them especially prospective for the development of laser materials.

(1)

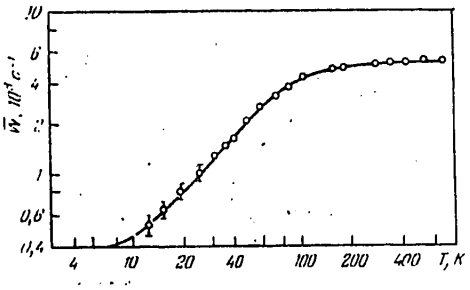

Figure 3.17. The experimentally found temperature dependence of the probability of migration-controlled quenching W in phosphate glass doped with Yb^{3+} and Tm^{3+} ions

Key:
1. $\overline{W}$, 10^3 sec^{-1}

6. For pairs of interest from the point of view of laser applications: namely, for Nd^{3+}-Yb^{3+}, Yb^{3+}-Er^{3+}, Er^{3+}-Nd^{3+}, Yb^{3+}-Ho^{3+}, Yb^{3+}-Tm^{3+}, Nd^{3+}-Nd^{3+} and many others, expression $\overline{C}_{DD} \geq \overline{C}_{DA}$ is satisfied, which indicates the discontinuous nature of the quenching process in the migration-controlled and kinetic stages.

§3.4. Ion-Vibrational Excitation Transfer

General State of the Art with Respect to the Problem. As has already been noted in §3.1, ion-vibrational BPV is a version of nonradiating energy transfer, and it is the process of replacement of a quantum of electron excitation energy by energy-equivalent number of phonons, local, quasilocal or crystalline excited in the first or more distant coordination spheres of the electron center (Figure 3.2). This process stimulates the effect of nonradiating relaxation of electron excitation leading to quenching of luminescence from the majority of excited states of electron centers in condensed media. In the general case, the degradation of the excited electron states of atoms and molecules can also have a chemical nature (electron transfer, isomerization, and so on). However, for trivalent rare earth ions in ion crystals and glass it has been established with reliability that in a wide temperature range, as a rule, the physical mechanism of degradation is realized which is not accompanied by chemical reactions. The probability of nonradiating relaxation depends strongly on the number of vibrational quanta or phonons participating in the elementary act of BPV. For single-phonon processes which predominate in the region of energy of gaps $\Delta E \leqslant \tilde{\nu}_{max}$, where the wave number $\tilde{\nu}_{max}$ corresponds to the maximum frequency of the extinguishing vibrations ω_{max}, very high relaxation rates are characteristic, in spite of the weakest binding of the ^4f-electrons of the rare earth ions to the surroundings compared to the binding in other known compounds. For example, judging from the uniform broadenings of the RZI lines and the EPR data [239], the excitation relaxation rates of the RZI on the lattic migrations reach values on the order of 10^{10} to 10^{11} sec^{-1}. With an increase in ΔE and, consequently, the number of generated phonons s, the probability of the relaxation process which is in the given case called multiphonon (MFR) decreases rapidly. At the same time, in some cases, in particular, in glass,

MFR can compete noticeably with other channels of radiative and nonradiating relaxation to $\Delta E \sim 8000$ to 10000 cm^{-1}, and in proton solutions, even to 13000 to 15000 cm^{-1} [239].

Another specific feature of nonradiating BPV is the exceptionally strong dependence of the probabilities of MFR for ΔE=const on the solvent matrix. As will be demonstrated below, even in a number of oxide glasses, they can differ by 10^4 to 10^5 times, and on comparing the various types of glass with certain ion crystals, the probability difference can reach 10 orders of magnitude or more.

The indicated facts force mixed attention to be paid to the study of the mechanisms of MFR in glass and the interrelations of their probabilities to the specific nature of electron transitions, the peculiarities of the vibrational spectra of the matrices and the values of ΔE. Clarity in these problems will permit facilitation of the solution of the basic applied problem, directional synthesis of glass with previously given properties for the same laser applications. Until recently, even qualitative understanding of the laws of MFR in glass was missing. This is indicated by the significant disparity in the interpretation of the experimental data by quantum yields of luminescence of rare earth ions from metastable states in glass, in particular, the dependence of the quantum yields on the glass composition and the technological factors connected with their manufacture.

Recently, in a number of experimental and theoretical studies of MFR in ion crystals [401] and glass [367, 404-412], basic qualitative laws of the MFR process were discovered. However, the problems of the physical mechanisms and the possibility of free experimental quantitative calculation of the probabilities of MFR for specific transitions of the rare earth ions in still univestigated matrices remain open. The original experimental data presented below, in our opinion, fill this gap. However, the theoretical concepts of the MFR and the experimental results published in the literature will be discussed briefly first.

On the theoretical level, the processes of MFR at the limit of weak binding usually are considered in the harmonic approximation of the dynamic Hamiltonian of the crystal field in the vicinity of the rare earth ions. For description of the perturbations generating nonradiating transitions, the nonadiabatic operator is used. The mechanism of electron-phonon interaction is not specified in this case. In various asymptotics of perturbation theory expressions were obtained for the probability of MFR W^s of order s (see, for example, the surveys [243, 258, 396, 401]). However, their use when calculating the quantitative laws of the processes of MFR for specific matrices and transitions is complicated in practice as a result of the absence of information about the frequencies of the vibrational modes in the vicinity of the rare earth ions, their polarization, mobility and strength of the vibron bond with the electron transition. Therefore a consistent analysis of the experimental results is possible only within the framework of the simplified phenomenological models. The so-called single frequency model of MFR has become widespread (first publication [397], for a detailed analysis see [401]), which presupposes that for $s \gtrsim 3$, the primary contribution to the $\overline{W}^s$ is made by the interaction with vibrations having frequencies which are close

at the high frequency boundary of the vibrational spectrum of the glass and strongly bound to the RZI-center. The binding strength can be judged by the electron vibrational spectra of the rare earth ions. For exchange of electron energy in this case a minimum number of phonons are required, and the order of the process is a predominant factor in the act of MFR. The specific properties of symmetry of the electron wave functions and vibrational modes and also dispersion of the force of electron-phonon binding with respect to modes are considered to be average as a result of the high order of the process, and they are not taken into account. The probability $\overline{W}^s$ basically depends on the magnitude of the normalized energy gap $\Delta E_{min}/\tilde{\nu}_{eff}$ and at low temperatures it can be described by the expression

$$\overline{W}^s \to \overline{W}_0^s = K \exp\left[-|\ln \varkappa| \Delta E_{min}/\tilde{\nu}_{эфф}\right], \qquad (3.15)$$

where $\tilde{\nu}_{eff}$ corresponds to the frequency of the most active vibrations in the act of MFR, K, κ-parameters characterizing the strength of the electron-phonon bond for the given matrix, where $\kappa=\overline{W}_0^s/\overline{W}_0^{s-1}<<1$, ΔE_{min} is the energy gap between the lower Stark component of the upper multipleth and the upper component of the lower multipleth. The temperature dependence of $\overline{W}^s$ in a single-frequency model is basically determined by the thermal population of the vibrational modes, and it has the form

$$\overline{W}^s(T) = \overline{W}_0^s \left[\frac{\exp\left(\hbar\omega^{(1)}_{эфф}/(k_B T)\right)}{\exp\left(\hbar\omega^{(1)}_{эфф}/(k_B T)\right)-1}\right]^s, \qquad (3.16)$$

Key: 1. eff

where the critical value even in the given case is considered to be the order of the process. The dependence on the exact value of ω_{eff} is much weaker. Consideration of the thermal population of the Stark components of the two multipleths gives only insignificant corrections to $\overline{W}^s$, so that the temperature dependence of the region $\hbar\omega_{eff}>>k_BT$ must be absent in practice. Exceptions are dictated only by the selection rules, on the basis of which for transitions between multipleths with J=1 and J=0 (for example, the transitions $^5D_1 \to {}^5D_0$ of the Eu^{3+} ions), the ion-vibrational BPV is forbidden.

Numerous experimental studies of the MFR processes in crystals activated by rare earth ions [401] confirm that the single frequency model qualitatively reliably describes the basic laws of the MFR. Recently it was modified considering the specific nature of the glass [412]. In Figure 3.18 the probabilities $\overline{W}^s$ measured in this experiment are presented for several transitions in different types of glass, and the experimental relations approximating them $\overline{W}^s(\Delta E_{min})$ are given. According to the conclusions drawn, the single-frequency model of MFR in oxide glass adequately describes the experimental data and permits quantitative prediction of $\overline{W}^s$ for new transitions. The greatest contribution to $\overline{W}^s$ is made by vibrations with $\tilde{\nu}_{eff} \to \tilde{\nu}_{max}$. The probability that MFR for defined transitions in a series of oxide glasses (from tellurite to borate) differ, according to [412], by 10^3 times, which is explained by the difference in values of $\tilde{\nu}_{max}$ (Table 3.8). On the whole, the values of $\overline{W}^s$ for equal ΔE_{min} in glass are higher than in crystals, which is explained by the great extent of the phonon spectrum

of the glass. Previously, the resolving effect of this factor in the glass was noted in references [404-411]. In [412] the conclusion was drawn of approximately equal strength of the electron-phonon binding in a number of oxide glasses. However, the latter conclusion does not correspond to the presented experimental data inasmuch as close slope angles of the curves $\ln[\overline{W}^s(\Delta E_{min})]$ for different ϑ_{eff} automatically indicate significant variations in the parameters K and κ for these types of glass. Let us also note that usually the values of κ in glass (about 0.012 to 0.007) are smaller than in crystals, that is, the electron-phonon binding in glass is obviously weaker.

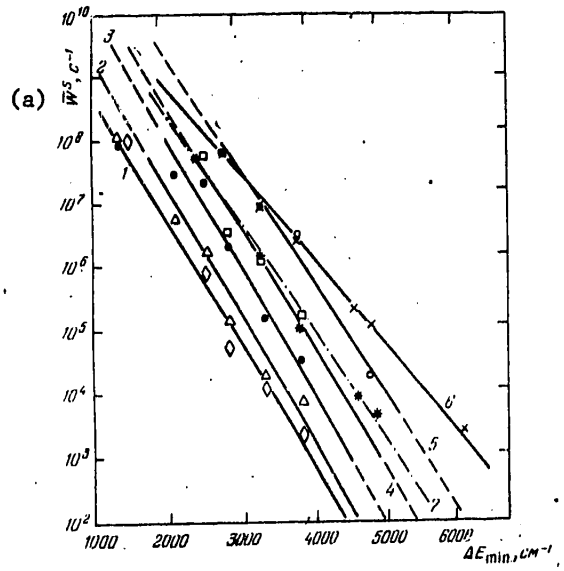

Figure 3.18. Dependence of the probability of multiphonon relaxation $\overline{W}^s$ on the magnitude of the energy gap ΔE_{min} in different glass.
1--tellurite, 2--germanate, 3--silicate, 4--phosphate, 5--borate glass [412]. Analogous relations for borate (6) and phosphate (7) glass according to the authors' data.

Key:
a. $\overline{W}^s$, sec^{-1}

Other noncorrespondences are discovered on comparison of the values of $\overline{W}^s$ predicted in [412] for the energy range of ΔE_{min}=5000 to 7000 cm^{-1} with those measured by us in systems of similar composition. For example, in borate glass the values we obtained for the transitions $^5I_7 \rightarrow {}^5I_8$ for the ions Ho^{3+} ($\Delta E_{min} \sim 4800$ cm^{-1}), $^3H_4 - {}^3H_6$ in the Tm^{3+} ions ($\Delta E_{min} \sim 4600$ cm^{-1}) and $^4I_{12/2} - {}^4I_{15/2}$ for the ions Er^{3+} ($\Delta E_{min} \sim 6100$ cm^{-1}) exceeded those predicted in [412] by 10, 7 and 17 times, respectively, in spite of the fact that our glass was carefully dehydrated, and in [412] this factor is not taken into account. The indicated noncorrespondence clearly illustrates the basic deficiency of single-frequency model--impossibility, with respect to minimum

number of preliminary spectroscopic data obtained on one to two samples, of predicting the quantitative value of $\overline{W}^S$ for any transition in a new matrix. On the contrary, it requires technically complex measurements of $\overline{W}^S$ directly on a large number of specially made samples. Of course, the averaging considering additional points permits a decrease in the average deviations (straight lines 6 and 7 in Figure 3.18), but here the problem of preexperimental calculation of W^S itself becomes meaningless.

Table 3.8

(1) Стеклообразователь	B^{3+}	P^{5+}	Si^{4+}	Ge^{4+}	Te^{4+}	Be^{2+}
(2) Атомный номер	5	15	14	32	52	4
(3) Координационное число	3 4	6	6	6	3	3
(4) Атомная масса, а. о. м.	10,8	31	28,1	72,6	127,6	9
(5) Ионный радиус, Å	0,10 0,20	0,34	0,41	0,54	0,52	0,31
ν_{max}, $см^{-1}$	≈1500	≈1250	≈1150	≈900	≈700	≈800

Key:
1. Glass former
2. Atomic number
3. Coordination number
4. Atomic mass, atomic units of mass
5. Ion radius, angstroms

Another highly significant deficiency of the single-frequency model, is that it is too formalized, and it sheds little light on the physical mechanisms of MFR. Actually, the mechanism of interaction in it is not specifically stated, it does not specifically take into account the degree of spatial localization of the damping vibrations, the concentration of the vibrational groups and their spatial distribution with respect to the electron center. In addition, the single-frequency model does not "operate" in the region s>3 or in the region greater than ΔE_{min} in the presence in the matrix of vibrational groups differing significantly with respect to frequencies and spatial distribution [401]. The latter situation is characteristic, nevertheless, for glass where along with the vibrations of the chemical bonds of glass forming elements in the nearest vicinity of rare earth ions, frequently there are oscillators of admixture origin, primarily OH-groups, the frequencies of the basic stretching vibrations of which (≈3000 $см^{-1}$) are appreciably higher than the vibrational frequencies of the glass forming elements. As a result of lower order of the MFR process, the OH-oscillators in the region of large ΔE_{min} (>4000 to 5000 $см^{-1}$), in spite of relatively low concentration of them in the glass, can compete with the lattice vibrations and quenchers of the rare earth ion luminescence. The quenching effect of the OH-group in the glass was first detected for Nd^{3+} and Er^{3+} ions in the phosphate systems of [181, 182, 193]. Later it was confirmed and studied on the phenomenological level for other transitions in phosphate, fluophosphate, silicate, borate and tellurite glass [101, 117, 183, 185, 187, 191, 229, 305, 345, 361, 403, 404, 413]. However, the mechanisms of electron-phonon interactions in the indicated papers were not specified; only the proposition was stated of

strong binding in the pair made up of rare earth ions and OH based on the erroneous interpretation of the linear nature of the dependence of the quenching probability on the concentration of OH-groups [101, 183]. In the indicated papers quenching was not taken into account even within the framework of formalism of multiphonon relaxation, although the nature of the spatial distribution of the vibrational groups and the difference in oscillator frequencies do not change the essence of the problem. Let us note that in all known papers on MFR in glass, except our paper [404], the possibility of competition on the part of the OH-groups is not considered in general. Nevertheless, for example, it significantly distorts the slope of the graph of $\ln W^S$ as a function of ΔE_{min} in [412] at least for tellurite and phosphate glass.

The presented arguments permit, in contradiction to [412], the conclusion to be drawn of insufficiency and nonphysicalness of the single-frequency model of MFR as a working theory for calculation and analysis of the MFR processes at least in glass. Another phenomenological model of MFR which uses the concept of induction resonance nature of the interaction of electron and vibrational oscillators appears to be more prospective. For a number of years the indicated model has been successfully developed in the papers by Yermolayev and Sveshnikova [239, 399, 400] as applied to the quenching of the luminescent of rare earth ions and transition metals in protonated and deuterated liquid solutions and also in hydrated crystals. For analysis of the MFR processes in ion crystals and glass, up to now it obviously has not been used (with the exception of [404]).

In the inductive-resonance model, a specific mechanism is proposed for ion-vibrational BPV-weak resonance dipole-dipole interaction of the electron oscillator with dynamic oscillators corresponding to overtones of local or quasilocal aggressions of chemical bindings in its vicinity. The dipole transition in the latter between the vibrational states with $\Delta s>1$ is partially permitted as a result of anharmonism of the vibrations. Thus, the elementary act of BPV in the given case is of a local nature, that is, a quantum of electron energy is replaced by vibrational quanta of a specific molecular group and not by quanta of collective vibrations of the surroundings as a whole. As was pointed out above, in the single-frequency model the nature and degree of localization of active vibrations in the MFR are not specified.

With this approach for calculation of the probability W^i_{ev} of interaction of an electron oscillator with the i-th vibration, it is possible to use the formula[1] analogous to (3.3):

$$W^i_{0n} = 2{,}3\cdot 10^{-4}\chi^2 R_i^{-6}(\tau_{0\text{Л}})^{-1}\int \sigma_{\text{К}}(\tilde{\nu})\, g(\tilde{\nu})\, n^{-4}(\tilde{\nu})\,\tilde{\nu}^{-4}\, d\tilde{\nu}, \qquad (3.17)$$

(1)

Key: 1. ev

---

[1] The factor $n^{-4}(\tilde{\nu})$ was introduced in (3.17) under the sign of the integral, for in the investigated region it is impossible to neglect the dispersion of the index of refraction.

where R_i is the distance from the RZI to the center of the i-th oscillator, $\sigma_k(\tilde{\nu})$ is the absorption cross section of the quenching vibrational groups, $g(\tilde{\nu})$ is the form factor of the luminescence band corresponding to the electron transition ($\int g(\tilde{\nu})d\tilde{\nu}=1$).

The probability of the MFR act for the j-th electron center is defined as the result of summation of W^i_{ev} with respect to all the quenching oscillators in the vicinity of the RZI:

$$W_j^s = \sum_i W^i_{ev(1)} \qquad (3.18)$$

Key: 1. ev

and the averaging procedure with respect to these centers in order to determine the effective macroscopic probability of $\overline{W}^s=\langle W^s_j\rangle$ depends on the nature of the spatial distribution of the vibrational oscillators with respect to the RZI-center. With regular arrangement of them in the nearest coordination sphere $\overline{W}^s\approx\sum_i W^i_{ev}$. For statistically uniform distribution of the impurity vibrational oscillators in the matrix, the kinetics of the MFR process become not exponential, but close to Foerster, and for its description it is possible to use formula (3.4a). In this case it becomes possible to determine the average parameters of the elementary act $\overline{W}_{ev}$ or $\overline{C}_{ev}=\overline{W}_{ev}R^6$ directly experimentally by the kinetics of the decay of the excited electron state. The first version is realized during quenching on the vibrations of the structural elements of the matrix, the second on the vibrations of the impurity oscillators, for example, the OH-groups.

Direct application of the formulas (3.17), (3.18) for interpretation of the experimental data with respect to MFR in the case of regular arrangement of the vibrational oscillators usually is complicated by the absence of reliable data on the coordination numbers of the first, and especially the second coordination spheres of the RZI. In addition, the vibrations themselves frequently are not completely localized. Therefore it is possible with good approximation to replace the summation in (3.18) by integration with respect to volume and then we obtain [239]

$$W_j^s = \frac{1}{10\pi^4 R_k^3 \tau_{0Д}} \int g(\tilde{\nu})\, k_м(\tilde{\nu})\, n^{-4}(\tilde{\nu})\tilde{\nu}^{-4} d\tilde{\nu}, \qquad (3.19)$$

where $k_M(\tilde{\nu})$ is the linear absorption coefficient of the matrix in the multiphonon region, R_k is the radius of the sphere around the RZI not containing high-frequency oscillators.

Thus, the inductive resonance model of MFR permits determination of the probability of MFR in terms of the experimentally measured spectroscopic characteristics of the electron transition (τ_{0D}, $G(\tilde{\nu})$) and the matrix ($k_M(\tilde{\nu})$). Here the function $\overline{W}^s(\Delta E)$ is defined by the dependence of k_M on $\tilde{\nu}$, in which automatic consideration is given to the contribution of all of the types of the vibrations active in the infrared spectra (which means in the MFR) determined by their anharmonism, both mechanical and electrooptical, connected with nonlinear dependence of the dipole moment on the vibrational coordinates. As is known from the theory of infrared spectra of amorphous

bodies (see, for example, [402]), in the multiphonon region basically these spectra are determined by the overtones and the component vibrations (among the highest frequencies of the given matrix), which also explains the applicability of the single-frequency approximation. Moreover, the spectrum $k_M(\tilde{\nu})$ in the multiphonon region in many cases can be calculated beginning with the structure of the matrices both for the crystals and for amorphous bodies [402]. The calculations show that for s>>1 where in the given case s has the meaning of the overtone number, the spectral function $k_M(\tilde{\nu})$ approaches the asymptotic $k_M(\tilde{\nu})\equiv\exp(-b\tilde{\nu})$, where b=const. Substituting it in (3.19), we obtain $\overline{W}\equiv\exp(-a\Delta E)$. Thus, within the framework of the inductive resonance model of MFR, the exponential dependence of $\overline{W}^s$ on ΔE is easily explained by the analogous function $k_M(\tilde{\nu})$. At the same time, this model explains numerous deviations from the exponential function, especially in the region of small s. Here the spectral function $k_M(\tilde{\nu})$ is less monotonic and $\overline{W}^s$ must follow its peculiarities. The inductive resonance model does not exclude consideration of the individual characteristics of the electron transition, explaining the differences in values of $\overline{W}^s$ for ΔE=const by the differences in the radiating probabilities of the transitions.

It must be emphasized that the effective value of the energy of the gap ΔE_{eff} which must be used in the framework of the applied model far from always coincides with ΔE_{min}. According to (3.17) ΔE_{eff} corresponds to the maximum of the expression $\sigma_k n^{-4} g\nu^{-4}$. Therefore $\Delta E_{eff}\to\Delta E_{min}$ in the region of large steepness $k_M(\tilde{\nu})$, and where $dk_M(\tilde{\nu})/d\tilde{\nu}\to 0$, the value of $\Delta E_{eff}>\Delta E_{min}$, and it corresponds to the center of gravity $g(\tilde{\nu})$. Considering that the Stark splitting of the electron states of the rare earth ions reaches 400 to 800 cm^{-1}, neglecting the indicated correction can significantly distort the results.

The temperature function $\overline{W}^s(T)$ within the framework of the inductive-resonance model corresponds to the temperature function $k_M(\tilde{\nu})$. In the region $k_BT>h\omega_{max}$, the latter is described by an expression similar to (3.16). In the low temperature range anomalies are possible which are connected with transformation of the spectra $g(\tilde{\nu})$ and variation of the radiative probabilities for thermal combination of populations of the upper Stark components. Within the framework of the given model, the term "electron-phonon bond strength" acquires specific physical meaning, and for other equal factors, it is determined by the distances from the RZI to the center of gravity of the vibrational oscillators ($\sim R^{-6}$), the nature of the distribution in the matrix and the degree of anharmonism of the vibrations. It is natural that in the matrices with less dense packing or for the OH-group, the bond strength is less, that is, for the same $k_M(\tilde{\nu})$, lower probabilities of MFR are observed. Finally, the inductive-resonance model presupposes the possibility of dispersion of the probabilities MFR even for regular arrangement of the vibrational acceptors the sources of which can be: 1) variation of the frequencies and degrees of anharmonism of the high-frequency vibrations as a result of local lattice deformation; 2) dispersion of the distances from the rare earth ions in the high-frequency groups; 3) dispersion of the radiating probabilities of the electron transitions; 4) dispersion with respect to the RZI-centers of the transition energies and, consequently ΔE_{eff}. The degree of the contribution of any of them a priori is not clear and requires experimental determination in each specific case. Let us only note that the first three factors in the single-frequency model are not taken into account,

so that the experimental isolation of their contribution will serve as one of the proofs in favor of the applicability of the inductive-resonance model. The vulnerable part of this model is the possible strong deformations of the given components in the vicinity of the RZI, whereas $k_M(\tilde{\nu})$ is determined integrally for the matrix as a whole. The degree of the influence of this factor requires experimental study.

Thus, the inductive-resonance model opens up new possibilities in the studies of the mechanisms of parameters of the MFR, and it has explicit advantages over the single-frequency model under the condition of obtaining weighty proofs of its applicability to vitreous matrices, theoretically permitting solution of the above-formulated basic problems. In [239], quite convincing, although indirect proofs of its suitability in the case of liquid solutions and hydrated crystals are presented. Beginning with the general principles, it can be stated that the situation in amorphous glass (in contrast to crystals with significantly different dynamic vibrational movements) does not differ in theoretical respects from the situation in liquid solutions, with the exception, perhaps, of significantly smaller frequencies of the high-frequency vibrations of the glass forming elements by comparison with uniquely high frequencies of hydrogen bonds. According to modern theoretical models of oxide glass [111], the high-frequency part of their vibrational spectrum is determined by the vibrations of the bonds of the glass-forming ions Si^{4+}, B^{3+}, P^{5+}, Ge^{4+} or Te^{4+} with oxygen. The frequencies of the vibrations connected with the modifier ions are 2 to 3 times less. The high-frequency vibrations are weakly bound to the lattice as a whole and are sufficiently well approximated by independent local oscillators. The number of oscillators in the first coordination sphere of the rare earth ions is equal to the product of the number of nearest glass-forming polyhedra (6 to 8 for oxide glass) times the number of high-frequency modes in each of them. The indicated oxygen bonds are sufficiently elastic, and their frequencies are close to the frequencies of the free elastic bonds of the oxygen and the glass former. Therefore the inhomogeneity of the crystal field in the vicinity of the rare earth ions is primarily obviously connected not with deformation of the polyhedron, but with variation of their mutual orientation. For this reason, it is not necessary to expect strong distortion of the phonon spectrum in the vicinity of the introduction of the rare earth ions by comparison with the lattice spectrum as a whole. However, in order to obtain reliable information, it is necessary to study the electron vibrational excitation spectra of rare earth ions in glass during selective excitation. Let us also note that in multiphase glass or systems with several glass-formers the rare earth ions can be introduced in different sublattices with essentially different vibrational structure. This fact must be considered when analyzing the processes of MFR in such systems.

The discussed arguments regarding the vibrational structure of glass favor the application of the inductive resonance model to the glass-forming matrices.

A description is presented below of the set of experimental data obtained by us[1] permitting reliable confirmation of its advantage and effectiveness for studying the processes of MFR for rare earth ions in glass.

Experimental Studies of the MFR Processes on Vibrations of the OH-Groups in Glass. As has already been noted, the admixture origin of the OH-groups and their statistically uniform distribution connected with this in glass create the prerequisites for quantitative testing of the applicability of the inductive-resonance model of MFR to the glass, and in the case of a positive result, for direct calculation of the integral parameters of the elementary act $\overline{C}_{ev}=\overline{W}_{ev}R^6$ and m according to the data on the decay kinetics of the residual luminescence of the set of rare earth ions after photoexcitation by a δ-pulse. Actually, the decay kinetics will be similar to Foerster kinetics (3.4) only in the case of multipole and local nature of the interaction. If the elementary act of MFR is the result of coherent interactions of the electron excitation with the collective of the vibrational oscillators or (and) the interactions of other types, for example exchange interactions) predominate, the kinetics will be significantly closer to exponential. In the literature devoted to studies of the quenching of the luminescence of the rare earth ions by OH-groups there were no data on the precision kinetic measurements. Moreover, the linear nature of the concentration functions $\tau_D^{-1}=f(N_{OH})$ noted in [101, 183, 185, 193] was not in favor of the multipole nature of the interaction. We measured the luminescence decay kinetics on 10 transitions in different RZI (Table 3.9) in phosphate glass with the composition $Ba_3AlLa(PO_3)_{12}$. The selective transitions correspond to energy gaps in the range of 5000 to 10000 cm^{-1}, where the quenching of the luminescence by the lattice is already quite weak, and it is possible to isolate the contribution of the quenching by the OH-groups which is more effective on the basis of the lower order of the MFR process. The concentration of the OH-groups in the investigated samples varied as a function of the technological procedures of founding and preparing the charge by almost 3 orders of magnitude, for $1\cdot10^{18}$ to $6\cdot10^{20}$ cm^{-3}. It was determined by the absorption level in the range of 3000 cm^{-1} with respect to the standard sample calibrated with an error of $\pm$20% by remelting in a vacuum with trapping of the water vapor in a nitrogen trap. The RZI concentration was $1\cdot10^{19}$ cm^{-3}, which almost excluded the possibility of migration of the excitation energy with respect to them. The luminescence kinetics were measured on the device described above. The experiment demonstrated that for all activators with an increase in N_{OH} the luminescence decay kinetics of the RZI vary from almost exponential for $N_{OH}\to0$ to sharply nonexponential for $N_{OH}>10^{20}$ cm^{-3}. The standard experimental decay curves are presented in Figure 3.19 in the form of a photograph from the screen of a multichannel analyzer. The result of the theoretical approximation of the luminescence decay kinetics is illustrated by expression (3.4). Complete coincidence of the theoretical and experimental curves was detected in a wide range of intensities. An analogous procedure performed for a large set of different samples demonstrated that for each activator

[1]The experiments were performed by the author jointly with Yu. Ye. Sverchkov and M. R. Syrtlanov. The samples were fixed by A. A. Izyneyev, A. K. Gromov and V. B. Kravchenko.

Table 3.9

Ion	Transistor	ΔE_{eff} cm^{-1}	$\tau_{\ell D}$ 10^{-3} sec	A, sec^{-1}	m	$\bar{C}^{e}_{ev}$ 10^{-40} $cm^{6}sec^{-1}$	$\bar{C}^{calc}_{ev}$ 10^{-40} $cm^{6}sec^{-1}$
Ho^{3+}	$^5I_7 \rightarrow {}^5I_8$	4800	0,37	57	6±0,3	23±2	26
Nd^{3+}	$^4F_{3/2} \rightarrow {}^4I_{15/2}$	5300	0,37	21	{6±0,1}	{4,6±0,5}	4,3
	$^4F_{3/2} \rightarrow {}^4I_{13/2}$	7500	0,37	300			0,18
Tm^{3+}	$^3H_4 \rightarrow {}^3H_6$	5250	0,21	130	6±0,3	25±3	27
Tb^{3+}	$^5D_3 \rightarrow {}^5D_4$	5700	1,1	62	6±0,1	4,7±0,5	—
Er^{3+}	$^4I_{13/2} \rightarrow {}^4I_{15/2}$	6500	8,2	100	6±0,1	1,2±0,3	1,6
Pr^{3+}	$^1D_2 \rightarrow {}^1G_4$	6800	0,25	2000	6±0,2	18±2	—
Sm^{3+}	$^4G_{5/2} \rightarrow {}^6F_{11/2}$	6950	3,1	19	6±0,2	0,1±0,05	—
Dy^{3+}	$^4F_{9/2} \rightarrow {}^6F_{3/2;1/2}$	7250	1,0	90	6±0,2	0,1±0,05	—
Yb^{3+}	$^2F_{5/2} \rightarrow {}^2F_{7/2}$	9900	1,15	870	6±0,2	0,055±0,2	0,035

at the given temperature there is a constant set of values of the parameters m and $\bar{C}^{e}_{ev}$ which does not depend on N_{OH} (Table 3.9), permitting description of the experimental luminescence decay curves by the expression (3.4). Here the parameter m was in all cases close to six. This result permits the conclusion to be drawn that the investigated MFR process is caused by the dipole-dipole interaction of local impurity centers [414].[1] The applicability of the inductive-resonance model of MFR is traced further if we calculate the value of the parameter $\bar{C}^{calc}_{ev}$, using formula (3.17). As is obvious from Table 3.9, quantitative correspondence of these values with the experimentally measured values is detected. Figure 3.20 shows the standard function $k_{OH}(\tilde{\nu})$ for the investigated glass (curve 2). The absorption spectrum of the matrix itself (curve 1) and the experimental values of the product $\bar{C}_{ev}(\Delta E)\tau_{\ell D}\tilde{\nu}^4$ are illustrated there for comparison. It is clearly obvious that the spectral dependence of this value strictly follows the function $k_{OH}(\tilde{\nu})$. Nevertheless, if we simply construct the graph of $\bar{C}_{ev}(\Delta E)$, quite strong deviations from the curve $k_{OH}(\tilde{\nu})$ are observed, which are connected with differences in the radiative probabilities of the transitions. Their difference is manifested especially clearly when comparing the transitions with close values of ΔE_{eff}, for example, for the pair Sm^{3+}-Pr^{3+} or Nd^{3+}-Tm^{3+}-Ho^{3+}.

The obtained results are of a fundamental nature, more precisely defining the mechanism of MFR in amorphous media and indicating the applicability of the dipole-dipole resonance model to the description of the ion-vibrational BPV

[1] Recently reference [238] also appeared, in which close values of the parameter C_{ev} were obtained for the Nd^{3+} ions in Li-La-Nd-phosphate glass.

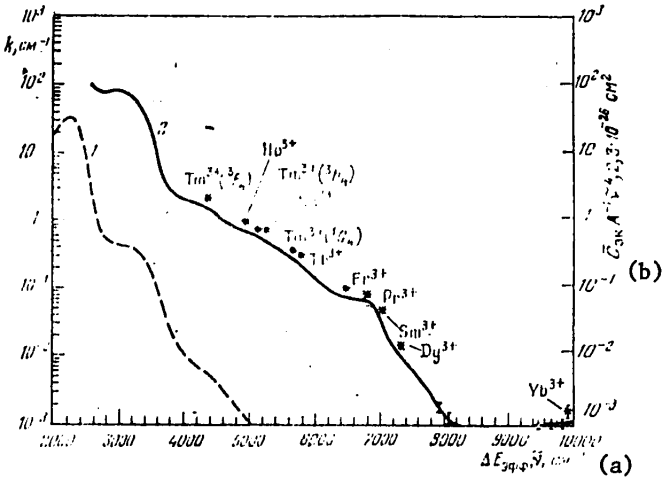

Figure 3.20. Spectral relations for the linear coefficients of absorption of the matrix (1) and OH-group (2) in glass with the composition $Ba_3AlLa(PO_3)_{12}$ and normalized experimental values of the microparameter $\bar{C}_{ev}$ for different transitions of rare earth ions (asterisks).

Key:
a. ΔE_{eff}, $\tilde{\nu}$, cm^{-1}
b. $\bar{C}_{ev}A^{-1}\tilde{\nu}^4$, $2.3\cdot10^{-26}$ cm^2

and its corollary--multiphonon relaxation of excited states of the RZI in glass. On the other hand, the possibility of calculating the probabilities of quenching luminescence of rare earth ions by OH-groups with respect to the absorption spectra and the known radiating probabilities without performing complex experiments and also the solution of the inverse problem--calculation of the radiating probabilities of the transitions with respect to the measured values of $\bar{C}_{ev}$ and k_{OH}--facilitate the development of new compositions of laser glass and determination of the required degree of their dehydration, and they also permit direct measurement of the radiating probabilities of the transitions between the high excited states, which is difficult or impossible in general by other methods.

Finally, let us note that the process of quenching of the luminescence of RZI by OH-groups is subordinate to all the laws of the theory of BPV discussed in §3.2 as applied to ion-ion interactions. In particular, a comparison of the data presented in Table 3.7 and 3.9 permits the conclusion that at least for the Nd^{3+}, Yb^{3+} and Er^{3+} ions, the migration controlled phase of quenching by OH-group must be considered within the framework of the jump model.

The studies of the functions $\bar{W}=f(N_{OH})$ indicates that, in accordance with (3.9), they are linear in a wide range of concentrations of N_{OH}. As examples, in Figures 3.21a, the relations are presented $1/\bar{\tau}=\bar{W}+1/\bar{\tau}_{\ell}=f(N_{OH})$ for ultraphosphate glass of the composition $La_{1-x}Nd_xP_5O_{14}$ [229], and in Figure 3.21b, for erbium glass with the composition $Ba_3AlLa(PO_3)_{12}$.

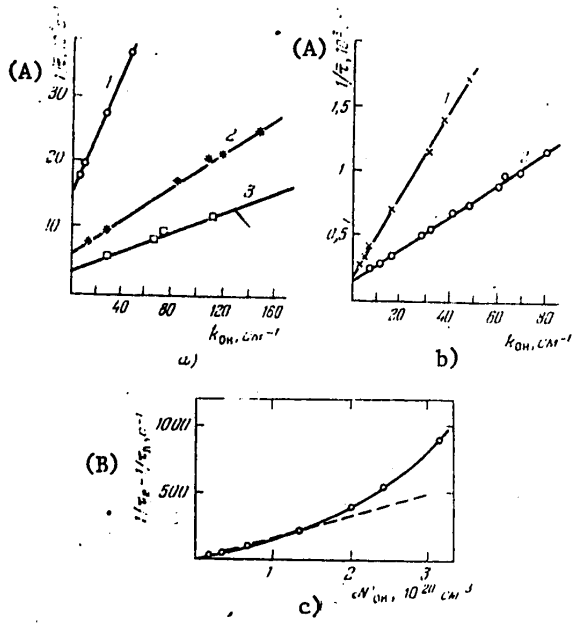

Figure 3.21. The probabilities $1/\bar{\tau}$(a,b) and $1/\tau_e - 1/\tau_\ell$ (c) of quenching of the luminescence of rare earth ions in phosphate glass as a function of the OH-group concentration. a) Glass with the composition $La_{1-x}Nd_xP_5O_{14}$, experiment; x=1 (1), 0.28 (2), 0.12 (3); b) glass with the composition $Ba_3AlLa(PO_3)_{12}$ with Er^{3+}, experiment; $N_{Er}=3.5\times10^{20}$ cm^{-3} (1), $1.3\cdot10^{20}$ cm^{-3} (2); c) glass with the composition $Ba_3AlLa(PO_3)_{12}$ with Er^{3+}; $N_{Er}=1.5\cdot10^{19}$ cm^{-3}; solid line--calculation.

Key:
A. $1/\bar{\tau}$, 10^3 sec^{-1}
B. $1/\tau_e - 1/\tau_\ell$, sec^{-1}

The linear behavior of these relations permits easy estimation of the maximum admissible values of τ_ℓ and q in the dehyrated glass without realizing the technologically difficult operation of removal of the OH-groups from the glass. This is especially convenient for erbium and highly concentrated neodymium-doped glass, where the degree of dehydration must be very high. For example, for neodymium-doped glass when x=1, it is required that $N_{OH}<1\cdot10^{19}$ cm^{-3} ($k_{OH}<1.5$ cm^{-1}), at the same time as for moderate concentrations of Nd^{3+} ions ($\sim(2\text{-}4)\cdot10^{20}$ cm^{-3} or x=0.05 to 0.1) usually used in laser elements, the admissible OH-group content is several times higher ($N_{OH}\sim(5\text{-}7)\cdot10^{19}$ cm^{-3}), which is easily achieved by ordinary technological procedures. In erbium-doped glass the situation is highly critical even for $N_{Er}\to0$, in spite of the smaller value of the parameter C_{ev} for N_{OH} must be smaller than or equal to $0.5\cdot10^{19}$ cm^{-3}, which is explained by the small radiating probability of the laser transmission of the Er^{3+} ions. It is obvious that glass with increased erbium concentration must be dehydrated to an even higher degree.

Values of $1/\tau_e - 1/\tau_\ell$ obtained experimentally and calculated by formula (3.4a) are presented in Figure 3.21, c, where τ_e is the time in which the intensity of the luminescence decreases by e times with respect to the maximum as a function of the concentration of OH-groups in $Ba_3AlLa(PO_3)_{12}$-glass with low concentration of Er^{3+} ions. These relations coincide in practice, confirming the conclusion of dipole-dipole nature of the interaction of the rare earth ions and OH. It is obvious that for $N_{OH} \leq (1\text{-}1.5).10^{20}$ cm^{-3} the function $1/\tau_e - 1/\tau_\ell = f(N_{OH})$ is easily taken as linear, just as the authors of [101, 183, 185, 193] did.

Experimental Studies of the MFR Processes on Matrix Vibrations. The basic evidence of the applicability of the inductive-resonance model in the given case is the presence of a correlation between the probabilities of multiphonon relaxation and the intensity of infrared absorption in the overtone region established by us on a large number of transitions of rare earth ions in several oxygen-containing glasses. This fact is indicated for the first time in the report [404]. In Figure 3.3 on the diagram of the energy states of rare earth ions, the solid vertical arrows indicate the investigated transitions. Figure 3.22 shows the relation $k_M(\tilde{\nu})$ in a wide spectral range for metaphosphate, borate, silicate, germanate, tellurite and fluophosphate glasses determined by computer processing of the data on the spectral transmission of samples from 10 microns to 15 cm thick in the corresponding regions of the spectrum obtained using the UR-20 and SF-8 spectrophotometers. All of the investigated types of glass were carefully dehydrated using the corresponding technological procedures, which permitted reliable isolation of the natural absorption of the glass and forming elements of the glass. For example, in phosphate glass the OH-group absorption coefficient on a frequency of the basic stretching vibrations ($\approx$3000 cm^{-1}) did not exceed 0.1 cm^{-1}. Analysis of the presented relations confirms that the linear absorption coefficient and its spectral behavior actually depend on the extent of the basic lattice vibration spectrum of the glass and $\tilde{\nu}_{max}$ (compare with the data in Table 3.8). A clear structure which is best expressed in phosphate glass is exhibited in all cases in the region of s=2-3. The average slope of the curve $k_M(\tilde{\nu})$ permits determination of the coefficients κ which, in the given case, characterize the degree of anharmony of the vibrations of the different matrices. In Figure 3.22 the experimental values of the probabilities of MFR are noted for different transitions. The explicit correlation between the functions $k_M(\tilde{\nu})$ and $\overline{W}^s(\tilde{\nu})$ is observed. At the same time, some of the points noticeably are removed from the general pattern which obviously is connected primarily with differences in the radiating probabilities of the transitions. Figure 3.23 shows the normalized values with the probabilities of MFR $\tau_{single}\overline{W}^s\tilde{\nu}4$ for transitions where it was possible to measure or calculate τ_{single} from the absorption spectra in phosphate (2) and borate (1) glass. The deviations turn out to be appreciably less in the given case.

Significant nonexponentialness of the luminescence decay curves must be noted in almost all of the investigated cases. Figure 3.24 shows the photographs of the luminescence decay curves for the Er^{3+} ions (the $^4S_{3/2}$-$^4F_{9/2}$ transition) in phosphate and fluophosphate glass. These photographs reflect the standard case. The more complicated curve corresponds to fluophosphate glass which obviously has two sublattices with frames based on phosphate fluorides. The probabilities of multiphonon relaxation of the rare earth ions introduced into each of them differ sharply from each other, and the decay curve is sharply nonexponential. This curve can be represented in the

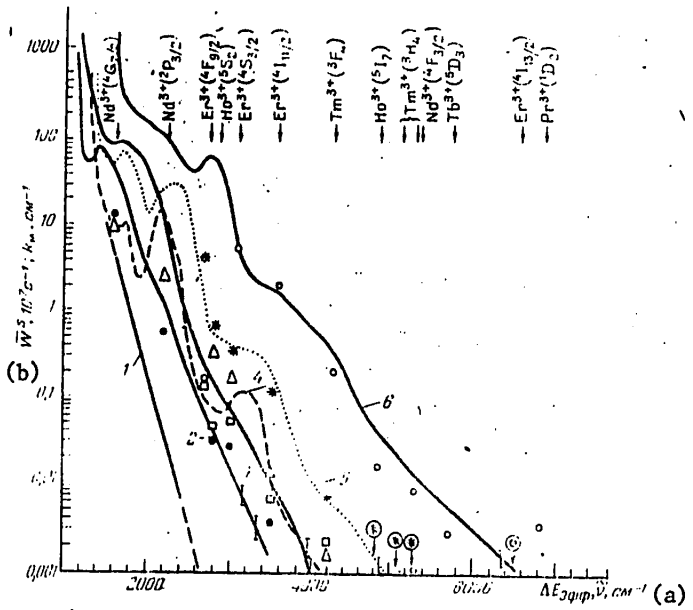

Figure 3.22. Correlation of experimental values of the probabilities of MFR $\overline{W}^S$ (the symbols) with natural absorption $k_M(\tilde{\nu})$ (lines) of the matrices in the overtone region. 1--tellurite glass, 2--germanate, 3--silicate, 4--fluophosphate, 5--phosphate, 6--borate. The symbols in the circles with arrows indicate the probability of MFR lying below the x-axis.

Key:
a. ΔE_{eff}, $\tilde{\nu}$, cm^{-1}
b. $\overline{W}^S$, 10^7 sec^{-1}; k_M, cm^{-1}

form of two quasiexponential components and, therefore, it is possible to define the probabilities of MFR and the percentage content of the rare earth ions in the two phases. The indicated fact opens up an interesting possibility for quantitative monitoring of the activator distribution in the multiphase vitreous system. So far as we know, there are no other methods of quantitative solution of the indicated problem at this time.

Analysis of the data presented in Figures 3.22, 3.23 also indicates that the probability of MFR in glass as a function of composition varies in the region of ΔE_{eff}=5000 to 7000 cm^{-1} by 4 to 5 orders, which is appreciably greater than was assumed earlier. Therefore the choice of composition for laser glass has exceptionally great significance. The possibility of quantitative prediction of the probabilities of MFR following from the obtained results greatly facilitates the solution of the indicated problem. Another consequence of these results is that the processes of relaxation of the excited states, skipping the nearest excited states, are almost completely excluded. Therefore the MFR process is a multistage, stepped process which must pass through all of the lower-lying electron states.

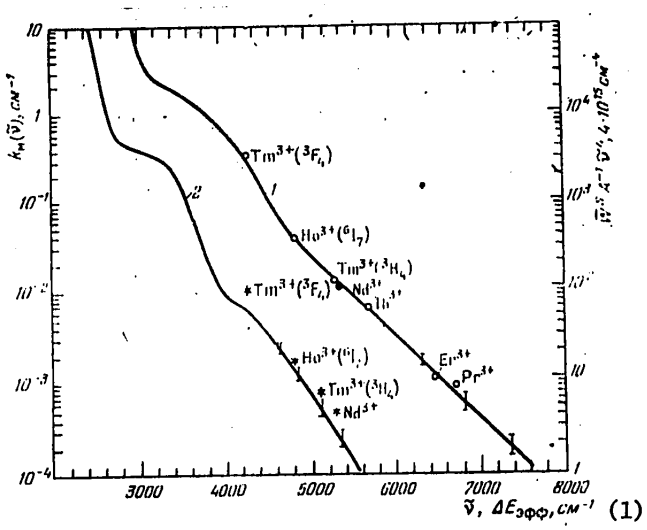

Figure 3.23. Correlation of the absorption coefficient (solid lines) of the glass matrix $k_M(\tilde{\nu})$ in the overtone region with experimental values of the probabilities MFR $\overline{W}^S$ (the symbols) from different excited states of the rare earth ions normalized by a unit radiating probability of an electron transition and $\tilde{\nu}^{-4}$.

Key:

1. $\tilde{\nu}$, ΔE_{eff}, cm^{-1}

CHAPTER 4. NEODYMIUM-DOPED PHOSPHATE GLASS

§4.1. General Description of Neodymium Laser Glass

Neodymium belongs to the group of lanthanoids, that is, elements with completing 4f-shell, whereas the shells of n=5 ($5s^2$, $5p^6$) and n=6 ($6s^2$) are completely filled. In oxide glass, the neodymium ion is surrounded by oxygen ions, as a rule, entering into the polyhedra of the glass former (the PO_4^{3-}, BO_3^{3-}, BO_4^{5-}, SiO_4^{4-} groups, and so on). The possible coordination polyhedra of Nd^{3+} and the symmetry of the environment are investigated in Chapter 2.

The excitation and luminescence of lanthanoid ions are realized as a result of internal electron transitions 4f→4f and 4f→5d. For the triple charged ions, the 4f→5d transitions correspond to the ultraviolet region of the spectrum, and the absorption and luminescence bands in the visible and infrared region are connected with the 4f→4f transitions. The optical electron is well shielded from the influence of the crystal fields of the matrix by the outer electrons, and therefore the general view of the spectrum for different matrices varies little. The influence of the matrix is felt only on variation of the relative intensity of the individual bands, their halfwidth and the amount of splitting of the components.

Neodymium-doped glass has become widespread as a result of its good laser characteristics. Active absorption of such glass is higher than glass doped with other rare earth elements. The neodymium-doped glass is colored a characteristic lilac color and has intense absorption bands in the regions of 0.58, 0.74, 0.80 and 0.90 micron (Figure 1.10). On excitation by emission from any of these wavelengths, intense infrared luminescence is observed with peaks of wavelengths of 0.9, 1.06, 1.35 and 1.8 microns. All of the luminescence bands correspond to the transition from the same metastable level $^4F_{3/2}$ to the lower-lying levels (Figure 4.1). The luminescence of Nd^{3+} from the higher levels ($^4F_{5/2}$, $^4F_{7/2}$) is weak, and it usually can be observed only at low temperature (see, for example, [417]).

Lasing is theoretically possible on all luminescent transitions from the levels $^4F_{3/2}$ to $^4I_{9/2}$, $^4I_{11/2}$, $^4I_{13/2}$, $^4I_{15/2}$, but the transition $^4F_{3/2}$→$^4I_{11/2}$ (1.06 microns) has the most practical significance. This is explained by the high induced emission cross section and four-level lasing diagram. The level $^4I_{11/2}$ "is raised" approximately 2000 cm^{-1} above the ground state, and therefore at room temperature it remains almost empty. In addition, from

this level there is rapid nonradiating relaxation of the excitation in the ground states $^4I_{9/2}$, which insures high lasing efficiency. According to the data of reference [418], the lifetime of neodymium in the state $^4I_{11/2}$ does not exceed 2 nanoseconds. Therefore neodymium-doped glass is a good material for generators and amplifiers of long light pulses.

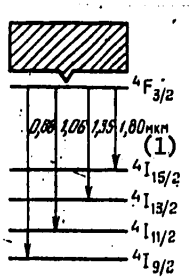

Figure 4.1. Diagram of Nd^{3+} levels in glass

Key:
1. micron

The luminescence bands of neodymium in glass are significantly wider than in the majority of crystal matrices. The broadening is of a nonuniform nature and depends weakly on the temperature. This arises from the irregular structure of the amorphous vitreous base, which leads to variation of the nearest surroundings of the Nd^{3+} ions and, correspondingly, to variation of the crystal field acting on them. The variations of strength of the crystal field and its symmetry cause variation of the amount of splitting of the terms. According to [419], the amount of splitting of the ^4I_J terms is determined by the field strength with cubic symmetry, and the terms $^4F_{3/2}$, by the strengths of the fields of lower symmetry.

When investigating alkali silicate glass [420] it was found that increasing the alkali content leads to growth of the nearest vicinity of the neodymium ionsand decreases the splitting of the $^4F_{3/2}$ level. Thus, with a content of 30 molecular % alkali oxide in the glass, this splitting is 135 cm^{-1} for Na_2O and 115 cm^{-1} for K_2O, whereas for 5 molecular % Na_2O, it reaches 160 cm^{-1}. Splitting of the ground state of the neodymium ion of the given glass almost does not depend on the composition and is about 500 cm^{-1}.

More complex relations can be observed in the process of rearrangement of the glass structure. For example, in sodium aluminum silicate glass the splitting of the $^4F_{3/2}$ varies from 150 to 220 cm^{-1} [421]. In contrast to the preceding case, the dependence of the composition is not smooth. With Al_2O_3 content of 13 to 15 molecular %, the splitting is maximal, which is connected with variation of the coordination above the aluminum. In these types of glass, analogous relations are also observed for the magnitude of the nonuniform broadening of the luminescence band of the resonance transitions $^4F_{3/2} \rightarrow {}^4I_{9/2}$. In sodium and potassium silicate glass, nonuniform broadening decreases as the alkali oxide content increases from 95 cm^{-1} to 83 cm^{-1} in sodium glass and to 78 cm^{-1} in potassium glass. In sodium aluminum silicate glass the nonuniform broadening varies from 90 cm^{-1} to 130 cm^{-1}; for Al_2O_3 content of 13 to 15 molecular %, maximum broadening is also observed.

The magnitude of the splitting of the $^4F_{3/2}$ level in phosphate glass usually is 100 to 140 cm^{-1}. Introduction of additives, for example, MgO or B_2O_3, leads to an increase in splitting.

During lasing, nonuniform broadening is accompanied by broadening of the lasing spectra [422]. Photometrizing the spectrogram of the lasing spectrum at low temperatures and with a high excess of pumping energy over the threshold, it is possible to determine the form and magnitude of the nonuniform broadening. In reference [85], the magnitude of the nonuniform broadening of 6.5 nm was found for silicate glass, and it was established that the band curve corresponding to nonuniform broadening is somewhat asymmetric. The remaining broadening of the luminescence band (usually the width of the luminescence band of the $^4F_{3/2} \rightarrow {}^4I_{11/2}$ transition in silicate glass at room temperature is 22.0 to 30 nm) is caused by Stark splitting and uniform broadening of the levels.

The Stark structure of the basic operating levels of Nd^{3+} in niobium phosphate glass was investigated in considerable detail in reference [202] (Figure 4.2). The magnitude of the splitting of the ground state $^4I_{9/2}$ in it will be about 400 cm^{-1}, which is somewhat less than in silicate glass, and more uniform distribution of the Stark halflevels indicates low symmetry of the surroundings. Nonuniform broadening of the luminescence bands for the transitions between the Stark halflevels of the $^4I_{9/2}$ and $^4F_{3/2}$ levels does not remain unchanged, but fluctuates within the limits of 40 to 200 cm^{-1} (Table 4.1).

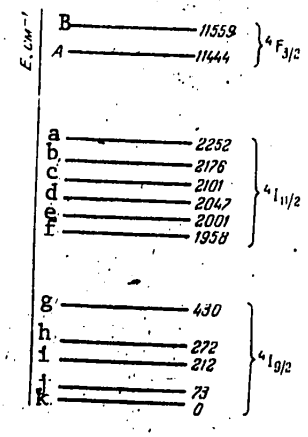

Figure 4.2. Stark structure of the basic operating levels of Nd^{3+} in niobium phosphate glass

Table 4.1.

Переход (1)	Частота полосы перехода, $см^{-1}$ (2)	Полуширина полосы, $см^{-1}$ (3)
a—A	11 444	40
a—B	11 559	80
A—a	11 444	58
A—b	11 371	110
A—c	11 232	175
A—d	11 172	195
A—e	11 014	200
A—f	9 486	67
A—g	9 441	68
A—h	9 397	71
A—i	9 343	94
A—j	9 288	94
A—k	9 192	120
B—f	9 602	115
B—g	9 542	89
B—h	9 509	80
B—i	9 459	80
B—j	9 389	100
B—k	9 301	80

Key:
1. Transition
2. Transition band frequency, cm^{-1}
3. Band halfwidth, cm^{-1}

The luminescence lifetime of neodymium in glass varies within broad limits (from 50 to 1000 microseconds [83-85]). With low activator concentration it is determined by the composition of the glass and the presence of quenching admixtures. In the borate base the luminescence lifetime of the neodymium has the least value (about 50 microseconds), and in the alkali earth silicate glass, the highest (to 1000 microseconds). The OH-groups [423], ions of transition and certain rare earth elements, which are acceptors of the neodymium excitation energy, can serve as quenching admixtures. This is discussed in more detail in Chapters 2 and 3.

Increasing the neodymium concentration above 1 to 2% by weight also leads to a reduction in the luminescence lifetime. This quenching is called concentration quenching and is explained by the cross relaxation interaction of close neodymium ions [424] (Chapter 3).

Other parameters characterizing the neodymium ion in glass are the quantum yield luminescence [118, 425], the branching coefficient [102, 118, 421, 426] and transverse cross section of the lasing transition [103, 104, 117, 118, 427, 429]. The quantum yield determines the efficiency of the conversion of the pumping light to luminescent emission, the branching coefficient gives an idea of the relative quantum yield in individual luminescence bands, and the magnitude of the induced emission cross section determines the choice of one glass or another for application in specific lasers and amplifiers.

At the present time lasing on neodymium is realized in a number of types of glass, but only silicate and phosphate bases have found broad practical application. This is explained by good luminescent and lasing characteristics of neodymium in such glass and also the possibility of achieving the required physicochemical parameters by variation of the composition of glass within broad limits.

§4.2. Spectral Luminescent Characteristics of Neodymium Phosphate Glass

The spectral luminescent characteristics of neodymium in glass are characterized by a set of parameters: the absorption and luminescence spectra, the magnitude of the Stark splitting of the levels, the magnitudes of the uniform and nonuniform broadening of the absorption and luminescence bands, probability of radiating and nonradiating transitions, the decay time of the excited state, the quantum yield of luminescence and also a number of other parameters. It is possible to find broad data and a list of papers on these questions, for example, in the survey [47]. In this section a study will be made primarily of the characteristics which, in our opinion, have direct influence on laser parameters. These are the width and the position of the luminescence band peak of the operating transition, the radiating lifetime, the resolution of the optical transitions, and the influence of the quenching admixtures.

Table 4.2.

Composition	$\Delta\lambda_{\ell}$, nm	Composition	$\Delta\lambda_{\ell}$, nm
$(PO_3)_6ZnLi_4$	20,4	$(PO_3)_{2,5}BaK_{0,5}$	20,6
$(PO_3)_6ZnK_4$	17,1	$(PO_3)_2BaK$	20,0
$(PO_3)_6CdK_4$	16,1	$(PO_3)_4BaK_2$	18,2
$(PO_3)_6CdCs_4$	16,0	$(PO_3)_6BaK_4$	15,3

The prospectiveness of neodymium phosphate glass of a material for lasers was demonstrated for the first time in [123, 430]. In reference [430], a study was made of the luminescent characteristics of neodymium in the systems P_2O_5+RMe_2O, where Me=Li, Na, K, Rb, and P_2O_5+RMeO, where Me=Be, Mg, Ca, Sr, Ba, Zn, Cd, Pb. The magnitude of R varied with respect to the entire region of glass formation In addition, studies were made of the characteristics of the mixed system $R(P_2O_5+Me_2O)+(P_2O_5+MeO)$, where R assumes values of 0, 5, 1, 2, 3, 4, 5.

For these investigations, primarily the high intensity of longwave bands in the neodymium absorption spectra by comparison with silicate glass was noted. In addition, the maximum of the luminescence band of the transition $^4F_{3/2}\rightarrow$ $\rightarrow{}^4I_{11/2}$ turned out to be shifted noticeably in the shortwave region of the spectrum. Thus, in the system P_2O_5+RCdO, the wavelength at the peak of this band was from 1051.5 to 1040.0 nm with variation of R from 0.6 to 1.2. It was also noted that the given luminescence band in a number of phosphate compositions is appreciably narrower than in any other glass base. Table 4.2 gives values of the halfwidth of this band for a number of types of glass

of the mixed system. As we shall see, increasing the alkali oxide content leads to noticeable decrease in the halfwidth. Introduction of Al_2O_3 into the glass composition is accompanied by broadening of the luminescence band.

The temperature and duration of founding have noticeable influence on the luminescent lifetime of neodymium in glass. On the average, it is 250 to 300 microseconds, and increasing the neodymium content leads to strong concentration quenching.

During lasing tests of this glass, very low threshold pumping energies were noted, which made it possible to obtain quasicontinuous lasing.

In reference [123] it was found that in phosphate glass the electron excitation transfer process between the rare earth ions proceeds more rapidly than in silicate glass. The actual lasing characteristics of phosphate glass were described there for the first time. It was discovered that phosphate glass differs from silicate glass by the narrower lasing spectrum, and the significantly larger gain of laser emission. All of this has served as an impetus to the expansion of operations in the given region.

A detailed study was made of two glass-forming systems: namely, $MePO_3$-BPO_4-MgO, where Me=Li, Na, K, and $Me(PO_3)_2$-$Al(PO_3)_3$, where Me=Mg, Ca, Sr, Ba, Zn, Cd, Pb [167, 430]. These two systems with different additives make up the base for the majority of industrial phosphate glass, both optical and laser glass.

In the noted papers it was demonstrated that luminescent and laser characteristics of neodymium in phosphate glass are determined to a significant degree by the structure of the latter. The structure of the glass is investigated in Chapter 2. The basis for the structure of the majority of pure phosphate glasses is the long polymer chains made of PO_4^{3-} tetrahedra connected with respect to the peaks. With an increase in the BPO_4 content in the glass, it is necessary to expect an increase in binding of the anion motif and partial replacement of the PO_4 groups in the coordination sphere of Nd^{3+} by BO_4 or BO_3. This increases the number of versions of the nearest vicinity of Nd^{3+} and leads to an increase in halfwidth of the nonuniformly broadened luminescence band. The nonuniform nature of the broadening is confirmed by studies of the luminescence spectra at helium temperatures. As has been demonstrated, significant variation in the magnitude of the Stark splitting of the $^4F_{3/2}$ and $^4I_{11/2}$ levels is not observed for these compositions.

Rearrangement of the glass structure found its reflection in the variation in halfwidth and position of the peak of the luminescence band of the transitions $^4F_{3/2} \rightarrow {}^4I_{11/2}$. The dependence of the halfwidth of the luminescence band on the BPO_4 content for lithium, sodium and potassium glass is presented in Figure 4.3. As follows from the performed measurements, very small halfwidth of the band is observed in glass based on sodium metaphosphate (14.4 nm); for lithium metaphosphate the halfwidth is somewhat greater (16.2 nm). Increasing the BPO_4 content to 45 molecular % leads to broadening of the band to approximately 18 nm; the least halfwidth is observed for potassium glass.

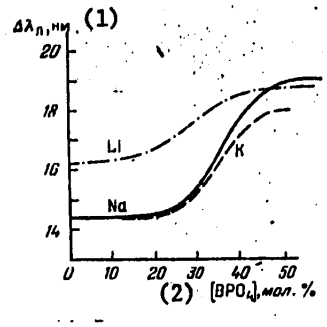

Figure 4.3. Halfwidth of the luminescence band of Nd^{3+} in glass of the $MePO_3$-BPO_4 system as a function of the BPO_4 content; Me=Li, Na, K.

Key:
1. $\Delta\lambda_0$, nm
2. $[BPO_4]$, molecular %

Increasing the broad orthophosphate content in the glass leads not only to variation of the nearest vicinity of the Nd^{3+}, but also to rearrangement of the glass structure. The presence of the BPO_4 groups corresponds to cross linking of the metaphosphate chains. By the Raman scattering spectra, it is well visible (Figure 4.4) how the transition takes place from the linear anion structure characteristic of sodium metaphosphate to the structure with high binding of the anion motif and glass with large boron orthophosphate content. In the luminescence spectra this is reflected in the shortwave shift of the luminescence band peak of the transition $^4F_{3/2} \rightarrow {}^4I_{11/2}$ in Nd^{3+} (Figure 4.5).

Another picture is observed on introduction of magnesium oxide. As its concentration in the glass increases, the content of pyrogroups and orthogroups must increase. Here the average length of the polyphosphate chains is quickly reduced, and the number of terminal groups PO_4^{3-} increases. In the Raman scattering spectra of glass the bands characteristic of metaphosphates disappear, and new bands appear corresponding to the orthogroups and pyrogroups. This rearrangement of the anion motif of glass from chain to predominantly island leads to a shift of the luminescence band peak of Nd^{3+} to the longwave region of the spectrum for sodium glass to 1056.5 nm (Figure 4.6). Strong deviation of the shift from linear is observed for potassium glass, which can be connected with partial transition of magnesium to quaternary coordination and the formation of MgO_4 groups. However, judging by the relations presented in reference [167] on the properties of glass as a function of its composition, the number of these groups must not be large.

As the MgO content in the glass increases, the halfwidth of the luminescence band of Nd^{3+} increases significantly (Figure 4.7). The probable cause is an increase in the strength of the disturbing fields caused by an increase in the second coordination sphere of Nd^{3+} ion of the number of high charge ions Mg^{2+} with small radius. However, in potassium glass the presence of MgO is felt weakly. Obviously, in this case primarily the K^+ ions are located in the second coordination sphere of neodymium.

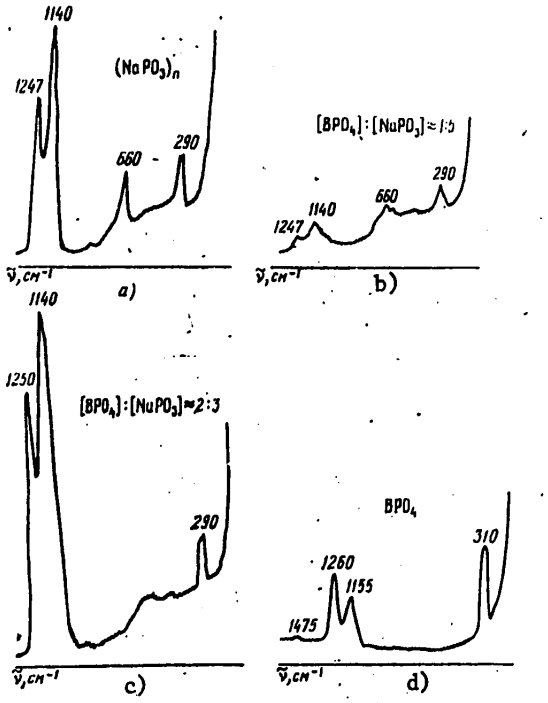

Figure 4.4. Spectra of Raman scattering of glass of the $NaPO_3$-BPO_4 system for different ratios of the components

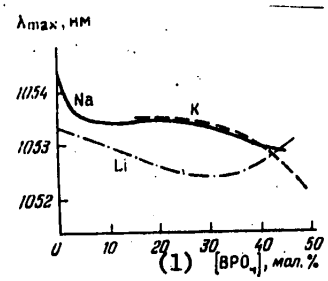

Figure 4.5. Position of the peak of the luminescence band of Nd^{3+} in glass of the $MePO_3$-BPO_4 system as a function of the BPO_4 content; Me=Li, Na, K
Key:
1. $[BPO_4]$, molecular %

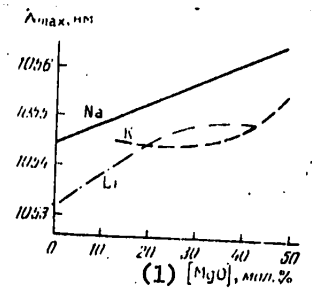

Figure 4.6. Position of the maximum of the luminescence band of Nd^{3+} in glass of the $MePO_3$-MgO system as a function of the MgO content; Me=Li, Na, K.
Key:
1. [MgO], molecular %

In glass of the ternary system $MePO_3$-BPO_4-MgO the indicated trends are retained. Consequently, on the basis of this system, it is possible to synthesize laser glass for lasing of different wavelengths and with different halfwidth of the luminescence band of the transitions $^4F_{3/2} \rightarrow {}^4I_{11/2}$. In this way it is possible to vary the lasing wavelength within the limits from 1052.0 to 1056.3 nm and, as will be demonstrated hereafter, the width of the lasing spectrum and magnitude of the cross section of the induced emission, and at the same time, the gain of the coherent signal.

In reference [167], a study was made of the glass of the $MePO_3$-B_2O_3 system, and it was demonstrated that the introduction of boron anhydride leads to broadening of the luminescence bands of Nd^{3+} and their shift to the longwave region of the spectrum for alkali metaphosphates of Li, Na and K (Figure 4.8, 4.9).

The spectral luminescent characteristics of glass based on metaphosphates of the elements Mg, Ca, Sr, Ba, Zn, Cd and Pb were studied for compositions of $(100-x)Me(PO_3)_2 \cdot xAl(PO_3)_3$ [431], where x assumed values of 0, 12.5, 25, 50 and 75 molecular %. For all pure metaphosphates of the basic subgroup (Mg, Ca, Sr, Ba) the peak of the absorption bands of the transitions $^4F_{3/2} \rightarrow {}^4I_{11/2}$ is found for the same wavelength of 1054 nm with small deviations. For Zn, Cd and Pb the peak is shifted to the shortwave region of the spectrum, especially for zinc glass. The halfwidth of the luminescence band of Nd^{3+} decreases monotonically in the series Mg-Ba from 22.6 to 18.0 nm. Here a linear correlation is observed between the radius of the cation Me^{2+} and the halfwidth of the luminescence band (Figure 4.10). This agrees well with the propostion of variation of the force of the disturbing crystalline field created by the modifier ions. The increase in aluminum phosphate content in the glass in all cases is accompanied by a shift of the luminescence band peak of Nd^{3+} to the shortwave region of the spectrum (Figure 4.11) and an increase in its halfwidth (Figure 4.12). The Ca and Mg metaphosphates constitute an exception; in the latter the halfwidth even decreases somewhat. The greatest shift in the peak is observed in zinc glass. For 50 molecular % $Al(PO_3)_3$ the lasing wavelength in it must be 1051.1 nm. Measuring the Einstein coefficients $A_{0.9}$, $A_{1.06}$, $A_{1.35}$ for luminescent transitions and Jadda coefficients Ω_2, Ω_4, Ω_6 (§4.3) demonstrated that the resolution of the transitions increases in the series Be-Ba, and the ratiosof the areas of the luminescence bands (the branching coefficients) remain almost constant (Table 4.3).

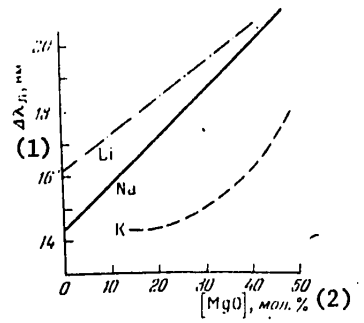

Figure 4.7. Halfwidth of the luminescence band of Nd^{3+} in glass of the $MePO_3$-MgO system as a function of the MgO content; Me=Li, Na, K

Key: 1--$\Delta\lambda_{\ell}$, nm; 2--[MgO], molecular %

The luminescent lifetime of neodymium in the investigated glasses based on alkali and alkali earth metaphosphate experiences significant fluctuation (within the limits from 200 to 350 microseconds). However, these fluctuations can be connected with the difference in residual water content as a result of inconstant synthesis conditions.

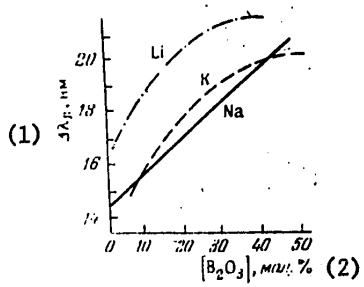

Figure 4.8. Halfwidth of the luminescence band of Nd^{3+} in glass of the $MePO_3$-B_2O_3 system as a function of B_2O_3 content; Me=Li, Na, K.
Key:
1. $\Delta\lambda_{\ell}$, nm
2. molecular %

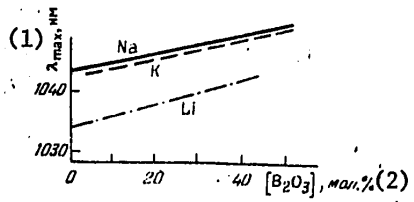

Figure 4.9. Position of the peak of the luminescence band of Nd^{3+} in glass of the $MePO_3$-B_2O_3 system as a function of the B_2O_3 content; Me=Li, Na, K
Key:
1. λ_{max}, nm
2. molecular %

The development in the USSR of experimental and industrial phosphate glass LGS-40, LGS-41, LGS-42, LGS-I, LGS-M and KGSS-1621 was a natural consequence of the performed research.

The results of studying the spectral luminescence characteristics of alkali alumophosphate glass are presented in [162]. A study was made of the glass of the Me_2O-Al_2O_3-P_5O_5 system. The phosphorus pentoxide concentration varied within the limits from 33 to 66 molecular %, and the ratio of Me_2O/P_2O_5 was selected equal to 1:1, 1:2 and 1:3. The absorption spectra of neodymium in such glass have the usual form, the most intense bands correspond to wavelengths of 590 and 794 nm. Significant variations of the spectra with temperature are not observed. The best resolution of the spectra occurs in potassium glass; the resolution becomes worse as the radius of the cation (Na^+, Li^+) decreases. The same thing also occurs with an increase in the P_2O_5 content. A decrease in the ratio Me_2O/Al_2O_3 gives the inverse effect.

The indicated variations are connected with the arrangement of the structure of the glass, the base of which is made up of the tetrahedra PO_4 and AlO_4. With a decrease in the ratio $Me_2O/Al_2O_3<1$ in the glass, AlO_6 octahedra appear. The luminescence lifetime of Nd^{3+} in the investigated glass containing 2% by weight Nd_2O_3 varies from 350 to 500 microseconds, increasing as the Me_2O content increases and the P_2O_5 content decreases. The residual water content has not been controlled.

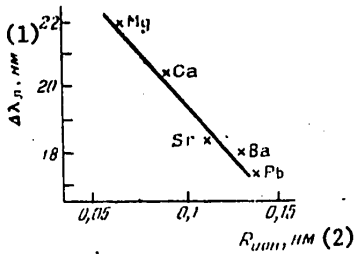

Figure 4.10. Halfwidth of the luminescence band as a function of the cation radius

Key:
1. $\Delta\lambda_{\ell}$, nm
2. R_{ion}, nm

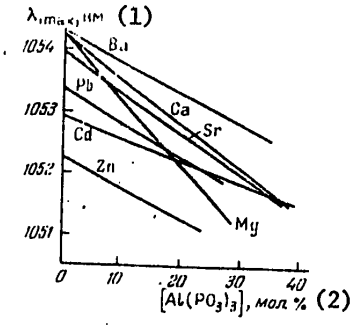

Figure 4.11. Postion of the luminescence band peak of Nd^{3+} in $Me(PO_3)_2$-$Al(PO_3)_3$ glass as a function of $Al(PO_3)_3$ content.

Key:
1. λ_{max}, nm
2. molecular %

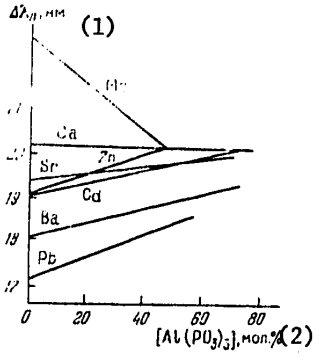

Figure 4.12. Halfwidth of the luminescence band of Nd^{3+} in glass of the $Me(PO_3)_2$-$Al(PO_3)_3$ system as a function of $Al(PO_3)_3$ content.

Key:
1. $\Delta\lambda_{\ell}$, nm
2. molecular %

In order to improve the physicochemical characteristics of alumium phosphate it is possible to introduce vanadium [433, 455] or niobium [159, 433] into their composition. On addition of vanadium pentoxide, part of the vanadium usually is reduced to tetravalent state, which leads to coloring of the glass a dark red color [416]. In order to avoid dyes when preparing the charge, yttrium orthovanadate (YVO_4) or neodymium orthovanadate ($NdVO_4$) is used. The introduction of even a relatively small quantity of YVO_4 (0 to 0.2% by weight) causes a sharp shift of the edge of the ultraviolet absorption of the glass to the longwave region of the spectrum (to 350 nm). The luminescence lifetime of the neodymium and the quantum yield of the luminescence first (to a concentration of YVO_4 of 0.35% by weight) increase, and with a further increase in the YVO_4 content, quickly decrease. The maximum of the luminescence band of neodymium corresponding to the transitions $^4F_{3/2}$-$^4I_{11/2}$

is shifted in the direction of longer wavelengths, which can be related to the rearrangement of the glass structure. Obviously, with a small content, vanadium forms the VO_4^{3-} tetrahedra which can be built into the polyphosphate chains without disturbing the overall structure of the glass, and a further increase in the V content leads to the fact that it begins to play the role of an ordinary ion modifier causing depolymerization of the vanadium phosphate anion motif.

Table 4.3

Me	Ω_4, 10^{-20} см^2	Ω_6, 10^{-20} см^2	Ω_4, 10^{-20} см^2	$A_{0,9}$, sec^{-1}	$A_{1,06}$, sec^{-1}	$A_{1,35}$, sec^{-1}	Branching coefficient	σ_ℓ, 10^{-20} см^2
Be	5,92	2,93	2,87	640	632	146	46 : 44 : 10	1,28
Mg	5,71	2,68	4,13	665	809	205	40 : 48 : 12	2,05
Ca	4,28	3,50	4,25	872	966	236	42 : 46 : 12	2,40
Sr	4,11	3,64	5,06	953	1136	286	40 : 48 : 12	2,94
Ba	2,94	4,58	5,38	1214	1316	320	43 : 46 : 11	3,00
Zn	4,80	3,26	4,51	832	991	249	40 : 48 : 12	3,0
Cd	4,23	3,42	4,75	932	1108	279	40 : 48 : 12	3,0
Pb	2,69	3,34	4,82	1241	1510	383	40 : 48 : 12	3,8

The glass composition in molecular %: 50 MeO-50P_2O_5-0.7Nd_2O_3;
σ_ℓ--value of the transverse cross section determined spectroscopically.

Analogous processes also take place in aluminum phosphate glass containing Nb [434], which indicates identical behavior of vanadium and niobium in them. Consequently, it is possible to consider that the introduction of small amounts of these elements is felt favorably in the spectral luminscence and, apparently, the lasing characteristics of aluminum phosphate glass.

The so-called fluophosphate glass is a version of phosphate glass. Fluophosphate glass, along with phosphate, can maintain up to 80 molecular % alkali earth element and aluminum fluorides. The spectral luminescence characteristics of neodymium in such a base were investigated in detail by the authors of references [115, 191, 345]. With respect to their structure, the fluophosphate glass is very similar to phosphate. For the systems investigated in reference [345], $Ba(PO_3)_2 \cdot (0.4)AlF_3 \cdot (0.6)CaF_2$ and $Ba(PO_3)_2 \cdot MgF_2$, the existence of magnesium fluoride and calcium fluoaluminate groups present in the products of crystallization of the glass along with the phosphate groupings and the fluophosphate groupings PO_3F is permissible. All of these groupings can serve as ligands in the complex molecules containing Nd^{3+}.

As the fluoride content increases, a significant shift of the peak of the luminescence band of the transition $^4F_{3/2} \rightarrow {}^4I_{11/2}$ of Nd^{3+} to the shortwave region of the spectrum is noted (Figure 4.13). For 80 molecular % fluorides, the wavelength of the peak is 1051.0 nm. The authors of [115] relate such shifts to the localization of neodymium in the fluoride component of the glass. However, beginning with the results obtained when investigating phosphate glass, the primary cause of this should be considered to be rearrangement of the structure of the glass. The halfwidth of the luminescence band of neodymium in aluminum fluophosphate glass [115] is 18 to 19 nm.

It must be noted that fluoridation is in itself a good method of dehydration of glass; therefore the fluophosphate glass contains an extraordinarily small amount of residual water and has high quantum yield of luminescence.

Table 4.4 gives the luminescence characteristics of some fluophosphate glasses: namely, the quantum yield of the luminescence q, the luminescent lifetime τ_{ℓ}, the total probability of luminescent transitions and the absorption of water contained in the glass on a wavelength of 3100 nm.

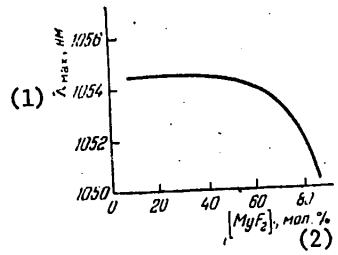

Figure 4.13. Position of the peak of the luminescence band of Nd^{3+} in barium magnesium phosphate glass as a function of the MgF_2 content

Key:
1. λ_{max}, nm
2. molecular %

Introduction of a small amount of silicon oxide into the composition of phosphate glass can be accompanied by an increase in the chemical stability and suppression of the inclination toward crystallization, which is extremely important for production. Some of the luminescence characteristics of a number of silicophosphate glasses based on alkali and alkali earth elements were studied in reference [436]. The presence of 15 to 20 molecular % SiO_2 in the composition of phosphate glass is felt little in the luminescence band width of neodymium. With a high SiO_2 content, just as in the case of the MgO and BPO_4 additives, broadening of the bands takes place.

An important luminescence parameter of the laser material is the quantum yield of luminescence. For Nd^{3+} ions in glass it is determined primarily by the concentration quenching of the luminescence and the scattering of the excitation energy of high-frequency vibrations of the molecular groupings, especially the OH-groups. The quenching of the luminescence of Nd^{3+} in glass by water was first indicated in reference [181]. The general mechanisms of quenching were investigated in Chapter 3. In [117] it was established that the luminescent lifetime of Nd^{3+} measured in the initial section of the luminescence quenching curve depends on the water content in the glass, and the lifetime measured on its "tail," almost does not depend on it and is determined by the neodymium ions with the least luminescence intensity. This process is analyzed in detail in §3.3.

At the present time it has been demonstrated that in condensed media, in the vibrational spectra of which there are no high-frequency components, the quantum yield of luminescence of neodymium with low concentration of it can approach one [412]. The highest frequency vibrations in the spectrum of phosphate glass lie in the region of 1000 to 1500 cm^{-1}, and therefore in them quite high quantum yield must also be observed. According to the data of references [118, 425], with careful dehydration it approaches 0.8.

Concentration quenching of the luminescence of neodymium as a function of the glass composition usually begins to be felt for Nd_2O_3 content of 1 to 3% by weight [117]. The quenching of luminescence is characteristic of all multicomponent systems, but homogeneous types of glass not subject to microstratification are the least subject to it (Chapter 2). A significant difference of the concentration quenching from water quenching is the possibility of the occurrence (with a quite large neodymium content) of the Nd^{3+} ion associates almost completely losing the possibility of luminescence as a result of strong exchange interaction.

Table 4.4.

No	Composition, molecular %	q	τ_l, microseconds	$\frac{A(^4F_{3/2})}{10^3}$, sec^{-1}	k_{3100}, cm^{-1}
1	$Ba(PO_3)_2$	0,70	310	2,26	1,250
2	$50Ba(PO_3)_2 \cdot 50MgF_2$	0,92	340	2,70	0,130
3	$30Ba(PO_3)_2 \cdot 70MgF_2$	0,95	410	2,32	0,143
4	$50Ba(PO_3)_2 \cdot 20AlF_3 \cdot 30CaF_2$	0,93	370	2,51	0,125
5	$10Ba(PO_3)_2 \cdot 36AlF_3 \cdot 54CaF_2$	0,95	530	1,79	0,075

Nd_2O_3 concentration in the glass was 1% by weight.

If in ordinary laser glasses the neodymium ion concentration fluctuates within the limits of $(1-4) \cdot 10^{20}$ cm^{-3} (1 to 4 % by weight Nd_2O_3), then, for example, in glass with the composition NdP_5O_{14} (neodymium pentaphosphate) it can reach $3.6 \cdot 10^{21}$ cm^{-3}. It is not possible to obtain homogeneous glass even for the ordinary multicomponent glass with this neodymium content as a result of the inclination of such glass to crystallization and stratification during the founding process. On the basis of mixed alkali and alkali earth metaphosphates and neodymium metaphosphate it is possible to obtain highly homogeneous glass containing up to 30% by weight or more Nd_2O_3. A number of luminescent characteristics of such types of glass are presented in Tables 4.5, 4.6 [229, 4362. As can be judged by the ratio of the radiating τ_0 and maximum τ_{max} luminescence lifetime obtained by approximation of the dependence of the lifetime on water content in the glass to its zero content, the quantum yield of neodymium luminescence in such glass for Nd^{3+} concentrations to $4 \cdot 10^{21}$ cm^{-3} can reach 0.15 to 0.2. This makes them an entirely suitable material, for example, for microlasers--devices where small volumes of working material are required. The maximum of the luminescence band of the

$^4F_{3/2} \rightarrow {}^4I_{11/2}$ transition for all mixed metaphosphates is located at 1053 nm, which is somewhat less than for the ordinary alkali and alkali earth metaphosphates (1054 nm). The halfwidth of the luminescence bands is high and depends weakly on the type of cation; both for sodium and for barium glass it is 21 nm. Attention is attracted by the broadening of the luminescence band in the glass with the composition $MePO_3(Me(PO_3)_2)\cdot xNd(PO_3)_3$ as the neodymium content increases. Whereas for a neodymium content in barium metaphosphate in the amount of several percentages the halfwidth was 18.0 nm, in glass with the composition $Ba(PO_3)_2\cdot Nd(PO_3)_3$ it reached 21.0 nm and increased to 22.8 nm in $Ba(PO_3)_2\cdot 2Nd(PO_3)_3$. The same thing occurs also in alkali metaphosphates, for with a small neodymium content in sodium metaphosphate or potassium metaphosphate the halfwidth is 14.0 nm. This dependence of the halfwidth on the concentration can indicate significant electrostatic interaction between the neodymium ions in such matrices, which nevertheless does not lead to strong quenching of the Nd^{3+} luminescence. It is also possible to state that a decrease in the cation radius, for example,

Table 4.5

Composition	N, 10^{21} см$^{-3}$	λ_{max}, nm	$\Delta\lambda_л$, nm
$LiPO_3\cdot Nd(PO_3)_3$	4,14	1053,0	21,6
$NaPO_3\cdot Nd(PO_3)_3$	3,95	1053,0	21,6
$KPO_3\cdot Nd(PO_3)_3$	3,76	1052,8	20,4
$Sr(PO_3)_2\cdot Nd(PO_3)_3$	—	1053,4	21,8
$Ba(PO_3)_2\cdot Nd(PO_3)_3$	3,1	1053,6	21,0
$Pb(PO_3)_2\cdot Nd(PO_3)_3$	—	—	20,8
$Ba(PO_3)_2\cdot 2Nd(PO_3)_3$	3,8	1053,5	22,8
$Ba(PO_3)_2\cdot 2Nd(PO_3)_3\cdot 2La(PO_3)_3$	—	1053,6	22,8
$Nd_2O_3\cdot 5P_2O_5$	3,6	1051,3	23,4
$Nd(PO_3)_3$	—	—	24,0

Composition	τ_0, 10^{-6} sec	$\tau_л$, 10^{-6} sec	τ_{max}, 10^{-6} sec
$LiPO_3\cdot Nd(PO_3)_3$	350	35	60
$NaPO_3\cdot Nd(PO_3)_3$	340	40	60
$KPO_3\cdot Nd(PO_3)_3$	330	60	65
$Sr(PO_3)_2\cdot Nd(PO_3)_3$	—	—	—
$Ba(PO_3)_2\cdot Nd(PO_3)_3$	330	30	30
$Pb(PO_3)_2\cdot Nd(PO_3)_3$	—	—	—
$Ba(PO_3)_2\cdot 2Nd(PO_3)_3$	420	29	30
$Ba(PO_3)_2\cdot 2Nd(PO_3)_3\cdot 2La(PO_3)_3$	—	—	—
$Nd_2O_3\cdot 5P_2O_5$	325	55	70
$Nd(PO_3)_3$	—	12	15

replacement of Ba by Sr leads to a noticeable increase in the probability of nonradiating relaxation, which can be explained by a decrease in the spacing between adjacent neodymium ions.

Table 4.6

Composition, molecular %	Ω_2, 10^{-20} cm^2	Ω_4, 10^{-20} cm^2	Ω_6, 10^{-20} cm^2	$A_{0,9}$, sec^{-1}	$A_{1,06}$, sec^{-1}	$A_{1,35}$, sec^{-1}	Branching Coefficient	τ, 10^{-6} sec
$22{,}6Al_2O_3 \cdot 2{,}4Nd_2O_3 \cdot 75P_2O_5$	7,64	2,89	4,74	718	936	243	38 : 49 : 13	2,08
$14{,}3Al_2O_3 \cdot 2{,}4Nd_2O_3 \cdot 83{,}3P_2O_5$	10,78	4,53	5,82	1053	1281	298	40 : 49 : 11	2,90
$22{,}6In_2O_3 \cdot 2{,}4Nd_2O_3 \cdot 75P_2O_5$	6,56	3,88	4,38	1088	1159	268	43 : 46 : 11	2,12
$14{,}3In_2O_3 \cdot 2{,}4Nd_2O_3 \cdot 83{,}3P_2O_5$	9,45	4,54	4,92	1213	1264	290	44 : 46 : 10	2,34
$22{,}6Y_2O_3 \cdot 2{,}4Nd_2O_3 \cdot 75P_2O_5$	7,11	2,35	4,32	692	955	253	37 : 50 : 13	1,70
$14{,}3Y_2O_3 \cdot 2{,}4Nd_2O_3 \cdot 83{,}3P_2O_5$	8,30	3,65	4,32	893	1038	237	41 : 48 : 11	2,00
$22{,}6La_2O_3 \cdot 2{,}4Nd_2O_3 \cdot 75P_2O_5$	5,88	2,93	4,04	809	962	242	40 : 48 : 12	1,99
$14{,}3La_2O_3 \cdot 2{,}4Nd_2O_3 \cdot 83{,}3P_2O_5$	7,18	3,04	4,47	664	1011	266	34 : 52 : 14	2,28
$12{,}2La_2O_3 \cdot 12{,}8Nd_2O_3 \cdot 75P_2O_5$	5,32	3,14	3,05	918	1038	247	42 : 47 : 11	2,24
$3{,}9La_2O_3 \cdot 12{,}8Nd_2O_3 \cdot 83{,}3P_2O_5$	6,19	3,28	4,56	923	1101	267	40 : 48 : 12	2,51

In contrast to the mixed metaphosphates, the wavelength of the maximum luminescence band for neodymium pentaphosphate is 1051 nm, and the halfwidth of the band is 23.4 nm. In recent times, luminescence of neodymium has also been detected in the form of the pure metaphosphate. The luminescence lifetime for glass not subject to careful dehydration was 12 microseconds.

In addition to the quantum yield of the luminescence, the neodymium ion in glass is characterized by the intensity of the luminescence bands arising on transition from the levels $^4F_{3/2}$ to the lower-lying levels $^4I_{15/2}$, $^4I_{13/2}$, $^4I_{11/2}$, $^4I_{9/2}$. The intensity of the luminscence band is determined by the Einstein coefficients for these transitions. These and other data for industrial phosphate glass are presented in Table 4.7 [47]. Table 4.8 gives comparative characteristics of the glass on a different base [103]. In our glass except the glass indicated in the last column of Table 4.8, Nd was introduced in the form of an oxide, and in the glass in the last column, in the form of the fluoride.

Table 4.7

Type of glass	Nd_2O_3, % by weight	N, 10^{20} cm^{-3}	q	$A(^4F_{3/2} \rightarrow {}^4I_J)$			τ, microseconds	λ_{max}, nm	$\Delta\lambda$, nm
				$J=9/2$	$J=11/2$	$J=13/2$			
GLS-21	1,11	1,38	0,73				340	1 055	19
GLS-22	1,63	2,0	0,74	1047	1557	278	300	1 055	19
GLS-23	2,89	3,6	0,0				250	1 055	19
GLS-24	4,59	5,7	0,44				210	1 055	19
LGS-40	3,1	2,75		1063	1489	303	220	1 054	14
LGS-41	3,2	3,06					230	1 054	18
LGS-42							260	1 054	18
LGS-54	2,0	2,01	0,7	1240	1660	359	280	1 055	17
LGS-55	2,0	1,90	0,56	860	1219	248	310	1 053	19
LGS-56	2,0	1,93	0,58	886	1186	257	300	1 054	19
LGS-N-1	1,11	1,33					300	1 055	19
LGS-N-2	1,92	2,33					280	1 055	19
LGS-M	3,0	3,17					260	1 054	18
LFG-11	4,0	1,52					645		32
LHG-5	3,31	3,17					290	1 056	18,6
LHG-6	3,62	3,39					277		18,8
LHG-7	3,38	3,04					305	1 054	18,2

§4.3. Spectroscopic Methods of Measuring Some Luminescence and Lasing Characteristics of Neodymium Glass

One of the widespread methods of determining the spectral luminescence characteristics of Nd^{3+} in glass is based on the results of references [437, 438]. The authors of these papers have demonstrated that the strength of the transition lines between levels of the trivalent rare earth ions can be described by the following expression:

$$\mathcal{P}(S, L, J \rightarrow S', L', J') = \sum_{b=2,4,6} \Omega_b |\langle J | U^b | J' \rangle|^2, \qquad (4.1)$$

where S, L, J are the main quantum numbers of the initial level, S', L', J' are the main quantum numbers of the final level, $|\langle J||U^b||J'\rangle|$ are the matrix elements of the unit tensor operator which do not depend on the composition of the base, Ω_b is the Jadda coefficient taking into account the influence of the base.

According to [444], it is possible to express the following values in terms of P:

The integral band intensity

$$\int k(\lambda)\, d\lambda = \frac{8\pi^3 e^2 \lambda N}{3ch(2J+1)} \frac{1}{n} \left[\frac{(n^2+2)^2}{9}\right] \mathcal{P}, \qquad (4.2)$$

where n is the index of refraction in the base, N is the volumetric concentration of the neodymium ions, e is the electron charge, λ is the average wavelength of the transition, c is the speed of light, h is the Planck constant, $k(\lambda)$ is the absorption coefficient on a wavelength of λ;

The probability of spontaneous transition

$$A(S, L, J \to S', L', J') = \frac{64\pi^4 e^2}{3h(2J+1)\lambda^3} n\left[\frac{(n^2+2)^2}{9}\right]\mathcal{P}; \tag{4.3}$$

The oscillator strength

$$f = \frac{mc^2}{\pi e^2}\frac{9n}{(n^2+2)^2}\frac{1}{N}\int k(\tilde{\nu})\,d\tilde{\nu}, \tag{4.4}$$

where m is the electron mass, N is the concentration of the neodymium ions.

Knowing the probabilities of spontaneous transitions from the metastable Nd^{3+} level, it is possible to find the branching coefficient[1]

$$\beta\left({}^4F_{3/2} \to {}^4I_J\right) = \frac{A\left({}^4F_{3/2} \to {}^4I_J\right)}{\sum_J A\left({}^4F_{3/2} \to {}^4I_J\right)}, \tag{4.5}$$

The usual lifetime

$$\tau_0 = \left[\sum_J A\left({}^4F_{3/2} \to {}^4I_J\right)\right]^{-1}, \tag{4.6}$$

Quantum luminescence yield

$$q = \frac{\tau_л}{\tau_0}, \tag{4.6a}$$

where $\tau_л$ is the luminescence lifetime of neodymium, and the value of the cross section of the induced emission at the maximum of the working transition band

$$\sigma_л = \frac{\lambda^4}{8\pi c n \Delta\lambda_{эфф}} A\left({}^4F_{3/2} \to {}^4I_J\right), \tag{4.7}$$

(1)

Key: 1. eff

where $\Delta\lambda_{eff}$ is the effective halfwidth of the luminescence band. The matrix elements used for these calculations were calculated in references [437, 439, 440], and the measurements reduce to determining the parameters Ω_b with respect to the absorption spectra. For example, in [439], 21 absorption bands of neodymium were used for this purpose; in [104], 9 bands were used. The investigation of the influence of the number of bands taken into account on the accuracy of determining the parameters Ω_b was performed in reference [102], and it was demonstrated that variation of their number from 6 to 10 does not lead to a significant change in the value of Ω_b.

[1]These branching coefficients differ from the ones presented in Table 4.6 by a constant factor.

Table 4.8

Glass composition, % by weight	$67P_2O_5$ 18BaO 15K_2O	$67B_2O_3$ 18BaO 15K_2O	$67GeO_2$ 18BaO 15K_2O	$67SiO_2$ 18BaO 15K_2O	$80TeO_2$ 20BaO	$11SiO_2$ 5BaO $32Al_2O_3$ $52CaO$	$50SiO_2$ 25Na_2O 25TiO_2	$80LiF$ $20Al(PO_3)_3$ ($0.5NdF_3$)
$\sum_J A_J$	2888	2326	2299	1602	4193	2660	2323	2695
$\beta=\frac{A_J}{\sum_J A_J}$ $J=9/2$	0,43	0,42	0,46	0,45	0,45	0,45	0,43	0,42
$J=11/2$	0,48	0,49	0,45	0,46	0,46	0,46	0,47	0,48
$J=13/2$	0,09	0,09	0,08	0,08	0,08	0,08	0,09	0,09
$J=15/2$	0,005	0,005	0,004	0,004	0,004	0,004	0,004	0,005
Radiation lifetime τ_R, microseconds	346	419	435	624	239	392	309	371
λ_{max}, nm	1055	1061	1062	1060	1063	1069	1064	1054
$\Delta\lambda_{eff}$, nm	25,3	36,8	34,7	34,9	28,9	43,1	38,6	27,2
σ_g, 10^{-20} cm^2	4,1	2,2	1,9	1,5	2,9	1,8	2,5	3,6

$\Delta\lambda_{eff}$ is the halfwidth of the luminescence band normalized to the gaussian curve [103].

The operation of determining the cross section of the induced emission was simplified somewhat by the author of [441]. For this purpose use is made of the fact that the ratios of the area of the absorption band on λ=750 nm ($^4I_{9/2}\rightarrow{}^4F_{7/2}$; $^4I_{9/2}\rightarrow{}^4S_{3/2}$) to the areas of the radiation bands on λ=1060 nm ($^4F_{3/2}\rightarrow{}^4I_{11/2}$) and λ=1335 nm ($^4F_{3/2}\rightarrow{}^4I_{13/2}$) depend weakly on the composition of the glass. Measurements by the proposed method reduce to determining the absorption band strength P_{750} and the calculation by the formulas

$$\sigma_{1060}=2{,}70\cdot10^{-6}\,\text{см}\cdot\mathcal{P}_{750}/\Delta\lambda^{(1)}_{эфф(1060)}, \quad (4.8a)$$

$$\sigma_{1335}=1{,}365\cdot10^{-6}\,\text{см}\cdot\mathcal{P}_{750}/\Delta\lambda^{(1)}_{эфф(1335)}. \quad (4.8b)$$

Key: 1. eff

Testing demonstrated good coincidence with the data obtained by other methods for various types of glass.

The band strength P_{750} is defined by the expression

$$\int k(\lambda)\,d\lambda=\frac{N8\pi^3e^2\lambda\xi\mathcal{P}}{3ch(2J+1)}, \quad (4.9)$$

where $k(\lambda)$ is the absorption coefficient (cm^{-1}), N is the volumetric concentration of Nd^{3+}, J is the quantum number of the lower level $^4I_{9/2}$, $\xi=(n^2+2)^2/9n$ is the correction factor of the local field in the dielectric.

In a number of papers, the lasing transition cross section is calculated in terms of the measured Einstein coefficients. For example, in [427] for determination of the probability of the transition, the formula

$$A\left({}^4F_{3/2}\rightarrow {}^4I_{9/2}\right)=\frac{A_1+\sum_{i=2}^{5}A_i}{A_1}\frac{8\pi n^2\nu_1}{N_1c^2}\int k_1(\nu)\,d\nu, \tag{4.10}$$

is used where A_1 is the probability of spontaneous transition between the lower Stark components of the ground state of $^4I_{9/2}$ and the excited state $^4F_{3/2}$, ν_1 is the frequency of this transition, $\sum_{i=2}^{5}A_1$ is the total probability of all spontaneous transitions on the lower component of the excited state to the upper halflevels 2, 3, 4, 5 of the ground state, N_1 is the population of the lower Stark component of the state $^4I_{9/2}$.

The value of A_1 is found from the resonance absorption spectrum and the helium temperature, and the ratio $(A_1+\sum_{i=2}^{5}A_1)/A_1$, from the luminescence spectrum of the same transition also at helium temperature. Hereafter the value of σ_ℓ will be defined by the expression

$$\sigma_n=\frac{\lambda_{1,06}^5}{8\pi n^2 c\lambda_{0,88}}\frac{1}{\Delta\lambda_{1,06}}\frac{1}{\tilde{\beta}}A\left({}^4F_{3/2}\rightarrow {}^4I_{9/2}\right), \tag{4.10a}$$

where $\tilde{\beta}$ is the ratio of the luminescence energies of the transitions $^4F_{3/2}\rightarrow{}^4I_{9/2}$ and $^4F_{3/2}\rightarrow{}^4I_{11/2}$.

In reference [118], a somewhat different formula is used, namely:

$$\sigma_n=A\left({}^4F_{3/2}\rightarrow {}^4I_{11/2}\right)\frac{\lambda^2}{4\pi^2n^2\Delta\nu}. \tag{4.10b}$$

Since the total probability of all radiation transitions from the metastable state is connected with the radiation lifetime of τ_0 (4.6), measurement of the luminescence lifetime and quantum yield of the luminescence permits determination of the value of $\tau_0=\tau_\ell/q$.

Normalizing the total luminescence spectrum of neodymium, it is possible to find the ratio of the number of quanta emitted during lasing transition to the total number of emitted quanta as the ratio of the area of the transition band $^4F_{3/2}\rightarrow{}^4I_{11/2}$ to the sum of the areas of all the luminescence bands and, consequently, to find $A(^4F_{3/2}\rightarrow{}^4I_{11/2})$. After substitution of the obtained result in formula (4.10b) we find σ_ℓ.

For determination of the quantum yield of the luminescence of neodymium glass frequently a traditional method is used utilizing the selective excitation source and integrating sphere [425].

§4.4. Cross Section of Induced Emission of Nd^{3+} Ions in Glass

The determination of the induced emission cross section of Nd^{3+} or other ions in glass has its peculiarities caused by nonuniform broadening of the levels in the energy spectrum of the laser ions. Nonuniform broadening is manifested not only in erosion of the electron states in some energy interval, but also the difference in resolution of the transitions between these states. It is also necessary to pay attention to the fact that the upper laser level of Nd^{3+} has two Stark components, and the lower, 6, and out of the 12 transitions, those for which the induced emission cross section on the lasing frequency is nonzero can participate in the induced emission. All of the indicated facts can be considered by defining $\sigma(\nu)$ as follows

$$\sigma(\nu, t) = \frac{\int_0^\infty \int_{\Delta Y} \sigma(A)\,\gamma(\nu, \nu')\,N(A, \nu', t)\,dA d\nu'}{\int_{\Delta Y} \int_0^\infty N(\nu', A, t)\,dA d\nu'}, \tag{4.11}$$

where $\sigma(A)$ is the integral cross section of the induced emission of a luminescence center with the probability of spontaneous emission A; $\gamma(\nu, \nu')$ is the form of the uniformly broadened line with peak at ν' normalized by 1; $N(A, \nu', t)$ is the inverse population of the Nd^{3+} ions on the level $^4F_{3/2}$ with resonance frequency ν' and probability of spontaneous emission A at the time t. Integration with respect to ν' is carried out in the spectral range of ΔY bounded by the complete width of the luminescence band of the transitions $^4F_{3/2} \rightarrow {}^4I_{11/2}$, and with respect to A, from 0 to ∞. Let us introduce the distribution function $\rho_i(A, \nu)$ normalized at each point in time such that

$$N(A, \nu, t) = N_i(t)\,\rho_i(A, \nu), \text{ т. е. } \int\int \rho_i(A, \nu)\,dA d\nu = 1. \tag{4.12}$$

Here $N_i(t)$ is the total number of excited particles per cubic centimeter. For the induced emission cross section $\sigma(\nu, t)$, we obtain

$$\sigma(\nu, t) = \int\int \sigma(A)\,\gamma(\nu, \nu')\,\rho_t(A, \nu')\,dA d\nu', \tag{4.13}$$

that is, at each point in time t $\sigma(\nu, t)$ is defined by the shape of the luminescence band given by the two-dimensional distribution function $\rho_t(A, \nu)$. The kinetic equation describing the variation in particle density distribution N(A, ν, t) in the case of the four-level system has the following form on neglecting the variation of the number of particles in the ground state $^4I_{9/2}$ [454]

$$\begin{aligned}\frac{\partial N(A, \nu, t)}{\partial t} = {} & (h\nu)^{-1}\varepsilon_m \rho_0(A, \nu) - N(A, \nu, t)\,A - \\ & - \sigma_0(A)\,N(A, \nu, t)\int \gamma(\nu, \nu')\,I(\nu', t)\,d\nu' + \\ & + w_m\left[\rho_0(A, \nu)\int N(A, \nu, t)\,dA\,d\nu - N(A, \nu, t)\right],\end{aligned} \tag{4.14}$$

where $(h\nu)^{-1}\varepsilon_m$ is the pumping rate, I(ν, t) is the emission intensity on a frequency of ν, $\rho_0(A,\nu)$ is the distribution function determing the population of the metastable state by pumping, w_m is the probability of energy exchange between ions. Using (4.14), let us demonstrate that even in the absence of induced emission and energy transfer, the cross section defined

by formulas (4.11) and (4.13) will vary as a function of the excitation conditions of the particle ensemble.

If the ion dispersion with respect to frequencies inside the nonuniformly broadened line does not correlate with the dispersion with respect to A[1], it is possible to represent the distribution function in the absence of induced emission in the form of the product of the distribution function with respect to A and the frequency ν:

$$\rho(A, \nu) = \rho(A)\rho(\nu), \tag{4.15}$$

where

$$\int \rho(A)\, dA = 1 \text{ and } \int \rho(\nu)\, d\nu = 1. \tag{4.16}$$

The solution of (4.14) in the absence of induced emission and in the case of rectangular shape of the excitation pulse lasting t_1 is represented in the form

$$N(A, \nu, t) = \frac{(h\nu)^{-1} e_m}{A} \rho_0(A, \nu)\left(1 - e^{-At}\right) \text{ for } t \leqslant t_1, \tag{4.17a}$$

$$N(A, \nu, t) = \frac{(h\nu)^{-1} e_m}{A} \rho_0(A, \nu)\, e^{-A(t-t_u)}\left(1 - e^{-At_1}\right) \text{ for } t > t_1. \tag{4.17b}$$

For a short excitation pulse ($At_1 \ll 1$) from (4.11), (4.12), (4.15), (4.17), considering that $\sigma = \alpha A$, where α is a constant coefficient, we obtain

$$\sigma(\nu, t) = \alpha F(\nu)\, \bar{A}, \tag{4.18}$$

$F(\nu) = \int \gamma(\nu, \nu')\, \rho(\nu')\, d\nu'$; $\bar{A} = \int A\rho(A)\, dA$ is the average value of A.

For the steady excitation mode $t < t_1 \to \infty$

$$\sigma(\nu, \infty) = \alpha F(\nu)\left(\overline{A^{-1}}\right)^{-1}. \tag{4.19}$$

Inasmuch as $\bar{A} \geqslant (\overline{A^{-1}})^{-1}$, then

$$\sigma(\nu, t) \geqslant \sigma(\nu, \infty).$$

---

[1] In the presence of a correlation it is easy to obtain the same results using a uniform distribution function.

Analogously, if the ensemble of Nd^{3+} ions is excited by the short pulse ($At_I<<1$), and luminescence decay of excitation then occurs,

$$\sigma(\nu, t') = \alpha F(\nu) \frac{\int \rho(A) A e^{-At'} dA}{\int \rho(A) e^{-At'} dA}, \qquad (4.20)$$

where $t'=t-t_i$. Obviously if $\rho(A)=\delta(A-A_0)$[1] (the case of absence of dispersion with respect to A), then $\sigma(\nu, t')=\alpha A_0 F(\nu)=\sigma(A)F(\nu)$. It is easy to demonstrate that for the distribution function with respect to A differing from the δ-function, $\sigma(\nu, t')$ decreases monotonically with an increase in t'.

Using equation (4.14), it is also possible to show that for a probability of energy exchange between the ions $w_m>>A$, the induced emission cross section does not depend on the excitation conditions and does not vary on damping of the excitation of the ensemble of particles as a result of the luminescence processes.

Thus, the induced emission cross section in the active medium with nonuniform broadening depends to a significant degree on the pumping conditions and evolution of the ensemble of excited particles at measurement time. Let us consider the procedures for determining the induced emission cross section of Nd^{3+} which have become quite widespread; one of them is based on using the spectroscopic methods to determine the value of the integral cross section of the laser transmission emission averaged with respect to the set of Nd^{3+} ions and the shape of the luminescence band. The induced emission cross section is naturally calculated by the formulas similar to formula (4.13).

Secondly, the laser procedure is used to determine the relative variation in the inverse population under the effect of the laser pulse with known energy density, and for calculation of $\sigma(\nu)$ expression (4.14) is used.

It must be noted that a value close to $\sigma(\nu_{max}, \infty)$ is determined by the spectroscopic methods (ν_{max} is the frequency of the maximum intensity of the luminescence band), whereas in the laser procedures, an effective cross section $\sigma_{eff}=\sigma(\tilde{E})$ is measured ($\tilde{E}$ is the energy density in the radiation pulse). It will be demonstrated below that for a narrow-band signal having small energy density and coinciding with respect to frequency with the peak luminescence band intensity, $\sigma_{eff}(\tilde{E})\underset{\tilde{E}\to 0}{\sim}\sigma(\nu_{max}, t)$. Consequently, in accordance with formula (4.19) $\sigma_{eff}(0)\geq\sigma(\nu_{max}, \infty)$. This fact is one of the causes leading to higher values of the cross section determined by the laser methods. Another cause consists in the difference in the integration intervals with respect to the spectrum: in the spectroscopic procedure the integration is carried out with respect to all transitions between levels $^4F_{3/2}\to{}^4I_{11/2}$; in the laser procedure only two transitions are actually considered--between the Stark components of the state $^2F_{3/2}$ and the lower components of the level $^4I_{11/2}$.

---

[1]Here and hereafter δ is the Dirac delta function.

Under the effect of coherent emission, the distribution function $\rho(A, \nu)$ and the form of the luminescence band of the laser transition can be significantly deformed, which leads to dependence of $\sigma(\nu, t)$ on the energy density of the emission, interacting with the inverse medium. Actually, with application of the laser pulse of duration $t_1 \ll \tau$ (τ is the lifetime of the state $^4F_{3/2}$), for which it is possible to neglect all processes, except the induced processes, the density of the inverse population $N(A, \nu, t)$ is defined by the solution of the equation (4.14):

$$N(A, \nu, t) = \\ = N(A, \nu, 0) \exp\left\{-\sigma(A) \int_{\Delta Y} \int_0^t \gamma(\nu, \nu') I(\nu', t')\, d\nu' dt'\right\}. \quad (4.2) \qquad (4.21)$$

Introducing the particle distribution function $\rho(A, \nu)$ at the time of arrival of the laser pulse and denoting by $N_1(0)$ the inverse population at the time (that is $N(A, \nu, 0) = N_1(0)\rho(A, \nu)$), we convert equation (4.13) to the form

$$\sigma(\nu, t) = \int_{\Delta Y} \int_0^\infty \sigma(A) \gamma(\nu, \nu'') N_{\text{н}}(0) \rho(A, \nu'') \times \\ \times \exp\left\{-\sigma(A) \int_{\Delta Y} \int_0^t \gamma(\nu, \nu') I(\nu', t')\, d\nu' dt'\right\} dA d\nu'' \times \\ \times \left[\int_{\Delta Y} \int_0^\infty N_1(0) \rho(A, \nu'') \times \right. \\ \left. \times \exp\left\{-\sigma(A) \int_{\Delta Y} \int_0^t \gamma(\nu, \nu') I(\nu', t')\, d\nu' dt'\right\} dA d\nu''\right]^{-1}. \qquad (4.22)$$

As we shall see, the magnitude of the induced emission cross section decreases in the process of forced emission.

For description of the propagation of the emission in the four-level medium with nonuniform broadening, a system of equations for emission intensity and for population is used:

$$\frac{\partial I(\nu, t, x)}{\partial x} + \frac{1}{c} \frac{\partial I(\nu, t, x)}{\partial t} = \\ = I(\nu, t, x) \int_0^\infty \int_{\Delta Y} \sigma(A) \gamma(\nu, \nu') N(A, \nu', t)\, dA d\nu' - \beta I(\nu, t, x). \qquad (4.23)$$

$$\frac{\partial N(A, \nu, t)}{\partial t} = \\ = -\sigma(A) N(A, \nu, t) \int_{\Delta Y} \gamma(\nu, \nu') I(\nu', t) d\nu' + e_m (h\nu)^{-1} \rho_0(A, \nu) - \\ - N(A, \nu, t) A + w_{\text{н}} \left[\rho_0(A, \nu) \int_{\Delta Y} \int_0^\infty N(A, \nu, t) dA d\nu - N(A, \nu, t)\right], \qquad (4.24)$$

where $I(\nu, t, x)$ is the emission intensity on a frequency ν at the time t in the cross section x, β is the loss coefficient.

The efforts to determine $\rho_0(A, \nu)$, which is needed for solution of equation (4.24) did not yield positive results, and therefore it is convenient to introduce the effective induced emission cross section σ_{eff} which describes the result of amplification of the spectrally nonuniform inverse medium.

If the rates of the induced processes are large, then by using equation (4.14) it is possible to determine σ_{eff} as follows:

$$\sigma_{\substack{\text{эфф} \\ (1)}} = \frac{h\nu}{\tilde{E}} \ln \frac{N_1(0)}{N_1(\tilde{E})}, \tag{4.25a}$$

Key: 1. eff

where $\tilde{E} = h\nu \int_{\Delta Y} \int_0^\infty I(\nu, t)\, d\nu dt$, $N_1(0)$ is the initial inverse population of the level $^4F_{3/2}$ of Nd^{3+}, $N_1(\tilde{E})$ is the inverse population after transmission of the laser pulse with energy density E and duration t_1:

$$N_1(\tilde{E}) = N_1(0) \int_0^\infty \int_{\Delta Y} \rho(A, \nu) \times \exp\left\{-\sigma(A) \int_{\Delta Y} \int_0^\infty I(\nu', t')\, \gamma(\nu, \nu')\, d\nu' dt'\right\} dA d\nu.$$

Consequently,

$$\sigma_{\substack{\text{эфф} \\ (1)}} = \sigma_{\substack{\text{эфф} \\ (1)}}(\tilde{E}) = \frac{h\nu}{\tilde{E}} \ln \left[\int_0^\infty \int_{\Delta Y} \rho(A, \nu) \times \exp\left\{-\sigma(A) \int_{\Delta Y} \int_0^\infty I(\nu', t)\, \gamma(\nu, \nu')\, d\nu' dt'\right\} dA d\nu\right]^{-1}.$$

Key: 1. eff

It is possible to show that

$$\sigma_{\substack{\text{эфф} \\ (1)}}(\tilde{E}, \nu_0) = \overline{\sigma(\nu_0, t)} = \frac{h\nu}{\tilde{E}} \int_0^t \sigma(\nu_0, t)\, I(t)\, dt.$$

Key: 1. eff

Under the condition $(h\nu_0)^{-1} \sigma_{\substack{\text{эфф} \\ (1)}}(\tilde{E}) \tilde{E} \ll 1$ we obtain

Key: 1. eff

$$\sigma_{\substack{\text{эфф} \\ (1)}}(\nu_0, \tilde{E}) = \int_{\Delta Y} \int_0^\infty \rho(A, \nu)\, \sigma(A)\, \gamma(\nu, \nu_0)\, dA d\nu, \tag{4.25b}$$

Key: 1. eff

where ν_0 is the laser signal frequency. Thus, $\sigma_{eff}(\nu, \tilde{E})$ for low energy density of the emission coincides with the induced emission cross section for the luminescence band not disturbed by the induced processes. The function $\sigma_{eff}(\nu, \tilde{E})$, being a characteristic of the laser material, at the same time permits proper calculation of the amplification of the emission in the active medium. Let us again consider the complete system of equations describing the propagation of the laser pulse in the four-level inverse medium; neglecting the luminescence processes and pumping, we have

$$\frac{\partial I(\nu, t, x)}{\partial x} + \frac{1}{c}\frac{\partial I(\nu, t, x)}{\partial t} = I(\nu, t, x)\int_0^\infty \int_{\Delta Y} \sigma(A)\,\gamma(\nu, \nu')\,N(A, \nu', t)\,dA d\nu' - \beta I(\nu, t, x), \tag{4.26}$$

$$\frac{\partial N(A, \nu, t)}{\partial t} = -\sigma(A)\,N(A, \nu, t)\int_{\Delta Y} \gamma(\nu, \nu')\,I(\nu', t)\,d\nu'.$$

Substituting the solution of the second equation in the first equation of system (4.26), using the definition of $\sigma_{eff}(\nu, E)$ and integrating the result with respect to time and frequency we obtain

$$\frac{\partial \tilde{E}}{\partial x} = h\nu N_1(0)\left[1 - \exp\left[-(h\nu)^{-1}\tilde{E}\sigma_{\text{эфф}}(\tilde{E})\right]\right] - \beta\tilde{E}. \tag{4.27}$$
(1)

Key: 1. eff

Equation (4.27) differs from the equations describing the amplification of the light pulse in the medium with uniform broadening [3] by replacement of $\sigma(\nu)$ by $\sigma_{eff}(\nu)$.

The effective cross section $\sigma_{eff}(\nu, \tilde{E})$ can be expressed in terms of the ratio of the intensities of the normalized luminescence bands on the frequency of the laser pulse ν_0 before and after transmission of this pulse. The intensity ratio is

$$\frac{\int_0^\infty \rho(A, \nu_0)\,dA}{\int_0^\infty \rho_t(A, \nu_0)\,dA} = \gamma \geqslant 1, \tag{4.28}$$

where $\rho(A, \nu_0)$ is the distribution function of the inverse population at the time of arrival of the laser pulse, $\rho_t(A, \nu_0)$ is the same function after passage of the pulse. Let us write solution of equation (4.26) in the following form:

$$N_1(\tilde{E})\,\rho_t(A, \nu_0) = N_1(0)\,\rho(A, \nu_0)\exp[-\alpha\tilde{E}A/(h\nu)].$$

Here $N_1(\tilde{E})$ is the inverse population after passage of the laser pulse, $\sigma(A)=\alpha A$. Then

$$\frac{N_{\text{н}}(0)}{N_{\text{н}}(\tilde{E})} = \frac{\int_0^\infty \rho_{\text{н}}(A, \nu_0)\, dA}{\int_0^\infty \rho(A, \nu_0) \exp\left\{-\frac{\alpha \tilde{E} A}{h\nu}\right\} dA} = \frac{1}{\gamma} \exp\left\{\frac{\sigma(\tilde{A})\,\tilde{E}}{h\nu}\right\}. \tag{4.29}$$

For $\sigma_{\text{eff}}(\tilde{E})$ we obtain

$$\sigma_{\text{эфф}}(\tilde{E}) = \frac{\sigma(\tilde{A}) \int_0^{\Delta\gamma} \int_0^t \gamma(\nu, \nu')\, I(\nu', t')\, d\nu' dt}{\int_0^t I(\nu_0, t')\, dt'} - \frac{h\nu}{\tilde{E}} \ln \gamma = \tilde{\sigma}(\nu_0) - \frac{h\nu}{\tilde{E}} \ln \gamma, \tag{4.30}$$

(1)

Key: 1. eff

where A is a value of the variable in the integration interval in (4.29).

The physical meaning of $\tilde{\sigma}(\nu_0)$ becomes clear if we consider the behavior of σ_{eff} for small energies in the laser pulse. In this case $\sigma_{\text{eff}}(\tilde{E})=\sigma(\nu_0)$, that is, it coincides with the cross section of the induced emission of the undisturbed luminescence band of the laser transition; therefore $\tilde{\sigma}(\nu_0)=\sigma(\nu_0)$.

Let us note that the value of $\sigma_{\text{eff}}(\nu, \tilde{E})$ depends on the excitation conditions and delay time of the laser pulse with respect to the beginning of the pumping pulse in the same way as $\sigma(\nu, t)$ defined by formula (4.20). Figure 4.14 shows the values of $\sigma_{\text{eff}}(\nu, \tilde{E})$ for a number of types of glass obtained for various time delays of the measuring pulse (energy density $\tilde{E}$ on the order of 1 joule/cm^2) with respect to the short (about 100 microseconds) pumping pulse[1]. In silicate glass ion dispersion with respect to radiating probabilities of A is clearly manifested. The picture of $\sigma_{\text{eff}} \neq \sigma_{\text{eff}}(t)$ observed in phosphate glass is explained either by the absence of the dispersion with respect to A or by rapid ($w_m >> A$) migration of excitation, which was noted in the studies of energy transfer.

[1]The experimental procedure for determining $\sigma(\tilde{E})$ will be discussed in §5.3.

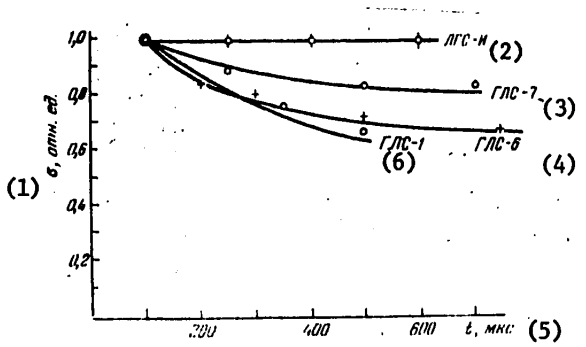

(1) (2) (3) (4) (5) (6)

Figure 4.14. The values of σ_{eff} obtained for different types of glass on variation of the time interval between the end of the pumping pulse and the time of measuring the cross section. The ratios σ_{eff} measured 100 microseconds after pumping to σ_{eff} measured 200 to 700 microseconds after pumping are plotted on the y-axis.

Key:
1. σ, relative units
2. LGS-I
3. LGS-7
4. LGS-6
5. t, microseconds
6. GLS-1

§4.5. Laser Methods of Determining the Induced Emission Cross Section

Effective cross section of induced emission can be calculated, measuring the energy parameters of the laser with sufficient accuracy (lasing threshold, energy of the induced emission for given amounts of pumping energy above the threshold), the resonator of which has known losses [428].

$\sigma_{eff}(\nu_0)$ can also be found, defining the variation of the population of the $^4F_{3/2}$ state of Nd^{3+} for generation or amplification of the light pulses of duration 10^{-7} to 10^{-8} seconds.[1] The variation of the inverse population can be found by measuring the luminescence intensity from the metastable level, for example, as a result of the transitions $^4F_{3/2}$-$^4I_{9/2}$. Let us consider the two procedures for determining $\sigma(\nu_0)$ in more detail.

Knowing the inverse population corresponding to the lasing threshold of the laser, the resonator of which has known losses, $\sigma_{eff}(\nu_0)$ can be calculated by the formula

$$\sigma_{эфф}(\nu_0) = \frac{\Pi}{N_{и,пор}}, \qquad (4.31)$$

(1) (2)

Key: 1. eff; 2. i, thresh

[1]For this pulse duration it is possible to neglect the variation of the inverse population as a result of luminescent processes and pumping.

where $\Pi = \frac{1}{2l}\ln\frac{1}{R_1R_2} + \beta$ are the losses on the mirrors and to absorption in the active elements, l is the length of the active element, R_1 and R_2 are the reflection coefficients of the mirrors, $N_{i,\ thresh}$ is the threshold inverse population. It can be found, measuring the energy obtained by the laser for different excesses of the pumping energy over the threshold energy. The following simple relation is used here

$$h\nu I(t) S = \underset{(1)}{\xi F \varepsilon_{\text{п}}}\left(1 - \frac{\varepsilon^{(1)}_{\text{пор}}}{\varepsilon_{\text{п}}}\right)\frac{k\sigma_{\text{эфф}} I(t)}{k\sigma_{\text{эфф}} I(t) + w_{\text{л}}}. \qquad (4.32)$$

Key: 1. thresh; 2. pump; 3. eff

Here ε_{pump} is the pumping power, S is the area of the end of the active element, $\xi F\varepsilon_{pump}/(h\nu)$ is the total number of particles excited to the metastable level by pumping per unit time (inverse population), $\varepsilon_{thresh}=h\nu(\xi F)^{-1}N_{i,\ thresh}w_l V$ is the pumping power spent on maintaining the threshold population in the active element during lasing of the laser, kI is the photon density inside the resonator, $k = \frac{1+R_1R_2}{1-R_1R_2}$, $w_{\text{л}}$ is the probability of the luminescence processes.

Performing the substitution in (4.32), $\sigma_{eff}=h\nu\Pi V w_l/\xi F\varepsilon_{thresh}$ and performing the corresponding algebraic transformations, we have

$$h\nu I(t) S = \underset{(1)}{\xi F}(\varepsilon_{\text{п}} - \underset{(2)}{\varepsilon_{\text{пор}}}) - \alpha\xi F\varepsilon_{\text{пор}},$$

Key: 1. pump; 2. thresh

where $\alpha=1/(k\Pi l)$.

Integrating the last expression with respect to time, we obtain the equation relating the emission energy, lasing threshold and pumping energy:

$$\underset{(1)}{\mathcal{W}_{\text{и}}} = \underset{(2)}{\mathcal{W}_{\text{п}}}\left[1 - \frac{\mathcal{W}^{(3)}_{\text{пор}}}{\underset{(2)}{\mathcal{W}_{\text{п}}}}(1+\alpha)\right]. \qquad (4.33a)$$

Key: 1. i; 2. pump; 3. threshold

Since the intensity of the emission ILN I(t) is proportional to $\varepsilon_{pump}(t)$, using a photomultiplier and oscillograph to record the kinetics of this emission and the lasing kinetics, it is possible graphically to define the integral

$$\int_{t_1}^{t_2} I(t)\,dt = \kappa\underset{(1)}{\mathcal{W}_{\text{п}}}. \qquad (4.33b)$$

Key: 1. pump

where t_1 and t_2 are the times of beginning and end of lasing, κ is the proportionality factor. Inasmuch as $I(t_2)=\kappa\varepsilon_{thresh}$, then $\kappa W_{thresh}=I(t_2)(t_2-t_1)$. If we perform measurements of W_i for different pumping energies it is possible to define, using the equation

$$\mathcal{W}_{\text{п}} = (\varkappa^{-1}\xi F)\int_{t_1}^{t_2} I(t)\,dt\left[1 - \frac{I(t_2)(t_2 - t_1)}{\int_{t_1}^{t_2} I(t)\,dt}(1+\alpha)\right], \qquad (4.33c)$$

the coefficient $(\varkappa^{-1}\xi F)$, to calibrate W_{thresh} in joules, and ε_{thresh} in watts (or in number of photons per second) and then by formula (4.31) to calculate N_i and σ_{eff}. The necessary measurements of the ratio W_{thresh}/W_{pump} can also be insured by varying the reflection coefficient of the output mirror and keeping the pumping energy constant.

The theoretical disadvantage of the investigated procedure is variation of the spectral composition of the ILN emission and the induced radiation cross section as a result of broadening of the spectrum of the laser emission with an increase in pumping energy.

The procedure for determining the effective emission cross section using a recording of variations of the inverse population and intensity of the Nd^{3+} ion luminescence for generation or amplification of light pulses was developed in references [117, 442, 443]. The layout of the experiment for determination of σ_{eff} is quite simple. An inverse population is created in a sample of Nd^{3+}-doped glass. When the maximum inversion is reached, a sounding laser pulse is fed to the sample. The luminescence of the Nd^{3+} ions and its variation are observed in small volumes of glass located at the entrance or exit end of the sample with respect to the sounding pulse on a wavelength of 880 to 920 nm. The energy in the laser pulse is measured simutaneously. The value of σ_{eff} is determined by the formula (4.25a). Obviously in order to insure the required accuracy of the measurement σ_{eff}, which depends only on the error in determining ΔN_i and the pulse energy, it is necessary that $\Delta N_i > 2N_0 \exp\{-\Delta E/k_B T\}(\delta N_i)^{-1}$ (δN_i is the error in determining the variation of the inversion), the intensity of the sounding beam must be uniformly distributed with respect to cross section, and the beam itself must completely fill the cross section of the sample.

In reference [443], σ_{eff} was measured as follows. The excitation of the active element (10 mm in diameter and 130 mm long) was carried out either by a IFP-1200 type pumping tube in a single tube illuminator or by the emission of a ruby laser operating in the monopulse mode or in the free-running mode (Figure 4.15). On excitation of the ILN sample, the luminescence at λ=880 nm was observed at a small angle to the direction of propagation of the sounding pulse from the direction of the exit end. The primary contribution to the observed luminescence, as the measurements demonstrated, is made by the part of the active element 1.5 cm long. In order to avoid spurious exposure to the ILN emission, when the maximum inversion is reached, the capacitor bank is shunted by a discharger, and the laser sounding pulse arrives at the sample 100 microseconds after cutoff of the current in the tube. The sounding pulse 50 nanoseconds long with respect to the base with a spectral width of less than 20 nm was generated by a laser and the laser amplifier. A uniform beam with respect to intensity, 10 mm in diameter was formed by a telescopic system with diaphragm. The emission energy was measured by an IKT-1M or IMO-2 calorimeter and if necessary it could be varied by using neutral light filters.

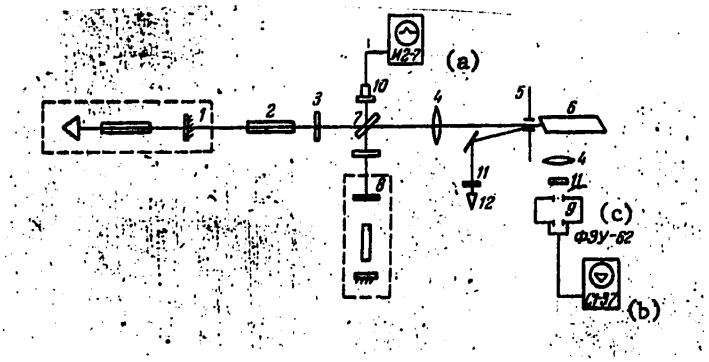

Figure 4.15. Diagram of the setup for measuring σ_{eff}. 1--neodymium glass master oscillator, 2--laser amplifier, 3--light filters, 4, 5--telescopic system with diaphragm, 6--investigated sample, 7--dielectric mirror with transmission coefficient for λ=1060 nm equal to 80% and reflection coefficient for λ=693 nm equal to 100%, 8--ruby laser, 9--monochromator, 10--photoreceiver; 11--light filter, 12--photocalorimeter.

Key:
a. I2-7
b. S1-37
c. FEU-62 photomultiplier

On excitation of the sample by the emission of the ruby laser luminescence is observed from the layer less than 1 mm thick from the entrance end perpendicular to the direction of propagation of the laser emission. The direction of propagation of the ruby laser emission was combined with the direction of propagation of the sounding pulse using a system of prisms and dielectric mirrors transparent for λ=1060 nm. The diameter of the neodymium laser beam was always equal to or somewhat greater than the diameter of the beam of emission with λ=693 nm.

The emission with λ=880 nm was recorded by means of an MDR-2 monochromator, the FEU-62 photomultiplier with cathode repeater and storing S1-37 oscillograph. The time resolution of the system was 0.2 microsecond. The results of measuring σ_{eff} agreed for the two methods of exciting the sample.

The authors of reference [117] determined σ_{eff} by measuring the inverse population and the gain in the glass. The inverse population N_1 on the metastable level of Nd^{3+} was found by varying the intensity of the luminescence on amplification of the monopulse and the increase in energy of this pulse. Since the intensity of the luminescence I is always proportional to the level population, then

$$N_{\text{(1)}_{\text{H}}} = \frac{\Delta \mathcal{F} I_0}{h\nu_0 \Delta I V}; \qquad (4.34)$$

Key: 1. i

where ΔW is the increase in pulse energy, I_0, ΔI is the luminescence intensity before passage of the pulse and variation of it, ν_0 is the frequency of induced emission, V is the volume of the sample. The effective cross section of the induced emission was calculated by the formula

$$\sigma_{эфф}^{(1)} = \frac{\ln K_0}{N_1 l}, \tag{4.34a}$$

Key: 1. eff

where l is the amplification length, K_0 is the gain of the weak signal related to the experimentally measured gain $K = \frac{W_{inp} + \Delta W}{W_{inp}}$ by the expression

$$K_0 = K\left[1 + (K-1)\ln\frac{I_0}{I_0 - \Delta I}\right]. \tag{4.34b}$$

The last expression was obtained by expansion of the complete solution of the equation of pulse amplification (4.27) for $(h\nu)^{-1}\sigma_{eff}\tilde{E}<1$.

The variation of the value of I with respect to length of the active element as a result of amplification of the sounding pulse leads to errors in determining the inverse population and emission cross section. Analysis shows that for $K_0 \leq 1.5$ the error in the value of N_1 does not exceed 5% for any energy of the sounding pulse. The required magnitude of K_0 for the given pumping conditions is achieved by selecting the length of the excited part of the active element.

The authors of the indicated paper characterize the energy efficiency of the laser material by maximum energy W_0, which can be converted to induced emission by a unit volume of active material under given pumping conditions:

$$W_{0_{(1)}} = h\nu_0 \int_0^\infty \frac{1}{\tau_0} N_{1(1)}(t)\, dt. \tag{4.35}$$

Key: 1. i

For the ensemble of particles which is uniform with respect to the luminescence output, this value is proportional to the total number of ions excited during the pumping pulse. In the presence of ions with short τ_l (for example, close pairs or groups of ions), their contribution to W_0 is negligibly small. Therefore among the glass with identical spectral characteristics the sample with noticeable proportions of ions with small τ_l will be distinguished by smaller values of W_0.

§4.6. Value of the Effective Cross Section of the Induced Emission of Nd^{3+} in Phosphate Glass

Systematic measurements of $\sigma_{eff}(\tilde{E})$ for phosphate glass were performed by the authors of references [117, 443]. In [443] results are presented from measuring $\sigma_{eff}(\tilde{E})$ for glass of the type LGS-40, LGS-I, LGS-M, GLS-22, and also for a number of types of glass based on the metaphosphates of the

second group on variation of the energy density in the laser pulse from 1 to 10 joules/cm^2. For comparison a study was made of silicate glass type GLS-6 and GLS-1. Figure 4.16 shows the relations for $N_i(0)/N_e(\tilde{E})$ as a function of $\tilde{E}$ for different glass for durations of the sounding pulse equal to 50 nanoseconds and 6 microseconds. In all cases the behavior of the ratio

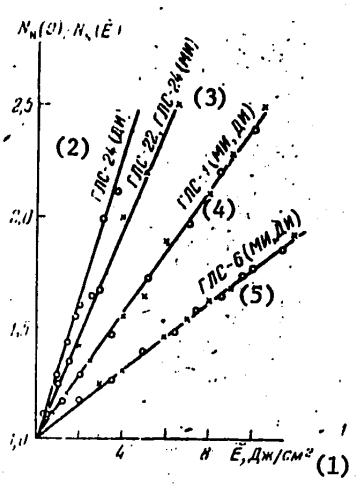

Figure 4.16. $N_i(0)/N_i(\tilde{E})$ as a function of energy density in the amplified laser pulse for different types of glass. DI--laser pulse lasting 6 microseconds, MI--laser pulse of 50 nanosecond duration
Key:
1. E, joules/cm^2
2. GLS-24 (DI)
3. GLS-22, GLS-24 (MI)
4. GLS-1 (MI, DI)
5. GLS-6 (MI, DI)

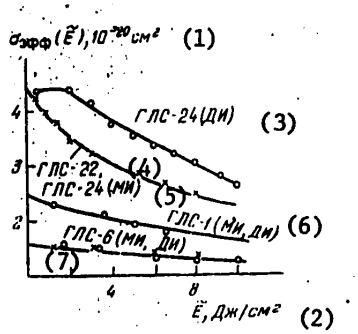

Figure 4.17. $\sigma_{eff}(\tilde{E})$ for different types glass.
Key:
1. $\sigma_{eff}(\tilde{E})$, 10^{-20} cm^2
2. E, joules/cm^2
3. GLS-24 (DI)
4. GLS-22
5. GLS-24 (MI)
6. GLS-1 (MI, DI)
7. GLS-6 (MI, DI)

$N_i(0)/N_i(\tilde{E})$ is described by linear functions. Increasing the pulse duration while retaining its energy does not lead to noticeable variations of this ratio in silicate glass, but in phosphate glass the values of $N_i(0)/N_i(\tilde{E})$ for t_i=6 microseconds are significantly larger than for t_i=50 nanoseconds. In Figure 4.17 relations $\sigma_{eff}(\tilde{E})$ are presented which were calculated by formula (4.25a) using experimental data presented in Figure 4.16. All of the curves $\sigma_{eff}(\tilde{E})$ for t_i=50 nanoseconds are approximated well by formulas of the type

$$\sigma_{\text{эфф}}(\tilde{E}) = \frac{h\nu}{\tilde{E}} \ln [1 + (-h\nu)^{-1} \tilde{E}\sigma(0)], \qquad (4.36)$$

(1)

Key: 1. eff

where $\sigma(0)$ is the induced emission cross section determined by the slope of the functions $N_1(0)/N_1(\tilde{E})$ for $\tilde{E}$ approaching zero.

Table 4.9 gives the values of $\sigma(0)$ and also values of $\sigma_{eff}(\tilde{E})$ for $\tilde{E}\approx 1.5$ joules/cm^2 for a number of types of phosphate and silicate glass. The observed relations of $\sigma_{eff}(\tilde{E})$ can be caused by the following factors: deformation of the shape of the luminescence band of the laser transition of Nd^{3+} ions, degeneration of the four-level amplification system to three-level, the simultaneous effect of both effects.

Table 4.9

Type of glass	$\sigma(0)$, 10^{-20} cm^2	$\sigma_{eff}(\tilde{E})$ 10^{-20} cm^2
Silicate		
GLS-1	2.5	2.3
GLS-6	1.5	1.4
Phosphate		
LGS-40	5.5	4.5
LGS-I	3.5	3.1
LGS-M	4.6	3.9
GLS-22	4.2	3.6

In reference [418] it was demonstrated that the magnitude of the $^4I_{11/2}$ level relaxation time, both in silicate and in phosphate glass, is less than 2.10^{-9} second. According to the data of reference [412], the rate of non-radiating excitation energy dissipation in phosphate glass is higher by several times than in silicate glass. Therefore with a sounding pulse duration of about 50 nanoseconds, it is possible to neglect the degeneration of the four-level amplification system to three-level.

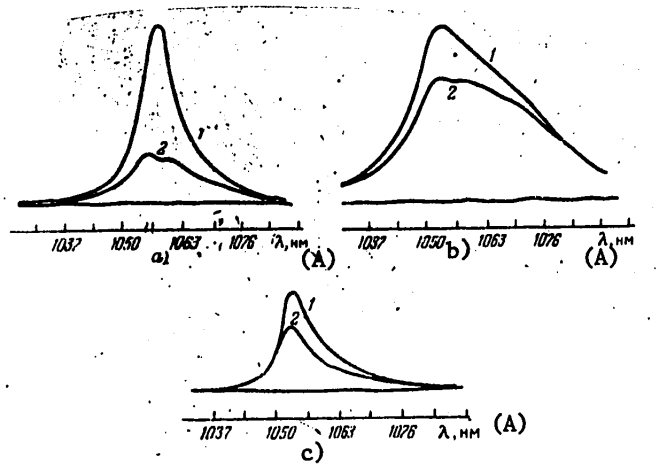

Figure 4.18. Luminescence spectra of GLS-1 glass (a), GLS-22 (b) and LGS-40 (c) before (1) and after (2) passage of the laser pulse

Key: A. λ, nm

In order to determine the degree of correlation between the deformation of the luminescence band of Nd^{3+} and the function obtained $\sigma_{eff}(\tilde{E})$, the luminescence band curves were recorded after passage of the laser pulse.

The spectrum was recorded with a time delay with respect to the laser sounding pulse from 3 to 100 microseconds. The scanning time in the entire spectrum was 10 microseconds. The spectral resolution of the spectrophotometer was ≤ 10 cm^{-1}. Figure 4.18 shows the luminescence band curves for silicate glass GLS-1 and phosphate glass LGS-40 and GLS-22 before and after passage of the laser pulse obtained at room temperature and with a delay time at the beginning of recording of the spectrum approximately equal to 3 microseconds. In silicate glass the deformation of the curve is significant. In LGS-I phosphate glass the deformation of the curve is noticeably less, and in LGS-40 glass the curve is close to equilibrium. Observation of the kinetics of restoration of the equilibrium curve of the luminescence band gives low false correlation rates: for silicate glass these rates are equal to $(0.5 \text{ to } 1)\times 10^4$ sec^{-1}; for phosphate glass GLS-22 and LGS-I, on the order of 10^5-10^6 sec^{-1}, and for LGS-40, obviously greater than 10^6 sec^{-1}. The deformation of the luminescence band of $^4F_{3/2} \rightarrow {}^4I_{9/2}$ was not observed in either type of glass, which is explained by absence of a correlation between the nonuniform broadenings of the Stark components of the $^4I_{9/2}$ and $^4I_{11/2}$ levels.

In silicate glass, the deformation of the curve for the luminescence band of the $^4F_{3/2} \rightarrow {}^4I_{11/2}$ transition, according to the calculations by formula (4.30) correlates with variation of $\sigma_{eff}(\tilde{E})$. Consequently, in these types of glass nonuniform broadening makes the basic contribution to the observed functions $\sigma_{eff}(\tilde{E})$. In phosphate glass the deformation of the luminescence band is significantly less than that which is required to match the deformation with the decrease in $\sigma_{eff}(\tilde{E})$ with an increase in energy in the laser pulse. This effect and the increase in $\sigma_{eff}(\tilde{E})$ which is observed in phosphate on variation of the pulse duration from 50 nanoseconds to 6-10 microseconds can be explained by rapid transfer of excitation between the Nd^{3+} ions or the quite large (about 50 nanoseconds) lifetime of the levels $^4I_{11/2}$. The latter proposition contradicts not only the previously presented data, but also our experiments. The variations of the dependence of $N_i(0)/N_i(\tilde{E})$ on the pulse duration cannot be matched with each other by varying only the value of τ_ℓ. On the contrary, introduction of the term describing the excitation migration into the equation (4.24) ($w_M \sim 10^5$-10^6 sec^{-1}) for $\tau_\ell \ll \tau_1 = 50$ nanoseconds, gives the required increase in the effective cross section and explains noncorrespondence between the relative deformation of the luminescence band of the laser transition and the measured values of $\sigma_{eff}(\tilde{E})$. This effect is connected with noticeable relaxation of the deformed curve to the equilibrium curve during the relaxation time inasmuch as the minimum delay time of the beginning of recording with respect to the sounding pulse was about 3 microseconds, and the recording of the entire spectrum took place in 10 microseconds.

The discussed experimental data indicate that in phosphate glass the effective induced emission cross section depends on the probability of this emission: on satisfaction of the conditions

$$\frac{(h\nu)^{-1}\sigma(0)\tilde{E}}{t_1} \gg w_M \sim 10^5\ c^{-1}$$

we have

$$\sigma_{\text{эфф}}(\tilde{E}) = \frac{h\nu}{\tilde{E}} \ln |1 + (h\nu)^{-1} \sigma(0) \tilde{E}|,$$
(1)

Key: 1. eff

and for $\frac{(h\nu)^{-1}\sigma(0)\tilde{E}}{t_1} \ll w_{\text{м}}$ we obtain

$$\sigma_{\text{эфф}} = \sigma(0).$$
(1)

Key: 1. eff

In intermediate cases with a magnitude of this ratio on the order of w_M, the exact value of $\sigma_{\text{эфф}}(E)$ must be determined beginning with the complete solution of equation (4.14). As an approximation it is possible to take the values obtained for $t_1 \sim 6$ microseconds.

§4.7. Amplification of Laser Pulses in Phosphate Glass Doped with Nd^{3+} Ions

The equations describing the gain of the laser pulse on propagation in a linearized inverse medium have the form

$$\frac{\partial I}{\partial x} + \frac{1}{c}\frac{\partial I}{\partial t} = (\sigma N_{\text{и}} - \beta) I, \tag{4.37a}$$
(1)

$$\frac{\partial N_{\text{и}}}{\partial t} = -\sigma N_{\text{и}} I - N_{\text{и}} \frac{1}{\tau_{\text{л}}}. \tag{4.37b}$$
(1)

Key: 1

Let us assume that the pulse duration is much greater than the equilibrium setup time between the excited laser ions and the medium, but much less than the characteristic pumping time. In the case of interest in practice where $t_1 \ll \tau_{\text{л}}$, the variation of the inverse population after transmission of the pulse is determined by the emission energy passing through the given cross section of the active element:

$$\Delta N_1 = N_1(0) \exp\left[-\sigma \int_0^{\infty} I(t', x)\, dt'\right]. \tag{4.38}$$

The system of equations (4.37) has quite simple analytical solution only under the condition of $\beta = 0$, that is, in the absence of inactive absorption [438]; then

$$I(x, t) = \frac{I_0(t - x/c)}{1 - \left\{1 - \exp\left[\sigma \int_0^x N_1(x')\, dx'\right]\right\} \exp\left\{-\sigma \int_0^{t-x/c} I_0(t')\, dt'\right\}}, \tag{4.39a}$$

$$\tilde{E}(x) = h\nu \int_0^\infty I(x, t)\, dt = \tilde{E}(0) + h\nu \int_0^x N_1\, dx + \\ + \frac{1}{\sigma} \ln \left\{ 1 + \exp\left[(h\nu)^{-1} \sigma \tilde{E}(0)\right] \left(\exp \sigma \left(- \int_0^x N_1\, dx \right) - 1 \right) \right\}. \qquad (4.39b)$$

The latter equation is easily converted to the form convenient for the calculations:

$$K_0(x) = (\exp\left[(h\nu)^{-1} \sigma \tilde{E}(x)\right] - 1)\,(\exp\left[(h\nu)^{-1} \sigma \tilde{E}(0)\right] - 1)^{-1}, \qquad (4.39c)$$

where $K_0(x) = \exp\left(\sigma \int_0^x N_1 dx\right)$ is the weak signal gain.

The inverse medium is called idealized, for a number of factors are not considered in the gain equations. The factors not considered include the presence of Stark structure of the levels of the ions interacting with the emission, nonuniform nature of broadening of these levels in glass. It is also proposed that the lower laser level is not populated in the induced emission process, that is, the time of its destruction $\tau_\ell = 0$, although it is known that in laser crystals and glass $\tau_\ell = 10^{-8}$ to 10^{-10} sec, and it depends on the magnitude of the energy gap between the ground state and the lower laser level of the phonon spectrum of the crystal or glass.

Let us consider what changes in equations (4.37) consideration of the indicated factors leads to. Obviously, equation (4.37b) is converted to a system of equations for populations of the Stark components which consider the setup time of the Boltzmann equilibrium between the components of the same level and the equilibrium setup time between the lower laser and ground levels. Inasmuch as the setup time of thermal equilibrium between the Stark components of the level on the rare earth ions is $< 10^{-12}$ second, it is possible to consider that for generation or amplification of pulses lasting more than 10^{-12} sec the Boltzmann distribution of the populations of the Stark components is not disturbed. In this case, the presence of the Stark structure of the upper laser level can be considered by introducing the averaged induced emission cross section with respect to transitions (for example, similarly to how average was done in §4.4). Let us note that the same magnitude of cross section is obtained from the previously described experiments in determining the induced emission cross section of Nd^{3+}.

Whereas some of the Stark components of laser levels do not participate directly in the induced emission ($\sigma(\nu_0) = 0$ for all transitions between these components) they play the role of the "reservoir" influencing the population of the components participating in the induced transitions.

The discussed arguments make it possible to reduce the system of equations for populations of the laser level components to the system of equations for integral population of these levels:

$$\frac{dN_m}{dt} = -\sigma I (N_m - \chi N_l), \tag{4.40}$$

$$\frac{dN_l}{dt} = \sigma I (N_m - \chi N_l) + \frac{N_l - N_l^0}{\tau_l}, \tag{4.41}$$

where χ is the ratio of the populations of the components participating in forced transitions to the total population of the lower laser level, $N_\ell^0 = N_0 \Sigma \exp[-\Delta\tilde{E}_\ell^i / k_B T]$ is the equilibrium population of this level. Here it is assumed that $N_m \ll N_0$ and significant variation of the population of the ground state on excitation does not take place.

Let us consider two limiting cases: amplification of the short laser pulse $t_i \ll \tau_\ell$ and amplification of the pulse of duration $t_i \gg \tau_\ell$. In the first case thermal destruction of the lower laser level in the time t_i can be neglected. Then

$$N_l = \frac{1}{1+\chi}[\chi - \exp[-(h\nu)^{-1}\sigma\tilde{E}(\chi+1)]]N_l(0), \tag{4.42a}$$

where $N_l(0)$ is the initial inverse population of the metastable level.

For neodymium-doped phosphate glass $\chi \approx 0.45$; for neodymium silicate glass $\chi = 0.6$ if we consider in accordance with [202], that the induced emission is participated in only by two Stark components of the $^4I_{11/2}$ state. From formula (4.42a) it follows that in phosphate glass on amplification of a short laser pulse, more than 70% of the excited Nd^{3+} ions can be involved in the induced emission, and more than 60% in the silicate glass. With a classical three-level gain (where the laser levels are assumed to be singlet levels) this value is 50%.

For $t_i \gg \tau_\ell$ we obtain the usual solution for the four-level laser system:

$$N_l = N_l(0)\exp\{-(h\nu)^{-1}\sigma\tilde{E}\}. \tag{4.42b}$$

In the intermediate cases $t_i \sim \tau_\ell$, it is necessary to solve the complete system (4.40), (4.41). According to the measurements performed in reference [418], $\tau_\ell < 2 \cdot 10^{-9}$ sec, and therefore the effects of degeneration of the four-level system must be noticeable for $t_i \sim 10^{-9}$ sec and radiation energy densities $\tilde{E} > h\nu/\sigma(\chi+1)$. The indicated energy densities for $t_i = 10^{-9}$ to 10^{-10} sec are achieved in the output amplifying stages of the laser units designed to obtain a thermonuclear plasma. The measurements of τ_ℓ for glass produced by USSR industry were taken by various methods [418, 444, 445]. In [444] the relaxation time of the $^4I_{11/2}$ level of Nd^{3+} in phosphate glass LGS-40 was determined by comparison of the "clearing" of the inverse population during generation of pulses of duration $3 \cdot 10^{-8}$ sec with different energy with variation of N_l calculated for the four-level system under the assumption of uniform broadening of the spectral band. The difference between the "clearing," defined experimentally and calculated was considered the consequence of the appearance of noticeable population of the lower laser level. The value of τ_ℓ was estimated by the difference between the experimentally found variation of N_l and that expected for the four-level system. For LGS-40 glass, $\tau_\ell = 3 \cdot 10^{-8}$ sec.

The more direct method of measuring the relaxation time of this level in the glass is based on determination of the variation of the gain of the weak signal after passage of a powerful laser pulse of duration $5 \cdot 10^{-11}$ sec through the amplifier with spectral width of 0.1 nm [445]. The authors considered that variation of the gain is caused only by relaxation of the $^4I_{11/2}$ level, although the pulse gain must be accompanied not only by redistribution of the population with respect to Stark components of the states $^4F_{3/2}$ and $^4I_{11/2}$, but also the deformation of the curve of the non-uniformly broadened luminscence band of the laser transition. According to their measurementa τ_ℓ for GLS-1 and LGS-40 glass is $(10 \pm 5) \cdot 10^{-9}$ and $(30 \pm 15) \cdot 10^{-9}$ sec, respectively.

In [418], the value of τ_ℓ was determined by the following procedure. The thermally equilibrium population of the lower laser level is about 10^{-4} of the population of the ground state neodymium. In standard laser glass at T=300 K this population corresponds to the absorption coefficient of λ=1060 nm on the order of $5 \cdot 10^{-4}$ cm^{-1}. In spite of such weak absorption, on irradiation by a laser pulse with a wavelength λ=1060 nm the population of the metastable level increases, reaching in the limiting case, for large energy densities of the pulse, the population of the Stark components of the $^4I_{11/2}$ level participating in the absorption. It is obvious that the maximum population of the $^4F_{3/2}$ level components will be equal to the thermal equilibrium population of the two lower components of the $^4I_{11/2}$ level for $t_i \gg \tau_\ell$. However, for pulse duration of $t_i < \tau_\ell$ the maximum populations of the $^4F_{3/2}$ level and corresponding components of the $^4I_{11/2}$ level will be less than the thermally equilibrium population. If it is considered that the Boltzmann equilibrium between the Stark components is set up instantaneously and $t_i < \tau_\ell$, then depending on the specific layout of the laser levels the limiting population of the states $^4F_{3/2}$ will be 1.5 to 1.7 times less than that observed for $t_i \gg \tau_\ell$. The increase in the $^4F_{3/2}$ level population can be monitored by luminescence, for example, on λ=880 nm.

Here the relations for the population (and luminescence intensity) of the $^4F_{3/2}$ level as a function of the energy of the exciting pulse for the indicated relations between t_i and τ_ℓ also differ noticeably, and the nonuniform nature of broadening of the spectrum of the Nd^{3+} ions has no significant influence on the observed relations. Consequently, by varying the duration and the energy of the laser pulse and comparing the observed increase in population of the $^4F_{3/2}$ level with that calculated for different ratios of t_i and τ_ℓ, it is possible uniquely to define the relaxation time of the $^4I_{11/2}$ level. As the experiment shows, in glass of the type GLS-1, LGS-247-2, LGS-40, LGS-I and GLS-22, the dependence of the $^4F_{3/2}$ level population on the energy of the laser pulse of duration $3 \cdot 10^{-8}$ sec does not differ from the four-level at the energy density for which $\sigma\bar{E}$=1.5 joules. According to the calculations, in this case τ_ℓ can be less than $2 \cdot 10^{-9}$ sec. In reference [446], a direct measurement was also made of the restoration of the gain of the laser amplifier using ED-2 silicate glass after passage of the pulse of 1.6 nanosecond duration. The energy density in the laser beam at the entrance of the amplifier was 2 joules/cm^2, the gain of the weak signal was 7. On interpretation of the experimental data, the system of kinetic equations describing the behavior of the $^4F_{3/2}$, $^4I_{11/2}$ and $^4I_{9/2}$ level populations of

neodymium and the laser pulse gain were used. The absorption from the $^4F_{3/2}$ level was also considered. The best agreement between experiment and calculation was obtained under the following conditions: absorption from the metastable level absent, degeneration of the levels participating in the induced transitions absent, $\tau_\ell=(1.25\pm0.2)$ nanosecond.

As was demonstrated in §4.1, the influence of nonuniform broadening in the energy spectrum of Nd^{3+} ions on the gain of a laser pulse can be considered by introducing $\sigma_{eff}(\tilde{E})$. The formula based on the experimental data is used:

$$\underset{(1)}{\sigma_{e\phi\phi}}(\tilde{E}) = \frac{h\nu}{\tilde{E}} \ln [1 + \sigma(0)\,\tilde{E}\,(h\nu)^{-1}]. \tag{4.43}$$

Key: 1. eff

For $t_1 >> \tau_\ell$, the equation describing the gain of a laser pulse in neodymium glass has the form

$$\frac{d\tilde{E}(x)}{dx} = h\nu \underset{(1)}{N_{\text{и}}}(x)\,[1 - \exp(-(h\nu)^{-1}\sigma(\tilde{E})\,\tilde{E}(x))] - \beta\tilde{E}(x) = \tag{4.44}$$

$$= \underset{(1)}{N_{\text{и}}}(x)\frac{\sigma(0)\,\tilde{E}(x)\,(h\nu)^{-1}}{1+\sigma(0)\,\tilde{E}(x)\,(h\nu)^{-1}} - \beta\tilde{E}(x).$$

Key: 1. i

In accordance with the solution of this equation the gain is defined by the expression

$$\ln K = \ln K_0 - \left(1 - \frac{\ln K_0}{\beta l}\right)\ln\frac{\ln K_0 - (h\nu)^{-1}\sigma(0)\,\tilde{E}(0)\,\beta l K}{\ln K_0 - (h\nu)^{-1}\sigma(0)\,\tilde{E}(0)\,\beta l}, \tag{4.45}$$

where K_0 is the gain of the weak signal, $\tilde{E}(0)$ is the energy density in the laser pulse at the entrance of the amplifier, ℓ is the amplifier length. It is easy to see that equation (4.44) coincides with the equation for the gain for a laser medium with uniform spectral broadening for $(h\nu)^{-1}\sigma\tilde{E}(0)<<1$ or $(h\nu)^{-1}\sigma\tilde{E}(0)>1$. The relations $K(\tilde{E}_{inp})$ for certain values of K_0(e, 10, 25) for $\beta=0$ are presented in Figure 4.19. Here relations are presented

$$K(\tilde{E}) = \frac{h\nu}{\sigma\tilde{E}(0)}\ln[1 + K_0(\exp[(h\nu)^{-1}\sigma\tilde{E}(0)] - 1)], \tag{4.46}$$

where σ is not a function of the energy flux density. The noted differences in the gains are manifested for quite large K; therefore in multistage laser systems based on glass consideration of the influence of the nonuniform broadening is necessary.

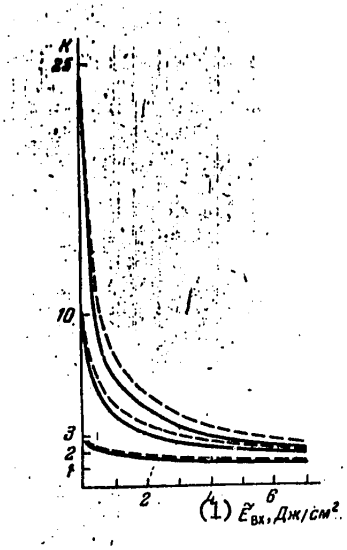

Figure 4.19. Gains of a laser amplifier considering (solid lines) and without considering (dotted lines) nonuniform broadening for values of the gain of the weak signal equal to e, 10, 25 and $\sigma(0)=5.5\times10^{-20}$ cm^2.

Key:
1. $\tilde{E}_{inp}$, joules/cm^2

§4.8. Lasing Characteristics of Neodymium-Doped Phosphate Glass

A distinguishing feature of phosphate glass doped with neodymium is significantly more narrow lasing spectra than in silicate glass. This fact was given attention in references [123, 354]. The results of investigating the dependence of the lasing spectrum width in a confocal resonator on the ratio of the pumping energy to the threshold energy for phosphate, borophosphate and silicate glass are presented in Figure 4.20. The LGS-40 glass (phosphate alkali glass of metaphosphate composition) has the most narrow lasing spectrum of all known types of glass--with a tenfold excess of the pumping energy over the threshold, the lasing spectrum width does not exceed 0.2 nm. The lasing spectrum of the borophosphate glass LGS-41 (0.4 nm) is somewhat broader. For silicate glass LGS-28, its width reaches 7 nm under the same conditions; this value is typical of silicate glass. In a flat cavity the width of the lasing spectrum is appreciably greater than in the confocal cavity (Fig 4.21).

Another characteristic feature of phosphate glass is the high gain [123]. The gain as a function of energy density of the entrance of the amplifier for phosphate glass LGS-40, LGS-41, LGS-I-3 and silicate glass LGS-28 is presented in Figure 4.22. With a weak signal the gain is 16 for LGS-40 glass, it is 12 for LGS-I-3 glass and 2.5 for LGS-28 or the gain is equal to 0.28 (LGS-40), 0.19 (LGS-I-3) and 0.07 cm^{-1} (LGS-28), respectively (rods 10 mm in diameter by 130 mm; pumping 80 joules/cm^3).

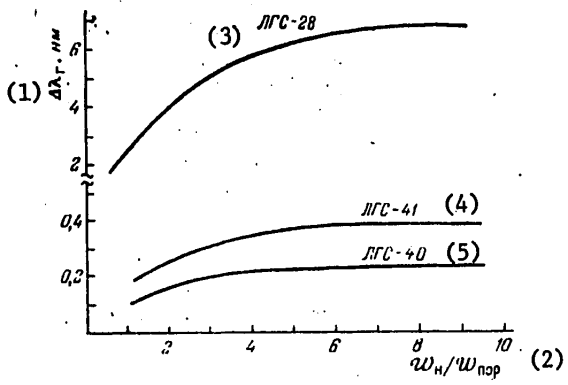

Figure 4.20. Width of the lasing spectrum as a function of pumping energy in a confocal resonator

Key:
1. $\Delta\lambda_{lase}$, nm
2. $W_{pump}/W_{threshold}$
3. LGS-28
4. LGS-41
5. LGS-40

The causes of narrow-band lasing in phosphate glass at the present time are considered to be a magnitude of nonuniform broadening less than for silicate glass and uncorrelated Stark splitting of the working levels [447]. Investigation of the time development of the lasing spectrum shows that in silicate glass the splitting of the lasing spectrum occurs by a pumping energy exceeding by one and a half times the threshold, and in phosphate glass LGS-40, splitting does not occur even for thirty-fold excess over the threshold.

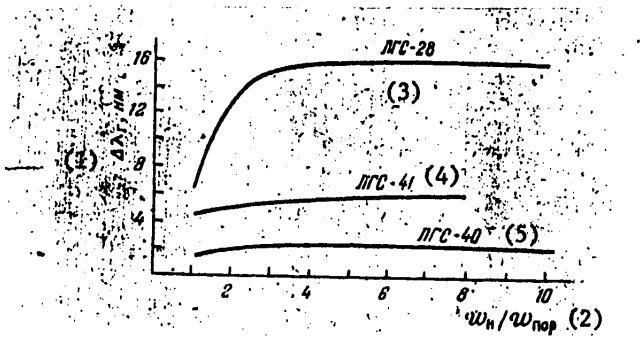

Figure 4.21. Lasing spectrum width as a function of pumping energy in a flat cavity.

Key:
1. $\Delta\lambda_{lase}$, nm
2. $W_{pump}/W_{threshold}$
3. LGS-28
4. LGS-41
5. LGS-40

Direct measurements of the inverse population of the working level $^4F_{3/2}$ and the induced emission cross section made it possible to explain the large gain [117]. It was discovered that although phosphate glass has lower luminescence lifetime than silicate glass, the phosphate glass is not inferior with respect to magnitude of inverse population and essentially is superior with respect to induced emission cross section. The energy stored in the inverse population of the Nd^{3+} ions usually is 0.7 to 1.5% of the energy fed to the pumping tube. At the same time, such glass is noticeably superior to silicate glass with respect to total excitation energy, that is, the total number of Nd^{3+} ions excited to the $^4F_{3/2}$ state during the pumping pulse. The combination of all of these properties determines the low lasing threshold and high efficiency of phosphate glass in the free running mode [167, 431]. Table 4.10 gives values of the induced emission cross section for laser phosphate glass produced in the Soviet Union and abroad.

By varying the glass composition it is possible to change the induced emission cross section and lasing wavelength, just as the position of the maximum luminescence band and its halfwidth. This is indicated by the results of references [167, 431], where a study was made of the dependence of the lasing spectrum width and magnitude of the cross section on the composition of the glass. From the data presented in Figure 4.23 it follows that increasing the BPO_4 content in metaphosphate alkali glass leads not only to broadening of the lasing spectrum, but also to a decrease in the induced emission cross section.

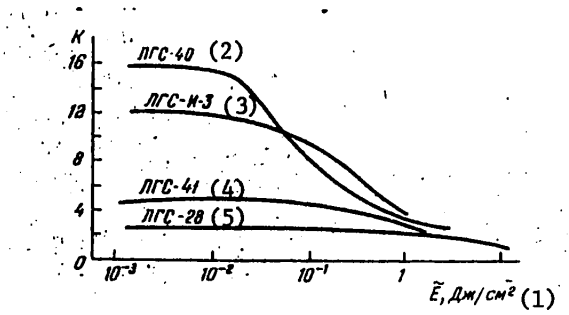

Figure 4.22. Gain as a function of energy density at the entrance of the amplifier

Key:
1. $\tilde{E}$, joules/cm^2
2. LGS-40
3. LGS-I-3
4. LGS-41
5. LGS-28

In glass based on phosphates of the elements of the second group, the magnitude of the cross section can be regulated by cation substitution [431]; whereas for magnesium metaphosphate the cross section is $1.8 \cdot 10^{-20}$ cm^2, on transition to barium, a smooth increase to $3 \cdot 10^{-20}$ cm^2 is noted. The lasing spectrum width $\Delta\lambda_{lase}$ for such substitution of cations is constricted from 2 nm for Mg to 0.4 nm for Ba (the data for all the alkali earth metaphosphates are

presented in Table 4.3 [432], Table 4.11 [430], and Figure 4.24). Whereas the constriction of the lasing spectrum can be explained by a decrease in nonuniform broadening of the Mg-Ba series, this is explicitly inadequate for the explanation of the growth of the induced emission cross section; obviously, on replacement of the cation, an increase in resolution of the lasing transition takes place.

Table 4.10

Type of glass	σ, 10^{-20} cm^2	Type of glass	σ, 10^{-20} cm^2
GLS-21	3.9	LGS-56	2.9
GLS-22	3.9	LGS-42	2.8
GLS-23	3.9	LGS-I	3.0
GLS-]3	3.9	LGS-M	4.0
LGS-40	4.3	LHG-5	3.9
LGS-41	2.6	LHG-6	3.7
LGS-54	4.3	LHG-7	3.8
LGS-55	3.3		

Data of [47] and measurements by the authors.

Table 4.11

Cation	$[Nd_2O_3]$, mol %	τ, мкс	N, 10^{18} см$^{-3}$	W_0, joule/cm^3	σ, 10^{-20} см^2	$\Delta\lambda_{laser}$, nm
Mg	0,7	260	2,8	1,6	1,8	2,0
Ca	0,7	250	3,2	1,9	2,2	0,9
Sr	1,2	255	5,7	3,6	2,5	0,4
Ba	1,2	240	6,0	3,6	8,0	0,4
Zn	1,2	200	3,7	2,5	2,3	0,5
Cd	1,2	210	4,8	3,1	2,5	0,5
Pb	0,7	230	3,0	1,7	2,6	0,4

N--maximum inverse population; W_0--excitation energy (energy per unit volume of the total number of Nd^{3+} ions excited during the pumping pulse); σ--induced emission cross section

The nature of narrow-band lasing of phosphate glass has been investigated inadequately at the present time. One of the primary factors influencing the spectral width of the emission of a free-running laser is narrowness of the luminescence band of the laser transition (the gain curves). The broadening of the luminescence band of this transition with variation in the composition of the glass has a negative effect on the selective properties of the gain curve, and it leads to noticeable broadening of the induced emission spectrum [432]. Another factor is comparability of the excitation migration rate with respect to Nd^{3+} ions for concentrations of $2 \cdot 10^{20}$ cm^{-3} with the destruction rate of the working level under the effect of induced emission. In niobium phosphate glass, a noticeable broadening of the lasing spectrum was noted for a reduction in the Nd^{3+} concentration to $5 \cdot 10^{19}$ cm^{-3}.

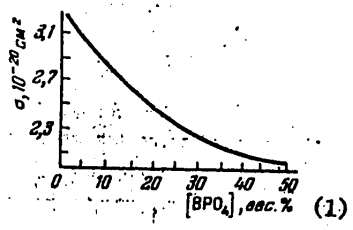

Figure 4.23. Induced emission cross section in glass of the system (90-x) $NaPO_3$-xBPO_4-10 MgO as a function of composition
Key:
1. % by weight

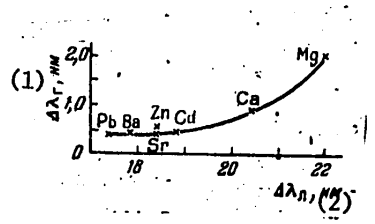

Figure 4.24. Width of the lasing spectrum as a function of halfwidth of the luminescence band in glass of the $Me(PO_3)_2$-$Al(PO_3)_3$ system
Key:
1. $\Delta\lambda_{lase}$, nm
2. nm

Higher values for the induced emission cross sections were obtained in reference [395]. Table 4.12 has the results for zero energy density of the sounding pulse and density of 1.5 joules/cm^2.

Judging by the results of measuring the magnitudes of the induced emission cross sections, silicophosphate glass is an extremely prospective material for lasers.

The magnitude of the induced emission cross sections, according to our measurements using the spectroscopic [441] and laser [117] procedure is $(2.6\text{-}4)\cdot10^{-20}$ cm^2.

Attention is attracted by high resolution of the laser transition ($\sigma=(3\text{-}4)\cdot10^{-20}$ cm^2, although the halfwidth of the luminescence band in this glass is also significant (20 to 23 nm). Broad luminescence bands and, consequently, absorption bands must promote more complete use of the light of the pumping source, and a high magnitude of the induced emission cross section must reduce the threshold pumping energy.

On a number of laser models 10 mm in diameter by 130 mm obtained from a small volume of glass of low optical quality, an efficiency exceeding 2% in the free running mode was easily achieved.

Data on the induced emission cross sections obtained by the spectroscopic method for a number of mixed metaphosphates of alkali and alkali earth elements and neodymium are presented in Table 4.13. For alkali metaphosphates the cross section is on the average $3.0\cdot10^{-20}$ cm^2, and it depends weakly on the type of cation. For alkali earth metaphosphates, its magnitude is somewhat lower. Data are presented in Table 4.6 [436] for glass containing aluminum, indium, yttrium and lanthanum.

The measurement of the cross section by the lasing procedure for neodymium pentaphosphate ($Nd_2O_3 \cdot 5P_2O_5$) gave a value of $2.2 \cdot 10^{-20}$ cm^2.

Table 4.12

Cation	$\sigma(\tilde{E}), 10^{-20}$ см^2	
	$\tilde{E}=0$	$\tilde{E}=1,5$ joule/cm^2
Mg	2,5	2,3
Ca	3,0	2,7
Sr	3,2	2,8
Ba	3,5	3,1
Zn	3,0	2,7
Cd	3,4	3,0

Glass composition in molecular %: 87.5% $(PO_3)_2$, 12.5% (Al_2O_3).

Table 4.13

Composition	$\sigma, 10^{-20}$ см^2
$LiPO_3 \cdot Nd(PO_3)_3$	3,0
$NaPO_3 \cdot Nd(PO_3)_3$	3,2
$KPO_3 \cdot Nd(PO_3)_3$	2,8
$Sr(PO_3)_2 \cdot Nd(PO_3)_3$	2,6
$Ba(PO_3)_2 \cdot Nd(PO_3)_3$	2,8
$Pb(PO_3)_2 \cdot Nd(PO_3)_3$	3,0

Lasing on glass with high neodymium concentration can be obtained for small sizes of the active element. Thus, for plates made of potassium neodymium glass LGS-K, 500 microns thick with longitudinal pumping by the second harmonic of a YAG laser, the threshold pumping energy was 700 microjoules [229]. Lasing was realized also on lithium neodymium glass [225].

In order to obtain a lasing effect with tube pumping, we used an element 10 mm in diameter by 130 mm made of pentaphosphate glass with the composition $xNd_2O_3(1-x)La_2O_3 \cdot 5P_2O_5$ containing 8% by weight Nd_2O_3. For a pumping energy of 800 joules, an efficiency of 2% was achieved.

The measurement of the inverse population and excitation energy for glass of this composition demonstrated that at least up to 8% by weight Nd_2O_3 the excitation energy increases as the square root of the neodymium concentration. For ordinary multicomponent glass the excitation energy growth stops with significantly less activator content [117].

As has already been stated, the concentration quenching of the neodymium in the glass is accompanied by a strong drop in luminescent lifetime and quantum yield of luminescence as the neodymium concentration increases. The data presented in reference [117] for the measurements for borophosphate glass LGS-41 and LGS-42 demonstrated that beginning with some concentration Nd^{3+}, a decrease in the excitation energy is noted. It was found that for micrononuniform glass the critical concentration is less than for uniform. The

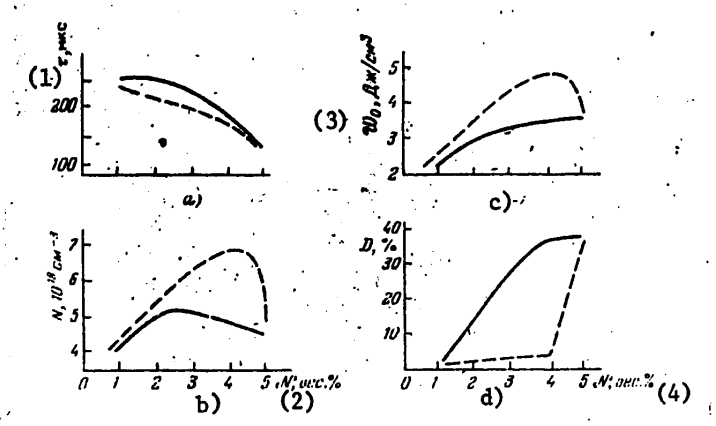

Figure 4.25. Lifetime τ, inversion density N, excitation energy density W_0 and proportion of nonluminescing ions D as functions of the Nd_2O_3 content.
Dotted line--LGS-42 glass, solid lines--LGS-41

Key:
1. τ, microsecond
2. *N*, percent by weight
3. W_0, joules/cm^3
4. *N*, percent by weight

same effect occurs in silicate glass. The authors of [117] relates to the formation of close groupings of neodymium ions with zero quantum yield of luminescence (pairs, triplets, and so on), the number of which increases quickly with exceeding of a critical concentration (Figure 4.25). From the obtained data it follows that the number of such associates can reach 40% of the total amount of neodymium. However, in reference [366] it is proved that in KGSS-1621 glass at least to a neodymium concentration of 2.1 molecular %, proportionality is retained between the quantum yield of the luminescence and the luminescence lifetime.

Study of the influence of water demonstrated that its presence does not lead to decrease in excitation energy, that is, each neodymium ion retains the capacity to luminesce, but the luminescence density decreases as a result of shortening of the lifetime [117]. An analogous result was obtained by the authors of reference [448].

§4.9. Free-Running Phosphate Glass Lasers

Good lasing characteristics of phosphate glass were noted in reference [430]. As a result of the low lasing thresholds of phosphate glass, a quasicontinuous lasing mode was obtained [74]. For this purpose, elements 3 mm in diameter by 50 mm were used, the pumping tube was fed by a rectified ac current without additional filtration. For a single halfperiod rectification, the threshold pumping power was 720 watts; for halfperiod, 1100 watts. Another attempt to realize continuous lasing was made in [73]. However, continuous lasing was obtained only on silicate glass, phosphate and fluoberyllate glass were destroyed as a result of thermal stresses before

attaining the lasing threshold. The experimental conditions were investigated above. It was found that emission in the free lasing mode was concentrated near the axis of the active element, and the emitted power (0.5 watts) was approximately 10 times less than the calculated power. At the present time continuous lasing is certainly obtained only on the so-called "selfocuses" made of silicate glass [72].

When using phosphate glass in pulsed lasers, the possibility of creating an extraordinarily narrow lasing spectrum without significant reduction in the laser efficiency is attractive. The simplest diagram of this laser is presented in Figure 4.26. The laser consists of a generator and amplifier, both of them are made of LGS-40 phosphate glass. In the generator the active element is placed in a semiconcentric resonator. The output mirror is made in the form of a plane parallel plate, on which a dielectric coating is applied. This plate simultaneously plays the role of a frequency selector with reflection coefficient of 15%. In order to increase the output energy, a single power amplifier is used. By using this device, a smooth lasing pulse is obtained with spectral width of the emission band of 0.05 cm^{-1}.

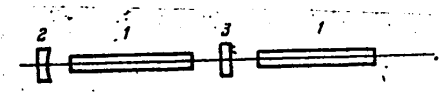

Figure 4.26. Diagram of an amplifier-laser with narrow emission spectrum.
1--active element, 2--spherical mirror, 3--plane parallel plate

The use of the resonator permitting realization of the traveling wave mode makes it possible to achieve further narrowing of the lasing spectrum [449]. In the system presented in Figure 4.27, a four-mirror ring cavity is used. In order to obtain the traveling wave mode, an additional return mirror is used. Three of the four mirrors placed at the corners of the rectangle are blind mirrors, with beveled rear surface, the fourth is semitransparent. It is used to output emission from the laser, and the return mirror is blind. Between the semitransparent and return mirrors there is a selector in the form of a Fabry-Perot etalon. The other etalon is placed directly in the resonator and is used for emission frequency tuning. For this purpose its surface is set an angle of 10^{-4} rad to each other. The laser uses two active elements, one made of phosphate glass and the other of GLS-1 glass. Both elements are excited simultaneously.

In the absence of the return mirror the time expansion of the lasing is a random series of peaks with spectral width on the order of 1 cm^{-1}. On including the return mirror, the width of the pulse spectrum decreases to 0.08 cm^{-1}. Placement of the selector between the return and semitransparent mirrors brings order into the series of peaks in time and is accompanied by excitation of only one or two axial modes. When the pumping energy exceeds the threshold by 4 to 6% and with small inclination of the selector, a single frequency lasing mode is achieved with spectral width of 0.005 cm^{-1}; regular emission pulsations are observed here. The duration of individual

peaks is 2 microseconds, the time intervals between them are 12 microseconds.

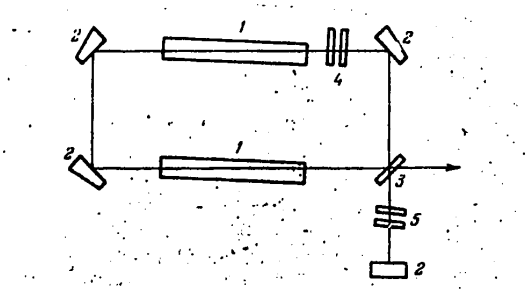

Figure 4.27. Diagram of a traveling wave laser with narrow emission spectrum:
1--active element, 2--reflector, 3--semitransparent mirror, 4,5--Fabry-Perot etalons.

Frequency tuning is realized by shifting the misaligned selector in a 1054-1070 nm range. It was noted that during tuning to the long wave region the width of the lasing spectrum increases somewhat.

As was stated above, efforts to obtain continuous lasing on phosphate glass were not crowned with success. Nevertheless, good results were obtained when using this glass in the frequency lasing mode [58]. On active elements 8 mm in diameter by 100 mm made of LGS-I and LGS-M glass, lasing was realized with pulse repetition of 10 hertz for an average emission power to 10 watts. For pumping the ISP-600 pulse tube was used which together with the active element was placed in a single module quartz illuminator. Cooling was realized by a liquid simultaneously serving as a filter for the ultraviolet pumping emission. The pumping power was 700 watts. In the LGS-M glass with attenuated dependence of the thermooptical constants on temperature, lasing was observed in the temperature range from -60 to +80°C, the variation of the lasing energy in the pulse on variation of temperature did not exceed 50%.

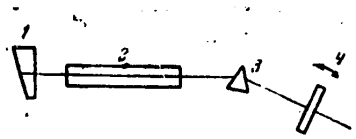

Figure 4.28. Simplest laser with dispersion resonator.
1--flat mirror, 2--active element, 3--prism, 4--rotating mirror.

Introduction of dispersion elements in the laser cavity (Figure 4.28) offers the possibility of obtaining smooth frequency tuning within the limits of the neodymium luminescence band [442, 450, 510]. Use of the Fabry-Perot etalon for frequency tuning made it possible in reference [453] to realize stable lasing in LGS-40 phosphate glass on a wavelength of 1.3 micron or simultaneously lasing on 1.06 and 1.3 microns. The possible tuning range inside the

luminescence band was determined by the dispersion characteristic of the etalon and it was 10.5 mm. Lasing was not obtained on silicate glass under the same conditions. Moreover, the introduction of silicate and phosphate glass simultaneously into the cavity leads to discontinuation of lasing at 1.3 microns, which indicates the appearance of large inactive losses in the silicate glass under the effect of pumping.

In conclusion, it can be stated that the use of phosphate glass in free-running lasers is extremely efficient. As a result of low lasing thresholds phosphate glass greatly increases the laser efficiency. References [167, 431] contain reports on obtaining an efficiency of 4 to 5% in elements 20 mm in diameter by 260 mm made of LGS-I, LGS-M glass. This is almost twice that, for example, for GLS-1 silicate glass. In reference [47], an efficiency to 6% was achieved for elements 45 mm in diameter by 600 mm.

§4.10. Use of Phosphate Glass to Obtain Short and Ultrashort Pulses

The narrowness of the lasing spectrum characteristic of phosphate glass can in some cases be useful to improve the characteristics of lasers operating in the self-synchronization modes.

Although silicate glass, as a result of the broad emission spectrum (50 to 100 cm^{-1}) theoretically permit us to obtain 10^{-13} second pulses with mode synchronization, the antireflection dyes used for realization of these conditions have insufficiently short absorption recovery time (10^{-11} sec), which leads to irregularity of the peak structure and difficulties in achieving reproducible conditions. In order to improve the reproducibility, it is necessary artificially to constrict the emission band of the laser using dispersion elements placed in the cavity. The application of phosphate glass with a narrow lasing spectrum must provide for simplification of the volume of this laser and provide stable, well-reproducible lasing conditions.

In reference [453], alkali niobium phosphate glass LGS-54 with an emission spectrum width in the free running mode of no more than 6 cm^{-1} was used for this purpose. A rod made of this glass 10 mm in diameter by 130 mm with ends beveled at the Brewster angle was placed in a plane parallel resonator 90 cm long. The resonator consisted of a blind mirror in direct contact with the transmitting filter 2 mm thick and a mirror with 50% transmission (Figure 4.29). The mirror backings and the filter opening had wedge shape. An iris 2.5 mm in diameter was used to limit the angle modes of the resonator. The initial transmission of the transmitting filter was 65%. When the pumping energy exceeded the threshold by 5 to 10%, the lasing occurred in the form of a regular train of pulses 20 nanoseconds in duration with contrast of 2.5. The width of the pulse spectrum was 1.3 to 1.7 cm^{-1}. The total energy of the pulse train was 6 to 9 millijoules with a peak power of 10^9 watts/cm^2. These conditions are highly reproducible for 30 to 40-fold pumping repetition. In addition to regularity of the pumping structure, the lasing wavelength is reproduced well, the average deviation from pulse to pulse does not exceed 0.5 cm^{-1}. Analogous results are also obtained for another phosphate glass--LGS-40 [453].

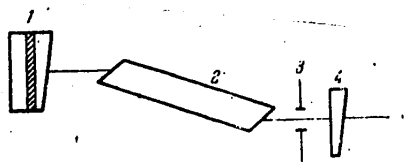

Figure 4.29. Diagram of a laser with passive mode synchronization. 1--cell filter combined with a mirror with 100% reflection, 2--active element, 3--iris, 4--mirror with 50% reflection.

As a result of the low thresholds and high efficiency, phosphate glass can be used in a number of devices to replace such expensive materials as yttrium aluminum garnet (YAG). Thus, when using a rotating prism based on elements 8 mm in diameter by 100 mm as the modulator, the periodic giant pulse lasing mode with a frequency of 10 hertz and energy per pulse of 0.5 joules was obtained [58].

The elements were made of LGS-I glass and they were subjected to special processing in order to improve their strength. The experimental conditions were analogous to those described above for the free lasing mode. The pumping energy per pulse was 50 joules. The efficiency of this laser in the giant pulse mode exceeded 1%. The presence of LGS-I glass by LGS-M with attenuated dependence of the thermooptical characteristics on temperature made it possible to obtain stable lasing in the range from -60 to +80°C with an emission divergence of 20' with respect to the 0.9 level and energy variation per pulse of no more than 50% in the entire temperature range. The parameters of such a laser as a function of thermooptical characteristics of the glass are investigated in more detail in §5.2.

CHAPTER 5. THERMOOPTICAL PROPERTIES OF PHOSPHATE GLASS AND SELECTION OF NEODYMIUM GLASS FOR LASERS OF VARIOUS TYPES

§5.1. Thermooptical Characteristics of Phosphate Glass

For the creation of phosphate glass with given thermooptical properties, it is necessary to know the thermooptical characteristics $\tilde{W}$, P and Q as a function of the glass composition. The value of $\tilde{W}$ which can be calculated by formula (1.32) [456] is the simplest to measure, but the interferometric methods of direct measurement of $\tilde{W}$ with uniform heating of the glass element [34, 455, 457, 458] or when determining the difference in path between two points of the cross section of a rectangular element having different temperature [32] are more convenient and exact. In the latter case, it is necessary to use a rectangular (desirably, plate) element with unattached ends, in which a linear temperature gradient does not create stresses [31, 32]. In the method discussed in [455, 457, 458], the temperature of the element is recorded, then it is varied by a defined amount, and the difference in optical path occurring in this case is measured. This gives an average value of $\tilde{W}$ for the temperature interval of the measurements. $\tilde{W}$ increases linearly with temperature. The temperature coefficient $d\tilde{W}/dT$ is $(0.05\text{-}0.30) \cdot 10^{-7}\ K^{-2}$ [33, 34, 49, 459]. For a value of $d\tilde{W}/dT$ equal to $0.2 \cdot 10^{-7}\ K^{-2}$ and a temperature gradient for two measurements at 50 K used, for example, in [457], the obtained average value of $\tilde{W}$ will differ from the values for the ends of the interval by $\pm 5 \cdot 10^{-7}\ K^{-1}$. When using values of $\tilde{W}$ presented by different authors, it is necessary to consider the variation of $\tilde{W}$ with temperature. In [34, 460], a method is proposed for continuous recording of the temperature dependence of the difference in optical path $\Delta p(T)$ with slow uniform heating of the sample, which permits construction of the curves $\tilde{W}(T)$ for a broad temperature interval and improvement of the accuracy of determination of $\tilde{W}$.

As was demonstrated in [461], and then in [34, 456, 460], the values of $\tilde{W}$ and $d\tilde{W}/dT$ for phosphate glass, as a rule, decrease with a decrease in the field strength of the cation modifier. In Figure 5.1 the values of $\tilde{W}$ are presented for metaphosphates of bivalent and trivalent metals [456] as a function of the ion radius r of the cation. Figure 5.2 shows the temperature dependence of $\tilde{W}$ for glass with the composition (in molecular percent) of 90 $Me(PO_3)_2$-10$Al(PO_3)_3$ [34]. The behavior of the curves $\tilde{W}(r)$ differs for the cations Mg, Ca, Sr, Ba with electron shells of the same type as for inert gases, and for ions of the Zn-Cd group with 18-electron shell. This was noted for the first time in [461], and then it was found for the dependence of other thermooptical

properties on the atomic characteristics of bivalent cations [456, 463, 464]. In Table 5.1 for glass with the composition of 90 $Me(PO_3)_2$-10 $Al(PO_3)_3$, values of $\tilde{W}$ obtained by two methods were compared. The value of $\tilde{W}_1$ was measured directly during continuous recording of the temperature dependence of the length of optical path of $\Delta p(T)$ [34]. We calculated $\tilde{W}_2$ by the values obtained in [456] for pure metaphosphates of bivalent metals and aluminum by measuring the coefficient of thermal expansion n and dn/dT and subsequent calculation of $\tilde{W}$ by formula (1.32). These values of $\tilde{W}$ are presented in Table 5.2 [456]. The values of B--the optical stress coefficient investigated below--are indicated there. When performing the calculation it was assumed that the contribution to $\tilde{W}$ depends linearly on the metaphosphate concentration. All of the values are presented for 70° C considering the values of $d\tilde{W}/dT$. In [34] $\tilde{W}$ was measured on a wavelength of 632 nm; in [456] it was measured on 508 nm. With an increase in wavelength the thermooptical constant $\tilde{W}$ decreases [33, 46]. Depending on the dispersion of the index of refraction the values of $\tilde{W}$ on λ = 508 nm must be (4-12) $\cdot 10^{-7}$ K^{-1} larger than for λ = 632 nm (Table 1.5).

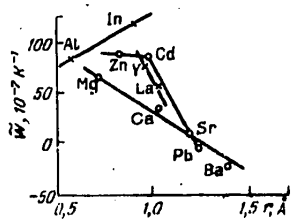

Figure 5.1. Thermooptical constant $\tilde{W}$ of vitreous metaphosphates of bivalent and trivalent metals as a function of the ion radius of the cation [456].

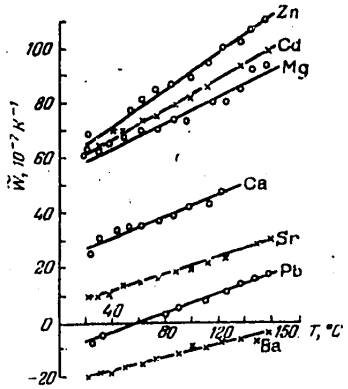

Figure 5.2. Temperature dependence of the thermooptical constant $\tilde{W}$ for glass with the composition (molecular percent) 90 $Me(PO_3)_2$-10 $Al(PO_3)_3$ [34].

Comparison of $\tilde{W}_1$ and $\tilde{W}_2$ (Table 5.1) demonstrates that both methods give results that agree satisfactorily considering the dispersion $\tilde{W}$ and the total

measurement and calculation error (on the order of $5 \cdot 10^{-7}$ K^{-1}); considering the dispersion of $\tilde{W}$, the values of $\tilde{W}_1$ are somewhat larger than $\tilde{W}_2$, except glass with Zn and Cd. At the same time, the values of the temperature derivative of $\tilde{W}$ differ by 1.5 to 2 times. The values of $d\tilde{W}/dT$ defined by different interferometric methods [34, 459], are larger than the values obtained by calculation using formula (1.32) [49, 456]. Therefore a quantitative comparison of $d\tilde{W}/dT$ is now possible only for the identical method of measurement. The course of the relation for $d\tilde{W}/dT$ as a function of the parameters of the modifier cations is identical for different measurement methods, and, namely, $d\tilde{W}/dT$ decreases with a decrease in the cation field strength. Alkali phosphate glass has the least values of these derivatives: for phosphate glass $d\tilde{W}/dT$ can be almost half that for barium glass having minimum value of $d\tilde{W}/dT$ in glass with the composition of 90 $Me(PO_3)_2$-10 $Al(PO_3)_3$. For example, in Table 5.3 compositions and thermooptical characteristics of certain glasses of the $MePO_3$-BPO_4-MgO (Me = Na, K) are presented which were studied in [34, 167, 461, 462]. The addition of B_2O_3, BPO_4 and MgO to the alkaline metaphosphates increases the values of $\tilde{W}$ and $d\tilde{W}/dT$ (Table 5.3). Potassium glass has appreciably smaller values of $\tilde{W}$ than sodium glass.

Table 5.1

Me	$\tilde{W}_1$, $10^{-7}K^{-1}$, 632,8 nm	$\tilde{W}_2$, $10^{-7}K^{-1}$, 508 nm	$\tilde{W}_1-\tilde{W}_2$, $10^{-7}K^{-1}$	$\frac{d\tilde{W}_1}{dT}$, $10^{-7}K^{-2}$, 632,8 nm	$\frac{d\tilde{W}_2}{dT}$, $10^{-7}K^{-2}$, 508 nm	$\frac{d\tilde{W}_1}{dT}-\frac{d\tilde{W}_2}{dT}$, $10^{-7}K^{-2}$
	T=70°C			T=20—120°C		
Mg	71	68,2	+2,8	0,235	0,163	+0,072
Ca	38	36,3	+1,7	0,205	0,154	+0,051
Sr	18	16,2	+1,8	0,155	0,136	+0,019
Ba	—15	—14,1	+0,9	0,15	0,109	+0,041
Zn	83	86	—3			
Cd	76	84,9	—8,9	0,27	0,136	+0,134
Pb	3	3,6	—0,6	0,18	0,163	+0,017

Table 5.2

Material	α_T, $10^{-7}K^{-1}$, T=70°C	$\frac{dn}{dT}$, $10^{-7}K^{-1}$, 508 nm	$\alpha_T(n-1)$, $10^{-7}K^{-1}$, 508 nm	$\tilde{W}$, $10^{-7}K^{-1}$, 508 nm	B, 10^{-7} см^2/kg, 550 nm
$Mg(PO_3)_2$	74	29	37,5	66,5	2,3
$Ca(PO_3)_2$	101	—25	56	31	1,65
$Sr(PO_3)_2$	119	—50	67	8	1,25
$Ba(PO_3)_2$	138	—106	81	—25	0,55
$Zn(PO_3)_2$	80	45	42	87	4,95
$Cd(PO_3)_2$	90	30	55	85	3,0
$Pb(PO_3)_2$	139	108	102	—6	0,35
$Y(PO_3)_3$	45,5	53	25	78	3,2
$La(PO_3)_3$	71	12	42,5	54,5	2,05
$Al(PO_3)_3$	57	54	30	84	2,6
$In(PO_3)_3$	62	85,5	35,5	121	3,0

Table 5.3

Glass Comp, mol-%				$\tilde{W}$, 10^{-7} K^{-1}, 20°C	$\frac{d\tilde{W}}{dT}$, 10^{-7} K^{-2}	α_T, 10^{-7} K^{-1}	n
$NaPO_3$	KPO_3	BPO_4	MgO				
70		15	15	—4	0,07	149	1,517
55		30	15	12	0,13	119	1,525
40		45	15	32	0,14	89	1,536
	70	15	15	—57	0,07	189	1,502
	55	30	15	—39	0,12	154	1,510
	40	45	15	—1	0,15	111	1,520
	60	20	20	—25	0,09	170	1,505

Glass Comp, mol-%				$\frac{dn}{dT}$, 10^{-7} K^{-1}	$\alpha_T(n-1)$, 10^{-7} K^{-1}	P, 10^{-7} K^{-1}	Q, 10^{-7} K^{-1}
$NaPO_3$	KPO_3	BPO_4	MgO				
70		15	15	—76	77	—32	9,8
55		30	15	—45	62	—	—
40		45	15	—11	48	23	8,7
	70	15	15	—147	95	—98	7,6
	55	30	15	—111	79		—
	40	45	15	—50	58	—9	8,1
	60	20	20	—107	86		

Now let us consider the contribution to $\tilde{W}$ from two terms of formula (1.32). In Table 5.2 these values are presented for metaphosphates of bivalent and trivalent metals [456], in Table 5.3 for glass based on alkaline metaphosphates. The contribution of $\alpha_T(n-1)$ is always positive, it is (25-100) $\cdot$ 10^{-7} K^{-1}, and for like ions, it increases monotonically with an increase in the atomic number of the cation. This is connected both with an increase in the coefficient of thermal expansion and with an increase in the index of refraction. Thus, the sign and the value of $\tilde{W}$ are determined primarily by the temperature dependence of n, which varies within significant limits (the value of dn/dT varies approximately from $-150 \cdot 10^{-7}$ to $+100 \cdot 10^{-7}$ K^{-1}). It depends on the ratio of the temperature coefficients of thermal expansion and polarizability. This is easy to demonstrate [467], using the known Lorenz-Lorentz formula:

$$\frac{n^2-1}{n^2+2}V = R, \tag{5.1}$$

where V is the specific volume, R is the specific refraction of the medium. The polarizability factor $\alpha_\pi = 3MR/(4\pi\mathcal{N})$, where M is the molar mass of the material, $\mathcal{N}$ is Avogadro's number. From (5.1) after transformations we obtain

$$\frac{dn}{dT} = \frac{(n^2-1)(n^2+2)}{6n}(\tilde{\varphi}-\tilde{\gamma}). \tag{5.2}$$

Here $\tilde{\gamma} = \frac{1}{V}\frac{dV}{dT}$ is the coefficient of volumetric expansion, $\tilde{\varphi} = \frac{1}{\alpha_\pi}\frac{d\alpha_\pi}{dT} = \frac{1}{R}\frac{dR}{dT}$ is the total thermal coefficient of polarizability (that is, considering all variations of the polarizability with temperature).

Let us consider three possible cases of the relations between $\tilde{\phi}$ and $\tilde{\gamma}$.

1. γ is always larger than $\tilde{\phi}$. The index of refraction decreases monotonically with temperature. As an illustration, in Figure 5.3 we have the temperature dependence of n, $\tilde{\gamma}$, $\tilde{\phi}$ for vitreous B_2O_3 [467], in which the bonds are significantly less strong than, for example, in SiO_2. This behavior is characteristic for "loose" structures with relatively weak bonds, and it can be expected for borate and phosphate glass containing large low-charge modifier cations.

2. $\tilde{\gamma}$ and $\tilde{\phi}$ are similar with respect to magnitude. This category includes the majority of silicate optical glasses with rigid silicate frame. For a wide temperature range the curves of the thermal dependence of $\tilde{\gamma}$ and ϕ intersect at three points where the function n(T) has peaks or minima. At low temperatures the index of refraction decreases slowly with temperature. Then at higher temperatures, n increases, reaching a maximum near the roasting temperature. In the region of transformation $\tilde{\gamma}$ becomes larger than $\tilde{\phi}$, and n decreases to the following minimum and then it again increases. As an illustration we have the behavior of n(T) for borosilicate crown glass (Figure 5.4).

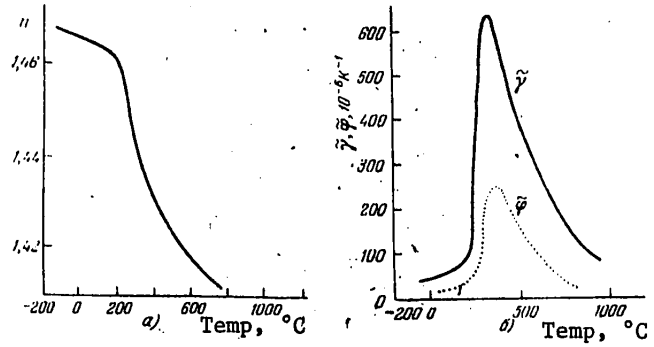

Figure 5.3. Temperature dependence of the index of refraction (a), the coefficient of volumetric expansion $\tilde{\gamma}$ and the total polarizability factor $\tilde{\phi}$ (b) for vitreous B_2O_3 [467].

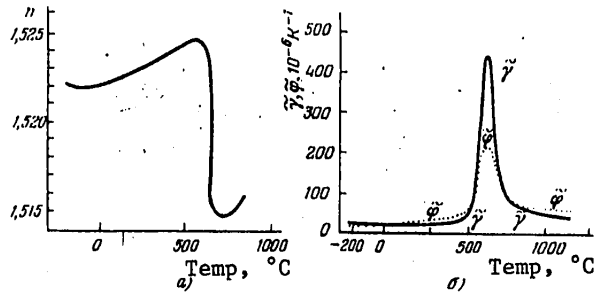

Figure 5.4. Temperature dependence of the index of refraction (a), the coefficient of volumetric expansion $\tilde{\gamma}$ and the total polarizability factor $\tilde{\phi}$ (b) for borosilicate glass [467].

3. $\tilde{\gamma}$ is always smaller than $\tilde{\phi}$. This is characteristic only for quartz glass with very small $\tilde{\gamma}$. Here the defining factor is the thermal variation of polarizability, and n increases monotonically with temperature to the region of transformation (about 1,300° C for quartz glass).

These relations are useful to consider when analyzing the general picture of the dependence of the index of refraction on temperature. For example, it can be expected that the values of dn/dT will increase for the transition from loose (with large volume calculated for one anion) phosphate glass containing large cations and having predominantly chain structure, to denser phosphate glass, the composition of which includes cations with large field strength (Mg^{2+}, Al^{3+}, and so on) and also ultraphosphate, borophosphate and silicophosphate glass having large binding of the anion motif and structure close to frame. Among the silicate glass the least values of dn/dT must also have glass with large content of the large cations (K, Cs, Ba, Sr).

Above, we did not investigate the physical mechanisms of variation of polarizability which, along with variation of density are responsible for the temperature dependence of the index of refraction. These mechanisms were analyzed in [465, 466], and then in [463, 468]. The Drude formula for molecular refraction or polarizability analogous to the Lorenz-Lorentz formula was used:

$$n^2 - 1 = 4\pi\tilde{N}\alpha_n,$$

where $\tilde{N}$ is the number of oscillators per unit volume. It was demonstrated that it is possible to isolate three contributions to dn/dT which we shall denote by $\mathcal{P}, \mathcal{Q}, \mathcal{R}$; they are related, respectively, to the variation in the number of oscillators per unit volume as a result of the thermal variation of the density ($\mathcal{P}$), with variation of the polarizability as a result of variation of the density ($\mathcal{Q}$) and with variation of the polarizability as a result of variation of the temperature ($\mathcal{R}$):

$$\begin{aligned} \mathcal{P} &= -\tilde{\gamma}\frac{n^2-1}{n^2+2}, \\ \mathcal{Q} &= \tilde{\gamma}\frac{E}{3(1-2\mu)}(C_1+2C_2) - \mathcal{P}, \\ \mathcal{R} &= \frac{dn}{dT} - (\mathcal{P}+\mathcal{Q}). \end{aligned} \tag{5.3}$$

When using the Lorenz-Lorentz formula, the value of $\mathcal{P}$ can be multiplied by $(n^2 + 2)/3$ [463]; the value of $\mathcal{Q}$ also varies correspondingly; $\mathcal{R}$ does not depend on the initial expression for refraction.

The value of $\mathcal{Q}$ permits estimation of the contribution of the photoelasticity to the temperature variation of n. Unfortunately, for such an analysis it is necessary to know the photoelastic constants of glass C_1 and C_2 which are measured only for optical glass of complex composition [469] and for metaphosphates of bivalent metals [464, 477].

Using the parameters $\mathcal{P}, \mathcal{Q}, \mathcal{R}$, it is possible to estimate the temperature variation of the polarizability factor of the glass $\alpha_\pi(T)$ [386, 388, 389, 391]:

$$\alpha_n(T) = \alpha_0(1 + \mathcal{L}\tilde{\gamma}T + \tilde{\varphi}_\rho T),$$

or

$$\frac{dn}{dT} = \frac{n^2-1}{2n}\left(-\tilde{\gamma} + \mathcal{L}\tilde{\gamma} + \tilde{\varphi}_\rho\right).$$

Here α_0 is the initial polarizability, $\tilde{\varphi}_\rho = \frac{1}{\alpha_n}\left(\frac{\partial \alpha_n}{\partial T}\right)_\rho = -\frac{\mathcal{R}\tilde{\gamma}}{\mathcal{P}}$ is the thermal coefficient of polarizability for constant density ρ (differing from the total coefficient $\tilde{\phi}$ in (5.2)), $\mathcal{L} = -Q/\mathcal{P}$ is the deformation-polarization coefficient determining the variation in the polarizability with variation of the volume.

Table 5.4 gives the values of $\mathcal{P}$, Q, $\mathcal{R}$, $\mathcal{L}$, $\mathcal{L}\tilde{\gamma}$ and $\tilde{\phi}_\rho$ according to Lorenz-Lorentz for metaphosphates of bivalent metals [464]; the values according to Drude are given in parentheses. Although the values of the coefficients calculated from the various expressions for the refractions can differ significantly, the general behavior of their variation on transition from one composition to another is retained. $\mathcal{P}$ and $(\mathcal{P}+Q)$ (the photoelastic effect) decrease in the series Mg-Ba and Zn-Cd-Pb. The values of $\mathcal{P}$, Q and $\mathcal{R}$ are comparable to each other, which distinguishes the glass from crystal in which the predominant contribution to the variation of the polarizability with temperature is made by the photoelastic effect ($\mathcal{P}, Q > \mathcal{R}$, $\mathcal{L}\tilde{\gamma} > \tilde{\varphi}_\rho$) [464]. Barium metaphosphate, which is similar with respect to the value of $\mathcal{R}$ to crystalline KBr [463, 466] is an exception. Figure 5.5 shows the dependence of the variation $\mathcal{P}$, Q and $\mathcal{R}$ in metaphosphates of bivalent cations on the variation of the coefficient of linear thermal expansion and the free cation refraction. $\mathcal{P}$ depends linearly on the coefficient of thermal expansion, Q and $\mathcal{R}$ depend on the refraction. The proportionality coefficients for $\mathcal{P}$ and $\mathcal{R}$ differ in the series Mg-Ba and Zn-Pb as a result of difference in degree of covalence of the Me^{2+}-O bond. As a result of different sign of the slope angles of the functions Q and $\mathcal{R}$ on the refraction, the sum $(Q+\mathcal{R})$ in the vitreous $Me(PO_3)_2$ varies little, and the dependence of dn/dT on the composition is determined in the given case by variation of the number of oscillators per unit volume, that is, the value of $\mathcal{P}$ [464]. As our measurements demonstrate, the analogous situation occurs for glass 0.9 $Me(PO_3)_2$-0.1 $Al(PO_3)_3$ and for glass based on alkaline metaphosphates. Thus, we obtain confirmation of the previously discussed arguments of the ratio of the values of $\tilde{\gamma}$ and $\tilde{\phi}$ for friable phosphate glass.

As is obvious from Tables 5.1-5.4 and Figures 5.1, 5.2, values of $\tilde{W}$ close to zero can be obtained on the basis of the compounds of Sr, Ba, Pb and also alkaline metals, which is understandable in the light of the previously discussed concepts. Therefore the influence of the oxides of these elements on the thermooptical characteristics of glass was studied recently in the greatest detail [470-476]. It was discovered that the contribution of the oxide additives to the value of $\tilde{W}$ depends on its value for the initial glass. The addition of SrO to glass with positive values of $\tilde{W}$ leads to a decrease in them; with negative values, to an increase in them. PbO has a similar influence [470, 471]. In all of the investigated phosphate glasses, BaO lowers $\tilde{W}$ [472]. Glass based on the alkaline metal oxides has the least value of $\tilde{W}$,

usually to $-50 \cdot 10^{-7}$ K^{-1} [34], although phosphate glass with a large content of Rb_2O and Cs_2O can also have much smaller values [473]. The determination of the contributions of individual components to $\tilde{W}$ made it possible to create a table for calculating its values in glass, predominantly based on phosphates of bivalent metals, inasmuch as for such glass data were obtained for different additives [478].

Table 5.4

	$MgO \cdot P_2O_5$	$CaO \cdot P_2O_5$	$SrO \cdot P_2O_5$	$BaO \cdot P_2O_5$	$ZnO \cdot P_2O_5$	$CdO \cdot P_2O_5$	$PbO \cdot P_2O_5$
$\mathscr{P}$, 10^{-7} K^{-1}	—130(—92)	—202(—137)	—246(—166)	—298(—197)	—151(—104)	—201(—132)	—399(—239)
$\mathscr{Q}$, 10^{-7} K^{-1}	73(35)	125(61)	130(50)	201(101)	66(20)	123(54)	233(72)
$\mathscr{R}$, 10^{-7} K^{-1}	86	52	57	—9	130	108	58
$\mathscr{L}$	0,56(0,38)	0,62(0,44)	0,53(0,30)	0,66(0,51)	0,44(0,20)	0,61(0,41)	0,58(0,30)
$\tilde{\varphi}_\rho$, 10^{-7} K^{-1}	147(207)	78(114)	82(122)	—13(—20)	206(298)	145(221)	62(102)
$\mathscr{L}\tilde{\gamma}$, 10^{-7} K^{-1}	125(84)	187(134)	189(107)	276(212)	105(48)	164(111)	242(126)
P, 10^{-7} K^{-1}	58	13	—14	—71	83	62	—37
Q, 10^{-7} K^{-1}	5,5	5,7	5,4	2,1	10	9,1	—0,7
$\tilde{W}$, 10^{-7} K^{-1}	66	31	8	—25	87	84	—7
$P/\tilde{W}$	0,9	0,4	—1,8	2,8	0,9	0,7	5,0

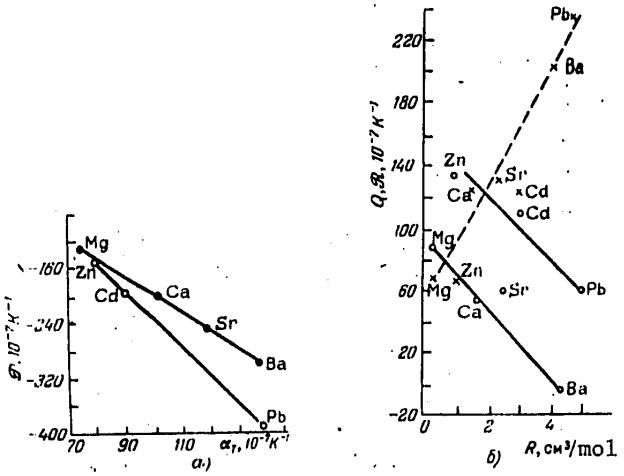

Figure 5.5. Dependence of the terms $\mathscr{P}$, $\mathscr{Q}$, $\mathscr{R}$, defining the variation of n with temperature on the coefficient of linear thermal expansion α_T (a) and on the refraction of the free cation R (b) in metaphosphates of bivalent metals [464]. Calculation by the Lorenz-Lorentz formula. The circles-- $\mathscr{R}$, the crosses-- $\mathscr{Q}$.

The calculation of an additive property Ω_c of the glass containing m components is made by the Demkina additiveness formula [479]:

$$\Omega_c = \sum_1^m \frac{a_0}{S_0}\Omega_0 \Big/ \left(\sum_1^m \frac{a_0}{S_0}\right) = \sum_1^m b_0\Omega_0,$$

where $b_0 = \frac{a_0}{S_0}\Big/\left(\sum_1^m \frac{a_0}{S_0}\right)$. Here Ω_0 is the partial value of the calculated parameter for components in glass; the coefficients S_0 called the structural mass serve for transition from the mass fractions a_0 to the volumetric fractions b_0. In Table 5.5 the partial values of the index of refraction n_0, the average dispersion $(n_F - n_C)_0$, the coefficient of thermal expansion α_T^0, the thermooptical characteristics $\tilde{W}_0$, Q_0 and the optical stress coefficient B_0 are presented for 28 oxides. The structural masses of S_0 of the oxides were determined by the experimental values of the index of refraction. The table offers the possibility of calculating the magnitudes of the coefficient of thermal expansion α_T and W with the arithmetic mean error $2.5 \cdot 10^{-7}$ K^{-1} and $3 \cdot 10^{-7}$ K^{-1}, respectively, and mean square error of $5 \cdot 10^{-7}$ K^{-1} for both values with a confidence interval of 0.85.

Table 5.5

Oxides	S_0	n_0	$(n_F - n_C)_0 \cdot 10^5$	α_T^0, 10^{-7} K^{-1} T=70°C	$\tilde{W}_0$, 10^{-7} K^{-1} λ=508 nm	B_0, 10^{-7} см^2/kg	Q_0, 10^{-7} K^{-1}	Oxide Content,* % by weight
P_2O_5	63	1,505	715	100	25	2,1	7,5	33—80
Li_2O	30	1,52	870	190	20	—1	5	0—6(17) (в стекле без PbO)[1]
	30	1,70	1670	190	20			0—6 (в стекле с PbO)[2]
Na_2O	62	1,45	950	400	—160	0	6	0—7 (30)
K_2O	94	1,42	620	490	—350	1	8	0—28 (40)
Rb_2O	187	1,44	800	430	—350	—2	3	0—21 (57)
Cs_2O	282	1,49	850	500	—500	—4	—8	0—25
Tl_2O	236					—12	—50	0—20
MgO	72					3	35	0—5 (в стекле с BaO и PbO)[3]
	40					3	5	0—5 (в стекле с K_2O и в метафосфате)[4]
CaO	198	1,85	1650	70	140	—1	10	0—10(28)
SrO	246	1,83	1500	210	—85	—4	4	0—10 (42)
BaO	295	1,94	1825	295	—230	—8	—23	0—36 (51)
ZnO	81					6	25	0—20

Key: a. (in glass without PbO)
b. (in glass with PbO)
c. (in glass with BaO and PbO)
d. (in glass with K_2O and in metaphosphate)

Table 5.5 (continued)

CdO	270	2,10	2800	25	425	7	35	0—20 (47)
PbO	223	2,23	4950	215	—30	—4	—18	0—56 (60)
Sc_2O_3	77	1,85	2500	—85	255	7	30	0—10
Y_2O_3	226	1,85	2500	—300	400	6	20	0—12 (33)
La_2O_3	171							
CeO_2	172	1,89	2085	—90	230	7	25	0—7 (45)
Nd_2O_3	176							
B_2O_3	43	1,59	750	—20	140	4	12	0—12
Al_2O_3	102	1,65	900	—205	400	5	25	0—17 (23)
Ga_2O_3	102	1,75	1500	—40	375	8	30	0—10 (31)
In_2O_3	147	1,78	2000	—55	270	7	40	0—10 (40)
SiO_2	60	1,49	635	—70	70	7	20	0—3
GeO_2	104	1,80	1800	—100	530	7	30	0—20
Nb_2O_5	125	2,05	6380	—185	370	6	25	0—10
Sb_2O_3	154	2,29	5500	130	280	1	15	0—20
Bi_2O_3	241	2,42	6900	100	280	7	25	0—20 (52)

* The numbers in parentheses indicate the maximum oxide concentration in the binary systems.

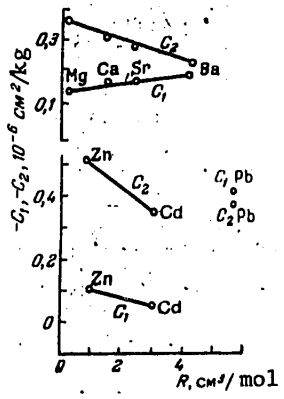

Figure 5.6. Photoelastic constants C_1 and C_2 as a function of the refraction of a free cation for vitreous metaphosphates $Me(PO_3)_2$ [464].

As a rule, the thermooptical characteristic P varies as a function of the glass composition in the same way as $\tilde{W}$. However, in connection with the great complexity of its determination, the number of papers in which the dependence

of P on the glass composition is analyzed, is very limited. P is calculated by mechanical and photoelastic characteristics of glass and values of dn/dT with respect to the formula (1.32). The photoelastic constants C_1 and C_2 in binary glass are measured only for metaphosphates of bivalent metals [400, 464, 477]. In the series Mg-Ca-Sr-Ba, the value of C_1 increases, and C_2 decreases (Figure 5.6). The optical stress coefficient $B = C_1 - C_2$ also decreases. A decrease in B is noted in the series of metaphosphates of Zn-Cd-Pb, however, C_1 and C_2 vary nonmonotonically here. This nature of variation of the photoelastic properties and small number of measurements on glass of simple composition make calculation of P difficult. The method of its independent determination proposed in [45] is highly complicated and requires samples with high optical quality. Now the values of P are measured by the method only for laser glass of complex composition (Table 1.3). In [55] it was demonstrated that P is connected linearly with $\tilde{W}$:

$$P = (-6{,}6 + 1{,}44\tilde{W}) \cdot 10^{-7}\ \text{K}^{-1}.$$

This relation was found for intervals of the values of the coefficient of linear thermal expansion of glass (35-112) $\cdot 10^{-7}$ K^{-1}, photoelastic constants $-(0.9\text{-}6) \cdot 10^{-7}$ cm^2/kg, Young's modulus 4,100-8,200 kg/mm^2 and values of P and $\tilde{W}$ (2-150) $\cdot 10^{-7}$ K^{-1}. The authors of [55] consider that in this case the value of P can be obtained with the mean square error not exceeding 4.5 $\cdot 10^{-7}$ K^{-1}. Figure 5.7 shows the relation of P and $\tilde{W}$ for glass [55].

If this expression is valid, the laws of variation of P and $\tilde{W}$ with glass composition in the phosphate systems are analogous, that is, P must decrease to large negative values for glass with large concentrations of large low-charge cations Na, K, Rb, Cs, Ba, Pb and, just as $\tilde{W}$, increase as the field strength of the cation modifier increases. This actually occurs, as the published data

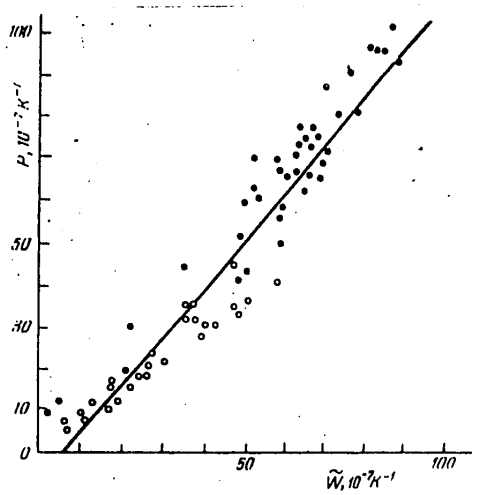

Figure 5.7. Relation of thermooptical constants P and $\tilde{W}$ for glass [55]. The circles are the experimental values, the dots are values found by the experimental values of optical, elastic, thermal and photoelastic parameters.

for phosphate glass [45, 46, 49, 51, 52, 463] and our calculations of P with respect to photoelastic, optical and mechanical characteristics for glass of the type 0.9 $Me(PO_3)_2$-0.1 $Al(PO_3)_3$ and for glass based on alkaline metal metaphosphates (see, for example, Table 5.3) show. Here the statistical relation between the calculated values of P and the values of $\tilde{W}$ determined experimentally, indicated in [55], is not always sustained, which can be seen from the data presented in Tables 5.3 and 5.4, but both characteristics vary symbatically. In calculating P, the greatest error is connected with measurements of the photoelastic constants C_1 and C_2, where for ordinary methods the total error reaches 15 to 20 percent. However, there are entirely sufficient data available on the correlation of the values of P and $\tilde{W}$ so that when developing phosphate glass with given thermooptical parameters initially the easily measured and calculated value of $\tilde{W}$ is used, and then a more precise definition is made of the composition after the more tedious measurements of P.

The value of Q characterizes the anisotropy occurring under the effect of mechanical stresses in the active elements. From formula (1.32) it is obvious that Q depends on the mechanical properties of the glass α_T, E and μ and on the optical stress coefficient $B = C_1 - C_2$. The laws of variation of B with phosphate glass composition were studied in a number of papers [46, 456, 463, 464, 469-477]. As is obvious from Figure 5.6 and Table 5.2, the Ba and Pb metaphosphates have the least values of B, and Zn and Y, the greatest. In the first approximation Q and B are related by the linear expression [55]: $Q = 3.75\ B$. A more detailed investigation demonstrated that for additives of certain oxides to glass of defined composition the contribution from α_T and E to the value of Q can predominate over the contribution to B, and the proportionality between B and Q in the general case is not satisfied (Figure 5.8). For example, additives of Na_2O and K_2O to the phosphate glasses lower B, but they increase Q as a result of a sharp increase in the coefficient of thermal expansion of glass. In [480], the molar contributions to Q are defined, that is, $\Delta Q/\Delta m$, where m is molecular percent of oxide, and the table is compiled which offers the possibility of calculating the values of Q and B for phosphate glass. Just as in the case of $\tilde{W}$, the calculation was made by the Demkina additiveness formula, the structural masses for calculating all of the thermooptical parameters coincide. The partial values of Q_0 and B_0 are presented in Table 5.5. They are minimal for heavy cations Cs, Tl, Ba, Pb where the values of Q_0 are negative. The values of B_0 and Q_0 can have different signs (Li, Rb, Ca, Sr, Table 5.5). The mean square deviation of the given calculations of Q_0 from the experiment is $\pm 0.3 \cdot 10^{-7}\ K^{-1}$, and $B \pm 0.1 \cdot 10^{-7}$ cm^2/kg, which almost corresponds to reproducibility of these parameters of the glass in different foundings of glass of the same composition. Let us again point out that the data in Table 5.5 are basically suitable for calculating the properties of glass based on metaphosphates of bivalent metals. For systems consisting, for example, predominantly of alkaline phosphates with additives of BPO_4 or B_2O_3 [101, 167, 462], the values of the calculation coefficients will differ significantly from those presented in Table 5.5. For example, the partial values of $\tilde{W}_0$ determined by us for alkaline phosphate glass for K_2O amount to $-420 \cdot 10^{-7}\ K^{-1}$, for Na_2O, $190 \cdot 10^{-7}\ K^{-1}$, that is, less than in Table 5.5. However, the majority of industrial optical glasses on a phosphate base contain high concentrations of bivalent oxides, and in this case, using the data in Table 5.5, it is possible to create laser phosphate

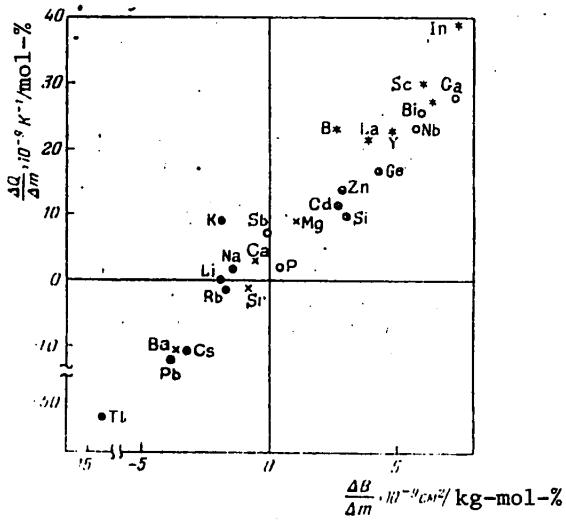

Figure 5.8. Relation between contributions to the values of B and Q per mole percent of added oxide for phosphate glass [480]. The element symbol corresponds to the oxide.

glass with values of Q close to zero. The primary component of such glass is PbO [46, 480]. Some characteristics of such glass were presented in Table 1.3. Birefringence in elements made of such glass with small Q is 3 to 4 times less than in analogous elements made of industrial phosphate glass GLS-22.

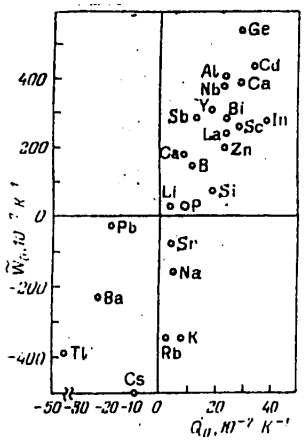

Figure 5.9. Relation between partial values of $\tilde{W}_0$ and Q_0 for oxides in phosphate glass [480]. The symbol of the element corresponds to the oxide.

For a small value of the thermooptical distortions in the active elements made of glass, closeness to zero of not only Q, but also P is needed. Glass with

small $\tilde{W}$, as a rule, has small values of P. In Figure 5.9 partial values of the thermooptical constants $\tilde{W}_0$ and Q_0 are compared [480]. This diagram, together with Table 5.5, offers the possibility of purposeful selection of the base of phosphate laser glass. Of course, when selecting, it is necessary to consider a number of other characteristics of the glass: spectral luminescence and lasing parameters, the technological properties, thermal conductivity, chemical and mechanical strength, and so on, but the condition of smallness of the thermooptical distortions is one of the most important. The primary components of phosphate glass with small thermooptical characteristics are the barium, lead, strontium, lithium, sodium, potassium, rubidium and cesium oxides. The phosphate glass with a high content of these oxides has high induced emission cross sections and small width of the luminescence and lasing bands of Nd^{3+} (Chapter 4), which makes it possible to create neodymium-doped laser glass with optimal combination of these properties for an entire series of laser systems [47, 48, 58, 59, 101, 395].

The relations studied at the present time for the thermooptical properties of phosphate glass as a function of glass composition are of a purely phenomenological nature. Unfortunately, even for simple binary crystals, the calculations, for example, of the photoelastic parameters determining the thermooptical characteristics of P and Q can be made only highly approximately [481, 482]. Efforts to explain the optical properties of crystal phosphates within the framework of the zone model in the approximation of a single-frequency oscillator [483] are known, which offers the possibility of prediction, for example, of the dispersion dependence of the photoelastic characteristics [481, 484]; work has been started in this area for certain types of glass (see, for example, [484, 487]). The thermooptical characteristics of phosphate glass within the framework of the model of a single-frequency oscillator have been investigated primarily by Kopylov [484]. Let us briefly remember the basic concepts of the model used. The dispersion equation of Zelmeer is most frequently the initial equation

$$n^2(\omega) - 1 = 4\pi s\tilde{N}/(\omega_0^2 - \omega^2).$$

Here n is the index of refraction, s is the oscillator strength, $\tilde{N}$ is the number of oscillators per unit volume, ω is the angular frequency. The dispersion of the optical properties of the material in the visible part of the spectrum depends on the position and strength of the most high-energy vibrations of the atoms in the ultraviolet region of the spectrum. In the Zelmeer model, the actual set of these vibrations is replaced by one "effective" equivalent oscillator with strength s and frequency ω_0. Wemple and Di Domenico have successfully used the zone model [481, 483, 485, 486] and a modified Zelmeer equation

$$n^2(\omega) - 1 = F/E_0^2 - (\hbar\omega)^2,$$

to describe a series of optical properties of solid states, where F is the strength of the interzone transitions, E_0 is their energy, $\hbar = h/2\pi$, h is the Planck constant.

The high-energy transitions which basically determine E_0 and F are related to the oxygen atom concentrations in oxygen-containing compounds. In this case the number of oscillators is identical with the number of oxygen atoms per unit volume. In [481, 483-486] it was demonstrated that it is expedient to use another value--the dispersion energy $E_d = F/E_0$--which for nonmagnetic nonmetals determines the dispersion of the electron part of the dielectric constant of the material. It turned out that for the majority of crystals and glass [481, 483-486], E_d is related simply to the structural characteristics of the material, namely to the coordination number N_c of the cation having the greatest bond strength with the anion, the anion valence Z_a and the number N_e of valence electrons on the anion: $E_d = \beta N_c Z_a N_e$. Here β is a constant which depends on the type of bond in the material and is equal to (0.26 ± 0.04) eV for ionic materials (halides and oxygen-containing compounds) and (0.39 + 0.04) eV for covalent materials. Measuring the dispersion of the index of refraction, it is possible to find F and E_0 and then calculate E_d and β. For phosphate glass based on univalent and bivalent cations the value of β turned out to be (0.27 ± 0.02) eV, which corresponds predominantly to the ionic bond in the Wemple-Di Domenico model.

The thermooptical and opticoelastic parameters of materials can be obtained [481, 484], differentiating the Zelmeer equation with respect to temperature and pressure. We shall present the corresponding formulas in the form used in [484]:

$$\frac{n(\lambda)B}{(n^2(\lambda)-1)^2} = -\frac{D_a}{E_d}\left[1 + k^{\eta}\left(1-\frac{\lambda_0^2}{\lambda^2}\right)\right],$$
$$\frac{n(\lambda)\frac{dn}{dT}}{(n^2(\lambda)-1)^2} = -\frac{z}{E_d}\left[1 + k^{T}\left(1-\frac{\lambda_0^2}{\lambda^2}\right)\right]. \qquad (5.4)$$

Here D_a is the potential of the deformation optical anisotropy characterizing the variation of the energy of the interzonal transitions for the uniaxial stress η, $D_a = \Delta E_0^{\eta}/\eta$; the value of $z = \Delta E_0^{T}/\Delta T$ characterizes the variation of the energy of the interzonal transitions with temperature, B is the optical stress coefficient. The values of k^{η} and k^{T} indicate variation of the oscillator strength on variation of its energy: $k^{\eta,T} \infty \left(\frac{\Delta F_0}{F_0}\right)^{\eta,T} \Big/ \left(\frac{\Delta E_0}{E_0}\right)^{\eta,T}$. The values of D_a, z, k^{η}, k^{T} are presented in Table 5.6 for glass with the composition 0.9 $Me(PO_3)_2$-0.1 $Al(PO_3)_3$ [484]. Values of B and dn/dT are presented there. The temperature is indicated for which k^{T}, dn/dT and z were calculated. For these types of glass $D_a < 0$, $\Delta F > 0$, that is, the oscillator strength increases, and its frequency decreases under the effect of uniaxial stress. The values of D_a and ΔF vary monotonically with B, which is connected with almost identical parameter k^{η} varying from -0.89 to -0.96 for these types of glass. For glass based on the metaphosphates of alkaline metals (Table 5.3), the values of k^{η} are small, that is, the oscillator strength varies little, and its energy varies approximately identically for all of the investigated alkaline glass. As a result, the values of B vary little--approximately from $1.5 \cdot 10^{-7}$ to $2 \cdot 10^{-7}$ cm^2/kg.

Table 5.6

Glass No	Basic Cation	D_a, 10^{-4} eV·см^2·kg^{-1})	k^n	B, 10^{-7} см^2/kg
1	Mg	—0,57	—0,90	2,02
2	Ca	—0,35	—0,91	1,78
3	Sr	—0,24	—0,82	1,37
4	Ba	—0,17	—0,96	0,59
5	Zn	—0,82	—0,92	3,66
6	Cd	—0,32	—0,89	2,52
7	Pb	—0,053	—0,90	0,42

Glass No	Basic Cation	ΔF, 10^{-4} eV^2·см^2·kg^{-1}	z, 10^{-4} eV/K	k^T	dn/dT, 10^{-7} K^{-1}	T, °C
1	Mg	21,5	—4,1	—0,94	44	124
2	Ca	12,7	3,4	—1,02	—11	126
3	Sr	7,4	4,5	—1,2	—42	94
4	Ba	6,2	5,3	—1,19	—82	122
5	Zn	25,7	0,8	—1,9	54	81
6	Cd	10,3	—4,7	—0,9	37	125
7	Pb	1,7	5,5	—1,1	—72	148

The sign of the parameter z for the majority of types of glass (except glass with Zn) does not coincide with the sign of the derivative dn/dT; their values vary symbatically. Here the proportionality is violated as a result of the variable value of k^T which varies by more than twofold in the metaphosphate glass series. When $z > 0$, the temperature increase leads to an increase in energy of the equivalent oscillator E_0, n decreases with temperature; for $z < 0$ the picture is the reverse.

Although the model of the single-frequency oscillator is also phenomenological, the parameters in it have an obvious physical meaning, and the formulas obtained with its help describe not only the variation of the optical properties with temperature and pressure well, but also the dispersion of these properties (formulas (5.4)). This approach supplements the one used earlier in the Ramachandran model [465, 466], and it also permits standardization of the description of thermooptical properties of crystals and glass.

§5.2. Phosphate Glass for Pulse-Periodic Lasers

Pulse-periodic lasers based on glass, primarily activated by Nd^{3+} ions, are finding broad application in various areas of technology. The parameters of these lasers vary within broad limits: the lasing energy varies from hundredths of a joule to tens of joules, the periodicity of the effect varies from fractions of a hertz to approximately 100 hertz, the emission power in the Q-switching mode varies from hundreds of kilowatts to hundreds of megawatts. The survey information about industrial periodic glass lasers can be found in [48, 119, 488], and information about the laser glass for them, in [47, 48, 119, 489, 490]. As a result of the wide range of variation of the spectral-luminescent and thermooptical properties of phosphate glass, they offer the possibility of detailed investigation of various lasing modes and

establishment of the physical principles of the optimal selection of the glass for application in various pulse-periodic laser systems.

In the given section, using the general concepts discussed in §§1.1, 1.4 and 1.5, let us specify the requirements for the active elements of pulse-periodic lasers using glass with Nd^{3+}. Inasmuch usually an effort is made to increase the average power of such lasers with given size of the active elements, the lasers operate in the mode with large heat release and, correspondingly, with high temperature gradient in the active element, which leads to powerful thermooptical distortions. We shall discuss these distortions in more detail on the basis of the results presented in §1.4. Let us consider the dependence of the energy characteristics of the lasers on the properties of the material of the active elements, and let us compare the parameters of the pulse-periodic lasers based on phosphate and silicate glass. Here we shall not consider the technical peculiarities of the structural design of such lasers, for we are interested primarily in the requirements on the material.

In §1.5 it was demonstrated that in order to improve the thermal conditions in pulse-periodic lasers it is expedient to use long and thin active elements made of glass having high thermal conductivity λ_h. Increasing the length of the active elements also leads to an increase in the gain and a decrease in the threshold pumping energy [491, 492]. The thermal conductivity of laser glass is approximately 0.4-2 watts/(meter-K) [47, 48, 490, 493, 494]. Among the silicate glass, lithiumcalciumsilicate ED-2 glass has the greatest thermal conductivity (about 1.2 watts/(meter-K)). The data on the thermal conductivity of phosphate glass are limited. Glass similar in composition to aluminum metaphosphate (Figure 5.10) has the largest values of λ_h (about 1.2 watts/(meter-K)), and potassium glass [111, 494, 495] has the least values ($\approx$0.3 watts/(meter-K)). Figure 5.11 shows the thermal conductivity of vitreous metaphosphates as a function of the ion potential Ze/R of the cation modifier [495]. The thermal conductivity increases with an increase in the ion potential of the cation. However, as was demonstrated in the preceding item, the values of the thermooptical characteristics of P and $\tilde{W}$ increase simultaneously, and the luminescence and lasing bands are broadened. The induced emission cross section of Nd^{3+} decreases (Chapter 4), and consequently the threshold pumping energy increases. Therefore when selecting the glass composition for active elements it is necessary to consider immediately the set of properties of the glass and the solution depends on the requirements on the output parameters, overall dimensions and pumping energy of the laser. In particular, the requirement of low energy threshold of lasing and high efficiency of the laser is usually the most important. For small threshold energy of pumping $\mathscr{W}_{threshold}$, the efficiency increases with the same values of the pumping energy $\mathscr{W}_{pump}$ in the pulse as a result of growth of the ratio $\mathscr{W}_{pump}/\mathscr{W}_{threshold}$.

The value of $\mathscr{W}_{threshold}$ decreases with an increase in the induced emission cross section and with an increase in the Nd^{3+} ion concentration; the laser efficiency also increases simultaneously. In Figure 5.12, we have the values of $\mathscr{W}_{threshold}$ (normalized for $\mathscr{W}_{threshold}$ at $\mathscr{N}_{Nd_2O_3}$ = 2 percent by weight) and the output energy $\mathscr{W}_{lase}$ (normalized for $\mathscr{W}_{lase}$ at $\mathscr{N}_{Nd_2O_3}$ = 6 percent by weight) as a function of the Nd_2O_3 concentration in silicate glass [496] for

cylindrical active elements 5 mm in diameter by 80 mm. The analogous picture occurs also for phosphate glass. With a diameter of the active elements of 6 to 8 mm, the optimal concentration of the Nd^{3+} ions is (3-4) $\cdot 10^{20}$ cm^{-3}; for a diameter of 3 to 5 mm it is (5-8) $\cdot 10^{20}$ cm^{-3}. In [497], for example, lasing on a frequency to 100 hertz was obtained using Li-Nd-La-phosphate glass with a concentration of Nd^{3+} 5.8 $\cdot 10^{20}$ cm^{-3}. Here a lasing power of 6.5 watts was obtained on an active element 5 mm in diameter by 50 mm with a pumping power of 1 kilowatt and pulse repetition frequency of 10 hertz. In this case the energy efficiency is low inasmuch as the dimensions of the active element, the illuminator and pumping tube do not match. For a laser with active element made of silicate glass 8 mm in diameter by 80 mm at a concentration of Nd_2O_3 of 6 percent by weight, an average free running power of 7 to 8 watts is obtained at a frequency of 7 hertz, a pumping power of 420 watts and efficiency of 1.8 percent and 7.5 watts at a frequency of 37 hertz and efficiency of 2.5 percent [492]. However, silicate glass providing such characteristics is not "athermal," and the divergence of the emission reaches 40-50'.

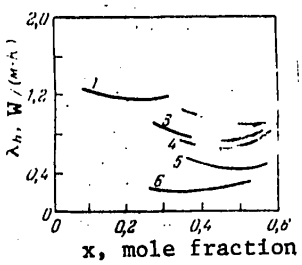

Figure 5.10. Thermal conductivity λ_h as a function of x for phosphate glass with the composition xMe_mO_n x $(1 - x)P_2O_5$ (where x is the mole fraction of the metal oxide) [495]. Me: 1--Al, 2--Mg, 3--Ca, 4--Ba, 5--Li, 6--K.

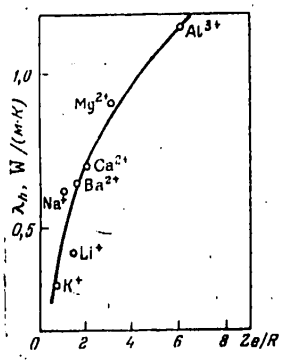

Figure 5.11. Thermal conductivity λ_h of vitreous metaphosphates as a function of the ion potential of the cation Ze/R [495].

The presence of a positive thermal lens in the active element of pulse-periodic lasers with moderate pumping powers improves the energy

characteristics of the laser. In a resonator of length l with lens introduced inside it with a focal length f, the diffraction losses are proportional to (1 - 1/2f) [492]. For small pumping powers f is large and the losses are significant. With a decrease in f with an increase in pumping power for glass with P > Q, the diffraction losses decrease, $W_{threshold}$ decreases, and the efficiency increases. For example, for the above-mentioned active elements 8 mm in diameter by 80 mm made of silicate glass with Nd_2O_3 content of 6 percent by weight $W_{threshold}$ decreases from 25 joules per pulse for the single pulse mode to 9-10 joules approximately every 8 seconds after the beginning of operation in the pulse-periodic mode with a frequency of 10 hertz (the thermal relaxation time of the active element in this case is less than 15 seconds). Therefore if the requirements on the radiation divergence are not very significant, it is preferable to use such glass.

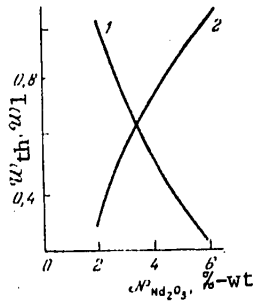

Figure 5.12. Threshold lasing energy (1) and lasing output power (2) as a function of the Nd_2O_3 concentration in silicate glass for an active element 5 mm in diameter by 80 mm [496].

Laser phosphate glass with large values of σ and optimal Nd_2O_3 concentration permit us to obtain low thresholds and high lasing efficiency. In Figures 5.13, 5.14, relations are presented for the lasing energy for single and repeated pulses in the free lasing mode and for Q-switching by a rotating prism (16,000 rpm) [81]. (The size of the active elements is 6.3 mm in diameter by 76 mm, the glass is Q-88* (strengthened version), 4.3 percent by weight Nd_2O_3, resonator length 20 cm for free lasing and 30 cm for giant pulse mode, silvered illuminator, water cooling.)

In the free running mode with single pulses and small repetition frequency (small average pumping power) the output energy of lasing, as shown by Figure 5.13, a and b, depends linearly on the pumping energy. The efficiency calculated by the slope of the curve is 4.5 percent for single pulses, 3 percent for a frequency of 1 hertz; the energy efficiency is equal to 3.5 and 2 percent, respectively. The lasing threshold for the periodic mode in the given case is almost half that for the single pulses. With Q-switching in the single pulse mode, the efficiency is 1.43 percent (mirror with 65-percent reflection, pumping energy 15.8 joules, emission energy 0.22 joules, Figure 5.13c). Q-88* glass is not "athermal," the magnitude of $\tilde{W}$ which we calculated according to the data of [493] is approximately $50 \cdot 10^{-7}$ K^{-1} for it. Therefore with an increase in the average pumping power, the divergence of the emission

θ increases, the output power decreases (when the diffraction losses become less than the losses to inactive absorption, and the effects of birefringence become important [50, 498]), for the Q-switching mode, the lasing pulse duration t_{lase} increases. The lasing energy drop per pulse is also observed for the above-mentioned active elements made of "athermal" Li-Nd-La-phosphate glass, where the average pumping power exceeds 0.3 kilowatt for the active elements and illuminators used in [497, 499] (Figure 5.15).

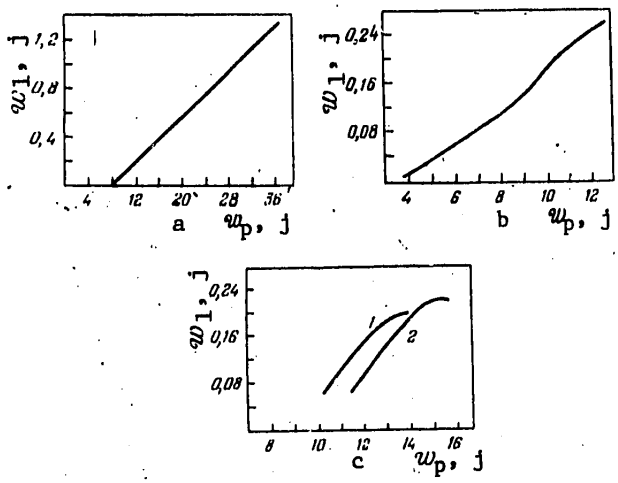

Figure 5.13. Lasing energy as a function of the pumping energy for an active element 6.3 mm in diameter by 76 mm made of Q-88* glass [81]. a) Single pulse mode; b) frequency 1 hertz, free lasing mode; c) single pulse mode, Q-switching, reflection coefficient of the output mirror 75 percent (1) and 65 percent (2).

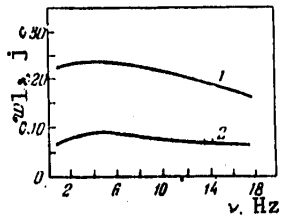

Figure 5.14. Lasing energy as a function of the pulse repetition frequency for an active element 6.3 mm in diameter by 76 mm made of Q-88* glass at a pumping power of 11 joules per pulse in the free lasing mode (1) and in the Q-switching mode (2) [81].

The values of t_{lase} and θ for active elements made of Q-88* glass with a pumping power of 11 joules per pulse and an increase in the pulse repetition frequency are as follows, respectively [81]: 25 nanoseconds and 8' (single pulses), 30 nanoseconds and 11' (1 hertz), 45 nanoseconds and 15' (5 hertz), 55 nanoseconds and 18' (10 hertz), 70 nanoseconds and 21' (15 hertz). The

lasing energy per pulse at ν = 15 hertz is about 0.07 joule (Figure 5.14). Thus, with an increase in the average pumping power as a result of growth of the pulse repetition frequency the lasing power in the giant pulse mode increases from 0.07 to 1.05 watts, the divergence increases by twofold, and the pulse duration by almost 2.5 times. The radiation energy flux density in each pulse decreases correspondingly by several times. The maximum efficiency for a laser with active element of the indicated size made of Q-88* glass with Q-switching is achieved for a frequency of 5 hertz, and it amounts to about 0.9 percent. The lasing energy in one pulse in the free lasing mode also passes through a peak at 5 hertz, the efficiency reaches 2.2 percent, the output power is 1.2 watts. For 15 hertz the free running power is about 2.9 watts at an efficiency of about 1.6 percent. Let us note that it is not the absolute values of the efficiency that depend on the optical quality and the machining of the active elements, the values of the inactive power in the glass and in the resonator or the pumping conditions and other factors that are significant, but the variation of the efficiency, energy and divergence of the emission with an increase in the average pumping power and lasing power (§1.5).

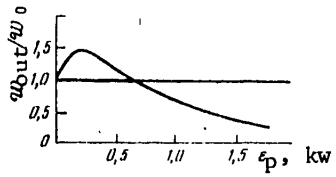

Figure 5.15. Output laser power (per pulse of emission) as a function of the average pumping power ε_{pump} [497]. Normalization by the lasing power W_0 in the single pulse mode.

When using "athermal" phosphate glass with low values of P ± Q/2 (for a cylindrical active element) in pulse-periodic lasers, the divergence of the emission decreases, and an increase in the average lasing power, especially in the giant pulse mode becomes possible. For "athermal" glass, some data were presented in §1.4, and shown in Figures 1.3-1.8. Let us consider in more detail the optical strength of the thermal lenses and lasing parameters for such glass under the conditions of a large temperature gradient between the axis of the active element and its edge [60]. Here the initial expression is expression (1.41). The thermal lens formed for large temperature gradients ΔT is nonideal, in contrast to the lenses with small gradients ((1.37), (1.38)). Actually, from expression (1.41) and the formula for the focal power

$$\frac{1}{f} = \frac{2\Delta p}{R^2}, \tag{5.5}$$

where Δp is the difference in optical paths between the axis and the edge of the lens, it follows that the thermal lens in an active element with focal power of $1/f$ can be represented as the sum of two lenses with focal powers of $1/f_1$ and $1/f_2$, where

$$\frac{1}{f_1} = 2\Delta T \frac{L}{R^2}\left(P_0 \pm \frac{Q_0}{2} + 0T\right), \tag{5.6}$$

$$\frac{1}{f_2} = 2(\Delta T)^2 \frac{L}{R^2} 0(2 - \xi^2). \tag{5.7}$$

The lens defined by expression (5.6) is a spherical lens, its sign and focal power depend on the thermooptical characteristics of the glass, the temperature gradient in the active element and emission polarization, and they do not vary with respect to cross section of the active elements. The lens defined by (5.7) is aspherical, always positive, its power does not depend on polarization and varies with variation of ξ; therefore the compensation of the distortions (closeness to zero of the focal power of the total thermal lens) is possible only for negative spherical lenses (5.6) and only in a sufficiently narrow ring zone with respect to the cross section of the active element. The temperatures T_1 and T_2 for which the focal power of the total thermal lens vanishes at the edge and on the axis of the active elements, are equal respectively [60] to

$$\begin{aligned} T_{1(r,\varphi)} &= -\Delta T - (P_0 \pm Q_0/2)/\theta, \\ T_{2(r,\varphi)} &= -2\Delta T - (P_0 \pm Q_0/2)/\theta. \end{aligned} \tag{5.8}$$

The resonator with negative lens introduced into it is unstable, and therefore it is expedient that the total thermal lens be positive with respect to the entire cross section of the active element, at least for r-polarization. Then T_1 defines the minimum temperature, for which the given glass can operate efficiently for the given value of ΔT determined by the pumping power. As follows from formula (5.8), T_1 is in the room temperature range only for $(P_0 \pm Q_0/2) < 0$. Expression (5.8) differs from the one used earlier in [52] (formula (1.44)) by considering the temperature gradient in the active element, which turns out to be highly significant for high average lasing power, when it can exceed 80 to 100 K [57-59].

As is obvious from formulas (5.5), (5.6), the focal power of a thermal lens in the active element depends on the temperature. Figure 5.16 shows the temperature dependence of the focal power of the thermal lens formed near the axis of a cylindrical active element for "athermal" phosphate glass GLS-22, LGS-I and LGS-M (r- and ϕ-polarizations) [60]; in Figure 5.17 we see the average free-running output power as a function of the pulse repetition frequency for a pumping energy per pulse of 100 joules.

The temperature gradients between the edge and the axis of the active elements are about 40 and 80 K for LGS-I and LGS-M glass with a pumping power of 250 and 500 watts, respectively. The measurement conditions were discussed in §§4.9 and 4.10, the surface temperature of the active elements was varied by means of the cooling liquid. With an increase in the pumping power $\mathscr{W}_{\text{lase}}$ increases linearly. In the free lasing mode the lasing power reached 10 watts with a pumping power of 700 watts. During Q-switching of the resonator using an opticomechanical shutter (rotation rate 21,500 to 43,000 rpm), the lasing energy on the active elements made of LGS-I glass obtained under optimal conditions was 0.6 joule with a pumping power of 40 joules and pulse repetition frequency of 10 hertz. The magnitude of the angular divergence with respect

to the 0,8 level of total power is 22' [59]. The "athermal" glass thus ensures higher radiation brightness than glass with large thermooptical constants.

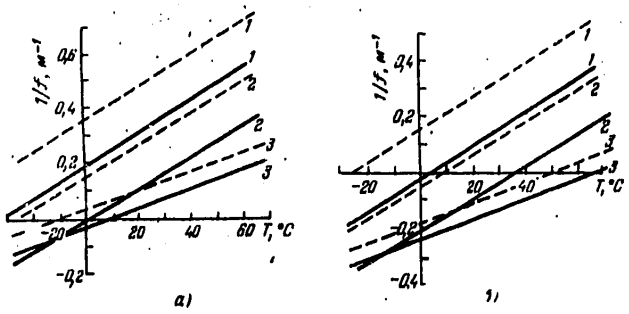

Figure 5.16. Temperature dependence of the focal power of thermal lenses for a temperature gradient of 30° C in active elements 8 mm in diameter and 200 mm long on a wavelength of the sounding pulse of 0.63 micron. a) r-polarization; b) ϕ-polarization. (r/R) = 0.5 (dotted lines), (r/R) = 0.82 (solid lines). The glass LGS-I (1), GLS-22 (2), LGS-M (3) [60].

The variation of the lasing energy with temperature depends on the temperature behavior of the focal power of the thermal lens that is formed. Since P decreases with temperature, the thermal lens with low focal power for "athermal" glass at room temperature can become negative at low temperatures, especially for ϕ-polarization (Figure 5.16). Here the magnitude of the temperature derivative of $\theta = dP/dT$ is significant: the smaller it is, the more slowly the focal power of the thermal lens varies. For LGS-M glass ($\theta = 0.09 \cdot 10^{-7}$ K^{-2}) the lasing power at negative temperatures decreases (by comparison with the lasing power at room temperature) appreciably more slowly than for GLS-22 glass ($\theta = 0.14 \cdot 10^{-7}$ K^{-2}) (Figure 5.18). This agrees with the temperature behavior of the focal power of thermal lenses in active elements (Figure 5.16). For negative lenses part of the beams leave the active element, the Q-factor of the resonator becomes worse, the resonator becomes unstable, the lasing efficiency decreases, and with high power of the negative lens the lasing stops. Accordingly, "athermal" glass, as has already been noted in §1.4, cannot operate efficiently in the pulse-periodic mode at temperatures appreciably below optimal [52], for which the combinations of thermooptical characteristics defining the optical difference in path for the ϕ-polarization vanish.

The above-presented arguments pertain to a fixed temperature gradient in the active elements. However, the focal power of the negative lens as a function of the temperature gradient in the active element is not monotonic under certain conditions. This is easily established from formula (1.41) for a cylindrical active element. Differentiating it with respect to ΔT and equating the obtained derivative to zero, let us define the value of the temperature gradient ΔT_{cr} for two polarizations of light:

$$\Delta T_{cr} = -\frac{P_0 \pm Q_0/2 + \theta T'}{20\,(2-\xi^2)}, \tag{5.9}$$

on exceeding of which instead of a further increase in focal power of the negative lens with an increase in ΔT, it begins to decrease, and then the lens becomes positive. Thus, the value of ΔT_{cr} corresponds to the minimum as a function of the focal power induced in the active element of the thermal lens as a function of the temperature gradient. Here expression (5.9) is meaningful only when the numerator is negative (or equal to zero), for the values of θ and ΔT_{cr} are positive, and $\xi \leq 1$ (§1.4).

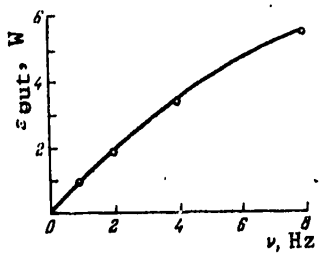

Figure 5.17. Average output power of free lasing as a function of pulse repetition frequency for a pumping power per pulse of 100 joules for LGS-I glass with active element 8 mm in diameter by 100 mm [59].

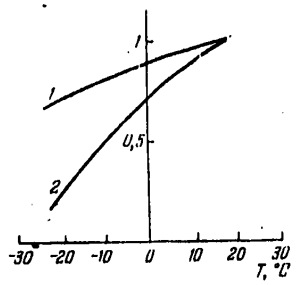

Figure 5.18. Lasing power as a function of the coolant temperature [60]. Pulse repetition frequency 10 hertz, active element 8 mm in diameter by 100 mm; LGS-M glass (1), GLS-22 glass (22). The ratio $W_{lase}/W_{lase,\ room}$ is plotted on the y-axis.

For the given glass the temperature gradient in the active elements is proportional to the pumping energy power. For example, for cylindrical active elements 8 mm in diameter by 10 mm made of LGS-I-3 glass in a highly efficient illuminator the temperature gradient increases by 16° C with an increase in pumping power by 100 watts [58, 59]. The focal power of the thermal lens changes correspondingly.

Let us consider an example of phosphate glass LGS-I and LGS-M, the thermooptical parameters of which were presented in Table 1.3. Table 5.7 shows the values of the combinations of thermooptical characteristics entering into formula (5.9) and the values of ΔT_{cr} for the temperatures of the side surface of the active element of 20 and -60° C, and Figure 5.19 shows the dependence on ΔT of the focal power of the total thermal lens in the active elements made of this glass for two polarizations and two values of ξ at T = 0° C. As we shall see, the smaller the initial values of the sums $(P_0 \pm Q_0/2 + \theta T)$, the greater the temperature gradient in the active element needed for variation of the course of the dependence of the focal power of the thermal lens on ΔT. Here the active element operates stably under two conditions--at $\Delta T \approx 0$ (rare pulse conditions) and at ΔT exceeding ΔT_0 corresponding to the intersection point with the x-axis of the curve $1/f(\Delta T)$, for r-polarization and $\xi = 0$ (curve 1 in Figure 5.19). In the region between $\Delta T = 0$ and $\Delta T = \Delta T_0$, where the negative lens under steady-state conditions occupies the entire cross section of the active element, the lasing power decreases, and the divergence increases [56]. In real active elements under transition conditions and on deviations from parabolic dependence of the temperature on the radius of the active element (the data in Table 5.7 and in Figure 5.19 are calculated under the assumption of parabolic dependence), the pattern of the variation of the thermooptical distortions with temperature gradient differs somewhat from idealized, but the general diagram of the variations is maintained. These arguments must be considered when selecting glass for pulse-periodic lasers with high average power, where phosphate glass turns out to be optimal. Under such conditions the active elements made of glass with a value of $(P_0 + Q_0/2 + \theta T)$ which for the given temperature gradient ensures a small positive lens for r-polarization near the axis of the active elements, give the least angular divergence of the emission, and in the Q-switching mode, the opticomechanical shutters ensure the shortest duration and high stability of the lasing pulse.

Table 5.7

			LGS-I		LGS-M	
			T=20 °C	T=−60 °C	T=20 °C	T=−60 °C
$(P_0+Q_0/2+\theta T)$, 10^{-7} K^{-1}			1,15	−10,05	−1,3	−8,4
$(P_0-Q_0/2+\theta T)$ 10^{-7} K^{-1}			−3,55	−14,75	−7,1	−14,3
ΔT_{cr}	r-pol.	ξ=0	−2,0	−18,0	−3,5	23
		ξ=1	−4,0	36	7	46
	φ-pol.	ξ=0	6,3	26,3	20	40
		ξ=1	12,6	52,5	40	80

Note: Negative values of ΔT_{cr} indicate that the thermal lens is always positive.

An important factor limiting the output power of such lasers is the limiting temperature gradient sustained by the active element without rupture.

Therefore the methods of improving the thermal strength investigated in §1.5 and used recently for "athermal" laser phosphate glass [58, 59, 70] have important practical significance. For certain types of technological lasers, the choice of phosphate glass with small values of the coefficient of thermal expansion (less than $100 \cdot 10^{-7}$ K^{-1}) and increased thermal conductivity makes it possible to increase the maximum temperature gradient in the active element [497, 499] and it ensures an increase in the output lasing power (with simultaneous increase in radiation divergence).

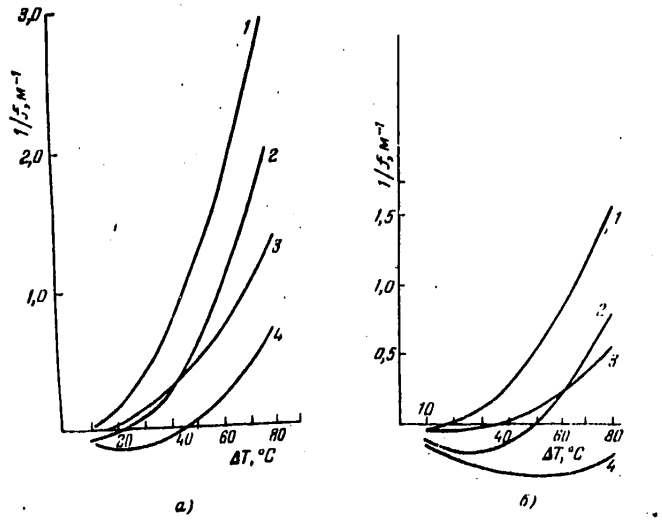

Figure 5.19. Focal power of a thermal lens as a function of the temperature gradient ΔT between the edge and the axis of the active element made of LGS-I glass (a) and LGS-M glass (b) for T = 0° C. 1, 3--r-polarization; 2, 4--ϕ-polarization; 1, 2--ξ = 0; 3, 4--ξ = 1.

Tables 5.8 and 5.9 show the parameters of pulse-periodic lasers using silicate and phosphate glass. The table data are not exhaustive and serve only to indicate the possibilities of active elements made of glass and approximate comparison of glass of various types, for the laser parameters depend on an entire series of factors. At the same time, from the tables it is obvious that phosphate glass ensures higher lasing power and efficiency and less angular divergence of the emission for active elements of similar size. According to the estimates of [500], the use of active elements made of phosphate glass in production lasers permits achievement of lasing efficiency which is 1.5 times greater than for silicate glass, 1.5 times less radiation divergence and twice the pulse repetition frequency. In reality, for "athermal" phosphate glass the gain in energy and divergence is even more. Here the lasing efficiency for "athermal" glass (type LGS-I, LGS-M, GLS-22, and so on) remains high for high average pumping power.

Table 5.8

Марка или тип стекла (1)	Режим генерации (2)	Тип АЭ (3)	Размер АЭ, мм (4)	Частота повторения импульсов, Гц (5)	Энергия накачки в 1 импульсе, Дж (6)	Энергия генерации, Дж (7)	К.п.д., % (8)	Угловая расходимость*), мин. (9)	Источник данных (10)
Ba – B-силикатное (12)	Свободный (15)	Цилиндр. (17)	Ø2×50	30	4	0,001	0,025		[501]
ГЛС-1	»	»	Ø6×130	25	100	0,15	0,15	(18)	[50]
				5	100	0,3	0,3		[50]
(12) Силикатное	»	Пластинч. (11)	2×6×76	85	19	0,07	0,4	верт. 7, гор. 28	[71]
»	Моноимпульсный (16)	»	8×20×175	1	490	1,0	0.2	—	[502]
ГД-2S	»	Цилиндр.	Ø6,3×77	10	23	0,1	0,4	34	[119]
(12) Силикатное	Свободный (15)	» (17)	Ø8×80	7	60	1,1	1,8	60	
»	»	»	Ø10×80	3	100	2,5	2,5	—	
»	»	»	Ø6×12	20	125	0,5	0,4		
»	Моноимпульсный (16)	»	Ø5×80	10	100	0,1	0,1		[492]
»	»	»	Ø10×80	3	125	1,0	0,8		
»	»	»	Ø6×120	10	200	1,0	0,5		
КГСС-7 (13)	Свободный (15)	»	Ø8×80	1	600	2,5	0,45	12	[57]
ЛГС-28-2 (14)	»	»	Ø7×130	1	980	6,3	0,65	—	[503]
ЛГС-24	»	»	Ø7×130	2	140	1,6	1,1	—	
ЛГС-24	Моноимпульсный (16)	»	Ø7×130	2	140	1,0	0,7	—	[504]

*) The divergences are presented in the vertical and horizontal planes for a plate element.

Key:
(1) Type of glass
(2) Lasing mode
(3) Type of active element
(4) Size of active element, mm
(5) Pulse repetition frequency, hertz
(6) Pumping energy per pulse, joules
(7) lasing energy, joules
(8) Efficiency, %
(9) Angular divergence*, minutes
(10) References
(11) Plate
(12) Silicate
(13) KGSS-7
(14) LGS-...
(15) Free
(16) Giant pulse
(17) Cylindrical
(18) Vertical 7, horizontal 28

Table 5.9

Марка или тип стекла (1)	Режим генерации (2)	Тип АЭ (3)	Размер АЭ, мм (4)	Частота повторения импульсов, Гц (5)	Энергия накачки в 1 импульсе, Дж (6)	Энергия генерации, Дж (7)	К.п.д., % (8)	Угловая расходимость *), мин. (9)	Источник данных (10)
(11)ГЛС-22	Моноимпульсный (14)	Пластинч. (16)	4×24×145	2	500	1,1	0,22	14(0.5)	[505]
ГЛС-22	»	»	4×24×145	5	500	0,75	0,15	—	
ГЛС-22	Свободный	Цилиндр.	Ø10×130	5	150	1,5	1,0	--	[76]
(12)ЛГС-И	» (15)	(17)	Ø8×100	10	70	1,0	1,4	—	[58, 59]
ЛГС-И	Моноимпульсный (14)	»	Ø8×100	10	40	0,6	1,5	22(0.9)	
Q-88*	Свободный	»	Ø6,3×76	5	11	0,24	2.2	14	
Q-88*	» (15)	»	Ø6,3×76	15	11	0,18	1.6	21	[81]
Q-88*	Моноимпульсный (14)	»	Ø6,3×76	5	11	0,09	0,8	14	
Q-88* (13)	»	»	Ø6,3×76	15	11	0,065	0.6	21	
Li-Nd-УФ	Свободный (15)	»	Ø5×50	10	100	0,65	0,65	--	[497]
Li-Nd-УФ	»	»	Ø5×50	1	32	0.45	1.40	--	[499]
Li-Nd-УФ	Моноимпульсный (14)	»	Ø5×50	1	32	0,15	0,47	—	

*) The proportion of the lasing energy in the given solid angle is indicated in parentheses

Key: (1) Type of glass
(2) Lasing mode
(3) Type of active element
(4) Size of active element, mm
(5) Pulse repetition frequency, hertz
(6) Pumping energy per pulse, joules
(7) Lasing energy, joules
(8) Efficiency, %
(9) Angular divergence*, minutes
(10) References
(11) GLS-...
(12) LGS-I
(13) Li-Nd-UF
(14) Giant pulse
(15) Free
(16) Plate
(17) Cylindrical

The possibility of obtaining short pulses investigated in Chapter 4 (pulses on the order of 10^{-10} to 10^{-11} seconds in duration) in phosphate glass can also be realized in the pulse-periodic mode. In [506], high power up to 0.5 gigawatt with a pulse duration of about 5 to 100 picoseconds and a pulse repetition frequency to 12 hertz was obtained on "athermal" phosphate glass LHG-7.

The most rigid requirements are imposed on active elements during operation of the laser in the continuous mode. As a result of large temperature gradients in this case it is necessary to make maximum improvement of the cooling conditions, which is achieved with small transverse cross section of the active elements. For effective absorption of light in the case of transverse pumping, high activator concentration is necessary. In this version the threshold pumping power $\varepsilon_{threshold}$ using the narrow-band radiation source with continuous mode is equal to [229]

$$\varepsilon_{th} \approx \frac{hc}{\lambda_p} \frac{(\Gamma_0 + \Gamma_p) \cdot 10^{-7}}{2\tau_1 L N \sigma k_\pi}, \qquad (5.10)$$

where Γ_0 and Γ_p are the nonresonance and resonance losses in the resonator, respectively, for a double pass, h is the Planck constant, c is the speed of light, λ_{pump} is the pumping wavelength, τ_1 is the luminescence lifetime of Nd^{3+}, N is the relative population of the upper half-level $^4F_{3/2}$, k_{pump} is the absorption coefficient in the pumping band, L is the length of the active element. The resonance losses $\Gamma_p = 2L\sigma\mathcal{N}\beta_1/Z$, where $\mathcal{N}$ is the activator concentration, β_1 is the Boltzmann factor for the lower laser level, Z is the distribution function. For glass with a concentration of Nd^{3+} on the order of 10^{21} cm^{-3} the resonance losses are significant, and they amount to several thousand cm^{-1} [48, 229, 232].

The product $\tau_1\sigma k_{pump}$ which enters into formula (5.10) and must be maximal depends to the highest degree on the composition. Since for small active elements k_{pump} must be large, glass is required which has long luminescence lifetimes of Nd^{3+} with concentrations to (2-4) $\cdot$ 10^{21} cm^{-3} and large induced emission cross section and, correspondingly, high quantum yield of luminescence. The magnitude of the quantum yield which depends weakly on the glass matrix in the dehydrated phosphate glass for a concentration of Nd^{3+} (4-6) $\cdot$ 10^{20} cm^{-3} (only if there is no inclination of the glass toward microstratification characteristic, for example, of zinc phosphate or boron phosphate glass) varies sharply with the glass composition at high Nd_2O_3 contents. It was demonstrated in Chapters 2-4 that the least luminescence quenching is observed in ultraphosphate and metaphosphate glass with approximately identical content of the oxides of univalent and trivalent metals under the condition of careful dehydration of the glass. Stronger quenching occurs in glass containing bivalent cations. When selecting the base of the glass for continuous microlasers, it is necessary to consider also the technological, thermooptical and physicochemical properties of glass. Absorption coefficients on a wavelength of 0.8 micron for phosphate glass reach approximately 70 cm^{-1} with Nd^{3+} concentration of (3.8-4) $\cdot$ 10^{21} cm^{-3}, and the maximum luminescence lifetime for such activator concentrations in the case of complete dehydration of the glass is 40 to 60 microseconds. Calculation shows [229] that for pumping by the emission of semiconductor light diodes the active elements of optimal size made of

phosphate glass with specially selected activator concentration and small inactive absorption can have lasing thresholds in the continuous mode which are comparable to lasing thresholds for YAG: Nd^{3+} crystals. The lasing on phosphate glass in the continuous mode is realized only for longitudinal pumping of the active elements by the emission of an argon laser [229].

§5.3. Glass for High-Energy Laser Systems

When studying the propagation laws of coherent radiation in the atmosphere, for experiments on the interaction of emission with the material and obtaining a thermonuclear plasma, lasers with an energy of more than 10^3 joules per pulse are required. Naturally, the divergence of the emission must be quite small, and the energy density in the laser beam the maximum possible. Since the ILN radiation energy flux density in the range of 0.3 micron to 1,000 nm is about 0.2 megavolt/cm^2, and in the best case 10 percent of the pumping energy or under giant pulse conditions 1 percent, is converted to induced emission under free lasing conditions, in order to obtain the indicated energy multitube, multistage laser systems are used with large total ILN surface and active elements, respectively. In these lasers the total number of ILN exceeds 10^2 to 10^3, and the total length of the active elements reaches several meters.

Let us consider the basic requirements imposed on the physical parameters of laser glass used in active elements of large laser systems.

For lasers operating in the free lasing mode, in accordance with what has been discussed above it is necessary to select glass which for the given magnitude of the absorption coefficient has minimal luminescence band width of the transition $^4F_{3/2} \rightarrow {}^4I_{11/2}$ and large quantum yield, that is, glass with maximum product $\sigma\tau_1$. As was demonstrated in §1.1, this glass will have minimum energy losses connected with luminescence processes and maintenance of threshold population.

Since the surface strength and nonlinear properties of the glass limit the operating energy density of the induced emission to values that are smaller than or equal to $h\nu/\sigma$, application of glass with high induced emission cross section in giant-pulse lasers promotes more efficient use of the energy stored in the inverse population of Nd^{3+}, especially in the preamplification stages. The increase in laser emission divergence (above the diffraction divergence) is determined by the following factors: distortions of the wave front of the emission on nonuniformities in the glass, deviation of the form of the working surfaces of the active elements from given, thermooptical and nonlinear effects.

Modern technology ensures high quality of active elements during series production of them. The distortion of the emission wave front on passage through an active element 100 cm long does not exceed 0.5λ (λ = 1.060 nm). Therefore thermooptical and nonlinear distortions are becoming the basic factors increasing the emission divergence.

The magnitude of the thermooptical distortions and the active elements (§1.4) is determined by the expression

$$\Delta p(x, y, z) = \Phi(T(x, y) - \overline{T})L$$

where $\Phi = P \pm Q$ for a plate active element and $\Phi = P \pm Q/2$ for a cylindrical active element, L is the length of the active element, $\overline{T}$ is the average temperature, T(x, y) is the local temperature in the active element. Let us estimate what value of Φ the glass must have which is used in a laser with total length of the active element equal to 1 meter so that $\Delta p \leq 0.5 \cdot 10^{-4}$ cm, that is, so that the thermooptical distortions will not exceed the distortions of the wave front caused by nonidealness of the glass. In giant-pulse lasers the energy (per unit volume) stored in the inverse population, as a rule, does not exceed 1 joule/cm^3, and at the time of achievement of the indicated population it goes for heating the glass as a function of the shape and duration of a pumping pulse of 1.5 to 2 joules/cm^3. Consequently, the maximum value of $(T(x, y) - \overline{T})$ does not exceed 1° C, and the value of Φ must be less than $5 \cdot 10^{-7}$ K^{-1}. In powerful lasers operating under free lasing conditions, the active element is heated by no more than 5° C. Therefore the magnitude of Φ must not exceed 10^{-7} K^{-1}. If the lasers operate in the repeated pulse mode with repetition period less than the time of complete cooling of the active elements, the established temperature gradient is tens of degrees, and more rigid requirements are imposed on the thermooptical characteristics of the glass: in addition to the condition $\Phi \approx 0$ for $T = \overline{T}$, it is necessary that $\partial\Phi/\partial T \approx 0$, for the latter value determines the temperature range inside which the conditions of smallness of the thermooptical distortions are satisfied. In the case where the laser emits a series of pulses (after which total cooling of the active elements takes place), the value of $(T(x, y) - \overline{T})$ increases continuously during the course of the working cycle, and the average temperature increases by $\Delta T > (\partial\Phi/\partial T)^{-1}$, it is possible to minimize the thermooptical distortions as follows.

For active elements, glass with $\Phi = -(\partial\Phi/\partial t)\Delta T$ is selected; the heating of the active element during lasing leads to a gradual decrease in the absolute magnitude of Φ, and at the end of the series, where the temperature gradients are maximal, $\Phi \approx 0$ and correspondingly $\Delta p(x, y) \approx 0$.

As the measurements show, the thermooptical distortions in the active elements in the form of a plane parallelepiped with a cross section of 40 x 240 mm made both from phosphate and silicate glass with neodymium concentration $(1.4\text{-}2.0) \cdot 10^{20}$ cm^{-3}, and the greater part of the cross section are close to cylindrical. They are about 0.2λ in an active element 720 mm long with pumping of 250 kjoules. In giant-pulse lasers which use these active elements, the thermooptical distortions can be compensated by a cylindrical lens, the curvature of which is connected at the time of lasing to the curvature of the wave front of the emission. In lasers operating in the free lasing mode, the thermooptical distortions are equivalent to a lens with variable focal length; therefore in order to compensate for the distortions, an optical system coupled to the thermooptical lens is required, the focal length of which varies proportionally to the pumping energy absorbed by the active element. It must be noted that the thermooptical distortions at the edges of a plate active element (in an

area making up 20 to 30 percent of the area of the output end) have complex form, and therefore they cannot be compensated by cylindrical or spherical optical system. In active elements of cylindrical form excited by the emission of illuminators with 4 to 6 tubes, nonuniformity is observed in the inverse population distribution and heat release both in the radial and in the azimuthal directions. However, the indicated nonuniformities can be decreased to 20 percent of the values at the center even in an active element with a diameter of about 100 mm by selection of the configuration of the reflectors and decreasing the Nd^{3+} concentration in the glass, and the thermal lens can be made almost spherical.

In lasers with disk active elements, the basic thermooptical distortions are caused by heating of the air between the individual active elements (dn/dT of the air is on the order of 10^{-6} K^{-1}), by the ultraviolet part of the pumping emission. In order to attenuate the pumping in the ultraviolet region, pyrex glass filters are used. The volumetric thermooptical distortions in disk active elements are small, for with uniform pumping with respect to aperture of the active element, the variation in the optical path in the glass as a result of volumetric thermooptical effects must have the same magnitude over the entire cross section of the laser beam even for poor thermooptical parameters of the glass. According to the experimental data, the total (surface and volumetric) thermooptical distortions in the laser containing six disk elements with light aperture of 10 cm and total glass thickness of 18 cm, amount to approximately 0.5λ for pumping of 70 kjoules [349].

The distortions of the wave front of the emission caused by nonlinearity of the index of refraction significantly increase the divergence of the emission and decrease the flux density which can be obtained, focusing the laser beam, if nonlinear variation of the phase on propagation of the emission in the laser system is much greater than π. Here the maximum radiation flux density which can be obtained for a given quality of the wave front, as was noted above, is proportional to $(\sigma N_1)^2/\gamma$. (The induced emission cross section σ and the nonlinearity coefficient γ are constants of the glass.) Obviously, the nonlinear phenomena are manifested completely for pulse durations such that the condition

$$\frac{2\pi n}{\lambda}\int_0^L \gamma J(l)\,dl > \pi$$

is satisfied for flux densities less than the threshold of optical breakdown of the glass surface.* For phosphate glass, the duration of these pulses is less than $(0.5\text{-}1) \cdot 10^{-9}$ seconds.

The authors of [507] propose selection of the glass for laser systems in the picosecond range by the cost of 1 joule of focused energy Z_j, using for this formula

* According to the data presented in [507], the surface breakdown threshold of the glass for different types of glass is 50 to 120 gigawatts/cm^2 with a laser pulse duration of about $2 \cdot 10^{-10}$ seconds.

$$Z_j \sim \frac{\lambda}{2\pi} \frac{n}{\gamma} S (\sigma N_1)^2 \frac{l}{C},$$

where C is the cost of the glass, S is the area of the output end. For lasers with a pulse duration of 10^{-9} to 10^{-10} seconds, the optimal phosphate and fluophosphate glass with $n_2 = (1\text{-}0.5 \cdot 10^{-13}$ cm^2/volts^2 and $\sigma > 3.5 \cdot 10^{-20}$ cm^2, and with a laser pulse duration of $\leq 10^{-10}$ seconds, the fluoberyllate glasses with $n_2 < 0.5 \cdot 10^{-13}$ cm^2/volts^2 are the best.

In lasers in the nanosecond range, nonlinear effects are not so significant, and the cost of the focused energy is determined by the ratio of the product of the energy density for which breakdown of the surface of the glass takes place, $\tilde{E}_p$ for the energy stored in the inverse population, to the magnitude of the saturating signal, $\tilde{E}_s = h\nu/\sigma$ multiplied by the thermooptical constant of the glass:

$$Z_E \sim \frac{\tilde{E}_p}{\tilde{E}_s} \frac{N_1 V}{C\Phi},$$

where V is the volume of the active element in the laser system.

The types of phosphate laser glass produced in the USSR are distinguished by good optical properties (and the LGS-M type glass also has a small value of $d(P \pm Q)/dT \approx 0.09 \cdot 10^{-7}$ K^{-2}), they have high values of the induced emission cross section of neodymium, and therefore they are used successfully in lasers in the nanosecond and millisecond range. For lasers that emit pulses shorter than 10^{-9} seconds, glass of the KGSS-1161 and LGS-M types, for which $n_2 \approx 10^{-13}$ cm^2/volts^2 are the most suitable.

CHAPTER 6. ERBIUM-DOPED LASER GLASS

§6.1. Specific Nature of Erbium Lasers and Requirements on the Active Medium

The induced emission of Er^{3+} ions in glass was first obtained in 1965 by Snitzer and Woodcock [312] on the resonance transition $^4I_{13/2} \rightarrow {}^4I_{15/2}$, $\lambda_{lase} = 1.536$ microns (Figure 3.3). The efforts [204, 508] to obtain lasing on transitions from higher excited states of Er^{3+} ions, for example $^4S_{3/2} \rightarrow {}^4I_{13/2}$ ($\lambda_{lase} \sim 0.85$ micron) or $^4F_{9/2} \rightarrow {}^4I_{13/2}$ ($\lambda_{lase} \approx 1.1$ microns), in contrast to crystals, did not yield positive results inasmuch as the luminescence from these states in glass is sharply quenched by the processes of multiphonon nonradiation relaxation of excitation (§3.4). The specific nature of erbium lasers consists primarily in the fact that the accumulation of the excitation energy on the upper laser level in erbium glass is realized predominantly (or completely) through the sensitization channel, for the effectiveness of direct excitation of the Er^{3+} ions is extremely low as a result of relatively weak and rare absorption bands of the latter and the necessity for introducing erbium ions into the active medium in the smallest possible concentrations on the basis of the three-level lasing system. For Er^{3+} ions, the Yb^{3+} ions turn out to be effective sensitizers. Yb^{3+} ions have a unique, but powerful (especially for high Yb^{3+} concentration) absorption band in the range of 0.9 to 1.02 microns with "effective" width on the order of 1000 cm^{-1} (Figure 3.3 and 6.1). At the same time, the Yb^{3+} ions can be in turn sensitized by Nd^{3+}, Cr^{3+}, Ce^{3+}, Mo^{2+} ions, and so on [48, 82], which theoretically permits the use coefficient of the emission of the pumping tubes to be increased still more. Under such conditions, the energy characteristics of erbium lasers (EL) are determined to a decisive degree by the BPV efficiency in the Yb^{3+}-Er^{3+} pair. The latter limits the minimum admissible concentration of the Er^{3+} ions, it forces an increase to the limit of $\mathcal{N}_{Yb}$ and basically gives the choice of the chemical composition of the glass. The maximum concentration of the Yb^{3+} ions which can be introduced into the glass without having a sharp negative effect on its technological properties (crystallization capacity, optical uniformity, and so on) usually is (1.5 to 2) $\cdot 10^{21}$ cm^{-3} (relatively rare glass compositions in which $\mathcal{N}_{Yb}$ can be increased to (3-4) $\cdot$ 10^{21} cm^{-3}, unfortunately, do not have the required level of adaptability to manufacture). For such $\mathcal{N}_{Yb}$ high quantum yield of the excitation energy transmission in the pair Yb^{3+} - Er^{3+} ($q_{da} \rightarrow 1$) can be insured (depending on the used matrix) for $\mathcal{N}_{Er} \geq (1{,}5-5) \cdot 10^{19}$ $см^{-3}$ (§3.3). Consequently, considering the losses in the laser cavity, in order to reach the lasing threshold it is necessary to excite at least (1-3) $\cdot 10^{19}$ cm^{-3} Er^{3+} ions. These

Figure 6.1. Standard absorption spectrum of Erbium-doped phosphate laser glass.

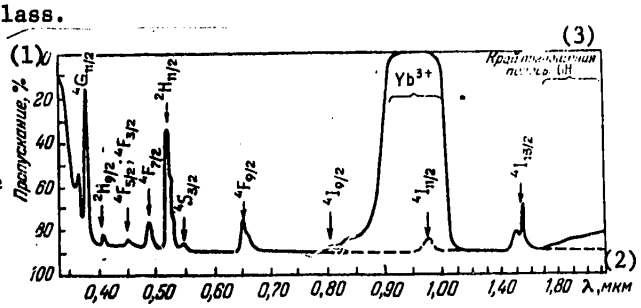

Key: (1) Transmission, %
(2) Microns
(3) Absorption edge of the OH band

excitation levels are already quite high. For comparison let us point out that in neodymium glass lasers with blind resonator mirrors the lasing threshold can be reached with a population of the metastable state of the Nd^{3+} ions on the order of $(1-2)\cdot10^{17}$ cm^{-3}, and under optimal operating conditions, the latter does not usually exceed $1\cdot10^{18}$ cm^{-3} under free lasing conditions and $(2.5-5)\cdot10^{18}$ cm^{-3} under the amplification conditions of short pulses (Chapter 4). In erbium glass, even the best with respect to BPV efficiency, the minimum Er^{3+} ion concentration must in practice be greater than the above indicated values, within the limits of $(\mathcal{N}_{Er})_{min} \geqslant (2,5-5)\cdot 10^{19}$ $см^{-3}$. The fact that is at high excitation levels, as the Er^{3+} ions accumulate in the metastable state under the effect of a pumping pulse, the BPV process efficiency decreases significantly. Frequently this is connected with impoverishment of the population of the ground state. Another effect appears to be more important. This effect consists in primary knockout of the acceptor centers from the quenching process with maximum probability of donor-acceptor interactions. According to what has been discussed in Chapter 3, for the above-indicated ratios of the Yb^{3+} and Er^{3+} ion concentrations in erbium laser glass, the kinetic phase of the BPV process is realized, that is, excitation energy migration with respect to the donor subsystem is so intense that the limiting factor of the quenching process is the excitation runoff rate to the acceptor subsystem. At low pumping levels the runoff takes place primarily through the acceptor centers, the donor vicinity of which approaches them to the maximum (to the minimum admissible distance R_{min} (§3.2)). At high pumping levels, under conditions where the migration process is absent in the acceptor subsystem ($\mathcal{N}_{Er}$ is small) and $t_{pump} \ll \tau_{1er}$, where t_{pump} is the pumping pulse duration, such centers, being excited to the first stage, are knocked out according to the pumping pulse effect from the BPV process, and the effective rate of the BPV process can drop significantly faster than would be expected beginning with the dynamics of the decrease in population of the ground state of the Er^{3+} ions. It is also possible to mention other important principles of the accelerated decrease in $\bar{W}$ during intense pumpings. In order to compensate for the indicated effects, it is also necessary to increase $(\mathcal{N}_{Er})_{min}$.

Thus, if we also consider the relatively low use coefficient of the emission of the pumping tubes (in spite of the presence of sensitizers), the lasing thresholds of erbium lasers with the traditional system of their execution using pulse tubes turn out to be very high, and under the conditions of limited reserve with respect to strength of the latter they are in practice reachable

only for cylindrical small-diameter active elements ($d \leqslant 10$ to 15 mm). The diameter restrictions are also imposed by the large values of the Yb^{3+} concentration, inasmuch as the active elements with $d > 7$ to 8 mm usually are pumped very nonuniformly. Thus, the possibilities of the tube version of the erbium laser (ELL) are highly limited. Introduction of sensitizers into the glass does not change the situation for the most effective of them, Nd^{3+}, cannot be used in sufficient amount as a result of the appearance of quenching of the luminescence of Er^{3+} with respect to the Er^{3+} $({}^4I_{13/2} \rightarrow {}^4I_{15/2}) - Nd^{3+}$ $({}^4F_{3/2} \rightarrow {}^4I_{15/2})$ (§3.3), and the others have low effectiveness. As a result, the energy characteristics of ELL are greatly inferior to the characteristics of neodymium glass lasers: the emission energy is less than one joule, the efficiency is $\leqslant 0.2$ to 0.4 percent [48, 85, 450]. At the same time, they find defined application as a result of absence of other, more efficient lasers for the 1.5 micron band, and also as a result of safety of their emission for the vision [48, 509], the presence of windows of transparency of the atmosphere [510, 511] and good radiation receivers [512].

Cardinal improvement of the energy characteristics of erbium lasers has been achieved by transition to excitation by the emission of neodymium glass lasers operating in the free running mode [247]. The pumping radiation in this case is absorbed by Yb^{3+} ions during the electron transition between the upper Stark component of the base level $^2F_{7/2}$ and the lower component of the metastable level $^2F_{5/2}$ (Figure 3.3). The initial level of the absorption transition at room temperature is weakly populated (about 1.5 to 2) $\cdot 10^{-2}$ N_{Yb}), but as a result of the large values of N_{Yb} it is possible to insure an absorption coefficient on the pumping frequency of k_{pump} approximately equal to (5 to 8) $\cdot$ $\cdot 10^{-2}$ cm^{-1}, for which the threshold densities of the stimulating emission, although quite high (30 to 100 joules/cm^2), are entirely attainable by neodymium glass lasers and, the main thing, they do not exceed the light strength of the glass (see § 1.3). At the same time, small absorption level permits uniform excitation of large volumes of the active medium. The theoretically possible energy coefficient of conversion 1.06 → 1.54 microns is defined by the ratio of the quantum energies of excitation and pumping, and it is $\eta^{max} \approx 0.69$. Although in a real experiment such values are hardly attainable, the application of the laser excitation system permits creation of erbium lasers with high energy characteristics as a result of high efficiency of the neodymium lasers in the free-running mode (to 5-6 percent) and elimination of restrictions on the thickness of the active elements. As will be demonstrated below (§6.5), the advantages of erbium laser reemitters (ELP) of neodymium lasers are especially perceptable when constructing powerful systems for the amplification of short and supershort pulses (KI and SKI). Indeed, high quantum yield (no less than 0.9), long excitation lifetimes in the metastable state (on the order of $1 \cdot 10^{-2}$ sec) and moderate values of the transverse cross section of the induced emission not exceeding $1 \cdot 10^{-20}$ cm^2 make the set of excited Er^{3+} ions almost the ideal medium for these operating conditions, and the application of the laser method of exciting the active medium to a high degree eliminates a number of the harmful effects accompanying tube pumping (for example, heating of the active elements or transverse nonuniformity of the distribution of the excited particles), and it permits achievement of record values of the specific stored energy in the amplification channel (to 5 to 10 joules/cm^3).

Let us consider in more detail the requirements imposed on erbium glass as an active medium in order to maximize the energy characteristics of erbium lasers. Let us perform a theoretical analysis of the processes of accumulating Er^{3+} ions in the metastable state and lasing of stimulated emission in the example of the model of the ELP excited by a monochromatic square pulse of emission of a neodymium laser ($I_{pump}(\nu,t) = I_0\delta(\nu - \nu_{pump})t$, $0 \leqslant t \leqslant t_{pump}$, where ν_{pump} and I_{pump} are the emission frequency (sec^{-1}) and intensity of the photon beam ($cm^{-2} \cdot sec^{-1}$) in the pumping laser pulse). The strict kinetic model of ELP is quite complicated. Figure 6.2 shows a simplified equivalent diagram of the levels and transitions between them determining the dynamics of the accumulation of the excitation energy in the metastable state and the lasing process. When compiling it, along with the excitation processes, consideration was given to BPV and lasing and also the presence of induced absorption of the Er^{3+} ions in the metastable state on pumping and lasing frequencies (ν_{lase}) for which the wings of the absorption bands corresponding to the transitions ${}^4I_{13/2} \rightarrow {}^4F_{9/2}$ ($\tilde{\nu}_0 \approx 8900$ см$^{-1}$) and ${}^4I_{13/2} \rightarrow {}^4I_{9/2}$ ($\tilde{\nu}_0 \approx 6100$ см$^{-1}$) are responsible. In the diagram in Figure 6.2 consideration is also given to the fact that in order to obtain lasing in the Er^{3+} ion system in glass, according to the analysis of the structure of their luminescence spectra (see below §6.2) the most favorable are the transitions from the ${}^4I_{13/2}$ level for one of three low Stark components of the level ${}^4I_{13/2}$ separated energywise by 40 to 50 cm^{-1} ($\Delta E << k_BT$). The transitions to the components 4-8 of the ${}^4I_{15/2}$ level lagging behind the lower component by 200 to 500 cm^{-1} ($\Delta E \geqslant k_BT$) have significantly smaller transverse cross sections (by 5 to 20 times) and, in addition, they overlap more sharply with respect to energy with the induced absorption band. Therefore the conditions for obtaining effective lasing on them, unfortunately, are unfavorable. It is also considered that according to the data discussed in §3.4, the probability of direct nonradiating transitions from the upper excited states of the Er^{3+} ions (states 3-5) to the ground state is negligibly small by comparison with the probabilities of staged relaxation with the participation of all of the intermediate levels.

Using the notation introduced in Figure 6.2, the system of kinetic equations describing the variation of the populations N_i of the levels of the Yb^{3+} and Er^{3+} ions during excitation accumulation on the metastable level ${}^4I_{13/2}$ (2 A) and generation of stimulated emission, can be written in the following form:

$$
\begin{aligned}
\dot{N}_{3Д} &= \sigma_{л} I_0 (N_{2Д} - N_{3Д}) - N_{3Д}\tau_{3Д}^{-1} - w_{ДА} N_{3Д}, \\
\dot{N}_{1A} &= \sigma_{л} I_л (N_{2A} - N_{1A}) + \tau_{0A}^{-1} N_{2A} - w_{ДА} N_{3Д} + w_{21} N_{2A}, \\
\dot{N}_{2A} &= w_{32} N_{3A} - (\tau_{0A}^{-1} + w_{21}) N_{2A} - \sigma_л I_л (N_{2A} - N_{1A}) - \\
&\quad - \sigma_{24} I_л (N_{2A} - N_{4A}) - \sigma_{25} I_0 (N_{2A} - N_{5A}), \\
\dot{N}_{3A} &= w_{ДА} N_{3Д} - w_{32} N_{3A} + w_{43} N_{4A}, \\
\dot{N}_{1A} &= w_{51} N_{5A} + \sigma_{24} I_л (N_{2A} - N_{4A}) - w_{43} N_{4A}, \\
\dot{N}_{5A} &= \sigma_{25} I_0 (N_{2A} - N_{5A}) - w_{54} N_{5A}, \\
N_{2Д} &= N_{1Д} \exp\left(-\frac{\Delta E_{12Д}}{k_B T}\right) = \text{const} \ll \mathcal{N}_{Yb}, \\
&\sum_{i=1}^{5} N_{iA} = \mathcal{N}_{Er}.
\end{aligned}
\tag{6.1}
$$

Key: (1) lase (2) pump

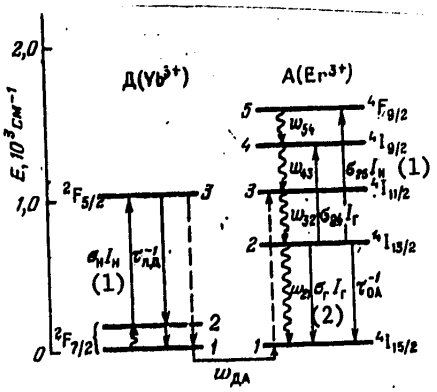

Figure 6.2. Equivalent diagram of the energy levels of the system of ions Yb^{3+}-Er^{3+} and transitions between them describing the operation of the ELP.

I_{pump} and I_{lase} are the intensities of the pumping and lasing emission ($cm^{-2} \cdot sec^{-1}$). σ_{pump} and σ_{lase} are the effective transverse cross sections of absorption on the pumping frequency and induced emission on the lasing frequency (cm^{-2}), σ_{ij} are the transverse absorption cross sections between the levels I and J of the acceptor (cm^{-2}). w_{ij} is the rate of nonradiating relaxation of excitation between the levels i and j (sec^{-1}), w_{DA} is the effective BPV rate in the pair Yb^{3+} - Zr^{3+}(sec^{-1}), τ_{1D} is the luminescent lifetime of Yb^{3+} on the levels $^2F_{5/2}$ (3D), τ_{0A} is the radiating lifetime of the Er^{3+} ions on the metastable level $^4I_{13/2}$ (2 A).

Key: (1) pump
(2) lase

The strict solution of the system (6.1) must be found jointly with the solutions of the equations for the emission density in the laser resonator (see, for example, [3]). Considering the complex form of the function $w_{DA}(N_{2A})$, it is difficult to obtain it. However, for the stationary pumping mode (t_{pump}; $t_{threshold} >> w_{DA}^{-1}$, w_{32}^{-1}; w_{54}^{-1}, w_{43}^{-1}, where $t_{threshold}$ is the time interval from the beginning of pumping until the threshold inverse population is reached $\Delta N_{threshold} = (N_{2A} - N_{1A})_{threshold}$) under acceptable conditions

$$w_{32},\ w_{43},\ w_{54} \gg \sigma_{21} I_r,\ \sigma_{25} I_0 \qquad (6.2)$$

(1)

Key: (1) lase

it is possible to replace system (6.1) by the equation for inverse population

$$\frac{d\Delta N}{dt} = -\underset{(1)}{(2\sigma_r I_r + \tau_{лА}^{-1})}\Delta N + \left(\frac{2w_{ДА}\sigma_н I_0 N_{2Д}}{\sigma_н I_0 + \tau_{лД}^{-1} + w_{ДА}} - \tau_{лА}^{-1} N_{Er}\right), \qquad (6.3)$$

(2)

Key: (1) lase
(2) pump

where $\tau_{1A}^{-1} = \tau_{0A}^{-1} + w_{21}$. Equation (6.3) is nonlinear, for $w_{DA} = f(\Delta N)$. If the form of the function f is known, its solution can be found by numerical methods. At the same time it is obvious that for minimization of $\Delta N_{threshold}$ it is necessary to insure satisfaction of the condition

$$w_{\text{Д}A} \gg \tau_{\text{Д}}^{-1} + \sigma_{\text{н}} I_0. \tag{6.4}$$
(1)

Key: (1) pump

In this case the solution of (6.3) presents no difficulties. In the initial phase of operation of the laser when the induced emission is absent ($I_{lase} = 0$) and the process of charge accumulation takes place on the level 2A,

$$\Delta N(t) = (\lambda - \mathcal{N}_{Er}) - \lambda e^{-t/\tau_{\text{л}A}}, \tag{6.5}$$

where

$$\lambda = 2\alpha_{\text{н}} I_0 N_{2\text{Д}} \tau_{\text{л}A}. \tag{6.6}$$
(1)

Key: (1) pump

Hence, it is easy to determine the time $t_{threshold}$:

$$t_{\text{пор}} = \tau_{\text{л}A} \ln\left\{\frac{\lambda}{\lambda - (\mathcal{N}_{Er} + \Delta N_{\text{пор}})}\right\}, \tag{6.7}$$
(1) (1)

Key: (1) threshold

and the threshold pumping energy density of the active medium of volume V:

$$\mathcal{W}_{\text{н пор}} = h\nu_{\text{н}} V I_0 [\sigma_{\text{н}} N_{2\text{Д}} + \beta_{\text{н}} + \sigma_{25} \cdot 0{,}25 (\mathcal{N}_{Er} + \Delta N_{\text{пор}})] t_{\text{пор}}, \tag{6.8}$$
(1) (2) (3)

Key: (1) pump threshold
(2) pump
(3) threshold

which must approach the minimum value

$$(\mathcal{W}_{\text{н пор}})^{\min} \approx 0{,}5 h\nu_{\text{н}} V (\mathcal{N}_{Er} + \Delta N_{\text{пор}}) \times \left[1 + \frac{\beta_{\text{н}} + 0{,}25\sigma_{25}(\Delta N_{\text{пор}} + \mathcal{N}_{Er})}{\sigma_{\text{н}} N_{2\text{Д}}}\right] \tag{6.9}$$
(1) (2) (3)

Key: (1) pump threshold
(2) pump
(3) threshold

on satisfaction of the condition $t_{threshold} \ll \tau_{1A}$ as a result of an increase in I_0. In these formulas β_{pump} is the coefficient of inactive losses in the glass on the pumping frequency (cm^{-1}), and $\Delta N_{threshold}$, as is easy to demonstrate, is defined by the expression

$$\Delta N_{\text{пор}}^{(1)} = \frac{\beta_{\text{г}} + \beta_{\text{и}}^{(3)} + 0{,}5\sigma_{24}\mathcal{N}_{\text{Er}}}{\sigma_{\text{г}}^{(2)} - 0{,}5\sigma_{24}}, \tag{6.10}$$

Key: (1) threshold (2) lase (3) i

where β_{lase} and $\beta_i = (1/2l_{lase})\ln(R)^{-1}$ are the coefficients of inactive losses on the lasing frequency and the losses to emission in the laser cavity (cm^{-1}), respectively, R is the reflection coefficient of the output mirror of the resonator, l_{lase} is the length of the active element with respect to the lasing channel. Then considering the known equations for the radiation density in the laser cavity [3], simple but awkward calculations permit us to obtain the following useful expressions for the output power ε_{out} and the efficiency (η) of ELP under quasisteady lasing conditions:

$$\varepsilon_{\text{вых}}^{(1)} \approx h\nu_{\text{г}} V q_{\text{ДА}}^{\text{г}}\,{}^{(2)}(k_{\text{и}})_{\text{эфф}}^{(3)} I_0 \frac{\beta_{\text{и}}^{(4)}}{\beta_{\text{и}} + \beta_{\text{г}} + 0{,}5\sigma_{24}\mathcal{N}_{\text{Er}}}\left(1 - 0{,}5\frac{\sigma_{24}}{\sigma_{\text{г}}}\right) \times \times \left[1 - \frac{0{,}5\,(\mathcal{N}_{\text{Er}} + \Delta N_{\text{пор}}^{(5)})}{q_{\text{ДА}}^{\text{г}}\tau_{\text{лА}}(k_{\text{и}})_{\text{эфф}} I_0}\right], \tag{6.11}$$

$$\eta \approx q_{\text{ДА}}^{\text{г}}\frac{\nu_{\text{г}}}{\nu_{\text{и}}}\frac{(k_{\text{и}})_{\text{эфф}}(1 - 0{,}5\sigma_{24}/\sigma_{\text{г}})}{(k_{\text{и}})_{\text{эфф}} + \beta_{\text{и}} + 0{,}5\sigma_{25}(\mathcal{N}_{\text{Er}} + \Delta N_{\text{пор}})} \times \times \frac{\beta_{\text{и}}}{\beta_{\text{и}} + \beta_{\text{г}} + 0{,}5\sigma_{24}\mathcal{N}_{\text{Er}}}\left[1 - \frac{0{,}5\,(\mathcal{N}_{\text{Er}} + \Delta N_{\text{пор}})}{q_{\text{ДА}}^{\text{г}}(k_{\text{и}})_{\text{эфф}} I_0}(\tau_{\text{лА}}^{-1} + t_{\text{и}}^{-1})\right]. \tag{6.12}$$

Key: (1) out (3) eff (5) threshold
(2) lase (4) i (6) pump

Here $q_{DA}^{lase} = \dfrac{w_{DA}^{lase}}{w_{DA} + \tau_{1D}^{-1}}$ is the quantum efficiency of energy transfer in the pair Yb^{3+}-Er^{3+} for the steady-state level of inversion

$$w_{\text{ДА}}^{\text{г}} \approx w_{\text{ДА}} \cdot 0{,}5\,(\mathcal{N}_{\text{Er}} - \Delta N_{\text{пор}}^{(1)}) = \text{const}, \tag{6.13}$$

$$(k_{\text{и}})_{\text{эфф}}^{(2)} = \sigma_{\text{и}}(N_{2\text{Д}}^{(3)} - N_{\text{эД}}) = \frac{(w_{\text{ДА}}^{\text{г}} + \tau_{\text{лД}}^{-1})N_{2\text{Д}}\sigma_{\text{и}}}{\sigma_{\text{и}} I_0 + w_{\text{ДА}}^{\text{г}} + \tau_{\text{лД}}^{-1}}.$$

Key: (1) threshold (3) pump
(2) eff

The last expression takes into account the possibility of violation of condition (6.4) leading to a decrease in the effective value of the absorption coefficient on the pumping frequency. The value of the probability w_{DA}^{lase} obviously is less than the values measured for low excitation levels. However, it is significant here that it approaches a steady-state value determined by the residual population of the basic level of 1 A, for with the occurrence of lasing, the effective radiating deactivation of the excited Er^{3+} ions permits the acceptor centers, the efficiency of the interaction of which with the donor surroundings is maximal, multiple participation in the BPV process even in the absence of migration of excitation energy with respect to them.

Analysis of expressions (6.8), (6.10), (6.11) permits discovery of the following conditions, on satisfaction of which the efficiency of the ELP must be close to the maximum value of $\eta^{max} = \nu_{lase}/\nu_{pump}$

$$
\begin{aligned}
&1)\ q^{r}_{\text{ДА}} \overset{(1)}{\underset{(3)}{\gtrless}} 1; \quad (5)\\
&2)\ (k_{\text{н}})_{\text{эфф}} \gg \beta_{\text{н}} + 0{,}5\sigma_{25}(\mathcal{N}_{\text{Er}} + \Delta N_{\text{пор}});\\
&3)\ \beta_{\text{н}} \gg \beta_{\text{г}} + 0{,}5\sigma_{21}\mathcal{N}_{\text{Er}}; \quad (4)\\
&4)\ \sigma_{21} \ll 2\sigma_{\text{г}}; \quad (\text{i})\\
&5)\ I_0 \ll w^{r}_{\text{ДА}}\sigma_{\text{н}}^{-1};\\
&6)\ I_0 \gg \frac{\mathcal{N}_{\text{Er}} + \Delta N_{\text{пор}}}{2q^{r}_{\text{ДА}} t_{\text{н}} (k_{\text{н}})_{\text{эфф}}}, \quad \frac{\mathcal{N}_{\text{Er}} + \Delta N_{\text{пор}}}{2q^{r}_{\text{ДА}}\tau_{\text{лА}} (k_{\text{н}})_{\text{эфф}}}.
\end{aligned}
\qquad (6.14)
$$

Key: (1) lase (4) threshold
(2) H = pump (5) i
(3) eff

Condition 1) defines the minimum Er^{3+} ion concentration in glass and, consequently, the threshold pumping energy and I_0. In order to decrease them, it is necessary to find matrices with the largest possible values of w_{DA}. According to the results of Chapter 3, the greatest efficiencies of transfer in the Yb^{3+}-Er^{3+} pair are realized in phosphate and borate glass. Considering that $w^{lase}_{DA} \approx w_{DA}$ (for $N_{2A} = (0.4 \text{ to } 0.5)\,\mathcal{N}_{Er}$), we find that in this glass usually $q^{lase}_{DA} \geqslant 0.9$ for $\mathcal{N}_{Er} \geqslant (3\text{—}4)\cdot 10^{19}$ см$^{-3}$. For comparison let us point out that in silicate glass it is required that at least $\mathcal{N}_{Er} \geqslant (8\text{—}10)\cdot 10^{19}$ см$^{-3}$.

The presence of induced absorption on the pumping frequency complicates the satisfaction of condition 2) For the actual values of $k_{pump} \approx 5\cdot 10^{-2}$cm^{-1}, $\beta_{pump} \approx (1\text{-}2)\cdot 10^{-3}$ cm^{-1} and $0.5(\mathcal{N}_{Er} + \Delta N_{threshold}) = 2\cdot 10^{19}$ cm^{-3}, the value of σ_{25} must be less than $(1\text{-}2)\cdot 10^{-22}$cm^2. Otherwise, this absorption will greatly decrease the efficiency of ELP. Experimental measurements of the level of induced absorption [413] demonstrated that condition 2) is critical. Phosphate glass in which σ_{25} is less than in silicate glass, has an advantage. In general, it is necessary to select matrices with large σ_{pump} and shift ν_{pump} as far as possible to the high-frequency region. Phosphate glass is also from this point of view preferable, for it has larger values of σ_{pump} compared to silicate glass, and as a result of larger w_{DA} under identical conditions $(k_{pump})_{eff} \to k_{pump}$ is insured for higher I_0.

Condition 3) reduces to the requirement of insuring the minimum level of inactive losses on the lasing frequency. The small cross section σ_{lase} limits the possibilities of satisfying the condition 3) as a result of an increase in β_i by decreasing R. In addition, the presence of induced absorption in the lasing region is equivalent to an additional decrease in the effective value of the induced emission cross section to a value of $\sigma^*_{lase} = \sigma_{lase} - 0.5\sigma_{24}$). Thus, the requirements on the purity and optical uniformity of erbium glass are much

more rigid than in the case of neodymium glass. Here, the glass must be purified not only of accompanying admixtures of rare earth elements and transition metals, but especially the hydroxyl groups dissolved in the glass. The absorption coefficient of the hydroxyl groups in the range of 1.54 microns increases compared to the region of 1.06 microns by 70 to 100 times (see Figure 3.21), and it becomes highly significant (about $1.5 \cdot 10^{-3} cm^{-1}$ for $N_{OH} = 1 \cdot 10^{19}$ cm^{-3} in phosphate glass). Consequently, erbium glass which is suitable for application in lasers must be carefully dehydrated. The requirement on the dehydration level ensuring minimization of β_{lase} approximately corresponds to the requirement $N_{OH} \leq (5-7) \cdot 10^{18}$ [illegible], following from the condition $q_{er} \to 1$. The influence of the induced absorption would be insignificant for $\sigma_{24} < 1 \cdot 10^{-22}$ см^2. This requirement is much more rigid than condition 4). To what degree it is satisfied has not been successfully established at the present time. The maximum of the corresponding absorption band (the transition $^4I_{13/2} \to {}^4I_{9/2}$) lies, as has already been pointed out above, near 6100 cm^{-1}, which is approximately 400 cm^{-1} less than $\tilde{\nu}_{lase}$. The intensity of this band, judging by the results of reference [361] is commensurate with the intensity of the transition $^4I_{15/2} \to {}^4I_{13/2}$. Therefore, in spite of significant shift of $\tilde{\nu}_{lase}$ with respect to the maximum, the value of σ_{24} can significantly exceed the above-indicated limit. Some estimates of σ_{24} will be presented in §6.3.

Condition 5) imposes an upper bound on the pumping emission intensity as a result of the finite value of w_{DA}^{lase}. Condition 6) is equivalent to the requirement that the intensity of the pumping emission significantly exceed the threshold, inasmuch as usually $t_{pump} \leq \tau_{1A}$. It imposes a lower bound on the optimal values of I_0. Let us estimate to what degree conditions 5) and 6) are satisfied in different matrices. For silicate glass when $N_{Er} = 8 \cdot 10^{19}$ см$^{-3}$ usually $w_{DA}^{lase} \simeq (2.5\text{-}4) \cdot 10^3$ sec^{-1}, $\sigma_{pump} \simeq 1 \cdot 10^{-21}$ cm^2. Then $I_0 \ll (2.5\text{-}4) \cdot 10^{24}$ cm^{-2}-sec^{-1}, which for pumping duration of $t_{pump} = 5 \cdot 10^{-8}$ seconds corresponds to a pumping radiation energy density of 2500 to 4000 joules/cm^2. On the other hand, condition 6) gives $I_0 \gg 2.2 \cdot 10^{23} cm^{-2}\text{-}sec^{-1}$ (210 joules/cm^2). Thus, it is difficult to satisfy both of the conditions 5) and 6) in the case of silicate glass immediately. For phosphate glass when $N_{Er} \approx 3{,}5 \cdot 10^{19}$ см$^{-3}$, $w_{DA}^{lase} \simeq 0.65 \cdot 10^4 sec^{-1}$, $\sigma_{pump} = 2 \cdot 10^{-21}$ cm^2 and $k_{pump} \simeq 6 \cdot 10^{19}$ cm^{-1}, condition 5) has the form $I_0 \ll 3{,}3 \cdot 10^{24}$ см$^{-2} \cdot sec^{-1}$ (3100 joules/cm^2), and condition 6) is the form of $I_0 \gg 8{,}2 \cdot 10^{22}$ см$^{-2} \cdot sec^{-1}$ (77 joules/cm^2). These conditions are less rigid than for silicate glass, but they are also quite stressed. Their satisfaction is complicated with a decrease in t_{pump}. It is also necessary to note that the pumping energy densities required for realization of high efficiencies are very high even for the laser method of excitation. For silicate glass, they exceed the radiation breakdown threshold of the glass with respect to platinum inclusions (700 to 1000 joules/cm^2).

Thus, the performed analysis demonstrated that under optimal conditions the energy efficiency of the ELP can approach the theoretical limits. Here the integral brightness of the emission of such ELP can exceed by one and a half to two orders the brightness of neodynium lasers [247, 413, 535]. However, the achievement of high energy characteristics of the ELP in the free running mode is possible only under very rigid conditions requiring optimization of the chemical composition of the glass and concentrations of the activators,

high radiating strength of the glass, high energy densities of the pumping emission and maximum shift of the emission wavelength of the pumping laser to the shortwave side (to 1.050 to 1.054 microns). The best matrices for the working material of the ELP are phosphate materials having decisive advantages over silicate. Only borate glass could compete with them with respect to BPV efficiency, but in borate glass the quantum yield of the Er^{3+} ion luminescence, unfortunately, is extremely low ($\leqslant 0.07$) as a result of the high efficiency of the MFR processes (§3.4). In the phosphate glass series preference must be given to the compositions permitting introduction of the largest possible concentrations of Yb^{3+} ions having both high σ_{pump}, σ_{lase} and maximum transfer efficiency in the Yb^{3+}-Er^{3+} pair without having negative effects on the technological characteristics. According to the results of §3.3, they should be found among the systems permitting maximum approach of the rare earth ions, that is, having minimum R_{min}.

§ 6.2. Spectral Luminescent Properties of Erbium Glass

Figure 6.1 shows the standard absorption spectrum of erbium phosphate laser glass. It consists of a small number of relatively weak and narrow bands in the visible and near intrared regions of the spectrum. The most intense are the bands with peaks about 522 and 378 nm (the oscillator strengths are $5.7 \cdot 10^{-6}$ and $12 \cdot 10^{-6}$, respectively). The remaining groups of the bands are at least an order weaker. A detailed analysis of the absorption spectra, detailed data on the powers of the oscillators of the transitions and positions of the band peaks and also the parameters calculated by them (in some cases) for the crystal field, can be found in the following papers: for silicate glass [361, 364, 516-518], phosphate glass [191, 193, 204, 361, 405, 411, 508, 516, 517], borophosphate glass [193, 361, 517], fluophosphate glass [191, 345, 517], borate glass [405, 411, 508, 517], germanate glass [405, 411, 508, 517], tellurite glass [361, 403, 411] and fluoberyllate [361, 517, 521, 522]. A comparison of the data presented in them permits the conclusion to be drawn that the chemical composition of glass has less influence on the form and the position of the bands than was observed for the Nd^{3+} ions. For example, in metaphosphate glass with different modifiers (elements of the first and second groups) and also in borophosphate glass the form and the position of the absorption bands of Er^{3+} do not change in practice [193]. Only on comparison of them with other types of glass are differences noticeable. It is possible to be convinced of this in the example of the resonance absorption band corresponding to the laser transition (Figure 6.3). The resolution of the transitions varies more significantly. With some exceptions, it increases in the series of fluoberyllate-alkali and alkali earth silicate-aluminocalciumsilicate-fluophosphate-borophosphate-phosphate-germanate-borate-tellurite glass (7-8 times for "supersensitive" transitions ${}^4I_{15/2} \rightleftarrows {}^4I_{11/2}$; ${}^2H_{11/2}$; ${}^4G_{11/2}$ with $\Delta J = 2$ and 2 to 3 times for the remaining transitions, including for ${}^4I_{13/2} \rightleftarrows {}^4I_{15/2}$, which, according to [518], correlates with the decrease in symmetry of the local crystalline field in the vicinity of the rare earth ions in this series of glasses. The resolution of the transitions varies noticeably also as a function of the type of modifier. For example, in binary alkali earth phosphate glass (50.5 MeO, 49.5 P_2O_5 molecular percent) the integral absorption cross section of the transition ${}^4I_{15/2} \rightarrow {}^4I_{13/2}$ increases by 1.35 times in the Mg-Cd series (to $4.2 \cdot 10^8 cm^2 \cdot sec^{-1}$), then it decreases somewhat for Ba [519].

In the luminescence spectra of the majority of compositions, a unique intense band is observed with peak at 1536 nm corresponding to the resonance transition $^4I_{13/2} \rightarrow {}^4I_{15/2}$ (Figure 6.3). Only in fluoberyllate and especially in the tellurite glasses do the bands corresponding to the transition $^4S_{3/2} \rightarrow {}^4I_{15/2}$ (550 nm), $^4I_{11/2} \rightarrow {}^4I_{15/2}$ (about 990 nm) and $^2P_{3/2} \rightarrow {}^4I_{15/2}$ (about 320 nm) [345, 361, 521, 522] have noticeable intensity, which is caused by lower probability of nonradiating degredation of the high excited states of the ions in these types of glass (Chapter 3).

In contrast to the corresponding absorption band, the form of the resonance luminescence band of Er^{3+} ions depends strongly on the glass composition (Figure 6.3). Its halfwidth in phosphate glass is greater than in silicate glass ($\Delta\nu \simeq 135$ and 115 cm^{-1}, respectively), and depends insignificantly on the type of modifier. In fluophosphate and especially in borate glass, the value of $\Delta\tilde{\nu}_1$ increases sharply (in the latter, to 400 cm^{-1}), which is connected first of all with growth of the relative intensity of the transitions from the upper Stark components of the $^4I_{13/2}$ level forming the high frequency wing of the luminescence band at 300K. Simultaneously, in the series of silicate-phosphate fluophosphate-borate glass, the transverse cross section of the induced

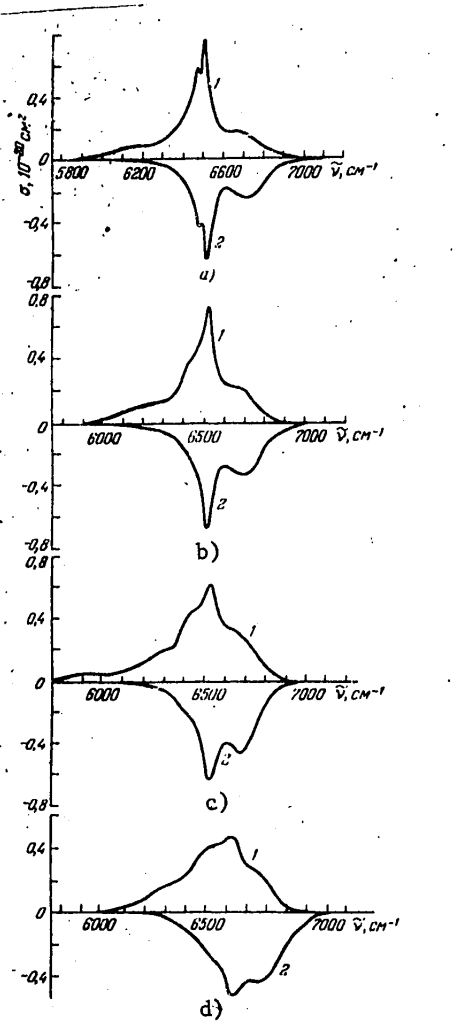

Figure 6.3. Luminescence (1) and absorption (2) bands of Er^{3+} ions corresponding to the transition $^4I_{13/2} \rightleftarrows {}^4I_{15/2}$ in Li-Mg-silicate (a), Ba-Al-phosphate (b), fluophosphate (c) and Na-borate (d) glass. 300 K.

Here and in Figure 6.4 the absorption cross sections are multiplied by -1.

emission decreases at the luminescence band peak σ_{lase}. Let us note that this series is almost inverse to the one presented above where we were talking about the integral cross sections of the absorption bands of Er^{3+} ions. This apparent contradiction is explained by differences in width and shape of the luminescence bands. In Table 6.1 complete information about σ_{lase} and the positions of the maximum resonance luminescence band taken from various sources are collected. The differences in the presented values of σ_{lase} do not exceed 50 percent. This is much less than the observed differences for neodymium glass where they reach three times (and even more) (Figure 4). Among phosphate glass, according to [519] the value of σ_{lase} increases from $6.3 \cdot 10^{-21}$ to $8 \cdot 10^{-21}$ cm^2 in the series of modifiers Mg-Ca-Sr, then decreases to $\approx 7.5 \cdot 10^{-21}$ cm^2 for Cd and Ba. However, the indicated differences are not too significant. Thus, it can be concluded that the possibility of a significant increase in σ_{lase} by finding the optimal compositions for erbium glass obviously is excluded.

Measurements of the absorption and luminescence spectra for low temperatures permit us to obtain information about the position of the Stark components of the levels $^4I_{13/2}$ and $^4I_{15/2}$ and also the magnitude of the nonuniform broadening of the bands corresponding to the transitions between these components. In Figure 6.4, the spectra of this type that we obtained are demonstrated for a temperature of 4.2 K for Na-K-La-Ba-silicate and Na-Mg-phosphate glass and also approximum expansion of these spectra into individual components. It is obvious that the degeneration of the indicated levels in glass is completely removed, and each of the terms is expanded in 2J + 1 halflevels. The opposite conclusion drawn previously in [517] is explained obviously by low accuracy of the recording. In Table 6.2 the positions of the Stark components on the energy scale and estimated values of nonuniform broadening of the absorption or luminescence bands connected with them are presented. The obtained values of $\Delta\tilde{\nu}_{pump}$ for phosphate glass turned out to be larger than for silicate glass, analogously to the results found by us for the Yb^{3+} ions, and opposite to the situation in neodymium glass. On the whole, the magnitude of the nonuniform broadening of the Er^{3+} ion bands is appreciably less than for the Nb^{3+} ions.

Few experimental studies have been made of the induced absorption spectra of Er^{3+} ions in glass. A strong band in the 20,880 cm^{-1} region was detected in reference [525]. This band was attributed to the transition to the $^2K_{15/2}$, $^2G_{7/2}$ levels, and weak bands were detected in the regions of 19,250 cm^{-1} ($\rightarrow {}^4G_{9/2}$) and 15,400 cm^{-1} (the transition is not established) in multicomponent silicate glass. More complete and exact data were obtained in [361, 526] for Li-Mg-Al-silicate and Na-Al-phosphate glass where the induced absorption bands corresponding to the transitions on the $^4I_{9/2}$ level (about 6100 cm^{-1}), $^4S_{3/2}$ (approximately 11,750 cm^{-1}), $^2H_{11/2}$ (12,450 cm^{-1}), $^4F_{7/2}$ (13,950 cm^{-1}), $^4F_{5/2}$ (15,550 cm^{-1}), $^4F_{3/2}$ (15,950 cm^{-1}), $^2G_{9/2}$ (18,050 cm^{-1}), $^4G_{11/2}$ (19,850 cm^{-1}), $^4G_{9/2}$ (20,850 cm^{-1}) and $^2G_{7/2}$, $^2K_{15/2}$ (21,550 cm^{-1} bands (Figure 6.5). Here the band with maximum at 6100 cm^{-1} turned out to be one of the most intense. Let us note that the authors of [361, 526] diverge with the generally accepted classification of Er^{3+} ion levels (see, for example, [95,

Table 6.1

Glass composition molecular %	$\sigma \cdot 10^{-20}$ см^2 lase	$\tilde{\nu}_s$, см$^{-1}$	Data Source
79,5 SiO_2, 8,1 Na_2O, 2,0 BaO, 2,4 Yb_2O_3, 8,0 K_2O, 0,04 Er_2O_3	0,56	6510	[312]
57 SiO_2, 26,4 Li_2O, 1,8 Al_2O_3, 13,8 MgO, 1 Er_2O_3	0,77	6510	[339, 519]
49,5 P_2O_5, 49,5 SrO, 1 Er_2O_3	0,80	6510	[519]
49,5 P_2O_5, 49,5CdO, 1 Er_2O_3	0,76	6510	[519]
49,5 P_2O_5, 49,5 MgO, 1 Er_2O_3	0,63	6510	[519]
56,3 P_2O_5, 25 ZnO, 12,5 Al_2O_3, 5,2 La_2O_3, 1 Er_2O_3	0,74	6510	[519]
84 B_2O_3, 14,8 Na_2O, 1,25 Er_2O_3	0,50 0,42	6650 6510	[519]
58,9 P_2O_5, 24,7 ZnO, 11,2 Al_2O_3, 5,2 Yb_2O_3, 0,18 Er_2O_3	1,11 *)	6510	[528]
50 P_2O_5, 37 BaO, 12,5 Al_2O_3, 0,5 Er_2O_3	0,70	6510	[101, 247]

*) The measurements were performed for 77K

100, 338] and so on), according to which the induced absorption bands with peaks in the vicinity of 18,050 cm^{-1} and 20,850 cm^{-1} must correspond to transitions to the levels $^2H_{9/2}$ and $^2G_{9/2}$, respectively. The band corresponding to the transition $^4I_{13/2} \rightarrow {}^4F_{9/2}$ (near 8800 cm^{-1}) was not detected in these experiments. On the contrary, in [527], the presence of induced absorption in the 9400 to 9250 cm^{-1} region in erbium glass was noted, which was later related by the authors to the indicated transition [413] (Figure 6.6). However, as a result of experimental difficulties, they were unable to reproduce the absorption band curve completely, and the presented data are limited to a segment of its short-wave wing. From Figure 6.6 it is obvious that on the pumping frequency of the ELP (1.055 micons) phosphate glass with a concentration of $N_{Er} = 3 \cdot 10^{19}$ см$^{-3}$ with specific absorbed energy of about 5 joules/cm^3 has an induced absorption level approximately equal to $7.5 \cdot 10^{-3}$ cm^{-1}, which is 1.3 times less than in

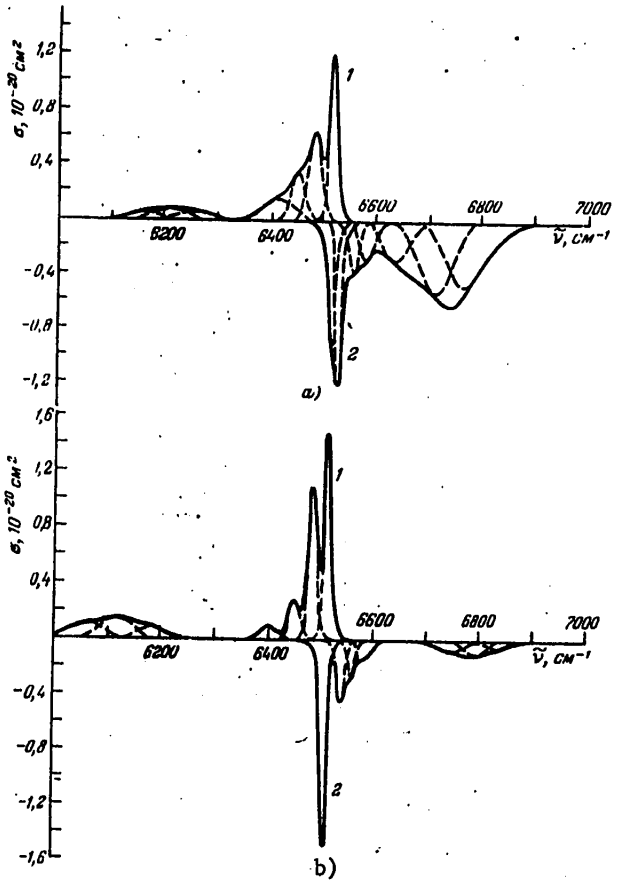

Figure 6.4. Luminescence (1) and absorption (2) bands of Er^{3+} ions in Na-Mg-phosphate (a) and Na-K-Ba-La-silicate (b) glass at 4.2K and the approximate position of the Stark components (dotted lines).

Data on the cross section are increased by five-fold in figure b in the 6000-6200 cm^{-1} range.

silicate glass. Hence, it is possible to obtain a value of $\sigma_{25} \simeq 3 \cdot 10^{-22} cm^2$, which must be considered as the lower limit, for the population of the metastable level is explicitly below the value estimated by the absorbed energy.

As was already noted in § 6.1, an important characteristic of erbium glass is the absorption coefficient k_{pump} in the region of emission of pumped neodymium lasers (1.055 to 1.06 microns). The form of the absorption band of Yb^{3+} ions in phosphate glass with high concentration of them is illustrated in Figure 6.1.

Table 6.2

Level	Na—K—Ba—La-SiO_2 glass		Ba—Al—P_2O_5-glass	
	$\tilde{\nu}_i-\tilde{\nu}_j$, $см^{-1}$	$\Delta\tilde{\nu}$ $см^{-1}$ pump	$\tilde{\nu}_i-\tilde{\nu}_j$, $см^{-1}$	$\Delta\tilde{\nu}$ $см^{-1}$ pump
$^4I_{13/2}$ Components				
1	0	13	0	17
2	28	18	29	26
3	62	30	51	50
4	107	35	74	64
5	≈220	≈60	≈130	≈68
6	≈390	≈70	≈270	≈70
7	≈440	≈70	≈320	≈70
8	≈500	≈75	≈370	≈80
$^4I_{13/2}$ Components				
1	0	13	0	17
2	33	16	18	18
3	51	18	41	26
4	75	25	69	35
5	≈230	≈40	≈132	≈60
6	≈280	≈45	≈190	≈65
7	≈330	≈52	≈250	≈80

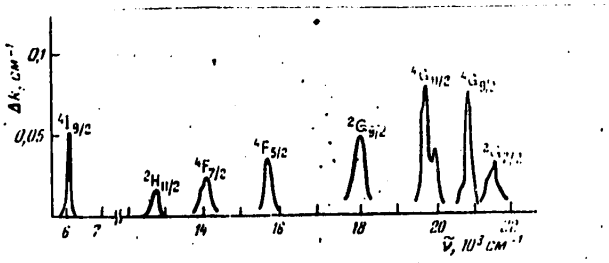

Figure 6.5. Induced absorption spectrum of the Er^{3+} ions from the $^4I_{13/2}$ level according to [361]. For transition to the $^4I_{9/2}$ level, the scale along the y-axis is dimished by twofold; for the transition to $^4G_{9/2}$ by tenfold.

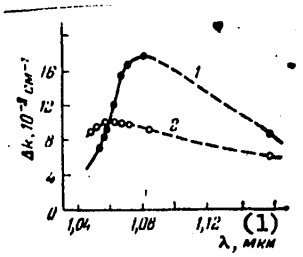

Figure 6.6. Spectrum of the induced absorption of Er^{3+} ions from the $^4I_{13/2}$ level in phosphate (1) and silicate (2) glass in the region of 1.05 to 1.15 microns; the absorped specific pumping energy is 5 joules/cm^3; $N_{Er} = 3 \times 10^{19}$ $см^{-3}$ [413].

Key: (1) microns

From this figure it is obvious that the pumping wavelength λ_{pump} comes at the edge of the long wave wing of the absorption band. The section of this wing of interest to us for a series of types of glass with identical concentration of Yb^{3+} ions ($1.5 \cdot 10^{21} cm^{-3}$) is presented in Figure 6.7 on an enlarged scale. As we shall see, the glass composition essentially determines not only the coefficient k_{pump}, but also another important characteristic--the slope of the spectral curve $dk_{pump}/d\lambda$ in the vicinity of λ_{pump} (§ 6.4). In Table 6.3 we have comparative data with respect to the magnitude of k_{pump} on $\lambda_{pump} = 1.055$ microns normalized to the concentration $N_{Yb} = 1,5 \cdot 10^{21}$ см$^{-3}$, in glass of different composition. Their analysis permits the conclusion to be drawn that the largest values of k_{pump} are characteristic of borate glass, which is connected both with the large oscillator strength of the transition $^2F_{7/8} \rightarrow {}^2F_{5/2}$ on the whole and with the higher relative intensity of the transition $^2F_{7/8}$ (4) $\rightarrow {}^2F_{5/2}$ (1) in these matrices. Unfortunately, the indicated glass is unsuitable as laser glass matrices with respect to other parameters. From Table 6.3 it is also obvious that the values of k_{pump} in phosphate glass exceed by one and a half times the values characteristic of silicate glass. Among the phosphate systems the variations of k_{pump} are insignificant. Germanium phosphate glass attracts attention by increased values of k_{pump}. In Figure 6.8 the relation is presented for k_{pump} as a function of the temperature of the sample, indicating that one way to increase k_{pump} is to increase the temperature within reasonable limits (by 50 to 70°C above room temperature).

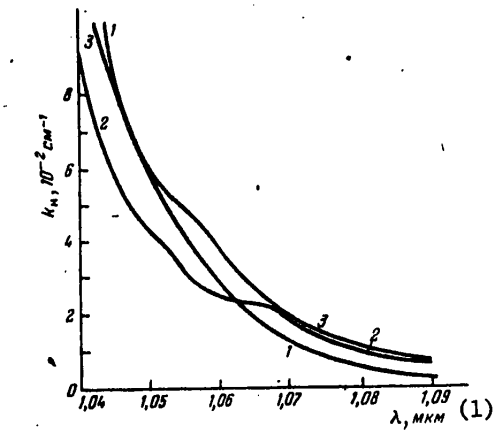

Figure 6.7. Spectral relations for the absorption coefficient k_{pump} of Yb^{3+} ions in the region of 1.04 to 1.09 microns in different glass. 1--Ba-Al-phosphate, 2--Na-K-La-Ba-silicate, 3--germanium phosphate.

Key: (1) microns

Table 6.3

Glass	k_{pump} (1.055 microns), $10^{-2}cm^{-1}$	W_{DA}, $10^{3}sec^{-1}$
Ba-Al-metaphosphate	6.0	11.0
Sr-Al-metaphosphate	5.9	10.8
Cd-Al-metaphosphate	5.9	10.7
Na-Mb-metaphosphate	5.0	10.5
Ba-La-metaphosphate	5.8	10.5
Ba-Pb-La-metaphosphate	5.0	12.6
K-Ba-Al-metaphosphate	5.9	10.7
Pb-La-ultraphosphate	6.8	10.8
Na-Mg-borophosphate	5.3	9.6
La-germaniumphosphate	5.3	12
Pb-La-germaniumphosphate	7.8	13
Fluophosphate	5.3	1.9
Pb-La-silicophosphate	5.0	8.2
LGS-E	6.0	10.9
Na-K-Ba-La-silicate	4.0	2.0
Ca-Li-Al-silicate (ED-2)	5.1	3.0
Ba-La-borate	9.8	18
Na-K-Ba-Al-germanate	4.5	2.9

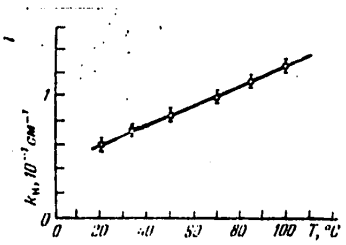

Figure 6.8. Absorption coefficient k_{pump} on λ_{pump} = 1.055 microns as a function of the sample temperature. Ba-Al-phosphate glass; $N_{Yb} = 1{,}5 \cdot 10^{21}$ см$^{-3}$.

The most important characteristics of erbium glass are, of course, the duration $\tau_{1\ Er}$ and quantum yield q_{Er} of the Er^{3+} ion luminescence. In earlier works [516, 517, 519], large scattering of the measured values of $\tau_{1\ Er}$ was noted in glass of different composition--from hundreds of microseconds to 15 milliseconds --which the authors explain by strong dependence on the structure of the vitreous matrices. However, in [193] we demonstrated that the quenching of the luminescence of Er^{3+} ions takes place primarily on vibrations of the OH-groups (see also § 3.4). Table 6.4 presents the data measured in this paper and also that of available in the literature on $\tau_{1\ Er}$ (in cases where low OH-group content is unquestioned). Values of q_{Er} which we estimated with respect to $\tau_{1\ Er}/\tau_{0\ Er}$ are also presented there ($\tau_{0\ Er}$ was determined using the known expression relating τ_0 to the integral absorption coefficient of the resonance band presented, for example, in [100]) and the values of q_{Er}^{calc} calculated or measured directly by other authors. When analyzing these data it must be considered that the decay times of the luminescence of Er^{3+} ions measured under ordinary conditions

can significantly exceed the true values of the luminescence lifetimes of $\tau_{1\ Er}$. The result of the measurements essentially depends on the configuration and the dimensions of the sample [193]. This fact is connected with reabsorption of the luminescence in the sample on the basis of resonance of the transition $^4I_{13/2} \rightleftarrows {}^4I_{15/2}$ combined with high quantum yield of the luminescence. The influence of these factors is illustrated by Figure 6.9 where concentration relations are presented for the true values of $\tau_{1\ Er}$ measured on powdered samples with a layer thickness of 500 microns and "ordinary" values obtained on samples 10x10x10 mm^3. As we shall see, for $\mathcal{N}_{Er} \geqslant 1 \cdot 10^{20}\ cm^{-3}$ in glass with high quantum yield, the measurement results can differ by 1.3 to 1.5 times in phosphate glass, and in fluophosphate glass, even by 1.7 times. In the published data of Table 6.4 this fact, as a rule, was not taken into account, and therefore the series of percentage values with respect to $\tau_{1\ Er}$ is explicitly high. The same thing must be said of values of q_{Er}. Whereas in germanate, fluoberyllate, fluophosphate and silicate glass the closeness of q_{Er} to one is unquestioned, in phosphate glass nevertheless $q_{Er} < 1$. This is indicated by our data on q_{Er} and

Table 6.4

Glass	$\mathcal{N}_{Er}$, $10^{19}\ cm^{-3}$	$\tau_{1\ Er}$, 10^{-3} sec	q_{Er}	q_{Er}^{calc}	Data Source
Na-K-Ba-Yb-silicate	2.3	14 *)	-	-	[312]
Silicate **)	4.7	13	-	1.0	[413]
K-Ba-silicate	4.5	13	-	0.97	[361]
Zn-Al-Yb-phosphate	-	9.0 *)	-	1.0 *)	[528]
Phosphate **)	3.0	8.4	-	1.0 *)	[413]
Fluophosphate **)	10	12 *)	-	1.0	[517]
Fluophosphate **)	6.8	8.0	-	1.0	[513]
Pb-germanate	10	5.5	-	1.0	[361]
Ca-Mg-Sr-Pb-Al-fluoberyllate	15	12.0 *)	-	0.96	[361]
Ba-Al-Yb-Phosphate	1-20	7.8	0.86		Data of the authors
LGS-E	0.35	7.7	0.88		The same
Na-Mg-phosphate	0.25	8.2	0.83	-	" "
Ba-La-borate	0.15	0.59	0.07	-	" "
Li-Ca-Al-silicate (ED-2)	0.33	12	1.0	-	" "
Na-K-Ba-Al-germanate	0.28	6.5	1.0	-	" "

*) The values are obviously high as a result of the influence of reabsorption.
**) The glass composition is not indicated.

also the calculation of the probability of MFR for Er^{3+} ions according to the results discussed in § 3.4. For phosphate glass the estimates give $\overline{W}^S \simeq 10\text{-}25\ sec^{-1}$ which corresponds to $q_{Er} = 0.8$ to 0.92. An indirect experimental confirmation of the difference of q_{Er} from 1 is also provided by the relations presented in Figure 6.9. They indicate that in phosphate glass the difference of the "ordinary" and true values of $\tau_{1\ Er}$ is less than in fluophosphate glass.

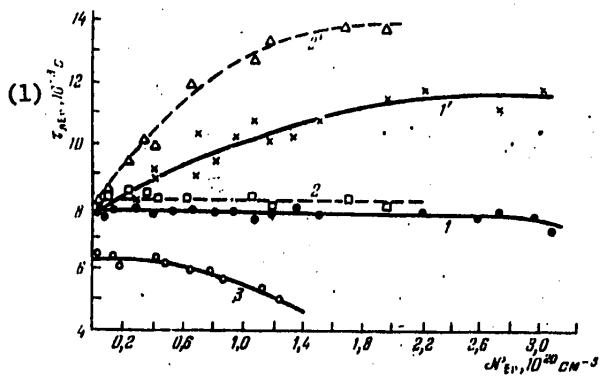

Figure 6.9. Concentration relations for the true values of $\tau_{1\ Er}$ (1, 2), and measured on samples with dimensions 10x10x10 mm^3 (1', 2', 3) for Ba-Al-phosphate (1, 1', 3) and fluophosphate (2, 2') glass at $N'_{OH} \leqslant 3 \cdot 10^{18}$ см$^{-3}$ (1, 1', 2, 2') and $N'_{OH} = 5{,}2 \cdot 10^{19}$ см$^{-3}$ (3).

Key: (1) $\tau_{1\ Er}$, 10^{-3} sec

The obvious reason for this is the smaller quantum yield. In phosphate glass with still lower q_{Er} ($\lesssim 0.6$ for $N'_{Er} \to 0$), concentration growth of $\tau_{1\ Er}$ is not observed in general as a result of introducing OH-groups for small N'_{Er}; but for high concentrations of Er^{3+} the value of $\tau_{1\ Er}$ begins to fall (curve 3), which is determined by the effect of excitation migration with respect to the Er^{3+} ions. The absence of the contribution of the latter to curves 1 and 1' confirms the intracenter nature of quenching.

Thus, the most probable value of q_{Er} in phosphate glass is about 0.9. Direct measurements that we performed by comparing areas under the luminescence decay curves of the samples made of fluophosphate and phosphate glass with $N'_{Er} \approx 0{,}6 \cdot 10^{20}$ см$^{-3}$ placed in the form of plates 500 microns thick under identical experimental conditions and excited by a short (t_{pump} = 35 nanoseconds) pulse of radiation of a neodynium laser (second harmonic) permitted direct determination of $q_{Er} = 0.88 \pm 0.2$.

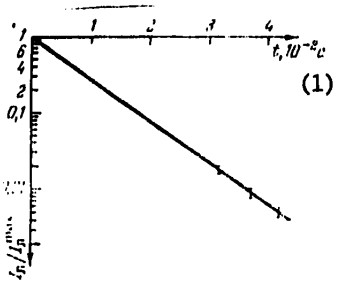

Figure 6.10. Standard form of the luminescence decay curve of Er^{3+} ions in phosphate glass with the composition $Ba_3Al(PO_3)_9$ taken in a large range of intensities.

$N'_{Er} = 1 \cdot 10^{19}$ см$^{-3}$;
$N'_{OH} \leqslant 3 \cdot 10^{18}$ см$^{-3}$; $d = 1$ мм.

Key: (1) seconds

The data presented in Figure 6.9 also indicate that the concentration quenching of the luminescence of the Er^{3+} ions noted in a number of papers [339, 361, 516, 517, 519] in carefully dehydrated glass founded from a pure charge is absent. It is also necessary to note that in phosphate erbium glass, the dispersion of the radiating probabilities of the transition $^4I_{13/2} \rightarrow {}^4I_{15/2}$ is weakly manifested, which is indicated by the exponential nature of the luminescence decay curve (Figure 6.10).

Thus, in the majority of vitreous materials in a wide range of concentrations the quantum yield of the luminescence of Er^{3+} ions can be close to one, and $\tau_{1\ Er}$, to the radiation value. Only borate glass, where quenching is highly significant on the matrix vibrations, constitutes an exception.

Values of the excitation lifetimes on higher excited states of Er^{3+} ions are also of theoretical interest for calculating the energy characteristics of erbium lasers. Insufficient deactivation rate of the $^4I_{11/2}$ level can limit the efficiency of the sensitization channel $Yb^{3+} \rightarrow Er^{3+}$ for high intensities of the pumping emission (§ 6.1), and also lead to the appearance of additional induced absorption of the pumping emission as a result of the transition $^4I_{11/2} \rightarrow {}^2H_{11/2}$. The efficiency of the multistage and cooperative processes of [245] and, consequently, the possible number of induced color centers of the glass which can significantly improve the level of inactive absorption on frequencies of ν_{pump} and ν_{lase} depend on the excitation lifetime on levels of $^4I_{9/2}$, $^4F_{9/2}$, $^4S_{3/2}$, and so on. Data on the excitation lifetimes on levels of $^4I_{11/2}$, $^4S_{3/2}$, and $^4F_{9/2}$ are presented in Figure 3.23. It is obvious from this figure that the excitation relaxation rates from these states are quite high. Borate and phosphate glass has predominance with respect to this parameter. In this glass, the values are equal to approximately $4 \cdot 10^7$, $1 \cdot 10^6$ and $3.5 \cdot 10^6$ sec^{-1}, respectively. For the $^4I_{9/2}$ level, the estimates give $\overline{W}^s > 10^8$ sec^{-1}. Thus, the quantum yield of the luminescence from these states in all types of glass is negligibly small which, along with the nature of the dependence of the probability of MFR on the energy gap between levels ΔE investigated in § 3.4, permits consideration of the results of the measurements of the quantum yield of the excitation relaxations from these states to the metastable state obtained in [517] to be considered incorrect inasmuch as [517] states that, as a rule, it is significantly less than 1. Inasmuch as the probability of MFR decreases sharply with an increase in ΔE, the excitation must unavoidably relax successively thrugh all intermediate states, including the metastable state.

The processes of nonradiating excitation energy transfer in the pairs Yb^{3+}-Er^{3+}, Nd^{3+}-Yb^{3+}, and Er^{3+}-Nd^{3+} and dependence of their efficiency on the glass composition were investigated in detail earlier (§ 3.3). Therefore we shall limit ourselves below to the presentation of some of the useful relations and tables. Figure 6.11 shows the standard relations for the parameters $\tau_{1\ Yb}$, $(\tau_{1\ Yb})^{-1}$ and q_{DA} as a function of the concentration of the Er^{3+} ions in phosphate glass measured for low excitation and concentration levels of the Yb^{3+} ions typical of laser glass. The concept of comparative efficiency of the BPV in various matrices with the same concentration $\mathcal{N}_{Yb}$ and $\mathcal{N}_{Er} = 3{,}5 \cdot 10^{19}$ $см^{-3}$ can be obtained

from Table 6.3 (the authors' data). As follows from this table, the largest values of w_{DA} for given concentrations are observed in borate and then in phosphate glass. In the latter, the quantum efficiency of the BPV is more than 0.9 already at $N_{Er} = (2 \text{ to } 2.5) \cdot 10^{19} \text{cm}^{-3}$. Within the limits of phosphate glass, the values of w_{DA} differ by no more than 1.3 times. With respect to efficiency these are also close to germanium phosphate glass which is attractive also because of its increased values of k_{pump}.

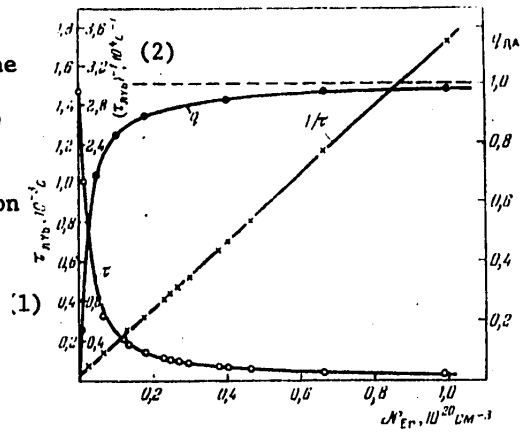

Figure 6.11. Standard relations for the duration of luminescence of Yb^{3+} ions ($\tau_{1\ Yb}$), the inverse duration ($1/\tau_{1\ Yb}$) and quantum efficiency of BPV (q_{DA}) as a function of the Er^{3+} ion concentration in phosphate glass; 300 K; $N_{Yb} = 1.5 \cdot 10^{21}$ см$^{-3}$.

Key: (1) $\tau_{1\ Yb}$, 10^{-3} sec
(2) $(\tau_{1\ Yb})^{-1}$, 10^{4} sec^{-1}

As was noted in § 6.1, in order to select the activator concentrations, it is extremely necessary to have information about the dependence of the efficiency of BPV in the pair Yb^{3+}-Er^{3+} on the excitation level. Figure 6.12 shows the functional relations that we obtained*) for the probability w_{DA} normalized by a value of w^0_{DA} characteristic of the lower excitation levels as a function of the relative population of the metastable levels $^4I_{13/2}$ for different concentrations of Er^{3+} ions. The measurements were performed by excitation of optically

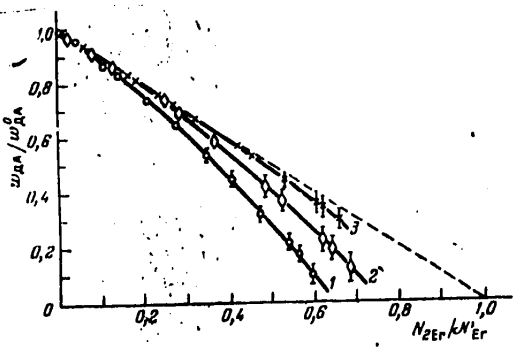

Figure 6.12. Relative rate of BPV in the pair Yb^{3+}-Er^{3+} as a function of the relative population of the metastable state of Er^{3+} ions.

Ba-Al-phosphate glass;

The dotted line is the calculated linear function.

*) The measurements were performed jointly with S.M. Matytsin.

thin samples by radiation pulses close to rectangular of a neodymium-doped phosphate glass laser (t_{pump} = 1.9 milliseconds, λ_{pump} = 1.055 microns) insuring an energy density on the surface of the sample to 500 joules/cm^2. The sample was secondarily excited 1 millisecond after the end of the pumping pulse by the pulse of another neodymium laser with duration of about 40 nanoseconds. The luminescence decay of the Yb^{3+} ions after the secondary excitation was recorded through a monochromator by a photomultiplier and it was recorded on the screen of a storing oscillograph with wideband logarithmic preamplifier insuring high quality logarithmization of two orders of signal intensity. The population of the metastable level was measured by monitoring the variation of the absorption coefficient of Er^{3+} ions based on the state in the band with maximum at 0.52 microns. As is obvious from Figure 6.12, for small concentrations $\mathcal{N}_{Er}$, an accelerated decrease in the value of w_{DA} is observed with an increase in the excitation level. With an increase in $\mathcal{N}_{Er}$ the function approaches linear because of a decrease in population of the ground state. This is promoted by the appearance of effective migration of the excitation energy in the subsystem of Er^{3+} ions. According to the estimate of $\overline{C}_{DD} \approx 30 \cdot 10^{-40}$ cm^6 sec^{-1} made in § 3.3, it is easy to calculate the average time in which an excitation jump takes place between the Er^{3+} ions. For $\mathcal{N}_{Er} = 1 \cdot 10^{20}$ см$^{-3}$, it is approximately 1.8 milliseconds, which is less than t_{pump}.

Table 6.5

Sensitizer	Transmission System	Data Source
Nd^{3+}	Nd^{3+}—Yb^{3+}—Er^{3+}	[528]
Cr^{3+}	Cr^{3+}—Er^{3+}	[361]
Mo^{3+}	Mo^{3+}—Er^{3+}; Mo^{3+}—Yb^{3+}—Er^{3+}	[330]
UO_2^{2+}	UO_2^{2+}—Er^{3+}; UO_2^{2+}—Nd^{3+}—Yb^{3+}—Er^{3+}	[323, 365]
Mn^{3+}	Mn^{3+}—Er^{3+}	[337]

The possible systems for the use of other sensitizers to increase the efficiency of erbium lasers proposed in various papers are presented in Table 6.5. The most prospective is the Nd^{3+}-Yb^{3+}-Er^{3+} system. However, complete use of it is interfered with, as has already been noted, by the inverse quenching of the luminescence of the Er^{3+} ions by the Nd^{3+} ions. In this pair the BPV was investigated in references [338, 339, 361, 517]. Quantitative estimates of the parameters of the elementary act of transfer are presented in § 3.3, where it is shown that the transfer in this pair, just as in others, is dipole-diplole, and for phosphate glass $\overline{C}_{DA} = 1 \cdot 10^{-40}$cm^6-sec^{-1}. Figure 6.13 shows the standard relation for phosphate glass of the magnitude of the characteristic time interval τ^e_{Er} for the static transfer during which the luminescence intensity decreases by e times with respect to the maximum as a function of the Nd^{3+} ion concentration. In practice this intensity coincides with the calculated value. From the figure it is obvious that for the Nd^{3+} concentration in the glass of more than $5 \cdot 10^{19}$ cm^{-3}, the duration and quantum yield of the luminescence of the Er^{3+} ions decrease. Other potential sensitizers of the Er^{3+} ions are much less efficient. The quantum yield of the luminescence of Cr^{3+} ions in glass is very small [361]. The quantum efficiency of the BPV for Mo, UO_2^{2+} and Mn^{2+}

ions exceeds 0.8 to 0.9 only for concentrations N_{Er} larger than $(2-3)\cdot10^{20}$ cm^{-3} [361]. The introduction of some of them (for example, UO_2^{2+}) into the glass is accompanied by an increase in the level of inactive absorption in the 1.5 micron range (as a result of the presence of other uranium forms) [246, 359].

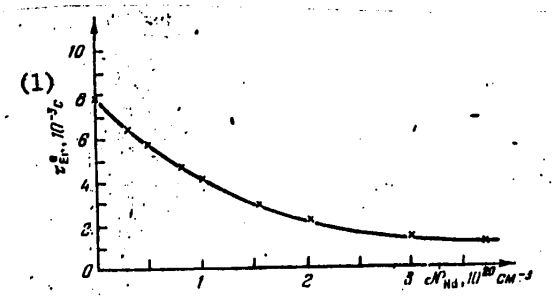

6.13. The effective energy transfer time of the excitation in the pair Er^{3+}-Nd^{3+} as a function of the Nd^{3+} ion concentration in the glass with composition $Ba_3Al(PO_3)_9$; $N_{Er} = 3\cdot10^{19}$ $см^{-3}$.

Key: (1) seconds

In conclusion, let us note that the studies that we made of the photochemical resistance of phosphate glass to solarization demonstrated that the laser emission with a wavelength of 1.055 microns at energy densities to 500 joules/cm^2 and a number of pulses to 10^3 does not lead to noticeable additional color of the glass. Concentration emission by the light of powerful pulsed xenon tubes is more dangerous. Therefore, the erbium elements operating in the ELL require filtration of the shortwave part of the pumping emission (see also [511]).

Thus, the performed analysis of the spectral luminescence characteristics of erbium glass confirms that phosphate glass has an optimal set of properties required for the creation of effective active material for ELL and ELP. These are similar only to germanium phosphate matrices, but the latter obviously are less adaptable to manufacture and contain an expensive component. At the present time the production of two high quality erbium laser glasses has been mastered by Soviet industry. Let us present the parameters of one of them, type LGS-E: $N_{Yb} = 1{,}5\cdot10^{21}$ $см^{-3}$, $N_{Er} = 3{,}5$; 6; $9\cdot10^{19}$ $см^{-3}$, $N_{OH} \leq 7\cdot10^{18}$ $см^{-3}$, $\tau_{1\,Er} \geq 7.6\cdot10^{-3}$ sec, $q_{er} \sim 0.9$, $\beta_{lase} \leq 1.5\cdot10^{-3}$ cm^{-1}, $\beta_{pump} \leq 2.0\times10^{-3}$ cm^{-1}, $k_{pump} \simeq 6\cdot10^{-2}$ cm^{-1}.

§ 6.3. Tube-Pumped Erbium Lasers

As has already been noted above (§ 6.1), the energy possibilities of ELL are highly limited. The basic efforts have been applied to improving them after the appearance of the first reports on obtaining the lasing effect in Na-K-Ba-silicate [514, 529], Li-Mg-Al-silicate [530] and fluophosphate [531] glass. Generalizing the conclusions of theoretical analysis of the energy characteristics of ELP to the case of ELL, it is possible to state that conditions 2) and 5) (6.14) in this case lose significance on the basis of the wideband nature of the pumping. On the contrary, condition 6) acquires decisive weight. In the given case this condition can be written in the form

$$\int_{\tilde{\nu}}^{\tilde{\nu}} I_{\text{п}}(\tilde{\nu})\, k_{\text{п}}(\tilde{\nu})\, d\tilde{\nu} \gg \frac{\mathcal{N}_{\text{Er}} + \Delta N_{\text{threshold}}}{2q^{\Gamma}_{\text{ДА}} t_{\text{pump}}} \quad \text{for} \int_{\tilde{\nu}}^{\tilde{\nu}} I_{\text{п}}(\tilde{\nu})\, d\tilde{\nu} = \text{const},$$
$$0 \leqslant t \leqslant t_{\text{п}}.$$

(1) (1) (1) (1)

Key: (1) pump
(2) Γ = lase

It is far from always possible to satisfy this relation fully on the basis of limited electric strength of the pumping tubes, especially for large-cross section active elements. From this condition we have two areas of improving the energy characteristics of ELL: selection of the compositions of the glass insuring minimum values of $\mathcal{N}_{\text{Er}}$ as a result of high efficiency of the BPV in the pair Yb^{3+}-Er^{3+} and finding means of improving the use coefficient of the emission of the pumping tubes.

Within the framework of the first area, a significant gain has been obtained from the transition to phosphate matrices realized for the first time in [528]. In such glass $\mathcal{N}_{\text{Er}} = (2.5\text{-}3)\cdot 10^{19}$ cm^{-3} is admissible. As an example let us present the characteristics of the ELL with active element 6.5 mm in diameter by 80 mm manufactured by us from LGS-E glass ($\mathcal{N}_{\text{Er}} = 1.5\cdot 10^{21}$ cm^{-3}, $\mathcal{N}_{\text{Yb}} = 3\cdot 10^{19}$ cm^{-3}) placed in a monomodular cylindrical quartz reflector and cooled by running heavy water (D_2O). The pumping tube of the IFP-800 type for the best matching with the Yb^{3+} ion absorption band operated under "soft" conditions, with current density of 1000 to 2000 amps/cm^2, which was achieved as a result of using a long pumping pulse ($\sim$ 4 milliseconds). The transmission coefficient of the output mirror was equal to 0.3, the resonator base was 300 mm. The lasing threshold in such a laser was reached for a pumping energy of $\simeq$ 350 joules, and for pumping energy of 1200 joules, 1.8 joules was emitted with a pulse duration of about 3.1 milliseconds. The lasing kinetics had ordinary peak structure with peak duration of 1 to 3 microseconds. In the case of Q-switching of the resonator by a rotating prism, with the exit mirror with R = 0.5 and pumping energy of 800 joules, a pulse was emitted with a duration of 30 nanoseconds and an energy of 0.5 joule.

A further decrease in $\mathcal{N}_{\text{Er}}$ would be possible by increasing $\mathcal{N}_{\text{Yb}}$ to the maximum admissible values of about $4\cdot 10^{21}$ cm^{-3}. However, the gain obtained in this case is approximately 1.5 times (§ 3.3), which is not so significant as to justify the difficulties connected with the negative effects on the radial uniformity of the pumping and the technological properties of the glass. In addition, in the Q-switching mode a further increase $\mathcal{N}_{\text{Er}}$ is generally inexpedient. The second area appears to be more prospective. At the present time several versions of increasing the efficiency of the use of pumping emission in ELL is proposed. The most radical of them is, as has already been noted above, introduction into the erbium glass of additional Nd^{3+} ions. A theoretical analysis in order to optimize the activator concentrations in the Nd^{3+}-Yb^{3+}-Er^{3+} is performed in reference [339]. Its authors have drawn the conclusion that it is expedient to introduce the Nd^{3+} ions into the glass in concentrations to $4\cdot 10^{20}$ cm^{-3}, compensating the decrease in $\tau_{1\,\text{Er}}$ accompanying this (§ 6.2) as a result of a decrease in the pumping pulse duration t_{pump}. As applied to the conditions of free lasing, it would be

possible to agree with this if the introduction of the Nb^{3+} ions were not accompanied by the introduction of additional inactive losses into the laser resonator on the lasing frequency which was not considered in [339]. According to our measurements, depending on the glass composition, these losses are (1.5 to 2.2)$\cdot 10^{-1}$ cm^{-1} for $\mathcal{N}_{Nd} = 1 \cdot 10^{20}$ cm^{-3}, which is highly significant, especially if we remember the small values of the cross section σ_{lase} (see also condition 3) in (6.14)). In the Q-switching mode the level of the inactive losses, as is known, has less influence on the lasing threshold and the efficiency, but the reduction of $\tau_{1\ Er}$ worsens the conditions of accumulation of the Er^{3+} ions in the metastable state, and therefore is extremely undesirable. For these reasons, in both operating modes of the ELL, obviously it is inexpedient to use $\mathcal{N}_{Nd} > (5-7) \cdot 10^{19}$ $см^{-3}$. The analogous conclusion is drawn in [361]. In [528], the optimal concentration of the Nd^{3+} ions is considered to be still less, approximately $2 \cdot 10^{19} cm^{-3}$. Their introduction into the glass even in such small quantity gave a gain in the lasing threshold by threefold. In this paper a study is made of the ELL with active element with dimensions of 4 mm in diameter by 76 mm made of Zn-Al-phosphate glass doped with Yb_2O_3 (15 percent by weight), Nd_2O_3 (0.2 percent by weight) and Er_2O_3 (0.5 percent by weight). With a pulse duration of the xenon pumping tube (4 mm in diameter) of about 6 milliseconds the lasing threshold was reached for a pumping energy of 95 joules, and at 350 joules in the free lasing mode, 0.86 joule was emitted (η = 0.25 percent). For Q-switching by a rotating prism and with pumping energy of 150 joules, a short pulse was obtained with duration of 25 nanoseconds and energy of 0.2 joule (η = 0.12 percent). Similar data were obtained later in other papers [85, 528, 533, 534].

Another way to improve the efficiency of using the pumping emission consists in placing reemitting shells around the active element. The active element itself in this case is made of glass activated only by Yb^{3+} and Er^{3+} ions. As the shell material most frequently Nd^{3+} and Yb^{3+} doped glass is used. A significant part of the emission of the latter falls inside the active element and is absorbed again by the Yb^{3+} ions. In [85] approximately double gain in radiation efficiency with respect to the active elements without the shell was achieved in this way. Inasmuch as the wall thickness of the shell must be as small as possible, highly concentrated neodymium glass with small additions of ytterbium are especially suitable for making the shells. Our estimates [534] demonstrated that such a shell 0.5 mm thick made of glass with the composition $KNd_{0.9}Yb_{0.1}P_4O_{12}$ increases the pumping use coefficient by 2 to 3 times. It is possible to obtain a still greater effect by applying an interference coating to the surface of the active element with reemitting shell reflecting the emission in the range of 0.95 to 1.1 microns and thus not emitting it from the active element. In reference [532] it is proposed that Mo^{2+} ions absorbing in the region of 0.36 to 0.55 microns and emitting in the region of 1.02 microns be used as the activator for the shell glass. However, nothing has been reported on the efficiency of this version. A study was also made of the possibility of making active elements by fusing a bundle of fibers consisting of glass activated by Yb^{3+} and Er^{3+} ions and shells made of Nd^{3+}-Yb^{3+}-glass [528]. A deficiency of such an element is increased radiation divergence (up to two angular degrees).

A prospective way to improve the output energy of an erbium laser is use of tubular elements, including with reemitting core, for example, made of Nd^{3+}-Yd^{3+}-glass [534]. Here it is possible to increase the transverse cross section of the active element without an increase in nonuniformity of pumping and therefore to match it with the large diameter pumping tube and, consequently, with high maximum emission energy. By using such elements with outside diameter of 14 mm, inside diameter of 8 mm and 120 mm long and optimizing the pulse duration and brightness temperature of the pumping source we were able to improve the radiation energy of the ELL to 4 joules in a pulse lasting 3.5 milliseconds and 1.5 joule for t_i = 40 nanoseconds.

An interesting possibility of improving the efficiency of ELL is connected with the application of interference dielectric coatings to the surface of the pumping tube emitting radiation only in the range of 0.89 to 1.05 microns. According to [543], in this way an increase in efficiency of the neodymium lasers by 1.5 to 1.7 times is achieved under certain pumping conditions as a result of partial transformation of the previously unused part of the pumping radiation to radiation in the spectral region of absorption by Nd^{3+} ions. For ELL absorbing in a narrow band, the effect of this transformation must be still more significant. This is indicated, in particular, by the smaller than expected lasing thresholds of erbium glass. For example, for ELL described at the beginning of the section, when $N_{Er} = 3 \cdot 10^{19}$ cm^{-3} the threshold absorbed specific pumping energy reduced to $\tilde{\nu}$ = 10,000 cm^{-1} must be more than 3 joules/cm^3. Such values are observed in ELP (see below, § 6.4), where they can be measured exactly. Consequently, for electric threshold pumping energy of 350 joules input to the pulse tube and for a volume of the active element of about 2.7 cm^3, an efficiency with respect to stored energy of more than 2.5 percent is realized. For ELL this is a very high value, and it indicates the partial transformation of the initially unused emission of the pumping tube, but then reabsorbed by the discharge plasma, to the emission falling in the absorption band of the Yb^{3+} ions. On application of interference coatings, this effect can be intensified significantly. An analogous result can be expected from the application of cavity pumping tubes. In the case of neodymium lasers they turn out to be less efficient than rod lasers on the basis of lower brightness temperature of the plasma and greater reabsorption of the pumping emission by the discharge plasma. For ELL, these deficiencies are surpassed by the advantages. In addition, the cavity tubes permit greater energy densities of pumping.

Along with the energy characteristics, the spectral characteristics of ELL emission are of great interest. In the first reports it was pointed out that the ELL based on silicate glass emit on a wavelength of 1.543 microns [312], and on phosphate glass, on λ_{lase} = 1.536 microns [528]. The reason for this is the differences in the form of the luminescence band of the Er^{3+} ions in this glass (§ 6.2). In silicate glass the relative intensity of the transition to the second Stark component ($\Delta E \simeq 26$ cm^{-1}) of the $^4I_{15/2}$ level is appreciably higher than in phosphate glass. Later, it was demonstrated that the lasing wavelength of the ELL in both cases depends on the reflection coefficient of the output mirror, the tuning accuracy of the resonator and the temperature of the laser element [510, 511, 533]. With high Q-factor of the resonator, lasing occurs on λ_{lase} = 1.543 microns, with low Q-factor, on λ_{lase} = 1.536 microns. In some cases (for example, blind mirrors) it is possible to observe lasing even in the range of 1.61 and 1.57 microns [361] with respect to the quasifour-level system ($\Delta E \approx 330$ cm^{-1}), although the efficiency of this lasing

is naturally low as a result of the small cross sections of the induced emission of Er^{3+} ions in this region and the presence of induced absorption (the transition $^4I_{13/2} \rightarrow {}^4I_{9/2}$). The width of the lasing spectrum is approximately 17 cm^{-1} for λ_{lase} = 1.543 microns and about 6 cm^{-1} for λ_{lase} = 1.536 microns.

On the whole, it must be noted that the energy and spectral characteristics of ELL have been investigated explicitly insufficiently. A more careful study will obviously help to reveal significant reserves for improvement of them. The application of ELL is primarily expedient where it is necessary to have emission in the spectral range of 1.5 microns or where the shorter wave emission presents a real danger for the eyes [537, 509]. The report was made on the development on the basis of ELL of a number of range finders and locators [85, 544, 510]. In [545] a description is presented of ELL developed for measuring the height of the lower bound of the cloud cover. It emitted pulses with 35 nanosecond duration and a power of 1 megawatt with a divergence of 10 milliradians. The reflected signal was received by an avalanche germanium photodiode. The range of the instrument was more than 10 km. Among the prospective areas of application it is also necessary to note scientific research, for example, spectroscopy [538] and also medicine. In [539] a report is presented on the successful experiments in treating diseases of the cornea of the eye using ELL.

§ 6.4. Erbium Laser Reemitters. Free Lasing Mode

Along with the search for new, more efficient compositions of erbium glass and optimization of the concentrations of the activators, the creation of the efficient ELP is connected with the solution of the nontrivial problem of optical coupling of the pumping laser to the erbium active elements. Let us consider some significant aspects of this problem. One of them consists in the necessity for simultaneous satisfaction of two, usually mutually exclusive requirements: 1) the pumping emission must be completely absorbed in the erbium active element; 2) the latter must be uniformly excited with respect to the entire operating volume. In order to satisfy the first of them, the active element must correspond to an optically thin element, and to satisfy the second, an optically dense layer with respect to the pumping radiation. However, these requirements can be combined if the active element is placed inside the resonator of a neodymium pumping laser. In this case the erbium active element plays the role of the useful load of this resonator, replacing the output mirror and, consequently, the losses introduced by it must be optimized in order to insure maximum efficiency of the neodymium pumping laser during operation on such a load. It is obvious that for this purpose the following relation must be observed:

$$\underset{(1)}{k'_{н}} = \frac{k_{н} l_{н}}{L} \gg \beta_{Nd} + \underset{(1)}{\beta_{н}} \frac{\underset{(1)}{l_{н}}}{L}, \qquad (6.15)$$

Key: (1) pump

where β_{Nd} and β_{pump} are the coefficients of inactive losses on the pumping frequency, respectively, in the neodymium and erbium active elements, L and L_{pump} are the lengths of the neodymium and erbium active elements along the pumping path and K'_{pump} is the coefficient of useful losses in the resonator of the

neodymium laser introduced by erbium active elements. For the available values of β_{pump}, $\beta_{Nd} \leqslant 1 \cdot 10^{-3}$ cm^{-1}, we obtain $k'_{pump} \leqslant 1 \cdot 10^{-2}$ cm^{-1}. Hence, it is possible to determine the minimum length of the erbium active element. For example, for a standard length of the neodymium active element, L = 600 mm and k_{pump} = 0.05 cm^{-1}, the length of the erbium active element must be no less than 120 mm. Here 45 percent of the pumping energy is absorbed in it in one pass or the density of the excited particles at the output of the active element for its location outside the resonator is two times less than at the entrance. In the case of intraresonator location, these values differ by no more than 20 percent. It is possible to obtain still greater uniformity (≤ 5 percent) on placing two neodymium elements in the resonator symmetric with respect to the erbium active elements (see below, 6.17).

A second aspect of the problem of coupling is connected with conditions 5) and 6) from (6.14) for the satisfaction of which in the free lasing mode, as was pointed out above, pumping emission energy densities in the erbium active element are required on the order of 500 to 700 joules/cm^2. These values are appreciably higher than those ordinarily realized in neodymium laser cavities (80 to 300 joules/cm^2). Consequently, the pumping emission beam inside the erbium active element must also be pinched. This is done most simply by using a lense telescope, but the introduction of the latter into the cavity is connected with the appearance of significant additional losses. The analysis that we made of various versions of increasing the pumping density demonstrated that the optimal version is to make erbium active elements in the form of special prisms, the geometric shapes of which in different versions are illustrated in Figure 6.14 [247, 515]. In elements of this type the pumping emission

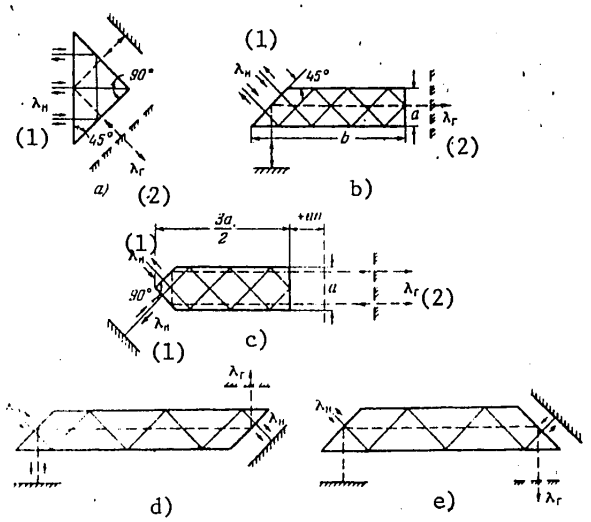

Figure 6.14. Various versions of the geometry of active elements of ELP for free lasing mode insuring optical coupling of the active element to the radiation beam of the pumping source and beam concentration.

Key: (1) lase (2) pump

density is twice the radiation density at the entrance as a result of several total internal reflections of the pumping beam from the side faces on which it is incident at an angle of 45°. An important problem of spatial separation of the lasing and pumping beams is solved simultaneously, and autocompensation of the nonuniformity of the pumping radiation density with respect to cross section of the beam at the entrance of the erbium active element and uniform energy pickup of the stored energy from the entire excited volume are also insured. Prisms of the type of a and b also satisfy the function of one of the mirrors of the pumping laser. The selection of the indicated versions is dictated by the required output energy of the ELP, the volume of the active medium and the possibilities of neodymium pumping lasers. The set of working faces, which complicates cooling of the active elements, high requirements on accuracy of their optical processing and the necessity for using neodymium active elements of rectangular cross section for pumping constitute the deficiencies of the indicated shapes.

Finally, a third aspect of the coupling problem is connected with the selective nature of loading introduced by erbium active elements into the neodymium laser resonator. For the last laser the threshold condition is defined by the relation

$$\underset{(2)}{\alpha_r}(\lambda) = \frac{[k_{\text{II}}(\lambda) + \beta_{\text{II}}]\, l_{\text{II}}}{\underset{(1)}{l}(1)} + \beta_{\text{Nd}}, \qquad (6.16)$$

Key: (1) pump
(2) lase

where $\alpha_{\text{lase}}(\lambda)$ is the gain of the active medium of the neodymium pumping laser on a wavelength of λ_{pump}. For $k_{\text{pump}} \gg \beta_{\text{pump}}$ and $k_{\text{pump}} l_{\text{pump}}/L \gg \beta_{\text{Nd}}$ we obtain

$$\underset{(2)}{\alpha_r}(\lambda) = \underset{(1)}{k'_{\text{II}}}(\lambda). \qquad (6.17)$$

Key: (1) pump
(2) lase

Figure 6.15 shows the relations $\alpha_{\text{lase}}(\lambda)$, $k'_{\text{pump}}(\lambda)$ and $k''_{\text{pump}}(\lambda)$ for active elements of the pumping laser and ELP made of phosphate glass. Inasmuch as the steepness of the function $k'_{\text{pump}}(\lambda)$ is greater than the steepness of the long-wave wing of the amplification curve, the condition for the beginning of lasing of a neodymium laser is satisfied primarily in the region of 1.07 to 1.08 microns. Thus, a shift of the pumping laser emission wave to this region must be observed, which is extremely undesirable, for it would lead to a sharp decrease in energy absorbed in the ELP element and to a decrease in the efficiency of the neodymium laser itself. Experimental studies of the emission spectrum of the pumping laser confirmed that the lasing frequency shift actually occurs. If under a load on the flat dielectric mirror with R = 0.5, the lasing spectrum width did not exceed 10 Å, and the center was located at 10,545 Å, then in the given case the lasing spectrum was broadened by approximately 200 Å (10,540 to 10,750 Å). Lasing began in the region of 10,750 Å, and then gradually shifted to the maximum of the luminescence band. This shift can be explained if we consider that as the ER^{3+} ions are accumulated in the metastable state, the

level of the induced absorption in the pumping region also increases, and its dependence on the wavelength is inverse to the dependence of k'_{pump} on λ (Figure 6.6). Analogous broadening of the lasing spectrum was observed by the authors of [535]. In order to improve the operating efficiency of the ELP it is necessary to take additional measures to stabilize λ_{lase} at the maximum of the amplification curve. This can be achieved if we introduce an element with inverse dispersion $k''(\lambda)$ into the resonator (Fibure 6.15, b, c). Here full compensation of k'_{pump} is not required, and it is sufficient to satisfy the condition

$$\frac{d\left[k'_{\text{н}}(\lambda)+k''(\lambda)\right]}{d\lambda} < \frac{d\alpha_{\text{г}}(\lambda)}{d\lambda}. \qquad (6.18)$$

Key: (1) pump
(2) lase

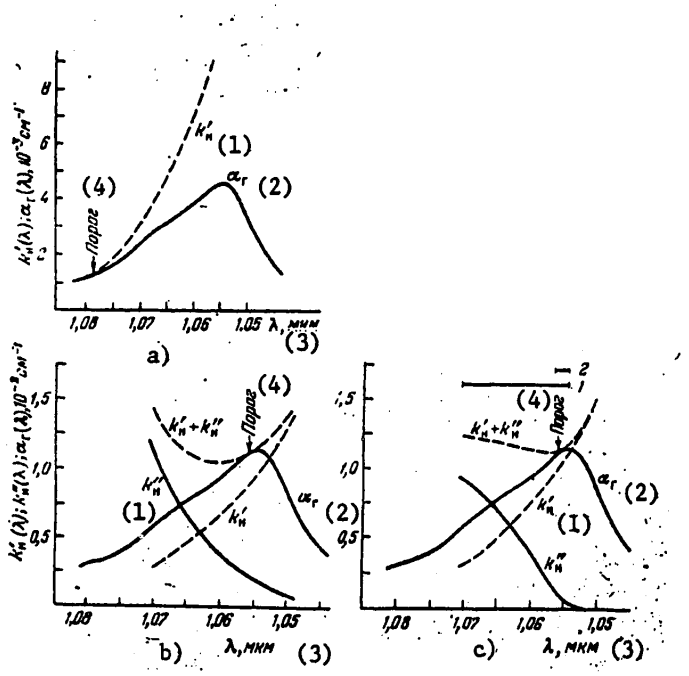

Figure 6.15. Spectral relations in the region of 1.05 to 1.08 microns of the gains $\alpha_{lase}(\lambda)$; $k'_{pump}(\lambda)$, $k''_{pump}(\lambda)$ are the losses in the resonator of the pumping laser introduced by absorption of the Yb^{3+} ions in the active element of the ELP and additional elements compensating the dispersion, respectively. a) Compensating element absent; (b) compensation using the glass plate activated by Sm_2O_3, 5 percent by weight ($k''_{pump} = \sigma_{Sm} N_{Sm}$); c) compensation using selective dielectic mirror ($k''_{pump}(\lambda) = \frac{1}{2L}\ln\frac{1}{R(\lambda)}$). The segments of a straight line at the top indicate the width of the lasing spectrum without compensation (1) and with compensation (2).

Key: (1) H = pump
(2) Г = lase
(3) microns
(4) threshold

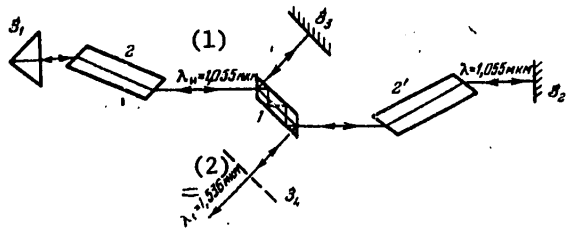

Figure 6.16. Diagram of an erbium converter with intraresonator symmetric excitation of the erbium element [247]. 1--erbium active element; 2,2'--neodymium active element; $З_1$, $З_2$--neodymium resonator mirrors; $З_3$, $З_4$--erbium resonator mirrors.

Key: (1) λ_{pump} = 1.055 microns
(2) λ_{lase} = 1.536 microns

Figure 6.16 shows one of the optical systems of ELP with intraresonator location of the erbium active element [101, 247] which we investigated. The latter was made of phosphate glass type LGS-E containing $N_{Yb} = 1.5 \cdot 10^{21}$ cm^{-3} and $N_{Er} = 2.5 \cdot 10^{19}$ cm^{-3} ($k_{pump} = 6 \cdot 10^{-2}$cm^{-1}, $\beta_{pump} \leqslant 2 \cdot 10^{-3}$cm^{-1}, $\tau_{1\ Er} = 9.0 \cdot 10^{-3}$ sec), in the form of a prism with side faces beveled at angles of 45°±5". The pumping radiation was introduced into it normally to one of the beveled faces and, undergoing several total internal reflections, it exited through the opposite face. The length of the erbium active element with respect to the pumping channel was 12.8 cm. The pumped volume was $\approx$ 8.2 cm^3. The resonator of the pumping laser consisted of a prism $З_1$ and dielectric mirror $З_2$ and also two active elements made of phosphate neodymium glass LGS-I made in the form of rectangular plates 2 and 2' with dimensions of 10x32x280 mm^3 and ends beveled at the Brewster angle arranged symmetrically with respect to the erbium active element. The base of the pumping resonator was 150 cm. The ELP resonator with base $\approx$ 20 cm was made up of flat dielectric mirrors $З_3$ (R = 1) and $З_4$ (R = 0.6). The pumping pulse duration $t_{pump} = 1.6 \cdot 10^{-3}$ second.

Two methods of compensation of $k'_{pump}(\lambda)$ were used. In the first method, a plane parallel plate of Sm_2O_3 pumped glass (5 percent by weight)was placed in the resonator at the Brewster angle to its axis. By selecting its thickness, it was possible to stabilize λ_{pump}, but the laser efficiency was reduced by 10 to 15 percent as a result of introducing additional losses into the resonator at the lasing frequency (Figure 6.15, b). The second method gave better results. A dielectric mirror with reflection band selected so that R (1.54 microns) = 0.95, and R (1.070 microns) = 0.45 (Figure 6.15, c) was made. In this case no noticeable decrease in pumping laser efficiency was observed. In both bases the lasing spectrum remained twice as wide as with a flat mirror, and it occupied an interval of 1.054 to 1.056 microns.

Measurements of the energy characteristics of this ELP demonstrated that the threshold absorbed specific pumping energy is 5.3 joules/cm^3, the lasing energy is about 40 joules with triple excess over threshold. The standard dependence

of the lasing energy ($\mathcal{W}_{lase}$) on the specific pumping energy absorbed in the erbium active element ($\mathcal{W}_{abs}$) is presented in Figure 6.17. From this relation it is possible to determine the differential efficiency of the ELP, reaching 30 percent. With somewhat altered resonator layout and greater pumping duration and excess over the threshold, the lasing energy of about 80 joules in a pulse with a duration of 3.5 milliseconds was achieved later with differential efficiency of about 39 percent and radiation divergence of $3 \cdot 10^{-4}$ rad [515]. The lasing spectra consisted of three lines: 1.536 microns with $\Delta\tilde{\nu}_{lase} = 7$ cm^{-1}, 1.543 microns with $\Delta\tilde{\nu}_{lase} = 7.5$ cm^{-1} and 1.538 microns with $\Delta\tilde{\nu}_{lase} = 6$ cm^{-1}. With a pumping density of $\approx$ 700 to 800 joules/cm^2, local deterioration of the glass of the erbium active elements with respect to platinum inclusions was observed.

Attention is attracted by the small divergence of the lasing emission achieved without the application of any special measures with a short resonator base and small cross section of the lasing beam of the ELP (about 1.4 cm^2). This is promoted by high uniformity of excitation and low specific heat release, which are distinguishing features of ELP.

In references [413, 535], a study was made of the extraresonator system of the ELP (Figure 6.18). A phosphate glass laser with active elements 45 mm in diameter by 620 mm (λ_{pump} = 1.543 microns) was used as the neodymium pumping laser. In order to increase the pumping density, a telescopic system 2 with multiplicity of about 4 was used. The pumping was done through the end of the ELP element (3) at an angle of approximately 20' to the axis of the ELP resonator. The latter was formed by the prism 4 and the flat mirror 5 with R = 0.2 to 0.8. The length of the resonator of the erbium laser was about 150 cm. The pumping pulse duration was $(2 \text{ to } 2.5) \cdot 10^{-3}$ seconds. The erbium active element was made of phosphate glass with the following parameters: $\mathcal{N}_{Yb} = 2{,}2 \cdot 10^{21}$ cm^{-3}, $\mathcal{N}_{Er} = 3 \cdot 10^{19}$ см$^{-3}$, $k_{pump} = 0.054$ cm^{-1}, $\tau_{1\ Er} = 7.5 \cdot 10^{-3}$, $\beta_{lase} = 0.006$ cm^{-1}. Under such conditions with absorbed specific pumping density equal to 31 joule/cm^3, a conversion efficiency was achieved which is equal to 35 percent, and the differential efficiency was 43 percent with a specific energy pickup of about 11 joules/cm^3, total emission energy of 27 joules (through a 5 mm iris) and divergence of 2.6'. The use of higher pumping densities led to the

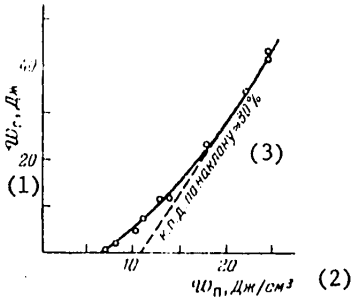

Figure 6.17. Standard dependence of the lasing energy $\mathcal{W}_{lase}$ of ELP in the free lasing mode on the specific pumping energy absorbed in the active elements, $\mathcal{W}_{abs}$ in the diagram with intraresonator location of the erbium active element.

Key: (1) $\mathcal{W}_{lase}$, joules
(2) $\mathcal{W}_{abs}$, joules/cm^3
(3) Efficiency with respect to slope $\approx$ 30 percent

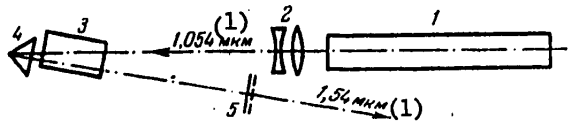

Figure 6.18. Diagram of an erbium ELP with active element outside the resonator [413].

1--Neodymium laser; 2--telecope; 3--erbium active element; 4--rectangular reflector prism; 5--output mirror.

Key: (1) microns

appearance of local damage to the investigated glass. The integral brightness of the emission of the ELP is almost an order greater than the brightness of the emission of the pumping neodymium laser. The emission spectrum consists of two spectral components with peaks at 1.536 and 1.545 microns, 8 and 16 cm^{-1} wide, respectively.

Thus, the performed experiments demonstrated that the ELP permit not only creation of laser sources in the region of 1.5 microns with good energy characteristics, but even an increase in the limiting values of the specific energy pickup from the active element (to 10 to 20 joules/cm^3) and integral brightness of the radiation to levels that are record levels for lasers in general, which opens up the prospects for their use in powerful laser systems. At the same time, a number of factors were discovered which prevent the achievement of maximum operating efficiency of the ELP in the free lasing mode. Above all, these include the following factors:

1) Extremely high required pumping emission densities (to 1000 joules/cm^2) commensurate with the radiating strength of the glass and complicating the problem of optical coupling of the ELP and the pumping lasers; 2) the necessity for operation with minimum possible concentrations of Er^{3+} ions, which does not permit insurance of sufficient efficiency of the excitation energy transmission in the pair Yb^{3+}-Er^{3+}, especially for high excitation levels; 3) relatively small cross section of the laser transition $^4I_{13/2} \rightarrow {}^4I_{15/2}$ which significantly increases the requirements on the level of inactive losses and the optical quality of the glass; 4) the presence of induced absorption on the lasing frequency.

The indicated difficulties are softened to a significant degree on using ELP in the lasing mode and on amplification of short (KI) and supershort (SKI) pulses.

§ 6.5. Possibilities of the ELP Under Lasing and Amplification Conditions of KI [Short Pulses] and SKI [Supershort Pulses]

In § 6.1 it was already noted that erbium glass is an almost ideal medium for amplification of KI and SKI. This fact was first indicated in [513]. The advantages of the erbium medium consist primarily in high quantum yield and

large values of $\tau_{1\ Er}$ permitting easy realization of the pumping mode $t_{pump} \ll \tau_{1\ Er}$. Low values of σ_{Er} are also favorably felt in the accumulation of the energy in the metastable state of $^4I_{13/2}$. As is known, (see, for example, § 5.3), neodymium glass corresponds to the requirements on the active medium for amplification of the KI and SKI to a much lesser degree, which causes a sharp decrease in their efficiency on transition to this operating mode.

Other advantages of ELP follow from the laser method of its excitation. Already for reasonable pumping radiation density of 400 joules/cm^2 it is possible to excite up to $1.0 \cdot 10^{20}$ Er^{3+} ions in one cm^3, which corresponds to a specific stored energy of $w_{stored} \approx 13$ joules/cm^3, exceeding by more than an order the value of w_{stored} in power amplifiers with large aperture based on neodymium glass and, the more so in gases. The optimal operating concentrations of Er^{3+} ions in the given case are $(6\text{-}10) \cdot 10^{19}$ cm^{-3}, which insures high excitation transmission efficiency in the Yb^{3+}-Er^{3+} pair (to inversions of $\Delta N/N_{Er} \geq 0{,}8$). For the indicated inversions, the gains up to 0.3 to 0.6 cm^{-1} become realistic, which permits a sharp decrease in the total length of the active elements in the amplifying channel and manufacture of elements of individual stages in the form of plates with l_{lase} = 2-3 cm, insuring, nevertheless, a gain K_0 in each of them for the weak signal of 3 to 6 times in one pass. In neodymium large cross section active elements, a value of l_{lase} of at least 20 to 40 cm is required to achieve such a gain. It is also known [540] that breakdown of the active elements into thin spatially separated discs (plates) significantly increasing the selffocusing thresholds and, consequently, the beam strength of the glass. In addition, the distortions of the wave front of the emitted radiation occurring as a result of thermal deformations decrease. Amplifiers based on ELP in this respect have unquestioned advantages over neodymium glass amplifiers for they permit easy solution of this problem without an extraordinary increase in the number of discs and the length of the amplifying channel as a whole. An important circumstance also is the smaller value of the index of refraction in the region of 1.5 microns and, obviously, its nonlinear component. In addition, it is highly significant that erbium active elements have almost unlimited "field of view," which permits use without any difficulties of diverging beams with any angle of aperture, full realization of the possibilities of multipass and telescopic amplifiers [541, 542] and also pickup of the maximum proportion of the excitation energy stored in the active element (which is especially urgent in the case of SKI) by passing several beams in series through it or one beam several times at different angles to the plane of the active element. Let us also note the simplicity of the effective suppression of superluminescence in the active elements. For this purpose it is sufficient to leave the peripheral parts of the active elements unexcited.

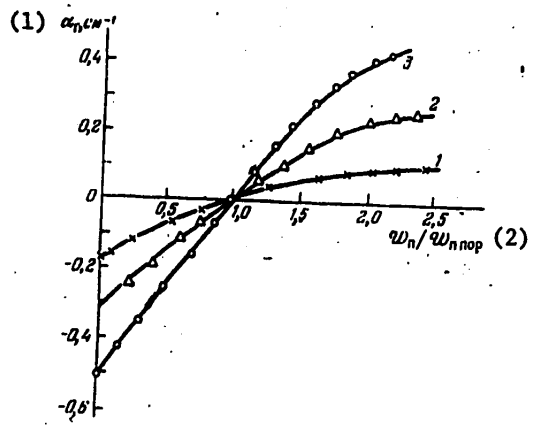

Figure 6.19. Experimental dependence of the gain α_{lase} on the specific absorbed pumping energy W_{abs} normalized by W absorbed threshold, in LGS-E glass.

$N_{Yb}=1,5\cdot10^{21}$ см$^{-3}$; $N_{Er}=3\times10^{19}$ (1), $5,2\cdot10^{19}$ (2), $8,6\times10^{19}$ см$^{-3}$ (3).

Key: (1) α_{lase}, cm^{-1}

(2) $w_{abs}/w_{abs\ threshold}$

In § 6.4, other advantages of the ELP have already been noted--low specific heat release and high uniformity of excitation, which permits simplification of the problem of achieving diffraction divergence of the radiation and also an increase in the repetition frequency of the amplified pulses. It is also important that in a neodymium pumping laser the tubes can operate under lighter conditions than in neodymium amplifiers, consequently, with high reliability. The theoretical analysis made by us [515] shows that in the amplification mode of short pulses at $t_n \geqslant 10$ nanoseconds, values of $\eta \simeq 0.15$-0.2 are entirely attainable; thus, the efficiency of the neodymium laser of about 3 percent can be counted on for a total efficiency of up to 0.4 to 0.6 percent.

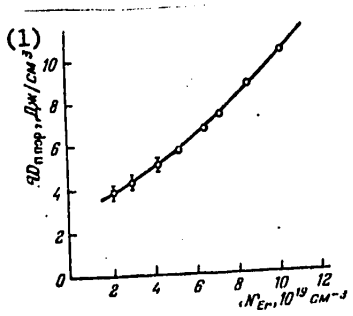

Figure 6.20. Experimental dependence of the specific absorbed pumping energy $W_{abs\ threshold}$ corresponding to the threshold of achievement of inversion as a function of the Er^{3+} ion concentration in LGS-E glass; $N_{Yb}=1,5\times10^{21}$ см$^{-3}$.

Key: (1) $W_{abs\ thresh}$, joules/cm^3

Figure 6.19 shows the experimental dependence of the gain of an erbium active element made of LGS-E phosphate glass with different erbium ion concentrations as a function of the relative magnitude of the absorbed specific pumping energy. The measurements were performed by sounding the active layer 5 cm thick uniformly excited by an external converging beam of neodymium laser emission (t_{pump} = 0.8 milliseconds), by a short pulse from the external ELL with Q-switching (the delay with respect to the beginning of pumping is about 1.0 millisecond). As we see, for small $\mathcal{N}_{Er}$ the investigated relation is nonlinear in a large range of values of $\mathcal{W}_{abs}/\mathcal{W}_{abs\ thresh}$. On the other hand, for $\mathcal{N}_{Er} = 8.6 \cdot 10^{19} cm^{-3}$, it is linear to values of α_{lase} = 0.26 to 0.3 cm^{-1}, which corresponds to a level population of $^4I_{13/2}$ of approximately $7 \cdot 10^{19} cm^{-3}$. The obtained maximum value of $\alpha_{lase} = 0.44\ cm^{-1}$ is not limiting. For large $\mathcal{N}_{Er}$ and $\mathcal{W}_{abs}$ it can reach up to 1 cm^{-1}.

The threshold specific absorbed pumping energy as a function of the erbium ion concentration in the glass is illustrated in Figure 6.20. From this relation it follows that for small $\mathcal{N}_{Er}$ the value $\mathcal{W}_{abs\ thresh}$ is somewhat higher than expected for $q_{DA}^{lase} \to 1$. These data agree with the results presented in Figure 6.12, and they independently confirm the contribution of the accelerated decrease in probability of BPV in the pair Yb^{3+}-Er^{3+} as the Er^{3+} ions are accumulated in the metastable state with low concentration of them in the glass.

The lasing characteristics of the ELP in the Q-switching mode will be illustrated in the example of the system used earlier to obtain free lasing (Figure 6.16). When using a rotating prism, output mirror with R = 0.5 and specific pumping energy of about 9.5 joules/cm^3, this ELP emitted 5.1 joules per pulse with 30 nanosecond duration.

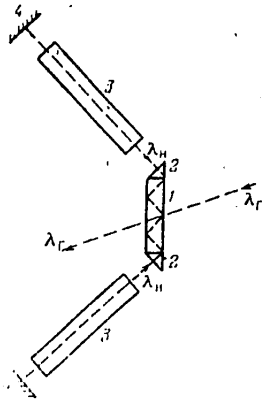

Figure 6.21. One version of the optical system of the power amplification stage for KI and SKI based on ELP.

1--erbium active element, 2--90° prism of erbium glass, 3--neodymiun active element, 4--selective dielectric mirrors.

Figure 6.21 shows one of the possible versions of the optical system of the output stage of a power amplifier based on ELP. The erbium active element is made in the form of a plate 14.1 mm thick and 60 mm long, on the two lateral faces of which 90 degree prisms made of glass of the same composition activated only by erbium ions in a concentration of $2 \cdot 10^{20}$ cm^{-3} are seated on a deep optical contact. Emission from two symmetrically arranged plates 20 mm thick made of neodymium glass which are placed in a common resonator with the erbium

active element is introduced through the indicated prisms into the active element. The manufacture of these prisms from glass with Er^{3+} permits efficient suppression of spurious lasing on the internal modes. It is obvious that the amplified beam of radiation can be transmitted at any angle of incidence with respect to the working planes of the active elements. The degree of nonuniformity of distribution of the inverse population in it does not exceed 5 percent. The total stored energy depends on the width H of the excited part of the active element and the erbium ion concentration. For example, for H = 60 mm and $\mathcal{N}_{Er}^{-} = 8.6 \cdot 10^{19}$ cm^{-3}, it can reach 500 joules. The amplifying characteristics of the active element are analogous to those presented in Figure 6.18, that is, the gain per pass on incidence of the beam at the Brewster angle will be about two.

BIBLIOGRAPHY

1. Bete, G., KVANTOVAYA MEKHANIKA [Quantum Mechanics], Moscow, Mir, 1975.

2. Sviridov, D. T.; Sviridova, R. K.; Smirnov, Yu. F., OPTICHESKIYE SPEKTRY IONOV PEREKHODNYKH METALLOV V KRISTALLAKH [Optical Spectra of Transition Metal Ions in Crystals], Moscow, Nauka, 1976.

3. Mikaelyan, A. L.; Ter-Mikaelyan, M. L.; Turkov, Yu. G., OPTICHESKIYE GENERATORY NA TVERDOM TELE [Solid-State Lasers], Moscow, Sov. radio, 1967.

4. Belostotskiy, B. R.; Lyubavskiy, Yu. V.; Ovchinnikov, V. M., OSNOVY LAZERNOY TEKHNIKI [Fundamentals of Laser Engineering], Moscow, Sov. radio, 1972.

5. Buzhinskiy, I. M.; Mamonov, S. K.; Mikhaylova, L. I., ZHPS [Journal of Applied Spectrometry], Vol 15, 1971, p 229.

6. NEODNORODNOYE USHIRENIYE SPEKTRAL'NYKH LINIY AKTIVNYKH SRED OKG [Nonuniform Broadening of Spectral Lines of the Active Media Lasers], Kiev, IF AN USSR, 1969.

7. Godenko, L. P.; Mashkevich, V. S., VVEDENIYE V KVANTOVUYU ELEKTRONIKU SPEKTRAL'NO NEODNORODNYKH SRED [Introduction to Quantum Electronics of Spectrally Inhomogeneous Media], Kiev, Naukova dumka, 1977.

8. Wang, C. C., PHYS. REV., Vol B2, 1970, p 2045.

9. Hellwarth, R.; Cherlow, J.; Yang Tien-Tsai, PHYS. REV., Vol B11, 1975, p 964.

10. Akhmanov, S. A.; Sukhorukov, A. P.; Khokhlov, R. V., UFN [Progress in the Physical Sciences], Vol 93, 1967, p 19.

11. Shen, Y. R., PROGR. QUANTUM ELECTRONICS, London, Pergamon Press, Vol 4, 1975.

12. Bliss, E. S.; Hunt, J. T.; Renard, P. A., et al., IEEE J. QUANTUM ELECTRONICS, Vol QE-12, 1976, p 402.

13. Bespalov, V. I.; Talanov, V. I., PIS'MA ZHETF [Letters to the Journal of Experimental and Theoretical Physics], Vol 3, 1966, p 471.

14. LAWRENCE LIVERMORE LAB., REP. UCRL 75628, Livermore, 1974.

15. Bliss, E. S.; Speck, D. R.; Simmons, W. W., APPL. PHYS. LETT., Vol 25, 1974, p 728.

16. Milam, D.; Weber, M. J., IEEE J. QUANTUM ELECTRONICS, Vol QE-12, 1976, p 512.

17. LAWRENCE LIVERMORE LAB., SEMIANNUAL REP. UCRL 50021-73-1, Livermore, 1973.

18. Boling, N. L.; Glass, A. J.; Owyoung, A., LAWRENCE LIVERMORE LAB., REP. UCRL 75628 SUPPL., Livermore, 1974.

19. Weiss, J. A. OPT. SPECTRA, Vol 11, 1977, p 39.

20. Blombergen, N., KVANTOVAYA ELEKTRONIKA [Quantum Electronics], Vol 1, 1974, p 786.

21. Khodakov, G. S.; Tsesnek, L. S., OPT.-MEKH. PROM. [Optical Mechanics Industry], No 9, 1976, p 55.

22. Glass, A. J.; Guenther, A. N., APPL. OPT., Vol 12, 1973, p 637; Vol 13, 1974, p 74; Vol 14, 1975, p 698; Vol 15, 1976, p 1510.

23. Danileyko, Yu. K.; Manenkov, A. A.; Prokhorov, A. M.; Mal'kov, V. Ya., ZHETF [Journal of Experimental and Theoretical Physics], Vol 58, 1970, p 31.

24. Hopper, R. W.; Uhlman, D. R., J. APPL. PHYS., Vol 41, 1970, p 4023.

25. Besarab, A. V., KVANTOVAYA ELEKTRONIKA, Vol 4, 1977, p 328.

26. Buzhinskiy, I. M.; Pozdnyakov, A. Ye., KVANTOVAYA ELEKTRONIKA, Vol 2, 1975, p 1550.

27. Aleshin, I. V.; Imas, A. Ya.; Milyukov, Y. Me., OPT.-MEKH. PROM., No 7, 1975, p 32.

28. Anan'yev, Yu. A.; Mak, A. A., OPT. I SPEKTR. [Optics and Spectroscopy], Vol 16, 1964, p 1065.

29. Dianov, Ye. M.; Prokhorov, A. M., DAN SSSR [Reports of the USSR Academy of Sciences], Vol 192, 1970, p 531.

30. Slyusarev, G. G., OPT. I SPEKTR., Vol 6, 1959, p 211.

31. Belostotskiy, B. R.; Rubanov, A. S., TEPLOVOY REZHIM TVERDOTEL'NYKH OPTICHESKIKH KVANTOVYKH GENERATOROV [Thermal Conditions of Solid-State Lasers], Moscow, Energiya, 1973.

32. Buzhinskiy, I. M.; Dianov, Ye. M.; Mamonov, S. K., et al., DAN SSSR, Vol 190, 1970, p 558.

33. Demkina, L. I.; Shchavelev, O. S.; Babkina, V. A., TRUDY GOI [Works of the State Institute of Optics], Leningrad, Vol 39, No 170, 1972, p 45.

34. Gromov, A. K.; Izyneyev, A. A., Kopylov, Yu. L.; Kravchenko, V. B., FIZ. I KHIM. STEKLA [Physics and Chemistry of Glass], Vol 2, 1976, p 444.

35. Vitrishchak, I. B.; Soms, L. N.; Tarasov, A. A., ZHTF [Journal of Technical Physics], Vol 44, 1974, p 1055.

36. Pavlov, V. I.; Pergament, A. Kh.; Ponomarev, A. V.; Chernyak, V. M., ISSLEDOVANIYE TERMOUPRUGIKH DEFORMATSIY TORTSEVYKH POVERKHNOSTEY AKTIVNYKH ELEMENTOV LAZERNYKH SISTEM [Study of Thermoelastic Deformations of End Surfaces of Active Elements with Laser Systems], preprint of the Applied Mathematics Institute, No 8, 1978.

37. Quelle, F. W., APPL. OPTICS, Vol 5, 1966, p 633.

38. Riedel, E. P.; Baldwin, G. D., J. APPL. PHYS., Vol 38, 1967, p 2720.

39. Berezina, Ye. Ye.; Demkina, L. I.; Kisin, V. I.; Orlova, L. A., FIZIKO-KHIMICHESKIYE OSNOVY PROIZVODSTVA OPTICHESKOGO STEKLA [Physico-chemical Principles of the Production of Optical Glass], Leningrad, Khimiya, 1976, p 161.

40. Zheltov, G. I.; Rubanov, A. S.; Chaley, A. V., ZHPS, Vol 14, 1971, p 226.

41. Zheltov, G. I.; Rubanov, A. S., ZHPS, Vol 22, 1975, p 418.

42. Baldwin, G. D.; Riedel, E. P., J. APPL. PHYS., Vol 38, 1967, p 2726.

43. Epstein, S., J. APPL. PHYS., Vol 38, 1967, p 2715.

44. Anan'yev, Yu. A.; Grishmanova, N. I., ZHPS, Vol 12, 1970, p 668.

45. Mak, A. A.; Mit'kin, V. M.; Soms, L. N., et al., OPT.-MEKH. PROM., No 9, 1971, p 42.

46. Shchavelev, O. S.; Babkina, V. A.; Yelina, N. N., et al., OPT.-MEKH. PROM., No 7, 1976, p 32.

47. Avakyants, L. I.; Buzhinskiy, I. M.; Koryagina, Ye. I.; Surkova, V. F., KVANTOVAYA ELEKTRONIKA, Vol 5, 1978, p 725.

48. Alekseyev, N. Ye.; Anikiyev, Yu. G.; Gapontsev, V. P., et al., ITOGI NAUKI I TEKHNIKI: SER. RADIOTEKHNIKA [Results of Science and Engineering: Radio Engineering Series], Moscow, VINITI, Vol 18, 1978.

49. Shchavelev, O. S.; Mit'kin, V. M.; Babkina, V. A., et al., OPT.-MRKH. PROM., No 1, 1975, p 30.

50. Mak, A. A.; Soms, L. N.; Stepanov, A. I.; Sudakov, A. B., OPT. I SPEKTR., Vol 30, 1971, p 1081.

51. Mit'kin, V. M.; Shchavelev, O. S.; Bunkina, N. N., ZHPS, Vol 23, 1975, p 218.

52. Vakhmyanin, K. P.; Mak, A. A.; Mit'kin, V. M., et al., KVANTOVAYA ELEKTRONIKA, Vol 3, 1976, p 196.

53. Bubnov, M. M.; Buzhinskiy, I. M.; Dianov, Ye. M., et al., DAN SSSR, Vol 205, 1972, p 556.

54. Bubnov, M. M.; Buzhinskiy, I. M.; Dianov, Ye. M., et al., KVANTOVAYA ELEKTRONIKA, Moscow, Sov. radio, No 4, 1973, p 113.

55. Shchavelev, O. S.; Mit'kin, V. M.; Babkina, V. A.; Bunkina, N. N., OPT.-MEKH. PROM., No 7, 1974, p 73.

56. Mit'kin, V. M.; Shchavelev, O. S., ZHPS, Vol 26, 1977, p 667.

57. Veyko, V. P.; Suslov, G. P., FIZ. I KHIM. OBRABOTKI MATERIALOV [Physics and Chemistry of the Working of Materials], No 6, 1968, p 27.

58. Alekseyev, N. Ye.; Gavrilov, G. S.; Gruzdev, V. V., et al., TEZISY DOKL. I VSESOYUZN. KONF. PO OPTIKE LAZEROV [Summaries of Reports of the First All Union Conference on Laser Optics], Leningrad, GOI, 1977, p 36.

59. Alekseyev, N. Ye.; Gruzdev, V. V.; Izyneyev, A. A., et al., KVANTOVAYA ELEKTRONIKA, Vol 5, 1978, p 2354.

60. Alekseyev, N. Ye.; Gromov, A. K.; Izyneyev, A. A., et al., KVANTOVAYA ELEKTRONIKA, Vol 6, 1979, p 140.

61. Dishington, R. H.; Hook, W. R.; Hilberg, R. P., PROC. IEEE, Vol 55, 1967, p 2038.

62. Yevdokimova, V. G.; Mak, A. A.; Soms, L. N.; Shaforostov, A. I., KVANTOVAYA ELEKTRONIKA, Vol 2, 1975, p 1915.

63. Mit'kin, V. M.; Shchavelev, O. S., OPT.-MEKH. PROM., No 9, 1973, p 26.

64. Buchenkov, V. A.; Mak, A. A.; Malinin, B. G., et al., KVANTOVAYA ELEKTRONIKA, Vol 2, 1975, p 2037.

65. Reitmayer, F.; Schroeder, H., APPL. OPT., Vol 14, 1975, p 716.

66. Bubnov, M. M.; Grudinin, A. B.; Dianov, Ye. M.; Prokhorov, A. M., KVANTOVAYA ELEKTRONIKA, Vol 5, 1978, p 464.

67. Buchenkov, V. A.; Kolesnikov, B. N.; Mit'kin, V. M., et al., KVANTOVAYA ELEKTRONIKA, Vol 2, 1975, p 728.

68. Ivanov, Yu. P.; Kolesnikov, B. N.; Kuznetsov, V. M.; Perlov, D. I., ZHPS, Vol 16, 1972, p 797.

69. Buzhinskiy, I. M.; Mamonov, S. K., OPTIKO-ELEKTRONNYYE PRIBORY [Optico-electronic Devices], Moscow, Mashinostroyeniye, No 7, 1974, p 181.

70. Mak, A. A.; Mit'kin, V. M.; Polukhin, V. N., et al., KVANTOVAYA ELEKTRONIKA, Vol 2, 1975, p 850.

71. Segre, J. P., SPACE AGE NEWS, Vol 12, No 11, 1969, p 21.

72. Ushida, T.; Yoshikawa, S.; Washio, K., et al., JAPAN J. APPL. PHYS., Vol 12, 1973, p 126.

73. Galaktionova, N. M.; Garkavi, G. A.; Zubkova, V. S., et al., OPT. I SPEKTR., Vol 37, 1974, p 162.

74. Deutschbein, O. K.; Pautrat, C. C., IEEE J. QUANTUM ELECTRONICS, Vol QE-4, 1968, p 48.

75. Bartenev, G. M., PROCHNYYE I SVERKHPROCHNYYE NEORGANICHESKIYE STEKLA [Strong and Superstrong Inorganic Glass], Moscow, Stroyizdat, 1974.

76. Mak, A. A.; Mikhaylov, Yu. N.; Stepanov, A. I.; Yastrebova, L. S., OPT.-MEKH. PROM., No 10, 1969, p 73.

77. Upton, L. O., US Patent 3982917, 1976.

78. LASER FOCUS, Vol 5, No 7, 1969, p 20.

79. Spanoudis, L., US Patent 3687799, 1972.

80. Kantorski, J. W., US Patent 3700423, 1972.

81. Meyers, J. D., OPT. SPECTRA, Vol 11, 1977, p 34.

82. Snitzer, E., APPL. OPT., Vol 5, 1966, p 1487.

83. Karapetyan, G. O.; Reyshakhrit, A. L., IZV. AN SSSR: SER. NEORGAN. MATER. [News of the USSR Academy of Sciences: Inorganic Materials Series], Vol 3, 1967, p 217.

84. Galant, Ye. I.; Karapetyan, G. O.; Lunter, S. G.; Reyshakhrit, A. L., OPT.-MEKH. PROM., No 11, 1969, p 48.

85. Snitzer, E.; Young, C. G., LASERS--A SERIES OF ADVANCES, New York, Dekker, Vol 2, 1968, p 191.

86. Gaprindashvili, Kh. I.; Gvatua, Sh. Sh.; Mumladze, V. V., et al., ZHPS, Vol 13, 1970, p 715.

87. Gaprindashvili, Kh. I.; Gvatua, Sh. Sh.; Mumladze, V. V., et al., ZHPS, Vol 17, 1972, p 715.

88. Stone, J.; Burrus, C. A., APPL. PHYS. LETT., Vol 23, 1973, p 388.

89. Gorovaya, B. S.; Demskaya, E. L.; Izotov, A. N., et al., KVANTOVAYA ELEKTRONIKA, Vol 4, 1977, p 922.

90. Stone, J.; Burrus, C. A., APPL. OPT., Vol 13, 1974, p 1256.

91. Yajima, H.; Kawase, S.; Sekimoto, Y., APPL. PHYS. LETT., Vol 21, 1972, p 407.

92. Saruwatari, M.; Izawa, T., APPL. PHYS. LETT., Vol 24, 1974, p 603.

93. Chen, B. U., Tang, C. L., APPL. PHYS. LETT., Vol 28, 1976, p 435.

94. Quinn, D. J.; Berak, J. M.; Cullen, D. E., J. APPL. PHYS., Vol 46, 1975, p 3866.

95. Dieke, G. H.; Crosswhite, H. M., APPL. OPTICS, Vol 2, 1963, p 675.

96. Matyushin, G. A.; Byalko, N. G.; Tolkachev, B. V., ZHPS, Vol 18, 1973, p 142.

97. Buzhinskiy, I. M.; Mamonov, S. K.; Mikhaylova, L. I., ZHPS, 1969, Vol 10, p 588.

98. Balagurov, A. Ya.; Kromskiy, G. I.; Chivilov, V. L., ZHPS, Vol 15, 1971, p 827.

99. Kishida, S.; Washio, K.; Yoshikawa, S.; Kato, Y., APPL. PHYS. LETT., Vol 34, 1978, p 273.

100. Kaminskiy, A. A., LAZERNYYE KRISTALLY [Laser Crystals], Moscow, Nauka, 1975.

101. Alekseyev, N. Ye.; Gapontsev, V. P.; Izyneyev, A. A., et al., ISSLEDOVANIYA V OBLASTI RADIOTEKHNIKI I ELEKTRONIKI [Research in the Field of Radio Engineering and Electronics], 1954-1974, Moscow, IRE AN SSSR, Part 2, p 401.

102. Brachkovskaya, N. B.; Grubin, A. A.; Lunter, S. G., et al., KVANTOVAYA ELEKTRONIKA, Vol 3, 1976, p 998.

103. Jacobs, R. A.; Weber, M. J., IEEE J. QUANTUM ELECTRONICS, Vol QE-12, 1976, p 102.

104. Sarkies, P. H.; Sandoe, J. N.; Parke, S., J. PHYS., Vol D4, 1971, p 1642.

105. Gandy, H. W.; Ginther, R. J.; Weller, J. F., J. APPL. PHYS., Vol 38, 1967, p 3030.

106. Singh, S.; Van Uitert, L. G.; Grodkiewicz, W. H., OPTICS COMMUN., Vol 17, 1976, p 315.

107. Michel, J. C.; Morin, D.; Auzel, F., REV. PHYS. APPL., Vol 13, 1978, p 852.

108. Reisfeld, R.; Bornstein, A., CHEM. PHYS. LETT., Vol 47, 1977, p 194.

109. Guittard, M.; Loireau-Lozac'h, A. M.; Purdo, M. P., et al., MATER. RES. BULL., Vol 13, 1978, p 317.

110. Appen, A. A., KHIMIYA STEKLA [Chemistry of Glass], Leningrad, Khimiya, 1974.

111. Mazurin, O. V.; Strel'tsina, M. V.; Shvayko-Shvaykovskaya, T. P., SVOYTSTVA STEKOL I STEKLOOBRAZUYUSHCHIKH RASPLAVOV [Properties of Glass and Glass Forming Melts], Leningrad, Nauka, Vol 1973, Vol 2, 1975, Vol 3, 1977, Part 1, Vol 3, 1978, Part 2.

112. Weber, M. J.; Cline, C. F.; Saroyan, R. A., et al., TOPICAL MEETING ON INERTIAL CONFINEMENT FUSION, San Diego, 1978, Tu B13.

113. Stokowski, S. E.; Weber, M. J.; Saroyan, R. A., et al., TOPICAL MEETING ON INERTIAL CONFINEMENT FUSION, San Diego, 1978, Tu B12.

114. Khalilev, V. D., SVOYSTVA I RAZRABOTKA NOVYKH OPTICHESKIKH STEKOL [Properties and Development of New Optical Glass], Leningrad, Mashinostroyeniye, 1977, p 62.

115. Golubtsov, V. A.; Yegorova, V. F.; Zubkova, V. S., et al., SPEKTROSKOPIYA KRISTALLOV [Spectroscopy of Crystals], Leningrad, Nauka, 1973, p 234.

116. Shchavelev, O. S., OPT.-MEKH. PROM., No 12, 1967, p 35.

117. Alekseyev, N. Ye.; Izyneyev, A. A.; Kravchenko, V. B.; Rudnitskiy, Yu.P., KVANTOVAYA ELEKTRONIKA, Vol 1, 1974, p 2002.

118. Dianov, Ye. M.; Karasik, A. Ya.; Kut'yenkov, A. A., et al., KVANTOVAYA ELEKTRONIKA, Vol 3, 1976, p 168.

119. Ryabov, S. G.; Toropkin, G. N.; Usol'tsev, I. F., PRINOTY KVANTOVOY ELEKTRONIKI [Instruments of Quantum Electronics], Moscow, Sov. radio, 1976.

120. Burdonsky, J. N.; Zhuzhukalo, E. V.; Kovalsky, N. G., et al., APPL. OPT., Vol 15, 1976, p 1450.

121. Auric, D.; Charles, C.; Dalmayrac, C., TOPICAL MEETING ON INERTIAL CONFINEMENT FUSION, San Diego, 1978, Tu B6.

122. Lewis, O.; Jacobs, S.; Lund, L., TOPICAL MEETING ON INERTIAL CONFINEMENT FUSION, San Diego, 1978, Tu B5.

123. Alekseyev, N. Ye.; Buzhinskiy, I. M.; Gapontsev, V. P., et al., IZV. AN SSSR: SER. NEORGAN. MATER., Vol 5, 1969, p 1042.

124. Petrovskiy, G. T., AVTOREFERAT DOKT. DISS. [Author's Review of Doctor's Dissertation], Leningrad, GOI, 1968.

125. Petrovskiy, G. T., STEKLOOBRAZNOYE SOSTOYANIYE [Vitreous State], Leningrad, Nauka, 1971, p 76.

126. Hagen, W. F.; Trenholme, J. B., TOPICAL MEETING ON INERTIAL CONFINEMENT FUSION, San Diego, 1978, Tu B6.

127. Bartenev, G. M., STROYENIYE I MEKHANICHESKIYE SVOYSTVA NEORGANICHESKIKH STEKOL [Structure and Mechanical Properties of Inorganic Glass], Moscow, Stroyizdat, 1966.

128. Demkina, L. I.; Yevstrop'yev, K. S.; Petrovskiy, G. T.; Yakhkind, A. K., FIZIKO-KHIMICHESKIYE OSNOVY PROIZVODSTVA OPTICHESKOGO STEKLA [Physico-chemical Principles of the Production of Optical Glass], Leningrad, Khimiya, p 33.

129. Porai-Koshits, E. A., J. NON-CRYST. SOLIDS, Vol 25, 1977, p 86.

130. Stevels, J. M.; Trapp, H. J. L., GLASTECHN. BER., 1959, B 32 K, p 31.

131. Ray, N. H., J. POLYMER SCI: POLYMER CHEM. BD, Vol 11, 1973, p 2169.

132. Ray, N. H., J. NON-CRYST. SOLIDS, Vol 15, 1974, p 423.

133. Corbridge, D. E. C., THE STRUCTURAL CHEMISTRY OF PHOSPHORUS, Amsterdam, Elsevier, 1974.

134. Corbridge, D. E. C., BULL. SOC. FRANC. MINER. CRIST., Vol 94, 1971, p 271.

135. Durif, A., BULL. SOC. FRANC. MINER. CRIST., Vol 94, 1971, p 314.

136. Hong, H. Y.-P., ACTA CRYATALLOGR., Vol B30, 1974, p 468.

137. Bondar', I. A.; Mezentseva, L. P.; Domanskiy, A. I.; Piryugko, M. M., ZHNKH [Journal of Inorganic Chemistry], Vol 20, 1975, p 2618.

138. Minacheva, L. Kh.; Poray-Koshits, M. A.; Antsyshkina, A. S., et al., KOORDINATSIONNAYA KHIMIYA [Coordination Chemistry], Vol 1, 1975, p 421.

139. Poray-Koshits, M. A.; Aslanov, L. A.; Korytnyy, Ye. F., ITOGI NAUKI I TEKHNIKI: SER. KRISTALLOKHIMIYA [Results of Science and Engineering: Crystal Chemistry Series], Moscow, VINITI, Vol 11, 1976, p 5.

140. Antsyshkina, A. S.; Poray-Koshits, M. A.; Minacheva, L. Kh., et al., KOORDINATSIONNAYA KHIMIYA, Vol 4, 1978, p 448.

141. Linde, S. A.; Gorbunova, Yu. Ye.; Lavrov, A. V., et al., TEZISY DOKL. I VSESOYUZN. SOVESHCH. PO NEORGANICHESKOY KRISTALLOKHIMI [Summaries of Reports of the First All Union Conference on Inorganic Crystal Chemistry], Moscow, Nauka, 1977, p 64.

142. Palkina, K. K., IZV. AN SSSR: SER. NEORGAN. MATER. [News of the USSR Academy of Sciences: Inorganic Materials Series], Vol 14, 1978, p 789.

143. Antsyshkina, A. S.; Poray-Koshits, M. A.; Minacheva, L. Kh.; Ivanova, V. G., KOORDINATSIONNAYA KHIMIYA, Vol 5, 1979, p 268.

144. Chudinova, N. N., IZV. AN SSSR: SER. NEORGAN. MATER., Vol 15, 1979, p 931.

145. Kravchenko, V. B., ZH. STRUKT. KHIM. [Journal of Structural Chemistry], Vol 6, 1965, p 88.

146. Van Vezer, FOSFOR I YEGO SOYEDINENIYA [PHOSPHORUS AND ITS COMPOUNDS], Moscow, Mir, 1969.

147. Belov, N. V., KRISTALLOKHIMIYA SILIKATOV S KRUPNYMI KATIONAMI [Crystal Chemistry of Silicates with Large Cations], Moscow, Izd. AN SSSR, 1961.

148. Belov, N. V., OCHERKI PO STRUKTURNOY MINERALOGII [Outlines of Structural Mineralogy], Moscow, Nedra, 1976.

149. Brady, G. W., J. CHEM. PHYS., Vol 28, 1958, p 48.

150. Jost, K. H.; Wolf, H.; Worzala, H.; Thilo, E., KRISTALL. U. TECHNIK, Vol 4, 1969, p 325.

151. Soklakov, A. I.; Portnova, N. L., KRISTALLOGRAFIYA [Crystallography], Vol 14, 1969, p 141.

152. Soklakov, A. I.; Portnova, N. L.; Nechayeva, V. V., STEKLOOBRAZNOYE SOSTOYANIYE. TRUDY V VSESOYUZN. SOVESHCH. [Vitreous State. Works of the Fifth All Union Conference], Moscow-Leningrad, Nauka, 1971, p 144.

153. Westman, A. E. R., MODERN ASPECTS OF VITREOUS STATE, London, Butterworths, Vol 1, 1960, p 63.

154. Pechkovskiy, V. V.; Cherches, G. Kh.; Kuz'menkov, M. M., USP. KHIM. Progress in Chemistry], Vol 44, 1975, p 172.

155. Poletayev, E. V. IZV. AN KAZ. SSR: SER. KHIM. [News of the Kazakh SSR Academy of Sciences, Chemistry Series], Vol 18, No 5, 1968, p 1.

156. Varshal, B. G.; Ilyukhin, V. V.; Belov, N. V., FIZ. I KHIM. STEKLA [Physics and Chemistry of Glass], Vol 1, 1975, p 117.

157. Voronkov, A. A.; Ilyukhin, V. V.; Belov, N. V., KRISTALLOGRAFIYA, Vol 20, 1975, p 556.

158. Zuca, S.; Sokolova, I. D.; Gagescu, D.; Olteanu, M., REV. ROMAINE CHIM., Vol 17, 1972, p 1497.

159. Atanov, I. G.; Buzhinskiy, I. M., KORYAGINA, Ye. I., et al., IZV. AN SSSR: SER. NEORGAN. MATER., Vol 10, 1974, p 909.

160. Galaktionov, A. D.; Shtin, A. P.; Malyushin, V. L., TEZISY KOKL. IV VSESOYUZN. SIMP. PO OPTICHESKIM I SPEKTRAL'NYM SVOYSTVAM STEKOL [Summaries of Reports of the Fourth All Union Symposium on Optical and Spectral Properties of Glass], Riga, 1977, p 85.

161. Beekenkamp, P., PHILIPS RES. REP. SUPPL., No 4, 1966, p 1.

162. Galaktionov, A. D.; Khodes, M. Ya.; Shtin, A. P., et al., ZHPS, Vol 21, 1974, p 460.

163. Shtin, A. P.; Fotiyev, A. A.; Galaktionov, A. D.; Khodes, M. Ya., FIZ. I KHIM. STEKLA, Vol 2, 1976, p 80.

164. Ushakov, D. F.; Baskova, N. F.; Tarlakov, Yu. P., FIZ . I KHIM. STEKLA, Vol 1, 1975, p 151.

165. Ushakov, D. F.; Baskova, N. F., FIZ. I KHIM. STEKLA, Vol 2, 1976, p 41.

166. Takahashi, K., ADVANCES IN GLASS TECHNOLOGY: TECHN. PAPER OF THE VI INTERN. CONGRESS ON GLASS, N.Y., Plenum Press, 1962, Pt 2, p 366.

167. Alekseyev, N. Ye.; Izyneyev, A. A.; Kopylov, Yu. L., et al., ZHPS, Vol 26, 1977, p 116.

168. Ray, N. H., PHYS. CHEM. GLASSES, Vol 16, 1975, p 75.

169. Nakamura, T.; Ohashi, Sh., BULL. CHEM. SOC. JAPAN, Vol 40, 1967, p 110.

170. Yun, Y. H.; Bray, P. J., J. NON-CRYST. SOLIDS, Vol 30, 1978, p 45.

171. Sedmalis, U. Ya.; Bol'shiy, Ya. Ya.; Eyduk, Yu. Ya., FIZ. I KHIM. STEKLA, Vol 1, 1975, p 549.

172. Finn, C. W. F.; Fray, D. J.; King, T. B.; Ward, J. G., PHYS. CHEM. GLASSES, Vol 17, 1976, p 70.

173. Kutukova, Ye. S.; Syritskaya, Z. M.; Vaysfel'd, N. M., FIZ. I KHIM. STEKLA, Vol 1, 1975, p 215.

174. Vitina, I. A.; Sedmalis, U. Ya.; Igaune, S. A., FIZIKA I KHIMIYA STEKLOOBRAZUYUSHCHIKH SISTEM [Physics and Chemistry of Vitreous Systems], Riga, No 5, 1977, p 19.

175. Vayvad, Ya. A.; Lagdzina, S. Ye.; Sedmalis, U. Ya., FIZIKA I KHIMIYA STEKLOOBRAZUYUSHCHIKH SISTEM, Riga, No 5, 1977, p 29.

176. Kutukova, Ye. S., AVTOREFERAT KAND. DIS. [Author's Review of Candidate's Dissertation], Moscow, MKHTI im. D. I. Mendeleyev, 1970.

177. Sedmalis, U. Ya.; Bol'shiy, Ya. Ya.; Sedmale, G. P., et al., UCH. ZZP. LATV. GU [Scientific Notes of the Latvian State University], Vol 231, 1975, p 160.

178. Vitina, I. A., AVTOREFERAT KAND. DISS [Author's Review of Candidate's Dissertation], Riga, 1974.

179. Naruse, A.; Abe, Y.; Inoue, H., J. CERAM. SOC., Japan, Vol 76, 1968, p 36.

180. Voskresenskaya, N. K.; Sokolova, I. D., USP. KHIM., Vol 38, 1969, p 1894.

181. Izyneyev, A. A.; Alekseyev, N. Ye.; Kravchenko, V. B.; Paramonova, N. A., TEZISY DOKL. III VSESOYUZN. SOVESHCH. PO FOSFATAM [Summaries of Reports of the Third All Union Conference on Phosphates], Riga, Einatne, 1971, p 214.

182. Alekseyev, N. Ye.; Gapontsev, V. P.; Gromov, A. K., et al., NOVYYE LEGKOPLAVKIYE GLAZURI, EMALI I FOSFOROSODERZHASHCHIYE STEKLA [New Low Melting Glasers, Enamels and Phosphorus-Containing Glass], Riga, Zinatne, 1973, p 154.

183. Alekseyev, N. Ye.; Gapontsev, V. P.; Gromov, A. K., et al., IZV. AN SSSR: SER. NEORGAN. MATER., Vol 11, 1975, p 323.

184. Plyshevskiy, S. V.; Makatun, V. N.; Kuz'menkov, M. I., FIZ. I KHIM. STEKLA, Vol 1, 1975, p 279.

185. Bondarenko, Ye. G.; Galant, Ye. I.; Lunter, S. G., et al., OPT.-MEKH. PROM., No 6, 1975, p 42.

186. Rzhevskiy, M. B.; Kuz'menkov, M. I.; Pechkovskiy V. V.; Plyshevskiy, S. V., ZHPS, Vol 17, 1972, p 1032.

187. Galant, Ye. I.; Lunter, S. G.; Mironov, A. N.; Fedorov, Yu. K., FIZ. I KHIM. STEKLA, Vol 2, 1976, p 351.

188. Khalilev, V. D.; Petrovskaya, M. L.; Nikolina, G. P., FIZ. I KHIM. STEKLA, Vol 1, 1975, p 508.

189. Petrovskiy, G. T.; Urusovskaya, L. N.; Yudin, D. M., IZV. AN SSSR: SER. NEORGAN. MATER., Vol 9, 1973, p 1615.

190. Smirnova, Ye. V.; Urusovskaya, L. N., TEZISY DOKL. IV VSESOYUZN. SIMP. PO OPTICHESKIM I SPEKTRAL'NYM SVOYSTVAM STEKOL [Summaries of Reports of the Fourth All Union Symposium on Optical and Spectral Properties of Glass], Riga, 1977, p 88.

191. Kolobkov, V. P.; Khalilev, V. D.; Vasylyak, Ya. P., et al., TEZISY DOKL. IV VSESOYUZN. SIMP. PO OPTICHESKIM I SPEKTRAL'NYM SVOYSTVAM STEKOL, Riga, 1977, p 115.

192. Vakhrameyev, V. I.; Raaben, E. L.; Fedorushkov, B. G., et al., TEZISY DOKL. III VSESOYUZN. SIMP. PO OPTICHESKIM I SPEKTRAL'NYM SVOYSTVAM STEKOL [Summaries of Reports of the Third All Union Symposium on Optical and Spectral Properties of Glass], Leningrad, GOI, 1974, p 84.

193. Gapontsev, V. P.; Gromov, A. K.; Izyneyev, A. A., et al., SPEKTROSKOPIYA KRISTALLOV [Spectroscopy of Crystals], Moscow, Nauka, 1975, p 337; IV VSESOYUZN. SIMP. PO SPEKTROSKOPII KRISTALLOV, AKTIVIROVANNYKH IONAMI REDKOZEMEL'NYKH I PEREKHODNYKH METALLOV [Fourth All Union Symposium on the Spectroscopy of Crystals Activated by Rare Earth and Transition Metal Ions], Sverdlovsk, 1973, p 84.

194. Bogomolova, L. D., FIZ. I KHIM. STEKLA, Vol 2, 1976, p 4.

195. Bandurkin, G. A.; Dzhurinskiy, B. F., DAN SSSR, Vol 168, 1966, p 1315.

196. Bokiy, G. B.; Kravchenko, V. B., KHIMICHESKIYE SVOYSTVA SOYEDINENIY REDKOZEMEL'NYKH ELEMENTOV [Chemical Properties of Compounds of Rare Earth Elements], Moscow, Nauka, 1973, p 7.

197. Aslanov, L. A., AVTOREFERAT DOKT. DISS. [Author's Review of Doctor's Dissertation], Moscow, IONKH AN SSSR, 1973.

198. Bandurkin, G. A.; Dzhurinskiy, B. F.; Tananayev, I. V., DAN SSSR, Vol 189, 1969, p 94.

199. Bandurkin, G. A.; AVTOREFERAT KAND. DISS. [Author's Review of Candidate's Dissertation], Moscow, IONKH AN SSSR, 1967.

200. Dzhurinskiy, B. F., AVTOREFERAT DOKT. DISS., Moscow, IONKH AN SSSR, 1972.

201. Robinson, Ch. C.; Fournier, J. T., J. PHYS. CHEM. SOLIDS, Vol 31, 1970, p 895.

202. Krasilov, Yu. I.; Solokha, A. F.; Tsapkin, V. V.; Ellert, G. V., KVANTOVAYA ELEKTRONIKA, Vol 1, 1974, p 370.

203. Zverev, G. M.; Onishchenko, A. M.; Semenov, A. A.; Smirnov, A. I., FTT [Solid-State Physics], Vol 13, 1971, p 2161.

204. Reisfeld, R.; Eckstein, Y., J. SOLID STATE CHEM., Vol 5, 1972, p 174.

205. Briskina, Ch. M.; Zhabotinskiy, M. Ye.; Artamonova, M. V., et al., ZHPS, Vol 22, 1975, p 61.

206. Weber, H. P.; Damen, T. C.; Danielmeyer, H. G.; Tofield, B. C., APPL. PHYS. LETT., Vol 22, 1973, p 534.

207. Alekseyev, N. Ye.; Gapontsev, V. P.; Gromov, A. K., et al., TEZISY DOKL. V VSESOYUZN. SIMP. PO SPEKTROSKOPII KRISTALLOV, AKTIVIROVANNYKH REDKIMI ZEMLYAMI I ELEMENTAMI GRUPPY ZHELEZA [Summaries of Reports of the Fifth All Union Symposium on the Spectroscopy of Crystals Activated by Rare Earths and Elements of the Iron Group], Kazan', 1976, p 11.

208. Bokiy, G. B.; Kravchenko, V. B., SPEKTROSKOPIYA KRISTALLOV, Leningrad, Nauka, 1973, p 7.

209. Dmitryuk, A. V.; Karapetyan, G. O.; Maksimov, G. V., ZHPS, Vol 22, 1975, p 153.

210. Galant, Ye. I.; Karapetyan, G. O., STEKLOOBRAZNOYE SOSTOYANIYE [Vitreous State], Leningrad, Nauka, 1971, p 186.

211. Stepanov, S. A., FIZ. I KHIM. STEKLA, Vol 2, 1976, p 228.

212. Zhilin, A. A.; Nemilov, S. V., FIZ. I KHIM. STEKLA, Vol 2, 1976, p 58.

213. Zhilin, A. A.; Nemilov, S. V., TEZISY DOKL. IV VSESOYUZN. SIMP. PO OPTICHESKIM I SPEKTRAL'NYM SVOYSTVAM STEKOL [Summaries of Reports of the Fourth All Union Symposium on Optical and Spectral Properties of Glass], Riga, 1977, p 76.

214. Zarubina, T. V.; Mokeyeva, G. A.; Stepanov, S. A., TEZISY DOKL. IV VSESOYUZN. SIMP. PO OPTICHESKIM I SPEKTRAL'NYM SVOYSTVAM STEKOL, Riga, 1977, p 60.

215. Tolstoy, M. N., AVTOREFERAT DOKT. DIS., Leningrad, GOI, 1977.

216. Dmitryuk, A. V., AVTOREFERAT KAND. DISS., Moscow, IKHF AN SSR, 1978.

217. Milyukov, Ye. M., OPT.-MEKH.PROM., No 3, 1976, p 66.

218. Arbuzov, V. I.; Galant, Ye. I.; Golubovskaya, M. P., et al., FIZ. I KHIM. STEKLA, Vol 3, 1977, p 242.

219. Dmitryuk, A. V.; Karapetyan, G. O.; Nikitin, S. V., ZHPS, Vol 18, 1973, p 869.

220. Antipenko, B. M.; Dmitryuk, A. V.; Zubkova, V. S., TEZISY DOKL. III VSESOYUZN. SIMP. PO OPTICHESKIM I SPEKTRAL'NYM SVOYSTVAM STEKOL [Summaries of Reports of the Third All Union Symposium on Optical and Spectral Properties of Glass], Leningrad, GOI, 1974, p 114.

221. Obraztsov, G. I.; Reyshakhrit, A. L.; Tolstoy, M. N., OPT. I SPEKTR, Vol 34, 1973, p 803.

222. Ageyev, L. Ye.,; Brachkovskaya, N. B.; Grubin, A. A., TEZISY DOKL. IV VSESOYUZN. SIMP. PO OPTICHESKIM I SPEKTRAL'NYM SVOYSTVAM STEKOL, Riga, 1977, p 103.

223. Komiyama, T., J. CERAM. SOC. JAPAN, Vol 82, 1974, p 637.

224. Kravchenko, V. B., TEZISY DOKL. I VSESOYUZN. SOVESHCH. PO NEORGAN. KRISTALLOKHIMII [Topics of Reports of the First All Union Conference on Inorganic Crystal Chemistry], Moscow, Nauka, 1977, p 24.

225. Voron'ko, Yu. K.; Denker, B. I.; Zlenko, A. A., et al., DAN SSSR, Vol 227, 1976, p 75.

226. Batygov, S. Kh.; Voron'ko, Yu. K.; Denker, B. I., et al. KVANTOVAYA ELEKTRONIKA, Vol 3, 1976, p 2243.

227. Denker, B. I.; Kil'pio, A. V.; Maksimova, G. V., et al., KVANTOVAYA ELEKTRONIKA, Vol 4, 1977, p 688.

228. Denker, B. I.; Maksimova, G. V.; Osiko, V. V., et al., DAN SSSR, Vol 239, 1978, p 573.

229. Alekseyev, N. Ye.; Gapontsev, V. P.; Gromov, A. K., et al., RADIOTEKHNIKA I ELEKTRONIKA, Vol 23, 1978, p 1896.

230. Hong, H. Y.-P., Chinn, S. R., MATER. RES. BULL, Vol 11, 1976, p 461.

231. Bondar', I. A.; Denker, B. I.; Domanskiy, A. I., et al., KVANTOVAYA ELEKTRONIKA, Vol 4, 1977, p 302.

232. Chinn, S. R.; Hong, H. Y.-P.; Pierce, J. W., LASER FOCUS, Vol 12, No 5, 1975, p 64.

233. Kaminski, A. A.; Sarkisov, S. E.; Tran Ngoc, et al., PHYS. STAT. SOLIDI (a), Vol 50, 1978, p 745.

234. Koizumi, H.; Nakano, J., ACTA CRYSTALLOGR., Vol B33, 1977, p 2680.

235. Hong, H. Y.-P.; Chinn, S. R., MATER. RES. BULL., Vol 11, 1976, p 421.

236. Denker, B. I.; Osiko, V. V.; Prokhorov, A. M.; Shcherbakov, I. A., KVANTOVAYA ELEKTRONIKA, Vol 5, 1978, p 847.

237. Kaminski, A. A.; Sarkisov, S. E.; Bohm, J., et al., PHYS. STAT. SOLIDI (a), Vol 43, 1977, p 71.

238. Avanesov, A. G.; Basiyev, T. T.; Voron'ko, Yu. K., et al., ZHETF, Vol 77, 1979, p 1771.

239. Yermolayev, V. L.; Bodunov, Ye. N.; Sveshnikova, Ye. B.; Shakhverdov, T. A., BEZYZLUCHATEL'NYY PERENOS ENERGII ELEKTRONNOGO VOZBUZHDENIYA [Nonradiating Transport of Electron Excitation Energy], edited by M. D. Galanin, Leningrad, Nauka, 1977.

240. Agranovich, V. M.; Galanin, M. D., PERENOS ENERGII ELEKTRONNOGO VOZBUZHDENIYA V KONDENSIROVANNYKH SREDAKH [Electron Excitation Energy Transport in Condensed Media], Moscow, Nauka, 1978.

241. Komiyama, T., J. NON-CRYST. SOLIDS, Vol 18, 1975, p 107.

242. Orbach, R., OPTICAL PROPERTIES OF IONS IN CRYSTALS, ed. Grosswhite and Moos, Intersci. Publ., 1967, p 445.

243. Orbach, R., OPTICAL PROPERTIES OF IONS IN SOLIDS, ed. B. DiBartolo, N.Y., London, Plenum Press, 1975, p 355.

244. Watts, R. K., OPTICAL PROPERTIES OF IONS IN SOLIDS, ed. B. DiBartolo, N.Y., London, Plenum Press, 1975, p 307.

245. Ovsyankin, V. V.; Feofilov, P. P., NELINEYNAYA OPTIKA [Nonlinear Optics], Novosibirsk, 1968, p 293.

246. Galant, E. I.; Gapontsev, V. P.; Zhabotinsky, M. E., et al., PROCEEDINGS MOGA-70, De Venter, 1970, pp 13-22.

247. Gapontsev, V. P.; Zhabotinskiy, M. E.; Izyneyev, A. A., et al., PIS'MA ZHETF, Vol 18, 1973, p 428.

248. Arbuzov, V. I.; Galant, Ye. I.; Lunter, S. G., et al., FIZ. I KHIM. STEKLA, Vol 4, 1978, p 439.

249. Aristov, A. V.; Kolobkov, V. P.; Kudryashov, P. I.; Shevandin, V. S., OPT. I SPEKTR., Vol 39, 1975, p 281.

250. Kangro, A. R.; Kariss, Ya. E.; Przhevuskiy, A. K., et al., PIS'MA ZHTF, Vol 2, 1976, p 652.

251. Avouris, ph.; Campion, A.; El-Sayed, M. A., J. CHEM. PHYS., Vol 67, 1977, p 3397.

252. Motegi, N.; Shionoya, Sh., J. LUMINESCENCE, Vol 8, 1973, p 1.

253. Alimov, A. K.; Basiyev, T. T.; Voron'ko, Yu. K., et al, ZHETF, Vol 72, 1977, p 1313.

254. Alekseyev, N. Ye.; Gapontsev, V. P.; Zhabotinskiy, M. Ye.; Sverchkov, Yu. Ye.; PIS'MA ZHETF, Vol 27, 1978, p 118.

255. Voron'ko, Yu. K.; Mamedov, T. G.; Osiko, V. V., et al., ZHETF, Vol 71, 1976, p 478.

256. Förster, Th., Z. NATURFORSCH., Vol 4A, 1949, p 321, ANN. PHYS., Vol 2, 1948, p 55.

257. Dexter, D., J. CHEM. PHYS., Vol 21, 1953, p 836.

258. Miyakawa, T.; Dexter, D. L., PHYS. REV., Vol B1, 1970, p 2961.

259. Nagibarov, V. R.; Nagibarova, I. A., OPT. I SPEKTR., Vol 20, 1966, p 815.

260. Nagibarov, V. R., FTT, Vol 8, 1966, p 484.

261. Nagibarova, I. A., SPEKTROSKOPIYA KRISTALLOV, Moscow, Nauka, 1970, p 96.

262. Nagibarova, I. A.; Shegeda, A. M., OPT. I SPEKTR., Vol 30, 1971, p 174.

263. Birgeneau, R. J., J. CHEM. PHYS., Vol 50, 1969, p 4282.

264. Kohli, M.; Huang Liu, N. L., PHYS. REV., Vol B9, 1974, p 1008.

265. Holstein, T.; Lyo, S. K.; Orbach, R., PHYS. REV. LETT., Vol 36, 1976, p 891.

266. Malyshev, V. A.; Shekhtman, V. L., XXVIII GERTSENOVSKIYE CHTENIYA: TEOR. FIZ. I ASTRON. [28th Hercene Lectures: Theory of Physics and Astronomy], Leningrad, Leningrad State University, 1975, p 27.

267. Shekhtman, V. L.; Shirokobrod, O. Ye., XXVIII GERTSENOVSKIYE CHTENIYA: TEOR. FIZ. I ASTRON., Leningrad, GLU, 1975, p 32.

268. De Losh, R. G.; Grant, W. J. C., PHYS. REV., Vol B1, 1970, p 1754.

269. Lowther, J. E., PHYS. STAT. SOLIDI (b), Vol 77, 1976, p 359.

270. Musin, I. Sh.; Trifonov, Ye. D.; Troshin, A. S., XXVII GERTSENOVSKIYE CHTENIYA: TEOR. FI Z. I ASTRON [27th Hercene Lectures: Theory of Physics and Astronomy], Leningrad, LGU, 1974, p 50.

271. Kozhushner, M. A., FTT, Vol 13, 1971, p 2601.

272. Bodunov, Ye. N.; Shekhtman, V. L., FTT, Vol 12, 1970, p 2809.

273. Golubov, S. I.; Konobeyev, Yu. V., PHYS. STAT. SOLIDI (b), Vol 56, 1973, p 69; Vol 70, 1975, p 373; Vol 71, p 777.

274. Golubov, S. I.; Konobeyev, Yu. V., FTT, Vol 13, 1971, p 3185.

275. Galanin, M. D., ZHETF, Vol 21, 1951, p 126; Vol 28, 1955, p 485.

276. Rozman, I. M., OPT. I SPEKTR., Vol 4, 1959, p 536; IZV. AN SSSR: SER. FIZ [News of the USSR Academy of Sciences, Physics Series], Vol 37, 1973, p 502.

277. Sveshnikov, B. Ya.; Shirokov, V. I., OPT. I SPEKTR., Vol 12, 1962, p 606.

278. Inokuti, M.; Hirayama, F., J. CHEM. PHYS., Vol 43, 1965, p 1978.

279. Sakun, V. P., FTT, Vol 14, 1972, p 2199; Vol 15, 1973, p 2277.

280. Rokenglaz, M. I.; Rozman, I. M., OPT. I SPEKTR., Vol 36, 1974, p 100, 106.

281. Shcherbakov, I. A., AVTOREFERAT DOKT. DISS., Moscow, FIAN SSSR, 1978.

282. Burshteyn, A. I.; Pusep, A. Yu., FTT, Vol 16, 1974, p 2318.

283. Artamonova, M. V.; Briskina, Ch. M.; Burshteyn, A. I., et al., ZHETF, Vol 62, 1972, p 863.

284. Burshteyn, A. I., ZHETF, Vol 62, 1972, p 1695.

285. Zusman, L. D., OPT. I SPEKTR., Vol 36, 1974, p 497; ZHETF, Vol 73, 1977, p 662.

286. Burshteyn, A. I., AVTOMETRIYA [Autometry], No 5, 1978, p 65; No 6, p 72.

287. Shekhtman, V. L., OPT. I SPEKTR., Vol 33, 1972, p 384.

288. Yokota, M.; Tanimoto, O., J. PHYS. SOC. JAPAN, Vol 22, 1967, p 779.

289. Doktorov, A. B.; Kipriyanov, A. A.; Burshteyn, A. I., ZHETF, Vol 74, 1978, p 1020.

290. Gapontsev, V. P.; Sverchkov, Yu. Ye., Preprint No 6, Moscow, IRE AN SSSR, 1979.

291. Vugmeister, B. E., PHYS. STAT. SOLIDI (b), Vol 76, 1976, p 161; Vol 90, 1978, p 711.

292. Mikhelashvili, M. S., IZV. AN SSSR: SER. FIZ, Vol 39, 1975, p 1859.

293. Basiyev, T. T.; Voron'ko, Yu. V.; Mamedov, T. G., et al., SPEKTROSKOPIYA KRISTALLOV, Moscow, Nauka, 1975, p 155.

294. Grubin, A. A.; Przhevuskiy, A. K.; Tr[illegible]onov, Ye. D.; Troshin, A. S., FTT, Vol 18, 1976, p 734.

295. Holstein, T.; Lyo, S. K.; Orbach, R., PHYS. REV., Vol B15, 1977, p 4693.

296. Huber, D. L.; Hamilton, D. S.; Barnett, B., PHYS. REV., Vol B16, 1977, p 4642.

297. Ching, W. Y.; Huber, D. L.; Barnett, B., PHYS. REV., Vol B17, 1978, p 5025.

298. Huber, D. L.; Ching, W. Y., PHYS. REV., Vol B18, 1978, p 5320.

299. Bernasconi, J.; Alexander, S.; Orbach, R., PHYS. REV. LETT., Vol 41, 1978, p 185.

300. Alexander, S.; Bernasconi, J.; Orbsch, R., PHYS. REV., Vol B17, 1978, p 4311.

301. Sevyast'yanov, Ye. A.; Przhevuskiy, A. K., FTT, Vol 21, 1978, p 796.

302. Tolstoy, M. N., SPEKTROSKOPIYA KRISTALLOV, Moscow, Nauka, 1970, p 124.

303. Peterson, G. E.; Bridenbaugh, P. M., APPL. PHYS. LETT., Vol 4, 1964, p 201; JOSA, Vol 54, 1964, p 644.

304. Karapetyan, G. O.; Tolstoy, M. N.; Feofilov, P. P.; Shapovalov, V. N., ZHPS, No 7, 1967, p 174.

305. Basiyev, T. T.; Mamedov, T. G.; Shcherbakov, I. A., KVANTOVAYA ELEKTRONIKA, Vol 2, 1975, p 1269.

306. Nakazawa, E.; Shionoya, S., PHYS. REV. LETT., Vol 25, 1970, p 1710.

307. Galant, Ye. I.; Gorovaya, B. S.; Demskaya, E. Kh., et al., FIZ. I KHIM. STEKLA, Vol 2, 1976, p 438.

308. Dianov, Ye. M.; Kutenkov, A. A.; Manenkov, A. A., et al., ZHETF, Vol 69, 1975, p 540.

309. Arbuzov, V. I.; Brachkovskaya, N. B.; Zhmyreva, N.A., et al., KVANTOVAYA ELEKTRONIKA, Vol 3, 1976, p 2005.

310. Hirayama, C.; Camp, F. E.; Melamed, N. T., J. NON-CRYST. SOLIDS, 1971, p 342.

311. Chrysochoos, J. J. CHEM. PHYS., Vol 61, 1974, p 4596.

312. Snitzer, E.; Woodcock, R., APPL. PHYS. LETT., Vol 6, 1965, p 45.

313. Reisfeld, R., STRUCTURE AND BONDING, ed. J. D. Dunity, et al., Berlin, Springer, Vol 13, 1973, p 53.

314. Reisfeld, R.; Greenberg, E.; Velapoldi, R. A.; Barnett, B., J. CHEM. PHYS., Vol 56, 1971, p 1698.

315. Gandy, H. W.; Ginther, R. J.; Weller, J. F., APPL. PHYS. LETT., Vol 4, 1964, p 188; Vol 6, 1965, p 46.

316. Gandy, H. W.; Ginther, R. J.; Weller, J. F., APPL. PHYS. LETT., Vol 5, 1964, p 220; PHYS. LETT., Vol 11, 1964, p 213.

317. Gandy, H. W.; Ginther, R. J.; Weller, J. F., APPL. PHYS. LETT., Vol 6, 1965, p 237; J. APPL. PHYS., Vol 38, 1967, p 3030.

318. Pearson, A. D.; Porto, S. P. S., APPL. PHYS. LETT., Vol 4, 1964, p 202.

319. Jacobs, R. R.; Layne, C. B.; Weber, M. J.; Rapp, Ch. F., J. APPL. PHYS., Vol 47, 1976, p 2020.

320. Peterson, G. F.; Pearson, A. D.; Bridenbaugh, P. M., J. APPL. PHYS., Vol 36, 1965, p 1962.

321. Pearson, A. D.; Northower, W. R., J. APPL. PHYS., Vol 38, 1967, p 2484.

322. De Shazer, L. G.; Cabezas, A. V., PROC. IEEE, Vol 52, 1964, p 1355.

323. Kitamura, A., J. PHYS. SOC. JAPAN, Vol 20, 1965, p 1283.

324. Melamed, N. T.; Hirayama, C.; French, C., APPL. PHYS. LETT., Vol 6, 1965, p 43.

325. Melamed, N. T.; Hirayama, C.; Davis, E. K., APPL. PHYS. LETT., Vol 7, 1965, p 170.

326. Snitzer, E.; Woodcock, R., JOSA, Vol 55, 1965, p 584.

327. Nakazawa, E.; Shionoya, Sh., APPL. PHYS. LETT., Vol 6, 1965, p 117.

328. Shionoya, Sh.; Nakazawa, E., APPL. PHYS. LETT., Vol 6, 1965, p 118.

329. Karapetyan, G. O.; Lunter, S. G.; Kovalev, V. P., OPT. I SPEKTR., Vol 19, 1965, p 951.

330. Dauge, G., IEEE J. QUANTUM ELECTRONICS (DIGEST OF TECHN. PAPERS), Vol QE-2, 1966, pp iv-iii-lix.

331. Kovalev, V. P.; Karapetyan, G. O., OPT. I SPEKTR., Vol 18, 1965, p 182.

332. Veynberg, T. I.; Zhmyreva, I. A.; Kolobkov, V. P.; Kudryashov, P. I., OPT. I SPEKTR., Vol 24, 1968, p 441.

333. Mokeyeva, G. A.; Kolobkov, V. P.; Karapetyan, G. O., ZHPS, Vol 9, 1968, p 326.

334. Kudrashov, P. I.; Kolobkov, V. P.; Veynberg, T. I., ZHPS, No 8, 1968, p 249.

335. Gapontsev, V. P.; Rudnitskiy, Yu. P.; Sverchkov, Ye. I., NEODNORODNOYE USHIRENIYE SPEKTRAL'NYKH LINIY AKTIVNYKH SRED OKG [Nonuniform Broadening of the Spectral Lines of the Active Media of Lasers], Kiev, 1969, p 180.

336. Tolstoy, M. N.; Feofilov, P. P.; Shapovalov, V. N., IZV. AN SSSR: SER. FIZ., Vol 31, 1967, p 2064.

337. Parke, S.; Cole, E., PHYS. CHEM. GLASSES, Vol 12, 1971, p 125.

338. Auzel, F., ANN. TELECOMMUN., Vol 24, 1969, p 363.

339. Edwards, J. G.; Sandoe, J. N., J. PHYS., Vol D7, 1974, p 1078.

340. Krayevskiy, S. L.; Rudnitskiy, Yu. P.; Sverchkov, Ye. I., OPT. I SPEKTR., Vol 36, 1974, p 1134.

341. Zhabotinskiy, M. Ye.; Izyneyev, A. A.; Krayevskiy, S. L., et al., OPT. I SPEKTR., Vol 32, 1972, p 758.

342. Yegorova, V. F.; Zubkova, V. S.; Karapetyan, G. O., et al., SPEKTROSKOPIYA KRISTALLOV, Moscow, Nauka, 1970, p 219.

343. Auzel, F.; Deutschbein, O. K., Z. NATURFORSCH, Vol 24a, 1969, p 1562.

344. Reisfeld, R.; Eckstein, Y., J. NON-CRYST. SOLIDS, Vol 11, 1973, p 261.

345. Kolobkov, V. P.; Khalilev, V. D.; Vasylyak, Ya. P., et al., FIZ. I KHIM. STEKLA, Vol 3, 1977, p 249.

346. Belan, V. R.; Briskina, Ch. M.; Grigor'yants, V. V.; Zhabotinskiy, M. Ye., ZHETF, Vol 57, 1969, p 1148.

347. Przhevuskiy, A. K., OPT. I SPEKTR., Vol 42, 1977, p 144.

348. Grigor'yants, V. V., ZHETF, Vol 58, 1970, p 1594.

349. Denisov, Yu. V.; Kovaleva, I. V.; Kolobkov, V. P.; Rastokuyev, V. V., OPT. I SPEKTR., Vol 38, 1975, p 98.

350. Weber, M. J., PHYS. REV., Vol B4, 1971, p 2932.

351. Gapontsev, V. P.; Gaygerova, L. S., TEZISY DOKL. V VSESOYUZN. SIMP. PO SPEKTROSKOPII KRISTALLOV, AKTIVIROVANNYKH REDKIMI ZEMLYAMI I ELEMENTAMI GRUPPY ZHELEZA [Summary of Reports of the Fifth All Union Symposium on Spectroscopy of Crystals Doped with Rare Earths and Elements of the Iron Group], Kazan', 1976, p 70.

352. Nakazawa, Ye.; Shionoya, Sh., J. PHYS. SOC. JAPAN, Vol 28, 1970, p 1260.

353. Antsiferov, V. V.; Chiner, A. V.; Deriy, N. M., et al., OPT. COMMUN., Vol 14, 1975, p 388.

354. Belokrinitskiy, N. S.; Zhabotinskiy, M. Ye.; Manuil'skiy, A. D., et al., DAN SSSR, Vol 185, 1969, p 557.

355. Artamonova, M. V.; Briskina, Ch. M.; Skleznev, A. G., ZHFKH [Journal of Physical Chemistry], Vol 69, 1975, p 353.

356. Kozlov, V. P.; Shapovalov, V. N., FIZ. I KHIM. STEKLA, Vol 2, 1976, p 145.

357. Ageyeva, L. Ye.; Przhevuskiy, A. K.; Tolstoy, M. N.; Shapovalov, V. N., FTT, Vol 16, 1974, p 1659.

358. Dmitryuk, A. V.; Karapetyan, G. O.; Nikitin, S. V., ZHPS, Vol 18, 1973, p 869.

359. Gapontsev, V. P., AVTOREF. KAND. DIS., Moscow, IRE AN SSSR, 1972.

360. Alekseyev, N. Ye.; Gapontsev, V. P.; Gromov, A. K., et al., TEZISY DOKL. III VSESOYUZN. SIMP. PO OPTICHESKIM I SPEKTRAL'NYM SVOYSTVAM STEKOL [Summaries of Reports of the Third All Union Symposium on Optical and Spectral Properties of Glass], Leningrad, GOI, 1974, p 107.

361. Kudryashov, P. I., AVTOREFERAT KAND. DISS., Leningrad, GOI, 1976.

362. Lebedev, V. P.; Lunter, S. G.; Ovsyankin, V. V., OPT. I SPEKTR., Vol 41, 1976, p 431.

363. Nakazawa, E.; Shidnoya, Sh., J. CHEM. PHYS., Vol 47, 1967, p 3211.

364. Reisfeld, R.; Eckstein, Y., J. NON-CRYST. SOLIDS, Vol 5, 1972, p 174.

365. Artamonova, M. V.; Briskina, Ch. M.; Zolin, V. F., ZHPS, No 6, 1967, p 112.

366. Kolobkov, V. P.; Zhmyreva, I. A.; Veynberg, T. I., SPEKTROSKOPIYA TVERDOGO TELA [Solid-State Spectroscopy], Leningrad, Nauka, 1969, p 150.

367. Reisfeld, R.; Eckstein, Y., APPL. PHYS. LETT., Vol 26, 1975, p 253.

368. Rapp, Sh. F.; Chrysochoos, J., J. PHYS. CHEM., Vol 77, 1973, p 1016.

369. Galant, Ye. I.; Kozlov, V. P.; Koricheva, I. V.; Shapovalov, V. N., FIZ. I KHIM. STEKLA, Vol 5, 1979, p 110.

370. Riseberg, L. A., PHYS. REV. LETT., Vol 28, 1972, p 786; Solid State Commun., Vol 11, 1972, p 469; PHYS. REV., Vol A7, 1973, p 671.

371. Denisov, Yu. V.; Dzhurinskiy, B. F.; Kizel', V. A., IZV. AN SSSR: SER. FIZ., Vol 32, 1968, p 1580.

372. Vasil'yev, I. V.; Zverev, G. M.; Kolodnyy, G. Ya.; Onishchenko, A. M., ZHETF, Vol 56, 1969, p 122.

373. Przhevuskiy, A. K.; Savost'yanov, V. A.; Tolstoy, M. N., KVANTOVAYA ELEKTRONIKA, Vol 5, 1978, p 104.

374. Speed, A. R.; Gorlick, G. F. J.; Hagston, W. E., PHYS. STAT. SOLIDI (a), Vol 27, 1975, p 477.

375. Avouris, Ph.; Campion, A.; El-Sayed, M. A., CHEM. PHYS. LETT., Vol 50, 1977, p 9.

376. Flash, R.; Hamilton, D. S.; Selzer, P. M.; Yen, W. M., PHYS REV. LETT., Vol 35, 1975, p 1034.

377. Selzer, P. M.; Hamilton, D. S.; Flash, R.; Yen, W. M., J. LUMINESCENCE, Vol 12/13, 1976, p 737.

378. Krasutsky, N.; Moos, H. W., PHYS. REV., Vol B8, 1973, p 1010.

379. Weber, M. J.; Paisner, J. A.; Sussman, S. S., et al., J. LUMINESCENCE, Vol 12/13, 1976, p 729.

380. Belokrinitskiy, N. S.; Manuil'skiy, A. D.; Soskin, M. S., UKR. FIZ. ZH. [Ukrainian Physics Journal], Vol 12, 1967, p 1720.

381. Zabokritskiy, B. Ya.; Manuil'skiy, A. D.; Soskin, M. S.; Odulov, S. G., SPEKTROSKOPIYA KRISTALLOV, Leningrad, Nauka, 1973, p 248.

382. Belan, V. R.; Grigor'yants, V. V.; Zhabotinskiy, M. Ye., PIS'MA ZHETF, Vol 6, 1967, p 721.

383. Brecher, C.; Riseberg, L. A.; Weber, M. J., APPL. PHYS. LETT., Vol 30, 1977, p 475.

384. Przhevuskiy, A. K.; Trifonov, Ye. D.; Troshin, A. S., FTT, Vol 19, 1977, p 1461.

385. Snitzer,E., JOSA, Vol 55, 1965, p 1547.

386. Snitzer, E., APPL. OPT., Vol 5, 1966, p 1487.

387. Basiyev, T. T.; Voron'ko, Yu. K.; Karasin, A. Ya., et al, ZHETF, Vol 75, 1978, p 66.

388. Basiyev, T. T.; Voron'ko, Yu. K.; Mirov, S. B.; Prokhorov, A. M., PIS'MA ZHETF, Vol 29, 1979, p 696.

389. Basiyev, T. T.; Voron'ko, Yu. K.; Prokhorov, A. M., SPEKTROSKOPIYA KRISTALLOV, Leningrad, Nauka, 1978, p 83.

390. Yen, W. M.; Susman, S. S.; Paisner, J. A.; Weber, M. J., Preprint UCRL 76481, Lawrence Livermore Lab., Livermore, 1975.

391. Avanesov, A. G.; Voron'ko, Yu. K.; Denker, B. I., et al., KVANTOVAYA ELEKTRONIKA, Vol 6, 1979, p 1583.

392. Malyshev, M. B.; Przhevuskiy, A. K.; Trifonov, Ye. D.; Troshin, A. S., FTT, Vol 19, 1977, p 1461.

393. Yen, W. M., J. LUMINESCENCE, Vol 18/19, Part II, 1979, p 639.

394. Przhevuskiy, A. K., SPEKTROSKOPIYA KRISTALLOV, Leningrad, Nauka, 1978, p 96.

395. Kravchenko, V. B.; Rudnitskiy, Yu. P., KVANTOVAYA ELEKTRONIKA, Vol 6, 1979, p 661.

396. Perlin, Yu. Ye., UFN [Progress in the Physical Sciences], Vol 80, 1963, p 553.

397. Riseberg, L. A., Moos, M. H., PHYS. REV., Vol 174, 1969, p 429.

398. Andriyesh, I. S.; Gamurar', V. Ya.; Vylegzhanin, D. N., et al., FTT, Vol 14, 1972, p 2967.

399. Sveshnikova, Ye. B., IZV. AN SSSR: SER. FIZ, Vol 39, 1975, p 1801.

400. Bodunov, Ye. N.; Sveshnikova, Ye. B., OPT. I SPEKTR., Vol 36, 1974, p 340.

401. Riseberg, L. A.; Weber, M. J., PROGR. IN OPTICS, Amsterdam, North Holland Publ. Co., Vol 14, 1976, p 90.

402. Boulos, E. N.; Kreidl, N. J., J. CANAD. CERAM. SOC., Vol 41, 1972, p 83.

403. Kovaleva, I. V.; Kolobkov, V. P.; Tatarintsev, B. V.; Yakhkind, A. K., ZHPS, Vol 23, 1975, p 1021.

404. Gapontsev, V. P.; Izyneyev, A. A.; Kravchenko, V. B.; Sverchkov, Ye. I., TEZISY DOKL. V VSESOYUZN. SIMP. PO SPEKTROSKOPII KRISTALLOV, Kazan', 1976, p 71.

405. Reisfeld, R.; Eckstein, Y., SOLID STATE COMMUN., Vol 13, 1973, p 265, 741.

406. Reisfeld, R.; Eckstein, Y., J. CHEM. PHYS., Vol 63, 1975, p 4001.

407. Reisfeld, R., J. NON-CRYST. SOLIDS, Vol 15, 1974, p 116.

408. Reisfeld, R.; Lieblich, N., J. PHYS. CHEM. SOLIDS, Vol 34, 1973, p 1467.

409. Reisfeld, R.; Velapoldi, R. A.; Boehm, L., J. PHYS. CHEM., Vol 76, 1972, p 1293.

410. Reisfeld, R.; Boehm, L.; Eckstein, Y.; Lieblich, N., J. LUMINESCENCE, Vol 10, 1975, p 193.

411. Reisfeld, R., STRUCTURE AND BONDING, ed. J. D. Dunitz, et al., Berlin, Springer, Vol 22, 1975, p 123.

412. Layne, C. B.; Lowdermilk, W. H.; Weber, M. J., IEEE J. QUANTUM ELECTRONICS, Vol QE-11, 1975, p 798; PHYS. REV., Vol B16, 1977, p 10.

413. Galant, Ye. I.; Kalinin, V. N.; Lunter, S. G., et al., KVANTOVAYA ELEKTRONIKA, Vol 3, 1976, p 2187.

414. Gapontsev, V. P.; Gromov, A. K.; Izyneyev, A. A., et al., PIS'MA ZHETF, Vol 29, 1979, p 234.

415. Denisov, Yu. V.; Kisel', V. A., OPT. I SPEKTR., Vol 23, 1967, p 473.

416. Khodos, M. Ya.; Fotiyev, A. A.; Shtin, A. P.; Galaktionov, A. D., ZHPS, Vol 24, 1976, p 529.

417. Yegorov, V. F.; Zubkov, V. S.; Mak, A. A., SPEKTROSKOPIYA KRISTALLOV, Moscow, Nauka, 1970, p 207.

418. Rudnitskiy, Yu. P.; Smirnov, R. V.; Chernyak, V. M., KVANTOVAYA ELEKTRONIKA, Vol 3, 1976, p 2035.

419. Shekun, L. Ya., FTT, Vol 9, 1967, p 948.

420. Brachkovskaya, N. B.; Karapetyan, G. O.; Reyshakhrit, A. L., et al., OPT. I SPEKTR., Vol 21, 1970, p 328.

421. Galant, Ye. I.; Reyshakhrit, A. L.; Tolstoy, M. N., OPT. I SPEKTR., Vol 31, 1971, p 266.

422. Mashkevich, V. S.; Soskin, M. S., PIS'MA ZHETF, Vol 5, 1967, p 456.

423. Heller, A., J. AMER. CHEM. SOC., Vol 88, 1966, p 2058.

424. Peterson, G. E.; Bridenbough, P. M., JOSA, Vol 54, 1964, p 644.

425. Arbuzov, V. I.; Brachkovskaya, N. B.; Zhmyreva, I. A., et al., KVANTOVAYA ELEKTRONIKA, Vol 3, 1976, p 2005.

426. Dianov, Ye. M.; Karasik, A. Ya.; Korniyenko, L. S., KVANTOVAYA ELEKTRONIKA, Vol 2, 1975, p 422.

427. Dianov, Ye. M.; Karasik, A. Ya.; Korniyenko, L. S., et al., KVANTOVAYA ELEKTRONIKA, Vol 2, 1975, p 1665.

428. Edwards, J. A., BRIT. J. APPL. PHYS., Vol 1, 1968, p 449.

429. Jacobs, R. R.; Weber, M. J., IEEE J. QUANTUM ELECTRONICS, Vol QE-11, 1975, p 846.

430. Deutschbein, O. K.; Pautrat, C. C.; Svirchevsky, J. M., REV. PHYS. APPL, Vol 2, 1967, p 29.

431. Alekseyev, N. Ye.; Izyneyev, A. A.; Kopylov, Yu. L., et al., ZHPS, Vol 24, 1976, p 976.

432. Lunter, S..G.; Raaben, E. L.; Shumilov, S. K., TEZISY DOKL. VI VSESOYUZN. SIMP. PO SPEKTROSKOPII KRISTALLOV, AKTIVIROVANNYKH IONAMI REDKOZEMEL'NYKH I PEREKHODNYKH METALLOV [Summaries of Reports of the Sixth All Union Symposium on Spectroscopy of Crystals Doped with Rare Earth and Transition Metal Ions], Moscow, 1979, p 271.

433. Galaktionov, A. D.; Shul'gin, B. V.; Khodos, M. Ya., et al., ZHPS, Vol 21, 1974, p 339.

434. Khodos, M. Ya.; Galaktionov, A. D.; Shtin, A. P., et al., ZHPS, Vol 24, 1976, p 631.

435. Alekseyev, N. Ye.; Izyneyev, A. A.; Kopylov, Yu. L., et al., TEZISY DOKL. IV VSESOYUZN. SIMP. PO OPTICHESKIM I SPEKTRAL'NYM SVOYSTVAM STEKOL, Riga, 1977, p 107.

436. Brachkovskaya, N. B.; Lunter, S. G.; Shumilov, S. K., TEZISY DOKL. VI VSESOYUZN. SIMP. PO SPEKTROSKOPII KRISTALLOV, AKTIVIROVANNYKH IONAMI REDKOZEMEL'NYKH I PEREKHODNYKH METALLOV, Moscow, 1979, p 64.

437. Judd, B. R., PHYS. REV., Vol 127, 1962, p 750.

438. Ofelt, G. S., J. CHEM. PHYS., Vol 37, 1962, p 511.

439. Krupke, W. F., IEEE J. QUANTUM ELECTRONICS, Vol QE-7, 1971, p 153.

440. Carnall, W. T.; Field, P. K.; Rajnak, K., J. CHEM. PHYS., Vol 49, 1968, p 4424.

441. Deutschbein, O. K., IEEE J. QUANTUM ELECTRONICS, Vol QE-12, 1976, p 551.

442. Belan, V. R.; Grigorjants, V. V.; Zhabotinsky, M. E., IEEE J. QUANTUM ELECTRONICS, Vol QE-3, 1967, p 425.

443. Rudnitskiy, Yu. P.; Smirnov, R. V.; Sokolov, V. I., TEZISY DOKL. I VSESOYUZN. KONF. PO OPTIKE LAZEROV [Summaries of Reports of the First All Union Conference on Laser Optics], Leningrad, 1976, p 68; preprint of the Atomic Power Institute im. I. V. Kurchatov, No 1417, 1979.

444. Grigor'yants, V. V.; Zhabotinskiy, M. Ye.; Markushev, V. M., ZHPS, Vol 14, 1971, p 73.

445. Mak, A. A.; Prilezhayev, D. S.; Serebryakov, V. A.; Starikov, A. D., OPT. SPEKTR., Vol 33, 1972, p 689.

446. Martin, W. E.; Milam, D., APPL. PHYS. LETT., Vol 32, 1978, p 816.

447. Nikitin, V. I.; Soskin, M. S.; Khizhnyak, A. I., PIS'MA ZHTF, Vol 3, 1977, p 14.

448. Bondarenko, Ye. G.; Galant, Ye. I.; Lunter, S. G., et al., TEZISY DOKL. NA III VSESOYUZN. SIMP. PO OPTICHESKIM I SPEKRAL'NYM SVOYSTVAM STEKOL, Leningrad, GOI, 1974, p 96.

449. Kravchenko, V. I.; Tarabrov, V. V., ZHPS, Vol 13, 1970, p 719.

450. Galich, G. A.; Kravchenko, V. I., UKR. FIZ. ZH., Vol 20, 1975, p 1732.

451. Pogorelyy, O. N.; Soskin, M. S.; Taranenko, V. B., PIS'MA ZHTF, Vol 2, 1976, p 49.

452. Zabokritskiy, B. Ya.; Manuil'skiy, A. D.; Orlov, S. G., et al., UKR. FIZ. ZH., Vol 17, 1972, p 501.

453. Veduta, A. P.; Solokha, A. F.; Furzikov, N. P., et al., KVANTOVAYA ELEKTRONIKA, No 5, 1973, p 36.

454. Treat, R. P.; Cabezas, A. Y., J. APPL. PHYS., 1966, Vol 37, p 3556.

455. Baak, T., JOSA, Vol 59, 1969, p 851.

456. Shchavelev, O. S.; Babkina, V. A.; Yelina, N. N., et al., FIZ. I KHIM. STEKLA, Vol 2, 1976, p 449.

457. Waxler, R. M.; Cleek, G. W.; Malitson, I. H., et al., J. RES. NAT. BUR. STAND., Vol 75A, 1971, p 163.

458. Waxler, R. M.; Cleek, G. W., J. RES. NAT. BUR. STAND, Vol 77A, 1973, p 755.

459. Blazhko, V. V.; Bubnov, M. M.; Dianov, Ye. M.; Chikolini, A. V., KVANTOVAYA ELEKTRONIKA, Vol 3, 1976, p 1151.

460. Gromov, A. K.; Izyneyev, A. A.; Kopylov, Yu. L.; Kravchenko, V. B., TEZISY DOKL. III VSESOYUZN. SIMP. PO OPTICHESKIM I SPEKTRAL'NYM SVOYSTVAM STEKOL, Leningrad, GOI, 1974, p 24.

461. Gromov, A. K.; Izyneyev, A. A.; Kopylov, Yu. L., et al., NOVYYE LEGKOPLAVKIYE GLAZURI, EMALI I FOSFOROSODERZHASHCHIYE STEKLA, Riga, 1973, p 152.

462. Alexeev, N. Ye.; Gapontsev, V. P.; Zhabotinsky, M. Ye., et al., PROC. XI INTERN. CONGRESS ON GLASS, Prague, Vol 3, 1977, p 69.

463. Levenberg, V. A.; Lunter, S. G., FIZ. I KHIM. STEKLA, Vol 2, 1976, p 63.

464. Berezina, Ye. Ye.; Levenberg, V. A.; Lunter, S. G., FIZ. I KHIM. STEKLA, Vol 3, 1977, p 617.

465. Ramachandran, G. N., PROC. INDIAN ACAD. SCI., Vol 25A, 1947, p 266.

466. Ramaseshan, S.; Vedam, K.; Kirshnan, R. S., PROGR. CRYST PHYS., Vol 1, 1958, p 139.

467. Prodhomme, L., PHYS. CHEM. GLASSES, Vol 1, 1960, p 119.

468. Chistyakov, A. N., OPT.-MEKH. PROM., No 1, 1975, p 60.

469. Berezina, Ye. Ye., OPT.-MEKH. PROM., No 9, 1974, p 63.

470. Kasymova, S. S.; Shchavelev, O. S., OPT.-MEKH. PROM., No 8, 1974, p 14.

471. Shchavelev, O. S.; Babkina, V. A.; Zelenskaya, M. V., OPT.-MEKH. PROM., No 3, 1975, p 64.

472. Shchavelev, O. S.; Zelenskaya, M. V., OPT.-MEKH. PROM., No 10, 1974, p 50.

473. Molev, V. I.; Shchavelev, O. S., ZHPKH, Vol 49, 1976, p 755.

474. Molev, V. I.; Shchavelev, O. S., OPT.-MEKH. PROM., No 4, 1977, p 27.

475. Kasymova, S. S.; Shchavelev, O. S., STEKLO. TRUDY GOS. IN-TA STEKLA [Glass. Works of the State Institute of Glass], No 2, (151), 1976, p 4.

476. Shchavelev, O. S.; Molev, V. I.; Yelina, N. N., OPT.-MEKH. PROM., No 9, 1976, p 22.

477. Gromov, A. K.; Izyneyev, A. A.; Kopylov, Yu. L.; Kravchenko, V. B., TEZISY DOKL. IV VSESOYUZN. SIMP. PO OPTICHESKIM I SPEKTRAL'NYM SVOYSTVAM STEKOL, Riga, 1977, p 46.

478. Shchavelev, O. S.; Babkina, V. A., FIZ. I KHIM. STEKLA, Vol 3, 1977, p 519.

479. Demkina, L. I., FIZIKO-KHIMICHESKIYE OSNOVY PROIZVODSTVA OPTICHESKOGO STEKLA [Physiochemical Principles of the Production of Optical Glass], Leningrad, Khimiya, 1976, p 78.

480. Shchavelev, O. S.; Plutalova, N. Yu., FIZ. I KHIM. STEKLA, Vol 4, 1978, p 98.

481. Wemple, S. H.; Di Domencio, M., PHYS. REV., Vol B1, 1970, p 193.

482. Bendow, B.; Gianino, P. D.; Tsay, Y. F.; Mitra, S. S., APPL. OPT., Vol 13, 1974, p 2382.

483. Wemple, S. H.; Di Domenico, M., PHYS. REV. LETT., Vol 23, 1969, p 1156.

484. Kopylov, Yu. L., AVTOREFERAT KAND. DISS., Moscow IRE AN SSSR, 1980.

485. Wemple, S. H., PHYS. REV., Vol B7, 1973, p 3767.

486. Wemple, S. H., J. CHEM. PHYS., Vol 67, 1977, p 2151.

487. Morozova, I. N.; Yakhkind, A. K., TEZISY DOKL. IV VSESOYUZN. SIMP. PO OPTICHESKIM I SPEKTRAL'NYM SVOYSTVAM STEKOL, Riga, 1977, p 21.

488. Veyko, V. P.; Libenson, M. N., LAZERNAYA OBRABOTKA [Laser Machining], Leningrad, Lenizdat, 1973.

489. Kaminskiy, A. A.; Mak, A. A.; Pashinin, P. P.; Popov, Yu. M., SPRAVOCHNIK PO LAZERAM [Laser Handbook], Moscow, Sov. radio, Vol I, 1978, p 237.

490. Buzhinskiy, I. M.; Dianov, Ye. M.; Mak, A. A., SPRAVOCHNIK PO LAZERAM, Moscow, Sov. radio, Vol I, 1978, p 329.

491. Mak, A. A.; Anan'yev, Yu. A.; Yermakov, B. A., UFN, Vol 92, 1967, p 373.

492. Mak, A. A.; Stepanov, A. I., OPT.-MEKH. PROM., No 10, 1967, p 17.

493. KIGRE Q-88* PHOSPHATE GLASS, USA, 1977 (Prospectus of the Kigre Company).

494. Stokowski, S. E.; Saroyan, R. A.; Weber, M. J., Nd-DOPED LASER GLASS. SPECTROSCOPIC AND PHYSICAL PROPERTIES, Lawrence Livermore Lab. M-095, Livermore, 1978.

495. Hattori, M.; Taubaki, T.; Murata, F.; Tanaka, M., J. CERAM. SOC, Japan, Vol 79, 1971, p 45.

496. Galaktionova, N. M.; Yegorova, V. F.; Zubkova, V. S., et al., DAN SSSR, Vol 173, 1967, p 1284.

497. Vodop'yanov, K. L.; Denker, B. I.; Maksimova, G. V., et al., KVANTOVAYA ELEKTRONIKA, Vol 5, 1978, p 686.

498. Zheltov, G. I.; Mamonov, S. K.; Rubanov, A. S., ZHPS, Vol 22, 1975, p 928.

499. Avanesov, A. G.; Vasil'yev, I. V.; Voron'ko, Yu. K., et al., KVANTOVAYA ELEKTRONIKA, Vol 6, 1979, p 1586.

500. Battista, A. D.; Shiner, W. H., PRODUCTION LASER HOLE DRILLING--NOW, Laser, Inc., 1976.

501. Komogawa, T.; Kotera, H.; Hayami, H., Japan, J. APPL. PHYS., Vol 5, 1966, p 449.

502. Gaponov, S. V.; Garin, F. V.; Paramonov, L. V., KVANTOVAYA ELEKTRONIKA, Vol 2, 1975, p 1554.

503. Grevtsev, N. V.; Yevdokimov, V. A.; Skripnichenko, A. S., FIZ. I KHIM. OBRABOT. MATER. [Physics and Chemistry of the Working of Materials], No 3, 1969, p 20.

504. Bespalov, V. I.; Gostev, V. I.; Gruzdev, V. V., et al., OPT.-MEKH. PROM., No 12, 1971, p 20.

505. Davidov, B. A.; Muratov, V. R.; Soms, L. N., et al., Kvantovaya ELEKTRONIKA, Vol 1, 1974, p 2518.

506. Kuroda, H.; Tomie, T.; Masuko, H.; Maekawa, S., IEEE/OSA CONF. ON LASER ENGIN. A. APPLICATIONS (DIGEST OF TECHN. PAPERS), Washington, 1977, p 51.

507. LASER PROGRAM--LAWRENCE LIVERMORE LAB. ANNUAL REP. NURCL 50021-76, Livermore, 1976.

508. Reisfeld, R.; Eckstein, Y., J. NON-CRYST. SOLIDS, Vol 12, 1973, p 357.

509. Quelle, F., PROC. CONF. ON LASER RANGE INSTR., California, SPIE, 1968, p 3.

510. Bruce, R. E.; White, K. O.; Magon, J. B.; Buser, R. G., IEEE J. QUANTUM ELECTRONICS, Vol QE-5, 1969, p 479.

511. White, K. O.; Holt, E. H.; Woodcock, R. F., LASER FOCUS, Vol 6, No 7, 1970, p 41.

512. Ross, M., LAZERNYYE PRIYEMNIKI [Laser Receivers], Moscow, Mir, 1969.

513. Gapontsev, V. P.; Rudnitskiy, Yu. P., TEZISY DOKL. VSESOYUZN. SOVESHCHANIYA PO INZHENERNYM PROBLEMAM UPRAVLYAYEMOGO TERMOYADERNOGO SINTEZA [Summaries of Reports on the All Union Conference on the Engineering Problems of Controlled Thermonuclear Fusion], Leningrad, 1974, p 3d.

514. Snitzer, E., AMER. CERAM. SOC. BULL., Vol 52, No 6, 1973, p 516.

515. Gapontsev, V. P.; Izyneyev, A. A.; Kravchenko, V. B.; Rudnitskiy, Yu.P., TEZISY DOKL. I VSESOYUZN. KONF. PO OPTIKE LAZEROV [Summaries of Reports of the First All Union Conference on Laser Optics], Leningrad, 1977, p 9.

516. Kudryashov, P. I.; Veynberg, T. I.; Kolobkov, V. P., ZHPS, No 5, 1966, p 434.

517. Auzel, F., ANN. TELECOMMUNIC., Vol 24, No 5-6, 1969, p 199.

518. Robinson, C., J. NON-CRYST. SOLIDS, Vol 15, 1974, p 1, 11.

519. Sandoe, J. N.; Sarkies, P. H.; Parke, S., J. PHYS., Vol D5, 1972, p 1788.

520. Mak, A. A., OPT.-MEKH. PROM., No 1, 1979, p 5.

521. Kolobkov, V. P.; Petrovskiy, G. T., OPT.-MEKH. PROM., No 3, 1971, p 53.

522. Zhmyreva, I. A.; Kovaleva, I. V.; Kolobkov, V. P., et al., OPT. I SPEKTR., Vol 22, 1966, p 509.

523. Judd, B. R., CHEM. PHYS., Vol 44, 1966, p 839.

524. Gapontsev, V. P., Kravchenko, V. B.; Rudnitskiy, Yu. D., TEZISY DOKL. III VSESOYUZN. SIMP. PO OPTICHESKIM SPEKTRAL'NYM SVOYSTVAM STEKOL, Leningrad, GOI, 1974, p 113.

525. Robinson, C., JOSA, Vol 57, No 1, 1967, p 4.

526. Kolobkov, V. P.; Kudryashov, P. I.; Rubinov, Yu. A., et al., ZHPS, Vol 17, 1972, p 161.

527. Kalinin, V. N.; Mak, A. A.; Prilezhayev, D. S.; Fromzel', V. A., ZHTF, Vol 44, 1974, p 1328.

528. Snitzer, E.; Woodcock, R. F.; Segre, J., IEEE J. QUANTUM ELECTRONICS (DIGEST OF TECHN. PAPERS), QE-4, 1968, p 360.

529. Snitzer, E.; Woodcock, R., JOSA, Vol 55, 1965, p 580.

530. Gandy, H. W.; Ginther, R. J.; Weller, J. F., PHYS. LETT., Vol 16, 1965, p 266.

531. Auzel, F., C. R. ACAD. SCI., Vol B263, 1966, p 765.

532. Snitzer, E.; Landry, J., USA Patent No 3675155, 1972.

533. Oshe, G. R., IEEE J. QUANTUM ELECTRONICS, Vol QE-7, 1971, p 252.

534. Gapontsev, V. P.; Kravchenko, V. B.; Sverchkov, Ye. I., TEZISY DOKL. I VSESOYUZN. KONF. PO OPTIKE LAZEROV, Leningrad, 1977, p 8.

535. Kalinin, V. N.; Mak, A. A., Prilezhayev, D. S.; Fromzel', V. A., PIS'MA ZHTF, Vol 1, 1975, p 449.

536. Sverchkov, Yu. Ye.; Gapontsev, V. P., TEZISY DOKL. VI VSESOYUZN. SIMP. PO SPEKTROSKOPII KRISTALLOV, AKTIVIROVANNYKH IONAMI P. Z. I PEREKHODNYKH METALLOV, Krasnodar, 1979, p 241.

537. Avdeyev, P. S.; Berezin, Yu. S.; Gudakovskiy, Yu. P., et al., KVANTOVAYA ELEKTRONIKA, Vol 5, 1978, p 220.

538. White, K. O.; Schlensener, S. N., APPL. PHYS. LETTS., Vol 21, 1972, p 419.

539. Avdeyev, P. S.; Berezin, Yu. D.; Volkov, V. V., et al., TEZISY DOKL. II VSESOYUZN. KONF. PO OPTIKE LAZEROV [Summaries of Reports of the Second All Union Conference on Laser Optics], Leningrad, GOI, 1979, p 280.

540. Baranov, N. B.; Bykovskiy, N. Ye.; Zel'dovich, B. Ya.; Sonatskiy, Yu. V., kvantovaya elektronika, Vol 1, 1974, p 2450.

541. Anan'yev, Yu. A., KVANTOVAYA ELEKTRONIKA, No 6, 1971, p 3.

542. Gorlanov, A. V.; Kalinina, A. A.; Lyubimov, V. V., et al., ZHPS, Vol 17, 1972, p 617.

543. Baranov, S. A.; Kolpakova, I. V.; Kononova, M. Yu., et al., KVANTOVAYA ELEKTRONIKA, Vol 5, 1978, p 174.

544. Snitzer, E., AMER. CERAM. SOC. BULL., Vol 52, 1973, p 516.

545. Segre, J. P.; Truscott, N. R.; Moroz, E. Y., IEEE J. QUANTUM ELECTRONICS, Vol QE-9, 1973, p 673.

10845

CSO: 8144/1223

- END -